Solution of the Crystal Structure of Human Milk Xanthine Oxidoreductase

Arwen Pearson

A thesis submitted for the degree of Doctor of Philosophy
in the University of St. Andrews, April 2001

For Mum and Dad

Declaration

i) I, Arwen Pearson, hereby certify that this thesis, which is approximately 40,000 words in length, has been written by me, that it is the record of work carried out by me and that it has not been submitted in any previous application for a higher degree.

Signature Date 24.04.01

ii) I was admitted as a research student in May 1999 and as a candidate for the degree of PhD in May 1999 at the University of St Andrews; the higher study for which this is a record was carried out in the University of Bath between October 1997 and April 1999, and in the University of St Andrews between May 1999 and February 2001.

Signature Date 24.04.01

iii) I hereby certify that the candidate has fulfilled the conditions of the Resolution and Regulations appropriate for the degree of PhD in the University of St Andrews and that the candidate is qualified to submit this thesis in application for that degree.

Signature of Supervisor Date 24/4/01

Copyright

In submitting this thesis to the University of St Andrews I understand that I am giving permission for it to be made available for use in accordance with the regulations of the University Library for the time being in force, subject to any copyright vested in the work not being affected thereby. I also understand that the title and abstract will be published, and that a copy of the work may be made and supplied to any *bona fide* library or research worker.

Signature

Date 21.04.01

Acknowledgements

Thanks first and foremost go to my supervisors, Garry, Roger and Robert for all their help and support during my PhD. Also owed special thanks are Justin, Sharmilla, Ben, Susan and Adrian at Bath, and Helen, Elaine, Rupert & Jim at St Andrews. I'm also grateful to all in the three labs (1.28, Taylor and Naismith) as well as the two departments (Bath and St Andrews) who answered questions, loaned me equipment and generally put up with me.

A very special mention is reserved for Catherine who got me through the molecular biology, helped me move house several times, let me walk the husky occasionally and was generally amazing.

Thanks are also due to Ursula Potter and Glyn Love in the Centre for Electron Optical Studies at University of Bath, Carrie Wilmot at The University of Leeds, Serena Radford at Daresbury Laboratory, Ed Mitchell and Tassos Perrakis at the ESRF and to Emil Pai at The University of Toronto who very kindly provided me with the co-ordinates of bovine milk xanthine oxidase.

I am also very grateful to the BBSRC and CeNeS for paying for it all.

"The pursuit of a structure is rather like hunting:
it requires some skill, a knowledge of the victim's habits,
and a certain amount of low cunning."

Crick and Kendrew, 1957.

Abstract

This thesis reports the crystallization, structure solution and preliminary refinement of the demolybdo form of human milk XOR to a resolution of 3.5 Å. Although the bovine milk XOR structure was also recently determined, this is the first demolybdo XOR structure to be determined and also the first structure of a human XOR. Also reported is the determination of the cDNA sequence of human mammary gland XDH.

Xanthine oxidoreductase is a complex molybdenum and iron-sulphur containing flavoprotein. Due to its abundance, the enzyme from bovine milk has been extensively studied over the last 100 years. More recently the human milk enzyme has been investigated and has been shown to have surprising properties, in particular a very low specific activity.

Traditionally associated with the last stages of purine catabolism, XOR has recently been shown to produce reactive oxygen species through reduction of oxygen and also to be capable of reducing nitrates and nitrites to NO. These findings implicate XOR in a variety of disease states, in particular ischaemia reperfusion injury.

The low specific activity of human milk XOR is due to a low content of molybdenum (~ 5 %). Higher molybdenum content and specific activity has been reported for certain other human tissues, notably liver and small intestine. This work aimed to investigate possible reasons for the low level of incorporation of molybdenum and its associated molybdopterin cofactor into the human milk enzyme.

Amino Acid three and one letter codes:

Alanine	ALA	A	Leucine	LEU	L
Arginine	ARG	R	Lysine	LYS	K
Asparagine	ASN	N	Methionine	MET	M
Aspartate	ASP	D	Phenylalanine	PHE	F
Cysteine	CYS	C	Proline	PRO	P
Glutamine	GLN	Q	Serine	SER	S
Glutamate	GLU	E	Threonine	THR	T
Glycine	GLY	G	Tryptophan	TRP	W
Histidine	HIS	H	Tyrosine	TYR	Y
Isoleucine	ILE	I	Valine	VAL	V

Abbreviations

A	Adenine
AMV	Avian myeloblastis virus
AO	Aldehyde oxidase
ATP	Adenosine triphosphate
CODH	Carbon monoxide dehdyrogenase
CODHL	Carbon monoxide dehdyrogenase, large subunit
CODHM	Carbon monoxide dehdyrogenase, medium subunit
CODHS	Carbon monoxide dehdyrogenase, small subunit
BAC	Bacterial artificial chromosomes
BMXDH	Bovine milk xanthine dehydrogenase
BMXO	Bovine milk xanthine oxidase
BMXOR	Bovine milk xanthine oxidoreductase
C	Cytosine
CS	Crystallographic symmetry
DMF	Dimethyl formate
DMSO	Dimethyl sulphoxide
DTT	Dithiothreitol
EDC	N-ethyl-N'-(3-dimethylaminopropyl) carbodiimide
EDTA	(disodium) ethylenediamine tetraacetate
EPR	Electron paramagnetic resonance
FAD	Flavin adenine dinucleotide
G	Guanine
HMXOR	Human milk xanthine oxidoreductase

IEF	Iso-electric focusing
IRI	Ischaemia reperfusion injury
MAD	Multiwavelength anomalous dispersion
MCD	Molybdopterin cytosine dinucelotide
MES	2-(N-Morpholino)-ethanesulfonic acid
MFGM	Milk fat globule membrane
MI	Myocardial infarction
ML	Maximum likelihood
Mo-co	Molybdenum cofactor
MOD	Aldehyde oxidoreductase from *D. desulfuricans*
Mo-MPT	Molybdenum containing molybdopterin
MOP	Aldehyde oxidoreductase from *D. gigas*
MPC	Magnetic particle concentrator
MPT	Molybdopterin
MR	Molecular Replacement
MurB	UDP-N-acetylenolpyruvylglucosamine reductase
NAD	Nicotinamide dinucleotide
NCS	Non-crystallographic symmetry
PBS	Phosphate buffered saline
PCR	Polymerase chain reaction
PEG 4K	Polyethylene glycol 4000
PFR	Protein to Flavin Ratio
RACE	Rapid amplification of cDNA ends
RLXO	Rat liver xanthine oxidase
r.m.s.d	Root mean standard deviation
ROS	Reactive oxygen species
RT	Reverse transcriptase
SDS-PAGE	Sodium dodecyl sulphate polyacrylamide gel electrophoresis
T	Thymine
TAE	Tris-acetate-ethanol
TEMED	N,N,N',N'-Tetramethylethylenediamine
THMXO	Human mammary gland XDH sequence (Briggs, 1997)
TLS	Translation/libration/screw-rotation
U	Uracil
UV	Ultraviolet
VAO	Vanillyl-alcohol oxidase
XDH	Xanthine dehydrogenase
XO	Xanthine oxidase
XOR	Xanthine oxidoreductase
X-ray SEM	X-ray microanalysis scanning electron microscopy

Table of Contents

Chapter 1

An Introduction to Xanthine Oxidoreductase

1.1 Xanthine oxidoreductase - A brief introduction

In 1891 Horbaczewski (Horbaczewski, 1891) observed the production of urate from nuclear material in the presence of tissue homogenates, and an increased level of *in vivo* urate production in clinical cases characterised by tissue damage/breakdown. This was followed by the recognition in 1899 by Spitzer (Spitzer, 1899) that the oxidation of hypoxanthine and xanthine to urate in the presence of aerated tissue homogenate was an enzymic process. The enzyme involved was named xanthine oxidase by Burian in 1905 (Burian, 1905). In 1902 Schardinger (Schardinger, 1902) proposed a new way to distinguish boiled and un-boiled milk, by showing that un-boiled milk was able to decolourise methylene blue on the addition of formaldehyde. He tentatively mentions, in a note appended to the paper, the possibility that the reductive activity may be due to some sort of enzyme-like bodies rather than metabolic products. By the 1920s it was well established that xanthine oxidase activity existed in milk, (Dixon, 1926; Dixon and Thurlow, 1924a; Dixon and Thurlow, 1924b; Dixon and Thurlow, 1924c; Morgan *et al.*, 1922) catalysing the conversion of hypoxanthine to xanthine to urate with the generation of reducing equivalents (Fig. 1.1). There was, however, considerable disagreement as to whether xanthine oxidase and "Schardinger's enzyme" were one and the same. By 1940, this identity was well established (Booth, 1938; Dixon, 1938) and protocols for the preparation of relatively pure xanthine oxidase from bovine milk were in use (Ball, 1939; Corran *et al.*, 1939).

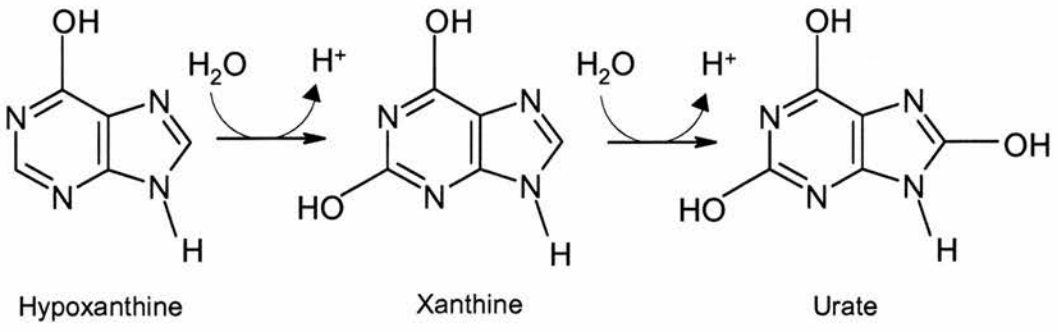

Hypoxanthine Xanthine Urate

Figure 1.1 The conversion of hypoxanthine to urate catalysed by xanthine oxidoreductase

The use of milk as a source for the enzyme meant that there was little contamination from other enzymes. This, and its abundance in bovine milk, has made xanthine oxidase one of the most extensively studied enzymes of the last 100 years.

1.2 The prosthetic groups of xanthine oxidoreductase

The xanthine oxidase preparations of Corran (Corran *et al.*, 1939) and Ball (Ball, 1939) consisted of a golden brown material, the visible spectrum of which indicated the presence of a flavin and another chromophore.

In 1950 Westerfield and Richert reported that they were unable to measure xanthine oxidase activity in the livers of newborn rats. Activity first began to appear after 12 days and even after weaning, at 21 days, xanthine oxidase activity was still only 50 % that of a mature animal. They went on to show that the development of xanthine oxidase activity was dependent on a dietary factor (Westerfield and Richert, 1950). In 1953, several groups identified the dietary factor required for xanthine oxidase activity as inorganic molybdenum (De Renzo *et al.*, 1953; Green and Beinert, 1953; Richert and Westerfield, 1953; Totter *et al.*, 1953).

Using similar studies, it was determined that supplementing the diet of newborn rats with iron also increased xanthine oxidase activity and Richert and Westerfield proposed that iron was the non-flavin chromophore of xanthine oxidase (Richert and Westerfield, 1954).

Over the next 15 years there were several attempts to determine the relative amounts of the xanthine oxidase prosthetic groups. Bray and co-workers, having made an extremely pure crystalline preparation of bovine milk xanthine oxidase (Avis *et al.*, 1955), reported that iron, flavin and molybdenum were present in the approximate ratio 4:1:1 (Avis *et al.*, 1956a), although they were unable to demonstrate a molybdenum content greater than 0.87 mols Mo/mol flavin. This, and the apparent presence of two electrophoretically identical

molecular species with differing activities in their preparation (Avis *et al.*, 1956b), led them to postulate the existence of molybdenum-poor species of xanthine oxidase.

In 1969 Massey and co-workers were able to show that fully active xanthine oxidase did indeed contain iron, molybdenum and flavin in the proportions 4:1:1 (Massey *et al.*, 1969) as suggested by Avis and co-workers (Avis *et al.*, 1956a).

1.2.1 Flavin

The flavin cofactor of xanthine oxidase was identified as a flavin adenine dinucleotide (FAD) by both Corran and Ball (Ball, 1939; Corran *et al.*, 1939), who noted its similarity to, and ability to substitute for, the flavin cofactor of amino acid oxidase reported by Warburg and Christian (Warburg and Christian, 1938) (Fig 1.2).

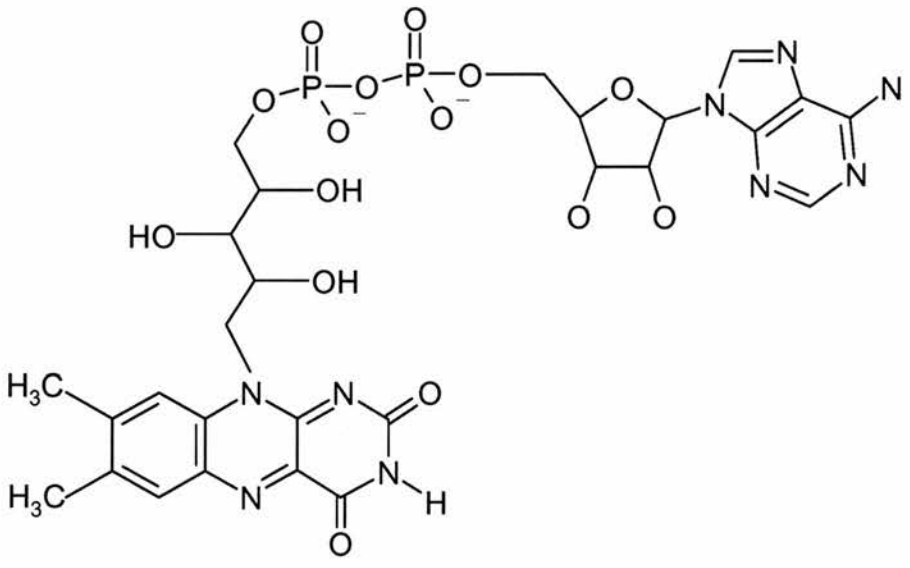

Figure 1.2 Flavin adenine dinucleotide. (Oxidised or quinone form)

Komai et al. (Komai *et al.*, 1969) prepared the deflavo enzyme, by treatment with calcium chloride and showed that it was unable to be reoxidised by molecular oxygen. It was, however, still able to oxidise xanthine in the presence of electron acceptors such as cytochrome c and ferricyanide.

1.2.2 Iron

Visible spectra and electron paramagnetic resonance (EPR) data collected by Massey and co-workers (Massey *et al.*, 1969) indicated that the iron is not associated with a porphyrin. Rather it is in an iron-sulphur complex similar to that seen in plant ferredoxins (Fig. 1.3).

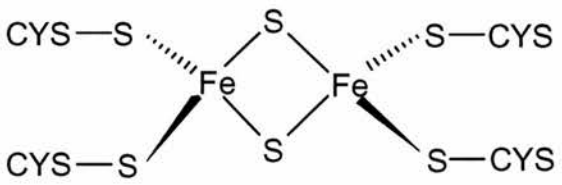

Figure 1.3 2Fe2S Iron sulphur cluster

They also showed that each mol of flavin is associated with two different iron sulphur centres (2Fe2S) assigned as FeS1 and FeS2 on the basis of EPR spectra (Palmer and Massey, 1969) and their measured reduction potentials. FeS2 has a reduction potential 100 mV higher than that of FeS1 (Porras and Palmer, 1982). Using Mössbauer spectroscopy, Hille has also observed an unusually large quadrupole coupling of 3.2 mm/s which he assigned tentatively to FeS1 (Hille *et al.*, 1985). Recent crystal structures of several xanthine oxidase related enzymes (Dobbek *et al.*, 1999; Rebelo *et al.*, 2000; Romão *et al.*, 1995), and a mutagenesis study on rat xanthine oxidase (Iwasaki *et al.*, 2000) has allowed the definitive assignment of the iron-sulphur motifs in the sequence to FeS1 and FeS2 (Fig 1.4).

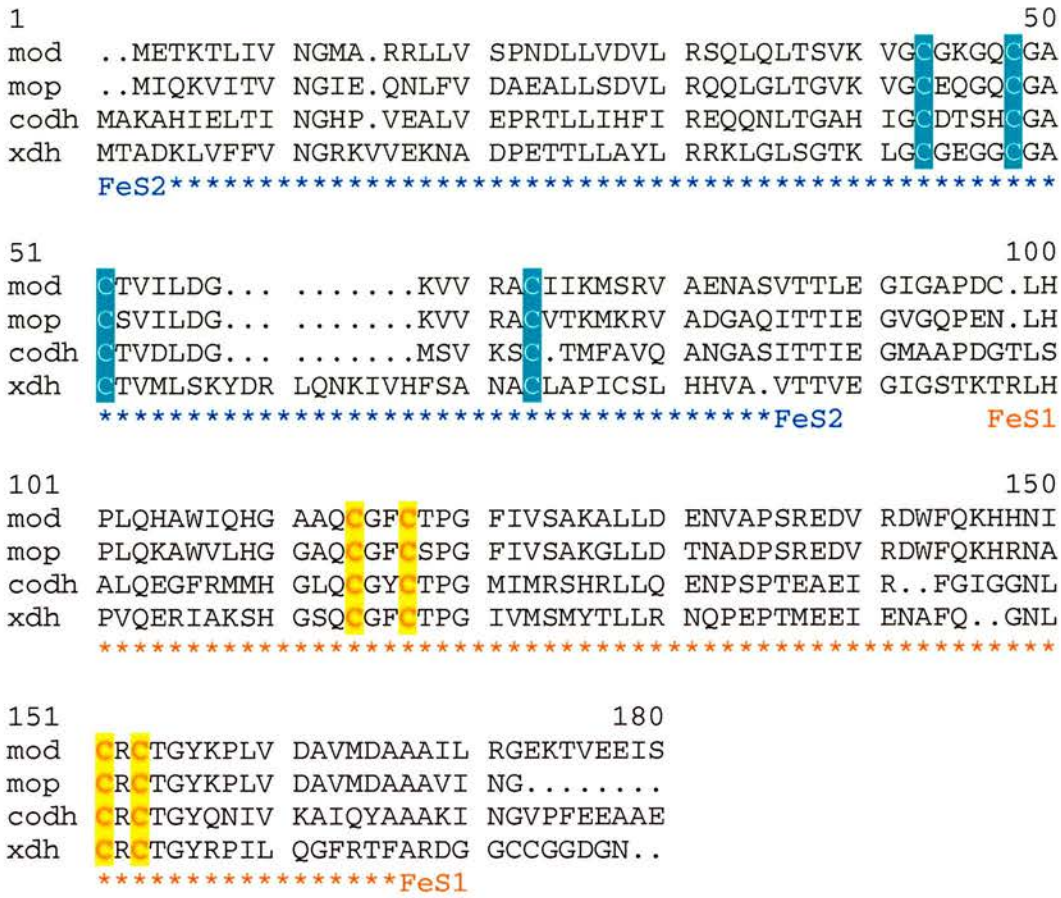

Figure 1.4 Sequence alignment of the Iron-sulphur domains of *D. Desulfuricans* Aldehyde oxidoreductase (MOD) 1-166 (Rebelo *et al.*, 2000), *D. Gigas* Aldehyde oxidoreductase (MOP) 1-158 (Romão *et al.*, 1995), **O. Carboxidovorans** CO dehydrogenase (CODH) 1-166 (Dobbek *et al.*, 1999) and Human liver Xanthine oxidoreductase (XDH) 1-175 (Ichida *et al.*, 1993). FeS1 is indicated in red and FeS2 in blue The Iron-sulphur cluster co-ordinating cysteines are highlighted.

An alternative nomenclature based on proximity to the molybdenum site has also been proposed (Dobbek *et al.*, 1999; Rebelo *et al.*, 2000) which assigns FeS1 as FeS_proximal and FeS2 as FeS_distal (Fig 1.5).

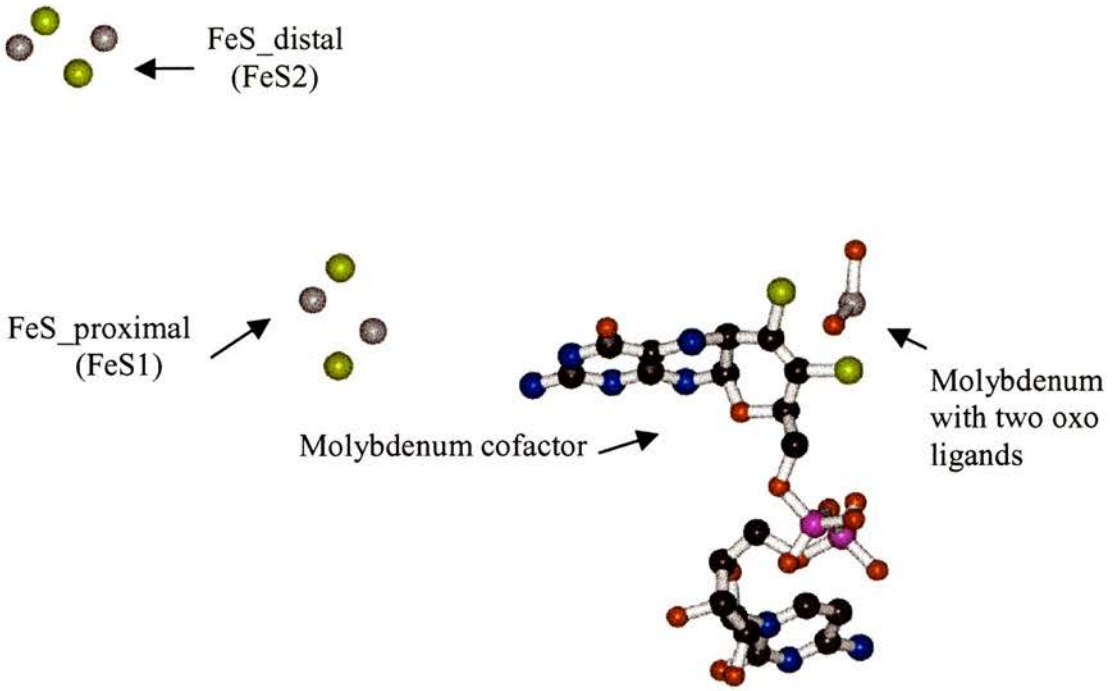

Figure 1.5 The cofactor arrangement in *D. sulfuricans* aldehyde oxidoreductase (Rebelo *et al.*, 2000). Atoms are coloured by type; metals - grey, S - yellow, C - black, O - red, N - blue and P pink. Image was generated using Molscript.

Given the relative positions of the iron-sulphur clusters and Mo, it can be seen that electrons entering the enzyme at the Mo will pass first to FeS1 then to FeS2. FeS2, located at the surface of the molecule, is then positioned to pass the electrons to the physiological electron acceptor (in the case of xanthine oxidase family members lacking the FAD domain), artificial acceptors (such as methylene blue or cytochrome c) or onto the FAD, which, in the CO dehydrogenase structure, is located 8.7 Å away (Dobbek *et al.*, 1999).

The crystal structures have also revealed the existence of two different 2Fe2S co-ordinating folds in the xanthine oxidase enzyme family. FeS2/FeS_distal is coordinated by a fold typical of the plant type ferredoxins, a five-stranded β

half barrel with an α-helix orthogonal to the strands (Fig. 1.6A), whereas FeS1/FeS_proximal is a new 2Fe2S coordinating fold consisting of a four helical bundle with the 2Fe2S cluster bound at the N-termini of the two central helices (Fig. 1.6B).

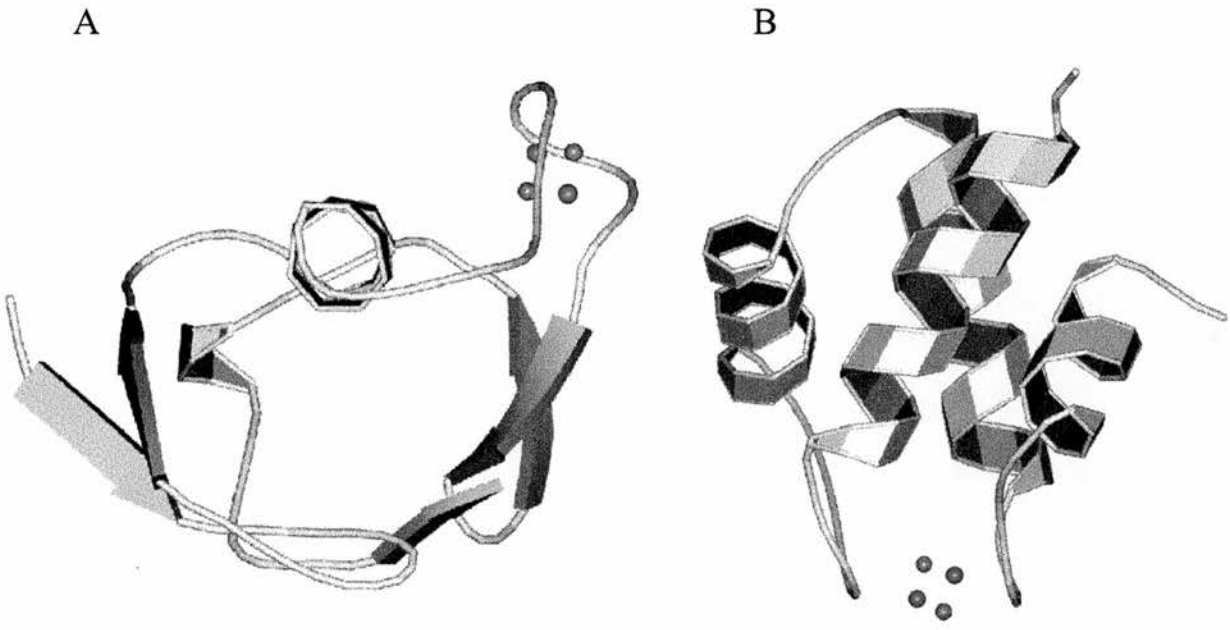

Figure 1.6 The FeS domains of *D. desulfuricans* Aldehyde oxidoreductase (MOD).
A: FeS_distal (FeS2) residues 1-76. B: FeS_proximal (FeS1) residues 84-156

1.2.3 Molybdenum

Early studies on the cyanide inactivation of xanthine oxidoreductase showed that cyanide does not bind to the protein, but is eliminated as thiocyanate in amounts directly proportional to active enzyme (Massey and Edmondson, 1970). This was interpreted as indicating the existence of a persulphide linkage to the molybdenum site and was supported by the demonstration that resulphuration with sulphide reactivates the enzyme. X-ray absorption spectroscopy studies on the oxidised form of the bovine enzyme revealed that it possesses both a sulphido and an oxo ligand to the Mo and that it was the sulphido group, rather than a persulphide, that was removed on treatment with cyanide (Bordas *et al.*, 1980). EPR studies also revealed the existence of further thiolate ligands to the Mo (Hawkes and Bray, 1984).

In 1964 studies on mutants of *Aspergillus nidulans* lacking functional nitrate reductase and xanthine oxidoreductase showed that at least six different genetic loci affected the observed phenotype (Pateman *et al.*, 1964). On the basis of this, it was suggested that five of the loci were actually concerned with the synthesis of a cofactor common to both enzymes. It was also suggested that, given the characteristics of the mutants, the cofactor was more likely to be associated with the Mo than the Fe or flavin.

Many attempts to elucidate the nature and structure of this cofactor followed, hampered by the fact that when the cofactor was released from the enzyme using standard methods (heating, acidification, treatment with denaturants) it was extremely unstable and was rapidly inactivated and degraded. An important step forward was the finding that a 6-substituted pterin could be

isolated from sulfite oxidase, xanthine dehydrogenase and a variety of other molybdoenzymes. The realisation that a number of fluorescent and relatively stable inactive derivatives of the cofactor could be isolated, led to their characterisation and the eventual proposal of the likely active cofactor structure (Johnson and Rajagopalan, 1982) (Fig 1.7).

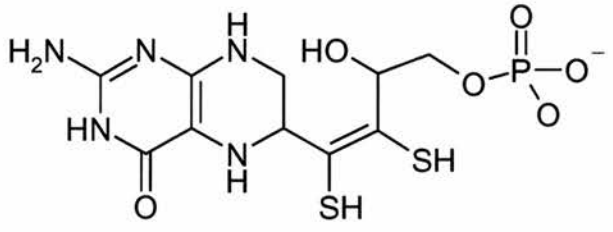

Figure 1.7 Structure of the molybdenum cofactor proposed by Johnson and Rajagopalan.

The first crystal structures of molybdopterin enzymes, aldehyde ferredoxin reductase (Chan *et al.*, 1995) and aldehyde oxidoreductase (Romão *et al.*, 1995), essentially confirmed this structure. *In situ*, however, the 3rd ring is actually closed, forming a pyran ring (Fig 1.8).

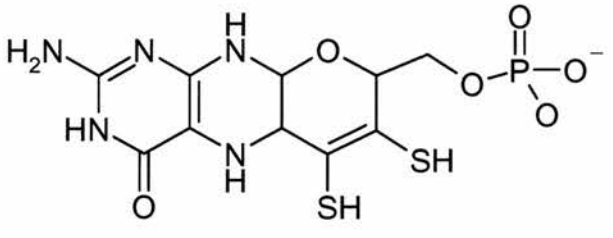

Figure 1.8 Structure of the molybdenum cofactor found *in vivo*.

In enzymes from eukaryotic sources the pterin is always in the form shown above but in enzymes from prokaryotic sources it is usually found as the dinucleotide of guanine, cytosine, adenine or hypoxanthine (Kisker *et al.*, 1999).

The structure of the *D. gigas* aldehyde oxidoreductase (Romão *et al.*, 1995) revealed that the Mo is pentaco-ordinated with two dithiolene sulphur ligands from the molybdopterin, and three oxygen ligands (Fig 1.9).

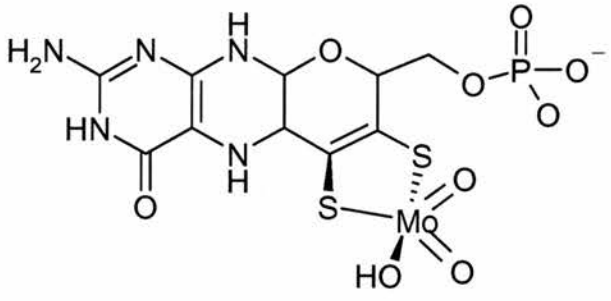

Figure 1.9 The molybdopterin structure and molybdenum co-ordination seen in D. Gigas AOR.

Romao and co-workers went on to propose that one of the oxo-ligands is replaced by a sulphido group in the active "sulpho" form of the enzyme. Further structural studies were carried out in order to define the co-ordination of the Mo more accurately and the structures of desulpho-, sulpho-, oxidised, reduced and alcohol-bound forms of MOP were solved at 1.8 Å resolution (Huber *et al.*, 1996).

1.3 Molybdenum hydroxylases and the xanthine oxidase family

Xanthine oxidoreductase is a member of a superfamily of proteins, the molybdenum hydroxylases, all of which contain molybdenum complexed to a derivative of the pterin cofactor described above (Hille, 1996).

The Mo cofactor-containing enzymes are ubiquitous in nature, and are currently divided into 4 families (Kisker *et al.*, 1999); dimethyl sulphoxide (DMSO) reductases, sulfite oxidases, aldehyde ferredoxin oxidoreductases and xanthine oxidases. This classification is based on sequence homologies, and includes tungsten-containing enzymes, but does not require the Mo/W centre to be co-ordinated in the same way for members of the same family. With the exception of the *Rhodobacter* DMSO reductase, all molybdenum cofactor-containing enzymes so far described also contain at least one additional cofactor, such as haem, FAD, FeS clusters or b_5 (Hille, 1996), which is involved in intramolecular electron transfer to or from the Mo/W centre.

Within each family there is moderate to high sequence homology, whereas no significant homology is detected between families (Fig. 1.10). The crystal structures so far determined, of proteins from all four families, support the sequence evidence that there is no common ancestral Mo-co containing protein. Rather, evolution has independently selected at least four different folds to co-ordinate the Mo-co.

Figure 1.10: Tree diagram showing the evolutionary relationships of all four molybdenum hydroxylase families, calculated from a multiple alignment of representative sequences and generated using GCG. The families are coloured as follows: xanthine oxidase family - blue, DMSO reductase family - green, sulfite oxidase family - red & the aldehyde ferredoxin oxidoreductase family - purple. Sequences used are as follows (the NCBI accession number is given in bold): *B. halodurans* xanthine dehydrogenase **BAB04467** (Takami *et al.*, 2000); *D. gigas* aldehyde oxidoreductase **A57429** (Thoenes *et al.*, 1994); *S. solfataricus* xanthine dehydrogenase **S73093** (Sensen *et al.*, 1996); *P. putida* quinoline-2-oxidoreductase **CAA66830** (Blase *et al.*, 1996); *O. carboxidovorans* carbon monoxide dehydrogenase **A56279**, **B56279** & **C56279** (Schubel *et al.*, 1995); *A. thaliana* xanthine dehydrogenase **CAB80207** (EU Arabidopsis Sequencing Project); *H. sapiens* aldehyde oxidase **NP_00150** (Wright *et al.*, 1993); *D. melanogaster* xanthine dehydrogenase **S07245** (Keith *et al.*, 1987); *G. gallus* xanthine dehydrogenase **XOCHDH** (Sato *et al.*, 1995); *B. taurus* xanthine dehydrogenase **CAA58497** (Berglund *et al.*, 1996); *R. norvegicus* xanthine dehydrogenase **NP_058850** (Amaya *et al.*, 1990); *F. catus* xanthine dehydrogenase **AAF97949** (Tsuchida and Tagawa, 2000); *H. sapiens* xanthine dehydrogenase **BAA02013** (Ichida *et al.*, 1993); *P. diminuta* isoquinoline-1-oxidoreductase **A56939** & **B56939** (Lehmann *et al.*, 1995); *B. subtilis* dissimilatory nitrate reductase **2203266A** & **2203266B** (Cruz Ramos *et al.*, 1995); *R. capsulatus* DMSO reductase **Q52675** (Shaw *et al.*, 1996); *B. halodurans* formate dehydrogenase **BAB06572** (Takami *et al.*, 2000); *N. crassa* assimilatory nitrate reductase **S16292** (Okamoto *et al.*, 1991); *A. thaliana* sulfite oxidase **AAF13276** (Brinkmann *et al.*, 1999); *H. sapiens* sulfite oxidase **AAA74886** (Garrett *et al.*, 1995); *G. gallus* sulfite oxidase **A34180** (Neame and Barber, 1989); *T. litoralis* formaldehyde ferredoxin oxidoreductase **Q56303** (Takami *et al.*, 2000); *P. horikoshii* aldehyde ferredoxin oxidoreductase **O58778** (Kawarabayasi *et al.*, 1998); *P. abyssi* glyceraldehyde-3-phosphate: ferredoxin oxidoreductase **F75005** (anonymous deposition from Genoscope) and *P. furiosus* glyceraldehyde-3-phosphate: ferredoxin oxidoreductase **AAC70892** (van der Oost *et al.*, 1998). This tree diagram is a modified version of that found in Hille (1996) and was compiled using the GCG programme suite.

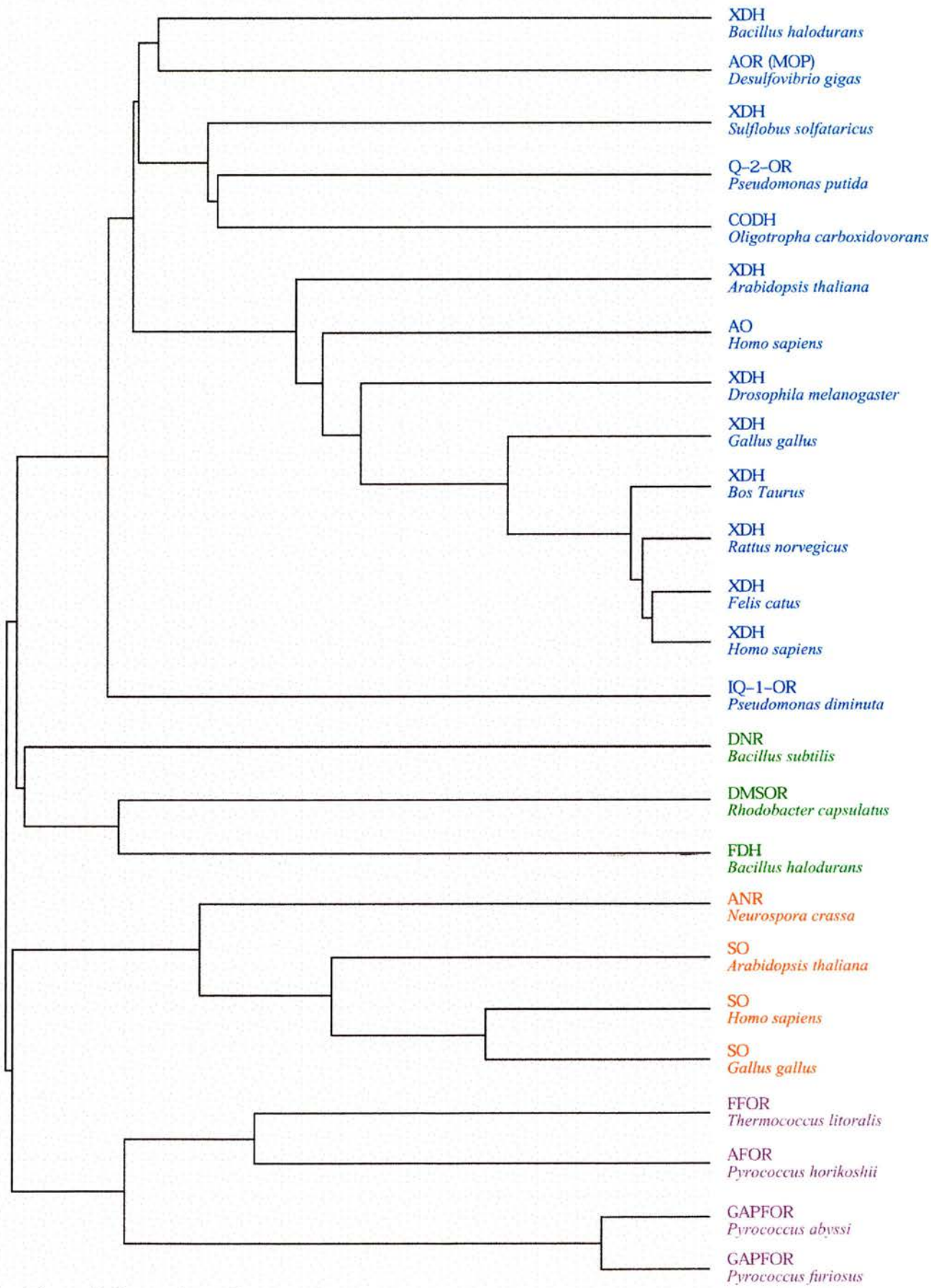

Figure 1.10: see legend on previous page

1.3.1 DMSO reductases

DMSO reductase family members are exclusively found in eubacteria, and include, amongst others, DMSO reductase, dissimilatory nitrate reductases, formate dehydrogenases and pyrogallol-phloroglucinol transhydroxylase. With the exception of the latter, these enzymes serve as terminal reductases in the absence of oxygen and the presence of substrate, thereby allowing the bacteria to generate energy in addition to that generated by fermentation. Three members of the DMSO reductase family have been characterised structurally; DMSO reductase from *R. sphaeroides* (Schindelin *et al.*, 1996) (Fig. 1.11) and *R. capsulatus* (Schneider *et al.*, 1996); *E. coli* Formate dehydrogenase (Boyington *et al.*, 1997) and dissimilatory nitrate reductase from *D. desulfuricans* (Dias *et al.*, 1999).

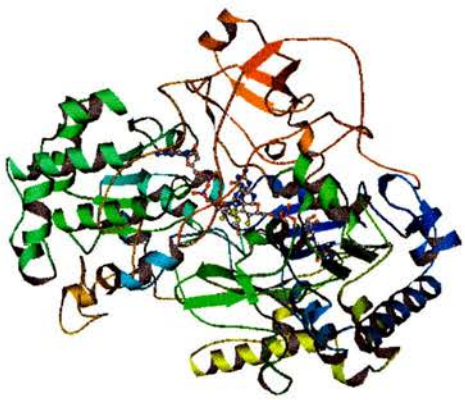

Figure 1.11
Ribbon diagram showing the fold of DMSO reductase (Schindelin *et al.*, 1996). Image generated using MICE (Bourne *et al.*, 1998; Tate *et al.*, 1999).

1.3.2 Sulfite oxidases

This family consists of the sulfite oxidases and the assimilatory nitrate reductases from algae, fungi and higher plants. Sulfite oxidase is mainly found in eukaryotes and is located in the mitochondrial intermembrane space where it catalyses the oxidation of sulfite to sulphate. This is the terminal reaction in the oxidative degradation of cysteine and methionine. Assimilatory nitrate

reductases catalyse the reduction of nitrate to nitrite which is subsequently converted to NH_4^+ by nitrite reductase. The crystal structure of a fragment of corn nitrate reductase (the FAD binding domain) has been published (Lu *et al.*, 1995) as has the structure of the complete chicken sulfite oxidase (Kisker *et al.*, 1997) (Fig. 1.12).

Figure 1.12
Ribbon diagram showing the fold of chicken liver sulfite oxidase (Kisker *et al.*, 1997). Image generated using MICE (Bourne *et al.*, 1998; Tate *et al.*, 1999).

1.3.3 Aldehyde ferredoxin oxidoreductases

Aldehyde ferredoxin oxidoreductase (containing a W centre) catalyses the interconversion of aldehydes and carboxylates and was the first molybdopterin containing enzyme to be characterised by X-ray crystallography (Chan *et al.*, 1995) (Fig. 1.13). With the exception of hydroxycarboxylate viologen oxidoreductase from *Proteus vulgaris,* all members of this family are tungsten containing enzymes. At present little is known about the catalytic mechanism of any member of this family.

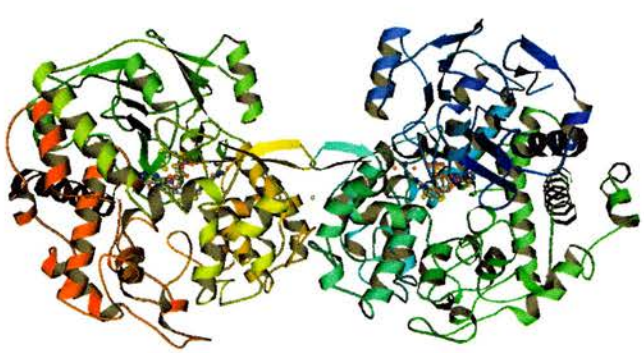

Figure 1.13
Ribbon diagram showing the fold of aldehdye ferredoxin oxidoreductase (Chan *et al.*, 1995). Image generated using MICE (Bourne *et al.*, 1998; Tate *et al.*, 1999).

1.3.4 Xanthine oxidases

Members of the xanthine oxidase family have been described from eukaryotic, eubacterial and archeael sources and generally catalyse hydroxylation reactions of the type shown in scheme 1.

$$RH + H_2O \rightarrow ROH + 2H^+ + 2e^- \qquad \text{Scheme 1}$$

The overall mechanism of the reaction catalysed by the xanthine oxidase family of enzymes is usually broken down into the oxidative and the reductive half reactions of the catalytic cycle, defined from the standpoint of the enzyme. It is usually the reductive half reaction in which the molybdenum centre participates, with the metal being reduced from Mo(VI) to Mo(IV) in the course of hydroxylation (Hille, 1996). The Mo centre is then reoxidised to an active state by the passing of electrons to a physiological electron acceptor via the iron sulphur clusters. In cases where a third cofactor is present (e.g. FAD in xanthine oxidoreductase & CO dehydrogenase) it is believed that the iron sulphur clusters pass the electrons onto FAD and thence onto an electron acceptor.

The xanthine oxidases are probably the largest and most diverse family of molybdenum cofactor-containing enzymes and have been extensively characterised spectroscopically and kinetically.

1.4 Structurally characterised members of the xanthine oxidase family

Three members of this family have been structurally characterised; aldehyde oxidoreductase from *D.gigas* (MOP) (Romão *et al.*, 1995) and *D. desulfuricans* (MOD) (Rebelo *et al.*, 2000), CO dehydrogenase (CODH) from *O. carboxidovorans* (Dobbek *et al.*, 1999) and *Hydrogena pseudoflava* (Hänzelmann *et al.*, 2000), and xanthine oxidase/dehydrogenase from *B. Taurus* (Enroth *et al.*, 2000) (Fig. 1.14).

The general architecture of the xanthine oxidase family of enzymes comprises (starting at the N-terminus) two 2Fe2S domains (one of the ferrodoxin type, one representing a new 2Fe2S co-ordinating fold), an FAD binding domain (not present in MOP or MOD) and two molybdopterin-binding domains which coordinate the molybdopterin between them. A few members of the family (e.g. CODH) have a different genetic architecture in which the domains are coded for by different genes, but the subunit/domain arrangement in the structures so far determined appears to be very similar.

Fig 1.14 Ribbon diagrams of the three xanthine oxidase family enzyme structures so far determined. **A**: *D. Gigas* aldehyde oxidoreductase (Romão *et al.*, 1995), **B**: *O .carboxidovorans* carbon monoxide dehydrogenase (Dobbek *et al.*, 1999) and **C**: Bovine milk xanthine oxidase (Enroth *et al.*, 2000). The iron sulphur domain is coloured red, the FAD domain/connecting peptide green & the molybdenum domain blue. Sequence identity with bovine milk xanthine oxidase for the different domains is as follows: MOP iron sulphur domain 44%, MOP molybdenum domain 27%, CODH iron sulphur domain 35%, CODH FAD domain 18% and CODH molybdenum domain 23%. These images were generated using MOLSCRIPT.

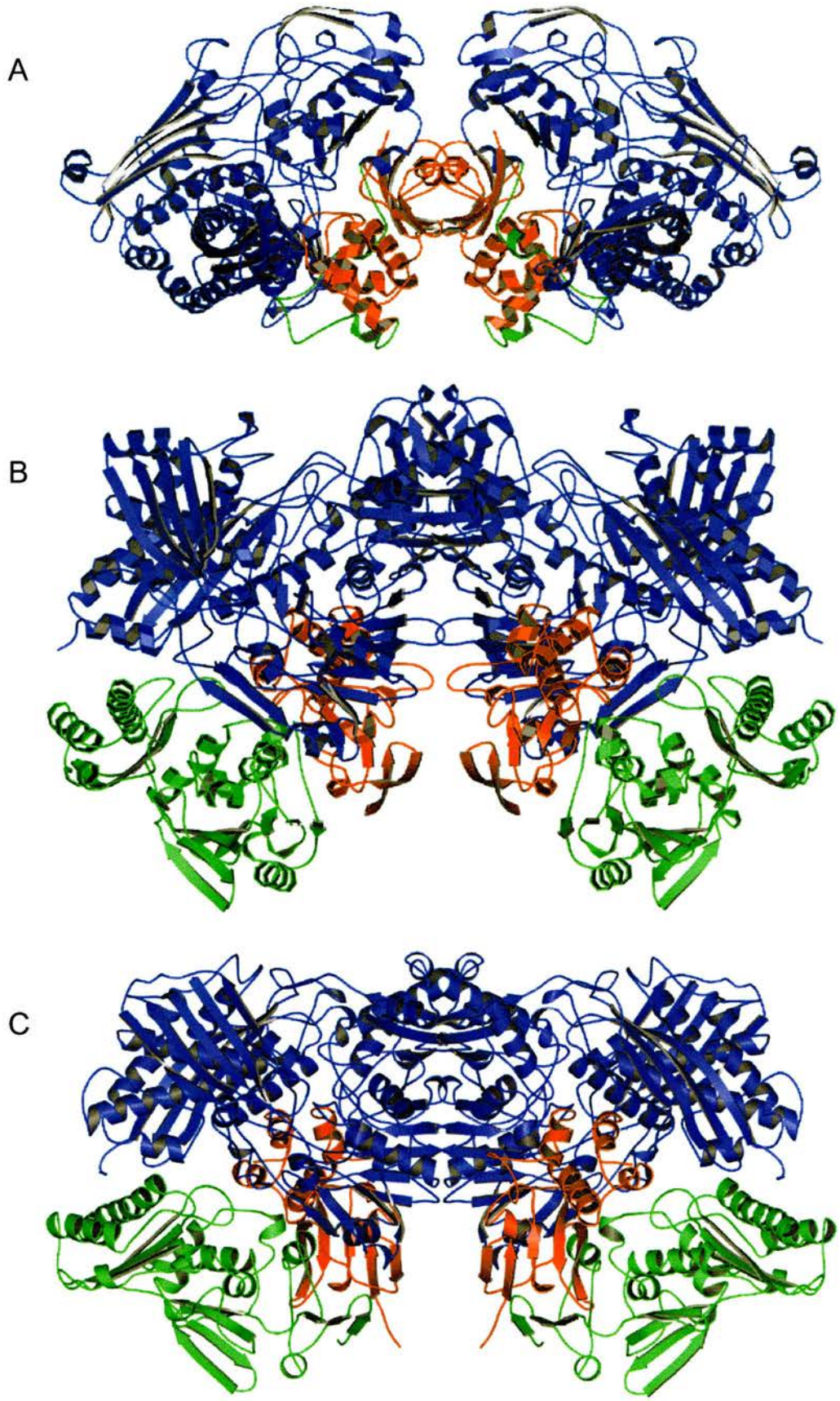

Figure 1.14 The legend for this figure is to be found on the previous page.

1.4.1 Aldehyde oxidoreductase from *D. gigas* (MOP) & *D. desulfuricans* (MOD)

MOP was the first true Mo/molybdopterin cofactor-containing structure to be solved (Romão *et al.*, 1995), although a W/molybdopterin enzyme was solved earlier in the same year (Chan *et al.*, 1995), and was also the first member of the xanthine oxidase family to be structurally characterised. MOP is a homodimer of 907 residues/monomer that oxidises aldehydes to carboxylic acids with little specificity for the nature of the side group and contains a molybdopterin moiety conjugated to a cytosine dinucleotide (MCD). It is part of a four protein electron transfer chain in *D. gigas* (Barata *et al.*, 1993) of which the other members are flavodoxin, cytochrome and hydrogenase.

MOP is organised into four domains; the N-terminus, containing the first 2Fe2S cluster (residues 1-76) which resembles plant and cyanobacterial ferrodoxins, the second 2Fe2S domain (residues 84-157) which represented a new 2Fe2S co-ordinating fold and is followed by an extended interconnecting peptide (residues 158-195) which then leads into the large MoCo domain. The MoCo domain is further subdivided into Mo1 (residues 196-581) which contributes two molybdopterin binding segments and Mo2 (residues 582-907) which contributes a third molybdopterin binding region and all of the nucleotide binding regions.

The molybdopterin is deeply buried between the two Mo subdomains, and is accessible through a 15 Å deep tunnel. In the original MOP structure to 2.25 Å resolution, the molybdenum was seen to be pentacoordinated with two dithiolene sulphur ligands from the molybdopterin, and three oxygen ligands. It was proposed that one of the oxo-ligands was replaced by a sulphido group in the active "sulpho" form of the enzyme. Further high resolution structural studies were carried out to define the exact co-ordination of the Mo (Huber *et al.*, 1996). These structures have been used to derive a mechanism for the hydroxylation reaction of MOP, and the xanthine oxidase family in general which will be discussed later.

The structure of the *D. gigas* MOP homologue from *D. desulfuricans* (MOD) was also solved recently to 2.8 Å resolution (Rebelo *et al.*, 2000). Like MOP it is a homodimer (2 x 98 kDa) with one molybdenum atom associated with an MCD type molybdopterin and two 2Fe2S clusters per monomer. Visible and EPR spectroscopy indicate a close relationship to MOP (Duarte *et al.*, 2000) and activity studies show a similar broad specificity. As is to be expected, the MOD structure shows the same overall globular structure as MOP and the same domain organisation.

1.4.2 CO dehydrogenase from *O. carboxidovorans* & *H. pseudoflava* (CODH)

CODH is a molybdenum-containing iron-sulphur flavoprotein that catalyses the oxidation of CO (Scheme 2), generating a proton gradient across the cytoplasmic membrane of *O. carboxidovorans* by channelling the electrons formed via cytochrome b_{561} into a CO-insensitive respiratory chain (Meyer *et al.*, 1993).

$$CO + H_2O \rightarrow CO_2 + 2e^- + 2H^+$$ Scheme 2

The enzyme is composed of 3 subunits; L (88.7 kDa), M (30.2 kDa) and S (17.8 kDa) and exists as a dimer of LMS heterotrimers. Each subunit contains one co-factor. The molybdenum is to be found, co-ordinated by MCD, on the L subunit, the FAD is bound by the M subunit and the two 2Fe2S clusters are located in the S subunit. Both the S and L subunits have a fold that closely resembles those of the FeS and MoCo1/2 domains in MOP and MOD. In addition the mutual orientation of the subunits is identical to that of the corresponding domains in MOP.

The structure of *O. carboxidovorans* CODH (Dobbek *et al.*, 1999) is of special interest as it is the first structural example of a xanthine oxidase family member containing an FAD domain/subunit. The FAD binding subunit (CODHM) can be subdivided into 3 distinct domains; N-terminal (res. 1-54), a middle domain (res. 60-174) and the C-terminal domain (res. 180-285). The

N-terminal and middle domains of CODHM show structural homology, and share some sequence motifs, with a recently described oxidoreductase family sharing a conserved FAD binding domain. Vanillyl-alcohol oxidase (VAO) (Fraaije *et al.*, 1998) and UDP-N-acetylenolpyruvylglucosamine reductase (MurB) (Benson *et al.*, 1996) are the only two other examples of this family whose structures have been solved. The C-terminal domain of CODHM and its counterparts in VAO and MurB are unrelated and Dobbek and co-workers postulate that they may confer class-specific properties.

Very recently, the structure of the CO dehydrogenase from *H. pseudoflava* has also been determined (Hänzelmann *et al.*, 2000). Interestingly, the structures of both the wild type and the inactive demolybdo form of this enzyme have been obtained. This is the first structure of a xanthine oxidase family member in the demolybdo form. Surprisingly, although certain catalytic residues are slightly displaced, there appears to be no alteration in the general fold of the molybdenum-binding subunit, or in its interactions with the other subunits, when the molybdenum cofactor is absent.

1.4.3 Xanthine oxidase from Bovine milk (BMXOR) & Rat liver (RLXO)

Crystals of bovine milk xanthine oxidoreductase (BMXOR) were reported as early as 1955 (Avis *et al.*, 1955), and diffraction to 2.1 Å was briefly reported in 1993 (Eger *et al.*, 1993). However, it was only very recently that the solution of the crystal structures of the oxidase and dehydrogenase forms of BMXOR complexed with the inhibitor salicylate was announced to 2.5 and 2.1 Å respectively. (Enroth *et al.*, 2000). Like CODH, the dimer interface is formed through the molybdenum domain, producing a butterfly shaped dimer with overall dimensions of 155 x 90 x 70 Å. Both forms of the enzyme are missing stretches of residues (Fig. 1.15). In the dehydrogenase form, only a few surface residues are undefined. This, in addition to the observation that the dehydrogenase form runs as a single band on SDS PAGE, leads Enroth and co-workers to conclude that these residues are disordered rather than missing. In the oxidase structure, however, considerably longer stretches are missing. Given that limited proteolysis was used to produce the oxidase form, they suggest it is likely these residues are not present in the molecule.

XDH	XO
1-2	1
166-191	166-223
532-536	529-570
1332	1316-1332

Figure 1.15 Residues without corresponding electron density in the bovine milk XOR structures (Enroth *et al.*, 2000).

The overall fold of the molecule is very similar to that observed for other members of the xanthine oxidase family. BMXOR is split into three domains. The N-terminal domain contains both iron sulphur clusters (1-165). There then follows a long connecting peptide (166-225) which leads onto the FAD domain (226-531). Another partially disordered segment (532-589) links the FAD domain to the C-terminal molybdenum domain (590-1332). Both the molybdenum and iron sulphur domains show the same fold as seen in all xanthine oxidase family members. The FAD domain, like the FAD subunit of CODH, is a VAO family member. The details of the structure, with respect to cofactors and dehydrogenase oxidase conversions, will be discussed in the relevant sections.

Diffraction to 2.6 Å has also been reported for rat liver xanthine oxidase (Carvalho *et al.*, 1998), although as yet, no solution has been found (Carvalho, personal communication).

1.5 Catalytic activity of XOR

Xanthine oxidoreductase catalyses hydroxylation reactions of the type:

$$RH + H_2O \rightarrow ROH + 2H^+ + 2e^-$$

Its overall reaction cycle is usually broken down into two half reactions. In the reductive half reaction electrons are removed from the substrate, reducing the enzyme. The enzyme then returns to its starting state via the oxidative half reaction, passing the electrons, *in vivo*, to a physiological electron acceptor - the oxidising substrate.

Mammalian xanthine oxidoreductase (XOR) exists in two kinetically distinguishable forms that differ in their choice of oxidising substrate. Xanthine dehydrogenase (XDH) displays a marked preference for NAD^+, whereas xanthine oxidase (XO) can only use molecular oxygen. The two are interconvertible via thiol-active agents, although an irreversible conversion to the oxidase form can be effected by limited proteolysis of the enzyme. Although there is as yet no consensus as to which thiols are involved in the conversion, a recent study by Rasmussen and co-workers (Rasmussen *et al.*, 2000) suggests that CYS535 and CYS992 (BMXOR) are the most likely candidates. Since the only difference between XO and XDH appears to be the preferred oxidising substrate, it is believed that the interconversion involves the FAD moiety. Indeed, the interconversion seems to involve a structural rearrangement of the FAD domain. By using flavin analogues, containing ionisable -OH or -SH groups, to replace the native FAD of XOR Massey and

co-workers obtained evidence of a strong negative charge in the flavin binding site of XDH which is absent in XO (Massey *et al.*, 1989).

1.5.1 Electron flow within XOR and associated reactivities

In the 1960s several EPR studies were carried out in order to determine the roles of the iron sulphur clusters, molybdenum and FAD in electron transfer from reducing to oxidising substrates. By following the appearance and disappearance of EPR signals associated with the various prosthetic groups it was determined that all three were involved in the transfer of electrons from substrate to electron acceptor. Early work seemed to suggest that the sequence of electron transfer was as shown below (Fig. 1.16):

Substrate (xanthine) → Mo → FAD → Fe → Acceptor (molecular oxygen/NAD^+)

Figure 1.16 Electron transfer scheme 1. Arrows indicate the direction of electron flow.

Then, in 1969, Komai and co-workers (Komai *et al.*, 1969) prepared deflavo XO, by treatment with calcium chloride, and showed that the deflavo-enzyme was unable to be reoxidised by molecular oxygen. It was, however, still able to oxidise xanthine in the presence of electron acceptors such as cytochrome c and ferricyanide. This led to a revised model for electron transfer (Fig. 1.17):

Substrate (xanthine) → Mo → Fe → FAD → Acceptor (molecular oxygen/NAD)

↓

Artificial acceptor (cytochrome c, ferricyanide)

Figure 1.17 Electron transfer scheme 2. Arrows indicate the direction of electron flow.

NADH can also act as a reducing substrate, donating electrons to the FAD (Hunt and Massey, 1994; Sanders *et al.*, 1997). Reoxidation of the enzyme can occur as normal with the reduction of molecular oxygen at the FAD. A scheme of electron transfer incorporating this reaction is shown in Fig 1.18. NADH is to date the only reducing substrate known that acts at the FAD site. NADH oxidase activity is higher in the dehydrogenase form of XOR.

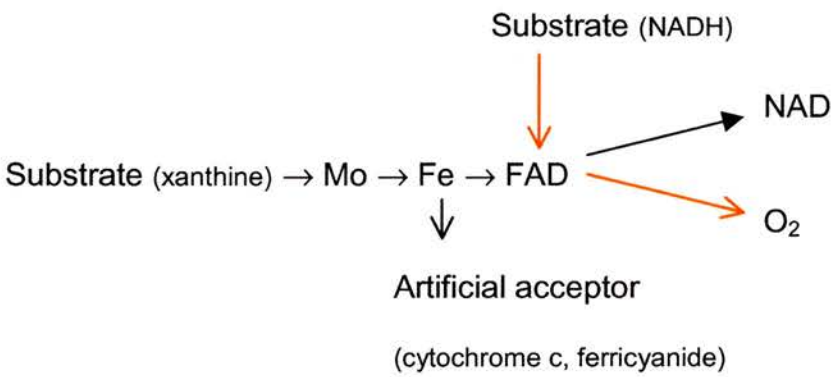

Figure 1.18 Electron transfer scheme 3. Arrows indicate the direction of electron flow.

Very recently, it has been shown that Xanthine oxidase is able to reduce glycerol trinitrate, inorganic nitrate and nitrite to NO under anaerobic conditions (Millar *et al.*, 1998). Godber and colleagues have demonstrated that XOR-catalysed nitrite reduction takes place in the presence of NADH or xanthine as reducing substrates, and that the reaction in the presence of NADH can be inhibited by allopurinol (a xanthine analogue known to act at the Mo site) (Godber *et al.*, 2000b). This leads to the currently accepted scheme for electron transfer in Xanthine oxidoreductase (Fig. 1.19):

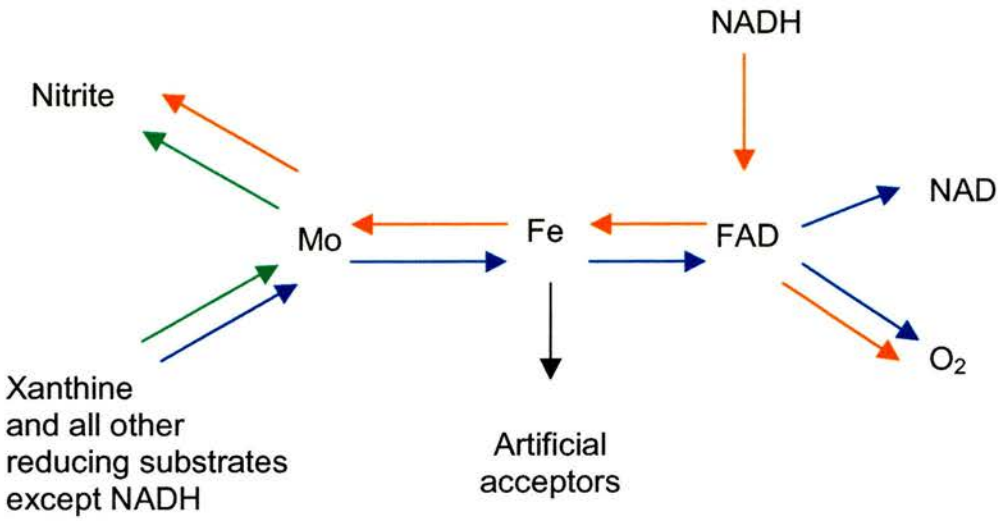

Figure 1.19 Current accepted scheme of e^- transfer within XOR. Arrows indicate the direction and source of electron flow within the enyzme.

1.5.2 Structural studies of xanthine oxidase family enzymes, and the catalytic and electron transfer mechanisms of XOR.

The recent crystal structures of several xanthine oxidase family members have provided a wealth of information on the environment and arrangement of the various prosthetic groups of XOR. This validates the overall electron transfer scheme described previously, certainly with respect to the relative positions of the prosthetic groups and has also allowed the proposal of structure based mechanisms for xanthine oxidase activity.

1.5.2.1 The molybdenum site and its role in catalysis

During the oxidation of xanthine, $2e^-$ are removed from the xanthine molecule when the purine C8 C-H bond is oxidised to C-OH. Until the availability of crystal structures of xanthine oxidase family members, a preferred mechanism

involved deprotonation of the purine C8 by the sulphido group co-ordinated to the molybdenum followed by the nucleophilic attack of the resulting carbanion on the Mo^{VI}=O group to give Mo^{IV}-OR (Hille, 1996). Dissociation of the product, and protonation from solvent would then be followed by regeneration of the Mo=O group from water (Fig 1.20). This rapid regeneration was required in order to explain XAS data obtained from reduced XOR complexed with violopterin or alloxanthine indicating clearly that both species possessed an Mo=O group. The 2.25 Å structure of MOP, showing a well defined water molecule complexed to the Mo, seemed to suggest that this regeneration might be accomplished by deprotonation of a metal complexed water rather than directly from bulk solvent (Fig 1.20).

Several groups, however, suggested that the catalytically labile oxygen required for xanthine oxidation could come from this Mo-bound water itself, rather than the M=O group, thus avoiding the mechanistic difficulties concerning regeneration of the Mo=O group (Fig 1.21).

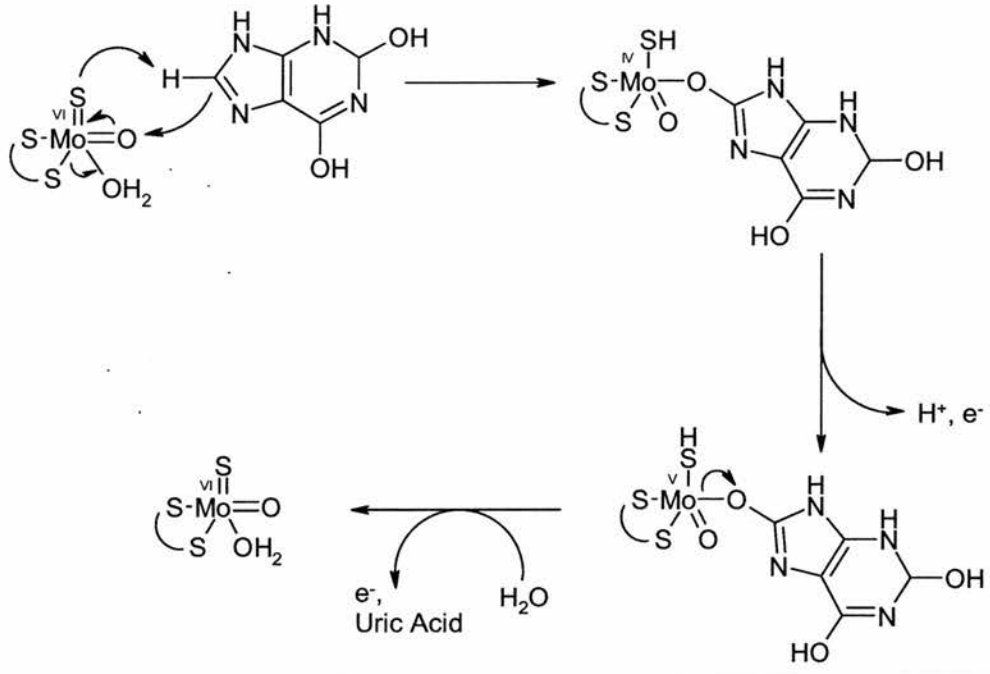

Figure1.20 Xanthine oxidase mechanism using the Mo=O as the catalytically labile oxygen. Requiring regeneration of the oxo group by deprotonation of a Mo bound water, and coordination of a new water from solvent to return the Mo to its resting state (MoVI) (Hille, 1996).

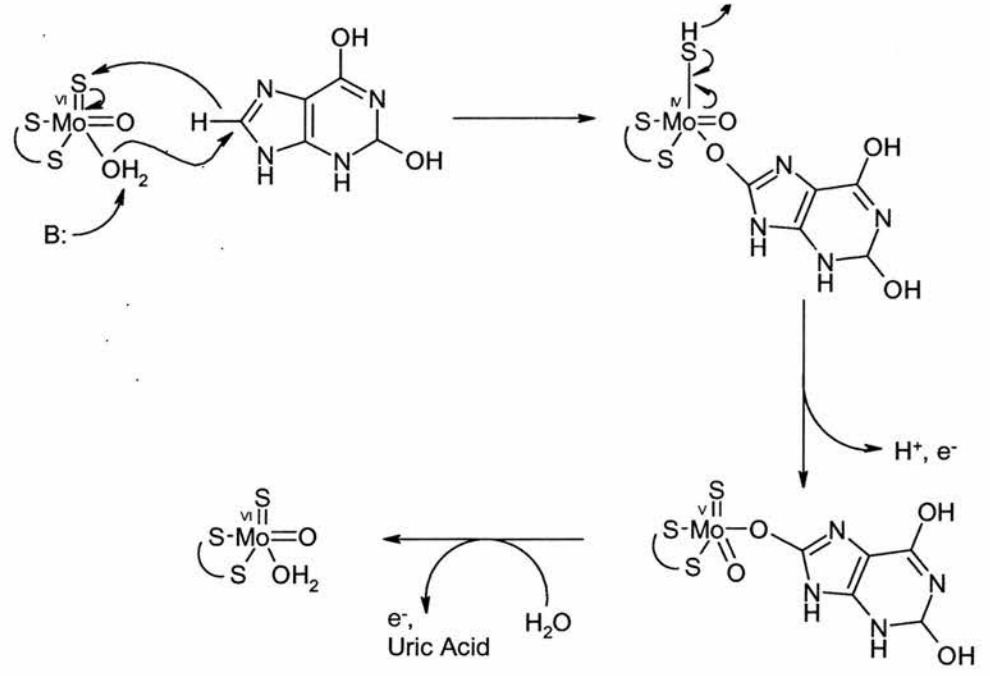

Figure 1.21 Xanthine oxidase mechanism based on that proposed for *D. Gigas* Aldehyde oxidoreductase (Hille, 1996; Huber *et al.*, 1996; Xia *et al.*, 1999).

The 1.8 Å structures of MOP containing a variety of ligands co-ordinated to the Mo, in particular a substrate analogue complex, allowed Huber and colleagues (Huber *et al.*, 1996) to differentiate between the two proposed mechanisms.

The likely substrate binding site was identified through the presence of an isopropanol molecule in the crystal structure, bound near the equatorial water ligand of the molybdenum. An aldehyde placed at this location would be adjacent to the water ligand, rather than the oxo or sulphido ligands. This supported the hypothesis that the water, not an oxo group, represents the oxygen species that attacks the carbonyl carbon of aldehyde substrates or the C8 carbon of purines.

They also propose that substrate access and product egress is via a ~ 15 Å channel formed by the interface of the two Mo binding domains of MOP. A similar channel is found in CODH, although in this case the channel is blocked by large hydrophobic residues, making it considerably narrower, reflecting the smaller size of the CODH substrate. The wider channel seen in MOP, and by extension likely in XOR, as well as the roomy binding pocket at the base of the tunnel containing the isopropanol molecule, explains the wide substrate specificity of both MOP and XOR.

The BMXOR structures from Enroth and co-workers (Enroth *et al.*, 2000) are not of high enough resolution to define the ligands to the molybdenum. However, they assign the =S, =O and -O ligands based on the high resolution

MOP structures described above. They crystallized XOR in the presence of 1 mM sodium salicylate, an XOR inhibitor, and visualised density for this in the active site. It does not bind directly at the molybdenum (6.5 Å distant) but they propose that it overlaps with the binding site for larger aromatics such as xanthine. Its interactions are summarised in the following figure (Fig 1.22).

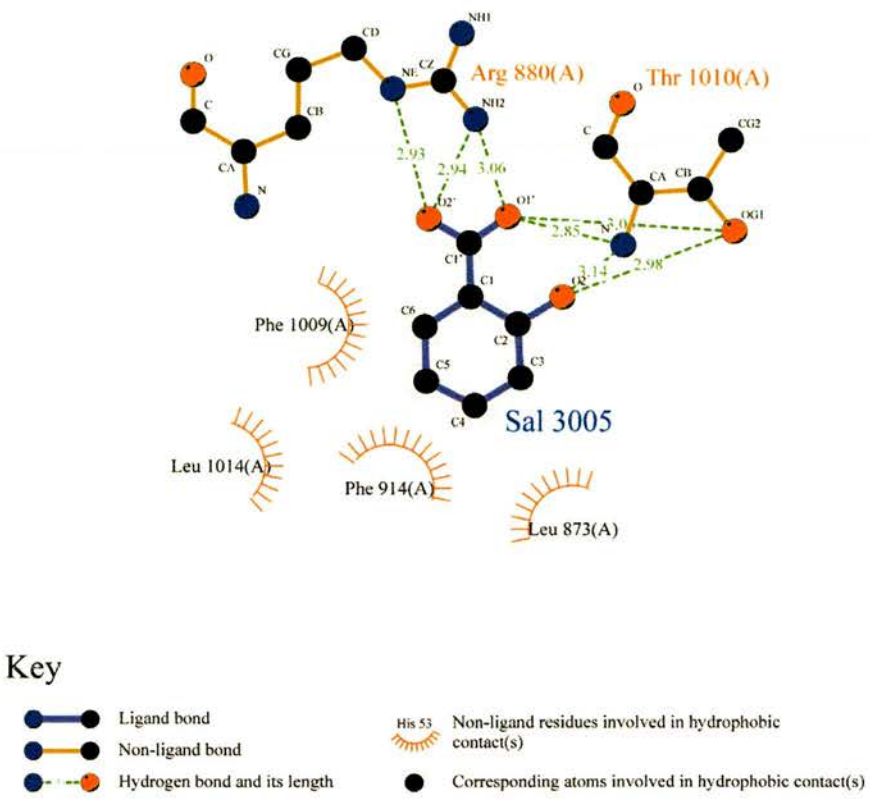

Figure 1.22: Summary of the interactions between bovine milk XDH and salicylic acid in the outer binding pocket of XDH. The image was generated using LIGPLOT (Wallace *et al.*, 1995).

1.5.2.2 Electron transfer between redox centres

The MOP structure also indicates a probable route for the transfer of electrons from the Mo to the iron sulphur centres. Although the distance between the Mo and the closest iron sulphur is about 15 Å, there is a direct interaction between the molybdopterin and FeS1 through a hydrogen bond formed between the N2 atom of the molybdopterin and the Sγ of the FeS ligand Cys139 (Cys150 in BMXOR). FeS1 is then further linked to FeS2 on the surface of the molecule through a series of covalent and hydrogen bonds linking Cys45 and Cys137, ligands to FeS2 and FeS1 respectively (Fig 1.23). In MOP the electrons are then transferred onto an external electron acceptor such as ferrodoxin, whereas in XOR they are further channelled onto the FAD.

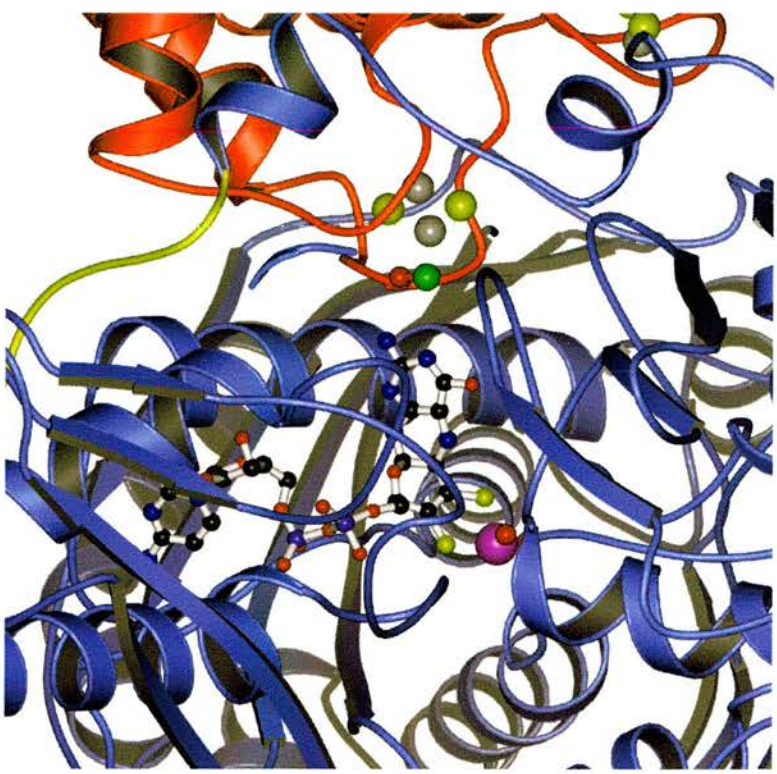

Figure 1.23:

View of the *D. Gigas* aldehyde oxidoreductase (MOP) illustrating the electron transfer pathway used to transfer electrons from the molybdenum to FeS1. The molybdenum (magenta) is complexed with the molybdopterin cofactor. The bridging cysteine (CYS 139) can be clearly seen between the molybdopterin and FeS1 (iron in grey, sulphur in yellow). The Cα trace is coloured as follows, red is the iron sulphur domain, yellow is the connecting peptide that joins the iron sulphur domain with the molybdenum domain (coloured blue).

The CODH structures indicate clearly that the FAD is well positioned to receive electrons from FeS2, the distance between C7 of the FAD and the closest iron atom is only 8.7 Å. However, no formal pathway for electron transfer has yet been described and, in the case of XOR, Enroth et al. (Enroth *et al.*, 2000) suggest tunnelling as the likely method, given the short distances involved (Fig 1.24).

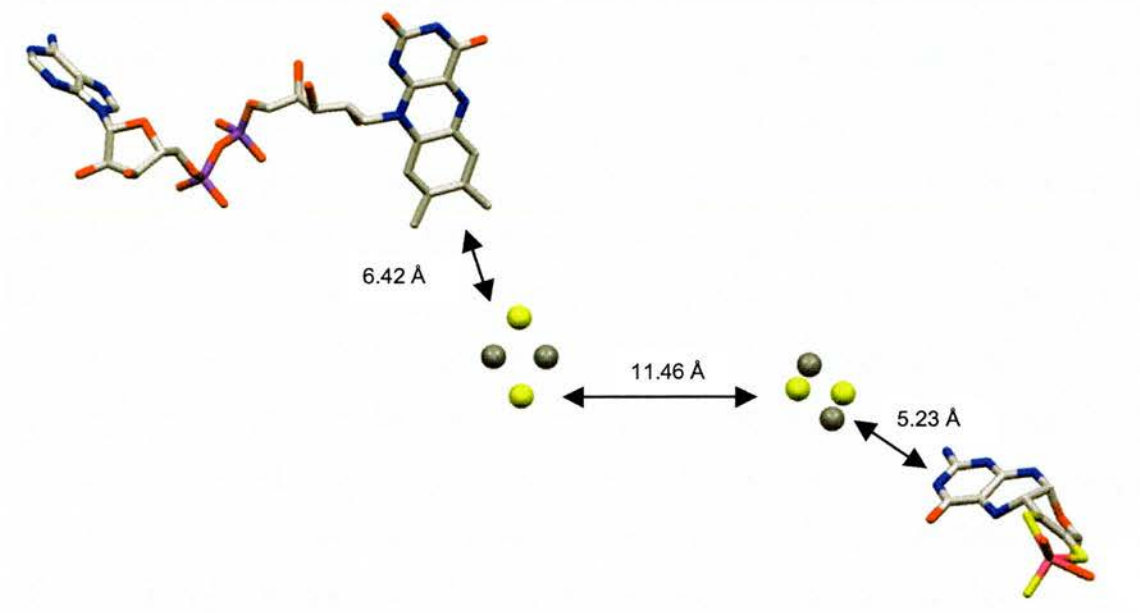

Figure 1.24: Alignment of the (from left to right) FAD, FeS2, FeS1, molybdopterin and molybdenum showing how close the four redox centres are. Distances are indicated in Å.

1.5.2.3 The FAD and its role in catalysis

The FAD is the site of electron egress from xanthine oxidoreductase and as such has been the focus of much spectroscopic and kinetic analysis. It is also the determinant of oxidising substrate specificity, possessing a binding site for NAD in the dehydrogenase form that is abolished in the oxidase form of the enzyme. However, until the solution of the crystal structure of CODH from *O.*

carboxidovorans (Dobbek *et al.*, 1999) no structural information was available, as the FAD domain showed no sequence homology to any known flavoproteins. In particular, it was clear that the FAD domain did not possess the classic Rossman fold associated with FAD binding.

Despite this, it was possible to define one of the residues responsible for forming the NAD binding site when it was shown that treatment of xanthine dehydrogenase with 5'-[*p*-(fluorosulphonyl)benzoyl]adenosine (FSBA) (an affinity labelling analogue of NAD^+ that reacts with tyrosine residues) resulted in covalent modification of a single tyrosine residue and abolition of NAD dehydrogenase activity (Nishino, 1989). Interestingly, as well as remaining reducible by xanthine, the labelled protein also retained unaffected oxidase activity. The modified tyrosine was identified as Tyr 419 in the chicken liver enzyme, and is conserved in all xanthine oxidases (Tyr 393 in bovine XOR), but not in aldehyde oxidases which lack dehydrogenase activity (Hille, 1996; Turner *et al.*, 1995) (Fig 1.25).

XDH	*H. sapiens*	383	VQMDHTFFPG**Y**RKTLLSPEEILLSIEIPYSRE	414
XDH	*F. catus*	381	VRMDHTFFPA**Y**RKTLLAPEEILLSIEIPYSRE	412
XDH	*R. norvegicus*	382	VRMDHTFFPG**Y**RKTLLRPEEILLSIEIPYSKE	413
XDH	*B. taurus*	383	VPMDHTFFPS**Y**RKTLLGPEEILLSIEIPYSRE	414
XDH	*G. gallus*	409	VMMDEKFFTG**Y**RKTIVKPEEVLLSVEIPYSKE	440
XDH	*D. melanogaster*	385	VHMGTGFFTG**Y**RRNVIEAHEVLLGIHFRKTTP	416
XDH	*A. thaliana*	415	IP-AKDFFLG**Y**RKVDMGSNEILLSVFLPWTRP	445
AO	*H. sapiens*	390	IPLNEQFLSK**C**PNADLKPQEILVSVNIPISRK	421

Figure 1.25 Alignment of several XDH sequences, as well as the sequence of human aldehyde oxidase for comparison, showing the Tyr residue that was labelled by 5'-*p*-FSBA, localising it to the NAD binding site. AO which lacks dehydrogenase activity, does not retain the conserved tyrosine. Alignments were created using Clustalx.

Evidence for further conformational change in the FAD domain came from studies of xanthine oxidoreductase in which the FAD was replaced by flavin derivatives. These results suggested that the dehydrogenase form of the enzyme possesses a strong negative charge in the vicinity of the flavin N1/C2=O which was absent in the dehydrogenase (Massey *et al.*, 1989).

The CODH structure from *O. carboxidovorans* revealed that its FAD domain, and by extension that of xanthine oxidase; a fact confirmed by the bovine milk XOR structure, is part of an emerging structural family of FAD binding proteins that share considerable structural homology but have a very low sequence identity. Two other members of the family have been structurally characterised, Vannillyl-alcohol oxidase (VAO) (Fraaije *et al.*, 1998), from which the family takes its name, and UDP-N-acetylenolpyruvylglucosamine reductase (MurB) (Benson *et al.*, 1996). Several putative members of this family, identified by the presence of two FAD binding motifs that appear to be conserved, possess a covalently bound flavin, although this does not seem to be the case for the xanthine oxidase family.

Study of the bovine milk XOR structure shows that the FAD isoalloxazine ring is accessible to solvent from two angles. There is a deep cleft on one side of the protein at the base of which lies the FAD. Substrates entering here would bind FAD, stacked against the *Si* face of the isoalloxazine ring. On the other side of the molecule, the edge and part of the *Re* face of the isoalloxazine ring are visible in a space-filling model, although access is limited. Sterically this would suggest that it is likely that, in the dehydrogenase form, NAD is binding in the deep cleft on the *Si* face of the FAD; and, in the oxidase form that molecular oxygen binds at the less accessible *Re* face. This assignment of

binding sites would also be consistent with the NADH oxidase activity of XOR in which electrons are passed from NADH via FAD to molecular oxygen, allowing both substrates to bind on opposite sides of the isoalloxazine ring.

The bovine milk XOR FAD domain, as stated above, also possesses a VAO type fold. The tyrosine (Tyr393) identified by labelling experiments can be seen to be positioned at the tip of a loop at the entrance to the probable NAD binding cleft and it is easy to imagine how attachment of a bulky derivative group could block NAD binding (Fig 1.26).

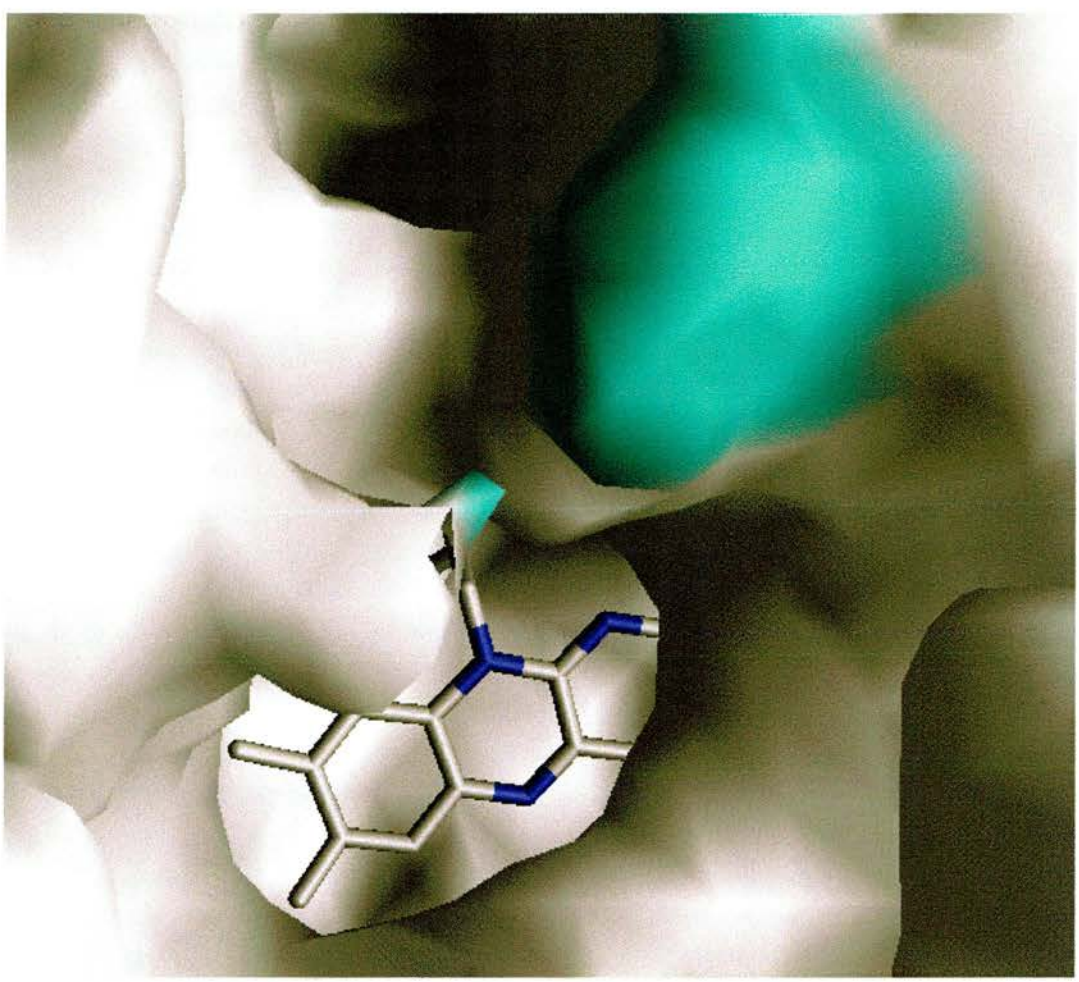

Figure 1.26: View of the FAD and NAD binding cleft in bovine milk XDH. TYR 393 is labelled in cyan, and can be seen to project over the entrance to the FAD site. Image generated using GRASP.

1.5.3 Irreversible dehydrogenase to oxidase conversion

XOR exists in two forms, dehydrogenase (XDH) and oxidase (XO), that differ in their choice of oxidising substrate; XDH utilising NAD and XO molecular oxygen. The two forms are interconvertible by manipulation of the oxidation state of various thiols in the enzyme. However, XDH can be irreversibly converted to XO by limited proteolysis of the enzyme. The two recent structures of the bovine milk xanthine XDH and XO (Enroth *et al.*, 2000) have provided some indication of the structural rearrangement that occurs on proteolysis of the enzyme to produce conversion to the oxidase form.

The most obvious difference between the two structures is the lack of several stretches of residues in the XO density, most probably caused by excision of these residues during proteolysis. However, there is a further large change in the FAD domain, as expected from biochemical studies. The result of the conversion is a drastic rearrangement of a highly charged loop (Gln423 - Lys433) on the *Si* side of the isoalloxazine flavin ring. This rearrangement, in which certain resides move by as much as 20 Å from their position in XDH has two effects on the putative NAD binding site. First, Asp429 that was in close contact with the FAD C6 is replaced by Arg426, producing a large change in the electrostatic environment of the flavin, as seen in the studies with 6- and 8- mercapto flavin probes. Secondly, the new position of the shifted loop now causes it to block access to the putative NAD binding cleft (Fig 1.27). On the *Re* side of the FAD where it is expected that molecular oxygen might bind, no such gross structural rearrangements are seen.

Interestingly, none of the cuts in the polypeptide chain, or indeed the amino acids implicated in causing the XDH/XO conversion by biochemical data, are in the vicinity of the putative NAD binding cleft. Rather, they are positioned on the opposite side of the FAD domain, at least 18 Å from the cofactor. This makes a direct influence on the residues surrounding the FAD/NAD binding site improbable. Enroth and colleagues do, however, suggest one candidate for triggering the large rearrangement of loop 423-433. Phe549, positioned in one of the loops missing in the XO structure (529-570), seems to form a close interaction with Arg427 (part of the shifted loop) in the XDH structure (Enroth *et al.*, 2000). Removal of this interaction, by proteolysis and loss of the 529-570 loop, is postulated to trigger the shift of the 426-ASP-ARG-GLU-ASP-ASP-ILE-ALA-LYS-433 loop that blocks the NAD binding site.

Figure 1.27: Surface representations of the electrostatic environment of the NAD binding cleft in bovine milk XOR. The FAD is shown as capped cylinders. The molecular surface is coloured by charge; blue for electropositive areas and red for electronegative areas. On the left is the environment seen in the dehydrogenase form, on the right is more occluded NAD binding site observed in the oxidase form of XOR. Images generated using GRASP.

1.5.4 Inactive forms of XOR

Evidence for the existence of inactive forms of XOR was first obtained by Lowry and colleagues (Lowry *et al.*, 1949) through titration experiments using a high-affinity molybdenum site binding inhibitor, 2-amino-4-hydroxy-6-formylpteridine. These workers showed that only 60% of the FAD present in their pure enzyme sample was associated with active enzyme. Subsequent studies established that two inactive forms of XOR are present *in vivo*, desulpho- and demolybdo-XOR.

1.5.4.1 Desulpho-XOR

As described in Section 1.2.3, a sulphido ligand to the molybdenum is absolutely required for catalytic activity. Inhibitor and titration studies such as that of Lowry *et al.* established that the desulpho form of XOR constitutes a considerable proportion of purified enzyme. Initially, the desulpho enzyme was assumed to be an artefact of purification procedures or storage of the enzyme (Bray, 1975). However, in 1986 Ikegami and Nishino showed that both crude and purified XOR preparations from rat liver contained ~40% desulpho enzyme, establishing desulpho-XOR as a naturally occurring form of the enzyme (Ikegami and Nishino, 1986).

The high resolution structure of MOP (Huber *et al.*, 1996), in both sulpho and desulpho forms, shows that the exchange of the sulphido ligand for an oxo group does not cause any distortion in the molybdenum active site.

Desulpho-XOR can be easily reconverted to active XOR by treatment with sulphide, leading to suggestions that *in vivo* resulphuration could be a mechanism for regulation of XOR activity.

1.5.4.2 Demolybdo-XOR

Analysis of molybdenum content in various preparations (Avis *et al.*, 1956a; Gardlik *et al.*, 1987; Hart *et al.*, 1970; Ikegami and Nishino, 1986) has shown the presence of demolybdo-XOR. Hart *et al.* (1970) estimated that as much as 40% of bovine milk XOR is present in a demolybdo form. An affinity purification method, based on the competitive XOR inhibitor folate (Nishino and Tsushima, 1981) which only binds intact molybdenum sites, allowed Ventom and co-workers (Ventom *et al.*, 1988) to isolate demolybdo-XOR from bovine milk. This demonstrated that, as well as lacking molybdenum, to some extent the preparation also lacked molybdopterin. These workers postulated that a related pterin-like molecule, possibly a degradation product of molybdopterin or an incompletely synthesised pterin, was present in the active site in demolybdo-XOR.

It has been observed using EPR (Bray *et al.*, 1999; Gardlik *et al.*, 1987; Godber, 1998) that demolybdo-XOR also appears to have a distorted or altered FeS1. As stated in Section 1.4.2.2, there is a direct interaction between the molybdopterin and one of the cysteine ligands to FeS1. It is therefore possible that loss or alteration of the molybdopterin affects the FeS1 centre as well.

The recent structure of demolybdo-CODH from *H. pseudoflava*, grown in the absence of molybdenum, shows that molybdenum deficiency affects only the molybdenum site of the protein, with no effect on the overall fold. Interestingly, in view of the suggestion by Ventom and co-workers (Ventom *et al.*, 1988) that an incompletely synthesised pterin molecule could be inserted in the demolybdo form, the demolybdo-CODH does contain the 5'-cytidine diphosphate section of the molybdopterin-MCD cofactor found in *H. pseudoflava,* but is lacking the Mo-pyranopterin moiety.

1.6 Human xanthine oxidoreductase

Largely due to the abundance and ease of preparation of XOR from bovine milk, the human enzyme was not well studied until recently. The implicit assumption made was that the behaviour of the bovine system could be extrapolated to the human. Despite the implication of defects in xanthine oxidase activity in the hereditary metabolic disorder xanthinuria, the human enzyme was not of great interest until the publication of work by Granger and co-workers (Granger *et al.*, 1981) citing xanthine oxidase activity as a source of damaging reactive oxygen species (ROS) during ischaemia reperfusion injury (IRI).

1.6.1 Properties of human XOR

Since 1981, XOR has been purified from several human tissues. Although levels of XOR activity were reported to be very low in most tissues studied, Krenitsky and co-workers (Krenitsky *et al.*, 1986) affinity purified XOR from human liver and were able to show that it had a specific activity very similar to that of the bovine enzyme. Small intestine also showed high levels of XOR activity, although no pure XOR has yet been prepared from this tissue (Sarnesto *et al.*, 1996). Abadeh and co-workers (Abadeh *et al.*, 1992) purified XOR from human breast milk (HMXOR) and showed that, despite physical properties very similar to those of the bovine milk enzyme (UV/Visible Spectra, M_w, A_{280}:A_{450}), its activity towards most reducing substrates was very low. In the case of xanthine, HMXOR activity was only 2-3% of that of the

bovine enzyme. Godber and colleagues (Bray *et al.*, 1999; Godber *et al.*, 1997) demonstrated that this lack of activity was due to the presence in HMXOR of large amounts of both the demolybdo and desulpho forms of the enzyme. Molybdo-XOR constitutes only 2-5% of total XOR in human milk and, of that molybdenum containing XOR, 30-40% is in the inactive desulpho form. Hence, only ~ 1% of HMXOR is fully active towards xanthine. This pattern of low activity is also seen in other tissues. Immunoaffinity purification of XOR from human heart demonstrated a protein with very similar specific activity to HMXOR (Abadeh *et al.*, 1993). It has been suggested (Harrison, 1997) that tissue specific isoforms of XOR might exist, giving high activity XOR in liver and small intestine, and low activity enzyme, like that of breast milk and heart, in the rest. It is also suggested that this low activity enzyme might be subject to some form of post-translation activation, such as resulphuration, as a method of XOR activity regulation.

1.6.2 The NADH oxidase activity of human milk XOR

XOR also possesses NADH oxidase activity with NADH acting as a reducing substrate at FAD, leading to the production of superoxide. As expected, NADH oxidase activity is unaffected by the lack of molybdenum (Sanders *et al.*, 1997), and the NADH oxidase activity of HMXOR was found to be equivalent to that of the bovine milk enzyme. NADH oxidase activity is higher in the dehydrogenase form of the enzyme. This is probably due to the reduced accessibility of the NAD(H) binding site seen in the oxidase form of the enzyme (Enroth *et al.*, 2000).

1.6.3 The role of XOR in ischaemia reperfusion injury (IRI)

Tissue localisation studies suggest that the dehydrogenase form of XOR is the predominant form *in vivo*. Since it is known that proteolysis converts the dehydrogenase to oxidase, McCord *et al.* (McCord and Roy, 1982) suggested the following scheme for XOR-mediated production of ROS during IRI (Fig 1.28). During an ischaemic event, the cells' energy charge falls, disrupting ion gradients across cell membranes, leading to an increase in cellular Ca^{2+} which activates Ca^{2+}-dependent proteases that convert XDH into XO. At the same time, hypoxanthine accumulates as cellular ATP is depleted, producing AMP which is catabolised to hypoxanthine. On reperfusion of the tissue, the accumulated hypoxanthine serves as a substrate for XO, generating superoxide, hydrogen peroxide and other ROS.

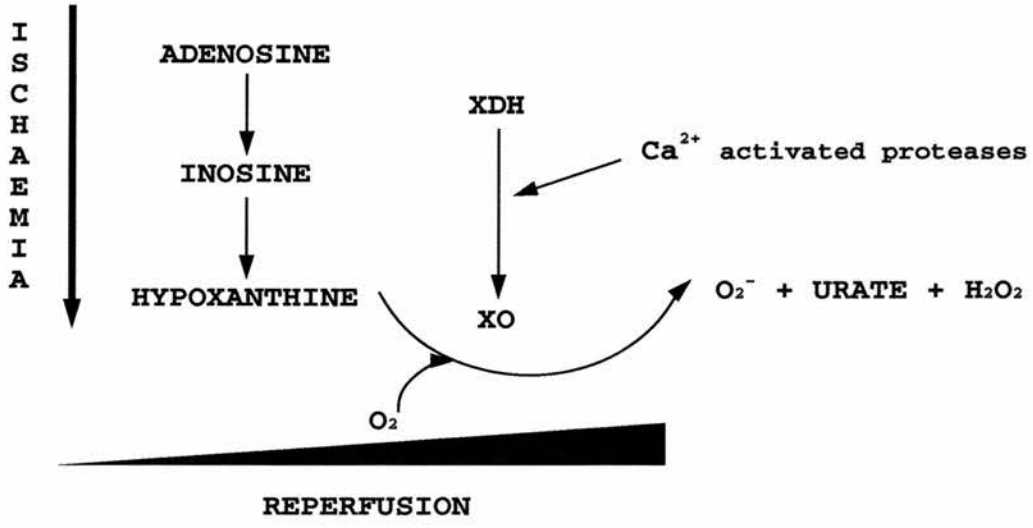

Figure 1.28: Schematic representation of the proteolytic theory of XOR involvement in ischaemia reperfusion injury (McCord and Roy, 1982).

The observations by Harrison and co-workers (Harrison, 1997) that human XOR has a very low specific activity towards xanthine, complicates the above

scheme somewhat. Both brain and heart, tissues severely damaged by IRI during stroke and heart attack, show low xanthine specific activity. This has led Harrison and co-workers to propose an alternative scheme for the role of XOR in IRI (Fig 1.29) in which the build up of NADH during an ischaemic event provides the source of reducing substrate for XOR, through its NADH oxidase activity. This scheme has the advantage of not requiring a XDH to XO conversion, the time scale and extent of which remains controversial.

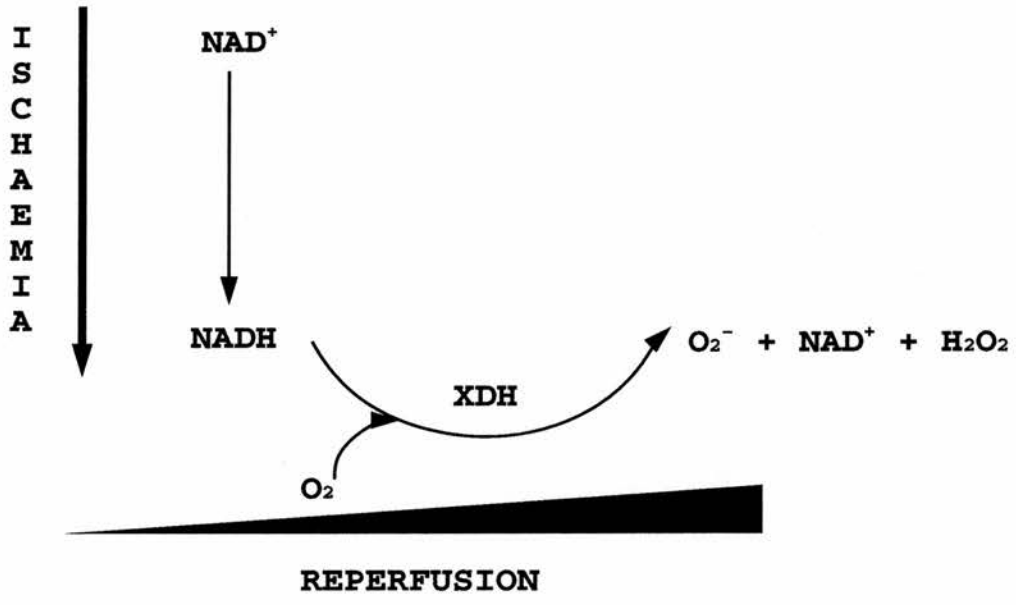

Figure 1.29: Schematic representation of the alternative theory of XOR involvement in ischaemia reperfusion injury, which proposes the NADH oxidase activity of XDH as a source of reactive oxygen species (Harrison, 1997).

1.6.4 Other roles of human xanthine oxidoreductase

In addition to its well established role in purine catabolism and its proposed involvement in IRI, many other functions for XOR have been suggested. Its ability to produce ROS has to lead to proposals that it may be involved in signal transduction in the cell. This is supported by recent work (Doel *et al.*, 2000; Godber *et al.*, 2000b) showing that XOR is able to catalyse the reduction of nitrates and nitrates to NO, a well established signalling molecule. This, coupled with the observation that XOR is heavily localised the endothelial cells of capillary walls (Jarasch *et al.*, 1986) implicates XOR in vasodilation in particular.

Other suggested physiological functions for XOR in healthy humans include a role in iron absorption from the gut (Topham *et al.*, 1989; Topham *et al.*, 1982a; Topham *et al.*, 1982b) and a proposal that it may act as an antimicrobial system in milk (Godber *et al.*, 2000a; Godber *et al.*, 2000b; Stevens *et al.*, 2000). Given its broad substrate specificity and high activity in liver, Krenitsky has also suggested that it has a general role in detoxification of N-heterocycles (Krenitsky, 1978).

Interestingly, XOR also appears to trigger a benign autoimmune response in humans that has been linked to otherwise undetectable myocardial infarction (MI) events (Benboubetra *et al.*, 1997; Harrison *et al.*, 1990). Harrison *et al.* (Harrison *et al.*, 1990) proposed that in the course of chronic minor lesions leading up to such an event, XOR leaks from the endothelial cells into the circulation. This could initiate an immune response and circulating anti-XOR would then act in a prophylactic way, clearing leaked XOR from the circulation

to prevent indiscriminate production of ROS. They also proposed the monitoring of levels of anti-XOR in serum in order to determine whether such minor events were occurring.

Chapter 2

Purification, Crystallization and Characterisation of Human and Bovine Milk Xanthine Oxidoreductase

2.1 Introduction: Outline of the purification of XOR

This chapter will discuss the purification of XOR from bovine and human milk, the crystallization of both enzymes and some methods under development for the characterization of the crystallized XOR species.

A purification procedure for both the human and bovine XOR was developed from that proposed by Nakamura & Yamazaki (1982) by Abadeh *et al.*, (1992), using a high ionic strength buffer to dissociate XOR from cream, followed by ammonium sulphate precipitation and calcium phosphate chromatography. Sanders *et al.* (1997) further modified the purification, replacing calcium phosphate chromatography with a heparin affinity column as Adachi *et al.* (1993) had demonstrated that XOR has a high affinity for heparin.

This procedure (Fig 2.1) is capable of producing high yields of relatively pure and unproteolysed XOR from both human and bovine milk. XOR is dissociated from the milk fat globule membranes (MFGM) of cream, by stirring in high ionic strength buffer. An ammonium sulphate cut then removes the majority of contaminating proteins and the addition of butanol solubilises membrane fragments. Heparin affinity chromatography yields relatively pure enzyme. Anion exchange column chromatography can be used as a final polishing step if enzyme of especial purity is required. Godber (1998) modified this protocol somewhat in order to increase the yield. This procedure is described in this chapter.

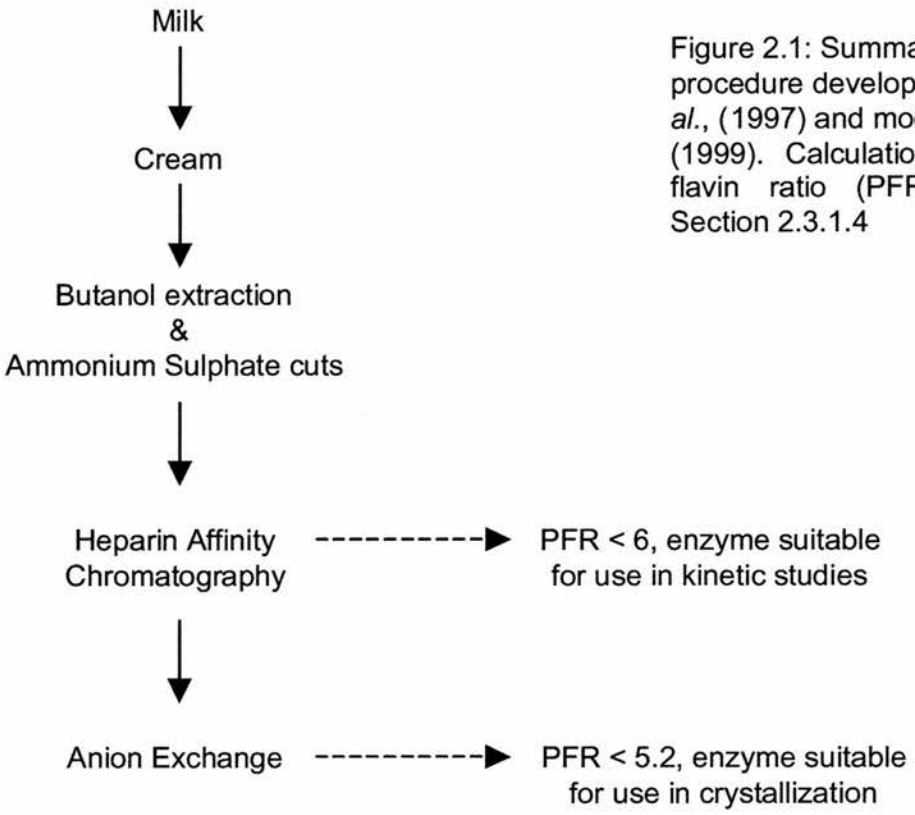

Figure 2.1: Summary of the purification procedure developed by Sanders *et al.*, (1997) and modified by Godber (1999). Calculation of the protein to flavin ratio (PFR) is described in Section 2.3.1.4

The above protocol is unable to differentiate between the various isoforms of XOR (dehydrogenase and oxidase, demolybo, desulpho, molybdo). Nishino and Tsushima (1981) described a further purification step that was able to separate demolybdo from desulpho and sulpho XOR using the substrate analogue folate (Fig 2.2). Only XOR possessing an intact molybdenum centre is able to bind folate and they were able to show a considerable enrichment of molybdenum-containing enzyme.

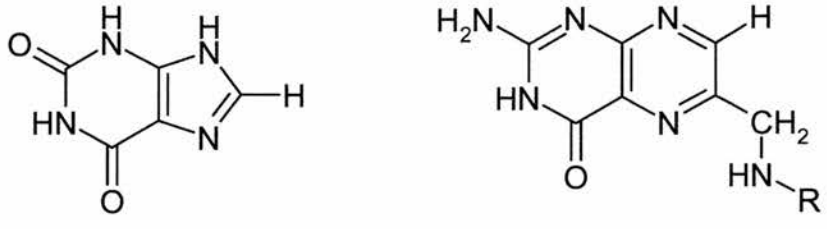

Figure 2.2: Structures of xanthine (left) and its analogue folate (right) used as an affinity ligand to purify molybdo-XOR.

2.2.1 Materials

DTT was obtained from Alexis Corporation. Molecular weight markers for SDS PAGE were obtained from BioRad. AH-sepharose was obtained from Amersham-Pharmacia. The Superdex 200 and HiTrap Mono-Q columns were also obtained from Amersham-Pharmacia.

Silanised coverslips, microbatch plates, Crystal Screens, crystal harvesting tools and paraffin oil were all obtained from Hampton Research, USA. Linbro plates were obtained from ICN.

All other reagents were obtained from Sigma-Aldrich.

2.2.2 Instruments

Formation of urate (during the spectrophotmetric assay) and XOR spectra were recorded using either a Cecil Series 6000 Double Beam Spectrophotometer or a Shimadzu UV-2101PC UV-Vis Scanning Spectrophotometer.

A Perkin-Elmer LS-5B Luminescence Spectrometer was used for the Fluorimetric assay.

IEF gel electrophoresis was carried out using the Pharmacia Phastgel system, Amersham-Pharmacia. IEF gels and markers were obtained from the same source.

Gel filtration was carried out using the Econo low pressure system, BioRad.

Anion exchange was carried out using a BioCad Sprint Perfusion Chromatography system, PerSeptive Biosystems.

X-ray SEM was carried out using a JEOL 8600 Electron-probe Microanalyser. Crystal Spectra were measured using the XSPECTRA Single Crystal Microspectrophotometer manufactured by 4DX, Sweden.

2.3 Methods

2.3.1 General Methods

2.3.1.1 Spectrophotometric XOR activity assay

XOR activity was determined by monitoring the rate of formation of urate from xanthine at 295 nm. Enzyme was added to assay buffer (50 mM Bicine, pH 8.3) to a final volume of 980 µl. 10 mM xanthine (10 µl) was added (final concentration 100 µM) and A_{295} monitored to give oxidase activity. 50 mM NAD^+ (10 µl) was then added (final concentration 500 µM) and A_{295} again monitored to give total (dehydrogenase + oxidase) XOR activity. The reaction was stopped by the addition of 1 mM allopurinol (50 µl) a specific XOR inhibitor.

2.3.1.2 Fluorimetric XOR activity assay

The fluorimetric assay (Beckman *et al.*, 1989; Page *et al.*, 1998) utilises the oxidation of pterin to its fluorescent derivative, isoxanthopterin. This oxidation occurs at the molybdenum site of XOR by the same mechanism used to oxidise xanthine. It is considerably more sensitive than the urate assay described above.

Briefly, enzyme was added to assay buffer (50 mM potassium phosphate, pH 7.4, 0.1 M EDTA) to a total volume of 980 µl. The fluorimeter (Perkin-Elmer LS-5B Luminescence Spectrometer) was set to an excitation wavelength of

345 nm and an emission wavelength of 390 nm with a slit width of 5 nm. After a stable baseline was obtained, 1 mM pterin (10 μl) was added (final concentration 10 μM) and fluorescence monitored to give oxidase activity. 10 mM methylene blue (10 μl) was added (final concentration 10 μM) and fluorescence monitored to give total XOR activity (dehydrogenase + oxidase). To ensure that all observed fluorescence was due to XOR activity, 1 mM allopurinol (50 μl) (a specific XOR inhibitor) was added to stop the reaction. The increase in fluorescence was calibrated by the addition of known concentrations of isoxanthopterin as an internal standard.

2.3.1.3 SDS-PAGE

SDS-PAGE was carried out essentially as described by Laemelli (Laemmli, 1970). 10 ml gels were prepared using the protocol in Table 2.1 and the gels were run in a 1/10 dilution of Tank buffer (0.025 M Tris, 0.1 % w/v SDS, ~1.9 M glycine. Samples were prepared for electrophoresis by boiling in a 1:1 ratio with Sample buffer (0.625 M Tris, 2 % SDS, 5 % 2-mercaptoethanol, 10 % sucrose, 0.02 % bromophenol blue). Gels were run at 20 mA until the dye front had reached the bottom of the gel. Broad range molecular weight markers (BioRad) were used. Protein was visualised using Coomassie blue stain (0.1 % Coomassie Blue R-250, in water:methanol:glacial acetic acid 5:5:2 by volume). Gels were destained in 30 % methanol, 10 % acetic acid.

Stacking gel		Resolving gel	
1756 µl	H_2O	1676 µl	H_2O
418 µl	30% bis-acrylamide	3000 µl	30% bis-acrylamide
312 µl	1 M Tris, pH 6.8	2800 µl	1 M Tris, pH 8.8
25 µl	10 % SDS	75 µl	10 % SDS
13 µl	10 % ammonium persulphate	32 µl	10 % ammonium persulphate
6 µl	TEMED	8 µl	TEMED

Table 2.1: Recipes for a 10 ml SDS-PAGE gel.

2.3.1.4 Spectral determination of XOR purity and concentration

As XOR contains several coloured prosthetic groups (Fe, FAD, Mo), it has a distinctive spectrum (Fig 2.3) which can be used to determine purity and protein concentration.

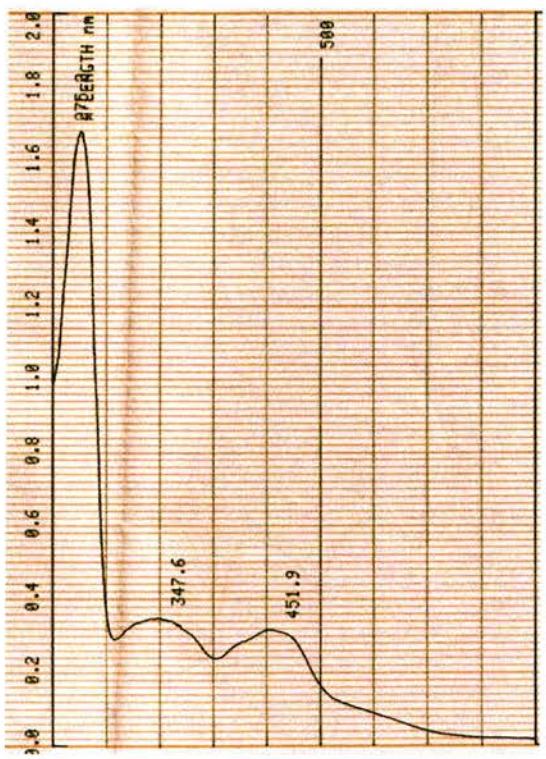

Figure 2.3 : Spectrum of human milk XOR, scanned from 220 nm to 700 nm, showing the characteristic three peaks at 280 nm (protein), 350 and 450 nm (FAD, 2Fe2S & Mo-MPT). Spectrum was scanned using a Cecil Series 6000 Double Beam Spectrophotometer.

The commonly used measure of purity is the protein to flavin (PFR) ratio. This is based on calculations by Avis *et al.* (1955) showing that in a totally pure preparation of XOR, containing a full complement of all cofactors, the ratio of protein (absorbance at 280 nm) to flavin (absorbance at 450 nm) should be 5. Preparations with PFR = 5-5.5 may be regarded as reasonably pure, those with PFR > 6 are very impure.

Protein concentration can be calculated from the absorbance measured at 450 nm using a molar extinction coefficient of 36000 $M^{-1}cm^{-1}$ as calculated by Bray (1975).

2.3.2 Purification of bovine milk XOR

2.3.2.1 Crude extraction & heparin affinity chromatography

This method is essentially that described by Sanders *et al.* (1997).

Bovine milk was obtained from a local dairy herd in Claverton, Bath and was used immediately. EDTA was added to the milk (typical volume 4 L) to a final concentration of 1 mM. The milk was then centrifuged at 3000 x g for 30 min at 4 °C. The cream was collected and resuspended in a 1:1 volume of 0.2 M K_2HPO_4, 1 mM EDTA by stirring for 2 h at 4 °C. The resulting suspension was centrifuged at 3000 x g for 30 min. The subnatant was collected and filtered through glass wool after which, whilst stirring at 4 °C, 15 % v/v ice-cold butanol was added dropwise followed by the slow addition of 15 % w/v finely ground ammonium sulphate. The mixture was then stirred for a further hour at 4 °C after which it was centrifuged at 10,000 x g for 30 min at 4 °C. The supernatant was collected and again filtered through glass wool. Whilst stirring at 4 °C, a further 20 % w/v finely ground ammonium sulphate was added slowly. The mixture was then stirred for 45 min at 4 °C, after which it was centrifuged at 10,000 g for 30 min at 4 °C. The resulting brown precipitate was collected and resuspended in a 1:1 volume of 20 mM MES, pH 6.5 and dialysed overnight at 4 °C against 3 L of the same buffer. Any remaining precipitate was removed by centrifugation at 27,000 x g for 1 h at 4 °C, followed by filtration through a 0.22 μm filter.

The heparin column was prepared by packing heparin (immobilised on cyanogen bromide activated 4 % cross-linked agarose in 20 mM MES, pH 6.5) into a small column (1 cm x 6 cm) under gravity. The column was then washed in 20 mM MES, pH 6.5, containing 1 M NaCl before being equilibrated in 20 mM MES, pH 6.5, ready for use. Heparin affinity chromatography was carried out at 4 °C.

The crude XOR solution was loaded onto the column in 20 mM MES, pH 6.5, under gravity and the XOR observed to bind strongly, colouring the column brown. Crude XOR solution was loaded until approximately half the column was coloured deep brown. The column was then washed with approximately 50 ml 20 mM MES, pH 6.5, containing 0.03 M NaCl (10 column volumes). XOR was eluted with 20 mM MES, pH 6.5, containing 0.4 M NaCl, and all the brown coloured eluate was collected. The column was then cleaned with 10 column volumes of 20 mM MES, pH 6.5, containing 1 M NaCl and stored in the same buffer at 4 °C.

If necessary (PFR > 6.5), the heparin affinity step was repeated, washing with 20 mM MES, pH 6.5, containing 0.08 M NaCl, and eluting in 0.25 M NaCl, 20 mM MES, pH 6.5.

2.3.2.2 Folate affinity chromatography

The column preparation is a modification of the method described by Nishino and Tsushima (1981). The procedure was modified in order to improve the coupling of folate to the column matrix, both folate and the coupling reagent EDC were added in excess and the coupling time was increased from 2 h to overnight. The column chromatography is as described by Ventom *et al.* (1988).

3 g AH-Sepharose was swollen in 0.5 M NaCl (400 ml), according to the manufacturers instructions. 52.5 mg of folate were dissolved in 18 ml of coupling solution (50 % v/v DMF, pH 5.8). The folate/coupling solution mixture was then added to the swollen gel and the pH checked. EDC (150 mg) was then added and reaction mixture left stirring gently overnight at room temperature in the dark. The coupled gel was then washed on a sintered glass funnel with 50 % DMF (60 ml) , pH 7, followed by 0.01 M NaOH (150 ml), then with 0.1 M Tris, pH 7, (150 ml) and finally with distilled water (300 ml). The folate-gel was then packed under gravity in water into a small column (1 cm x 6 cm) and washed with water until no further yellow colour eluted from the column. The column was seen to be a bright yellow and was then stored in water at 4 ^{o}C in the dark to avoid degradation of the folate.

Column chromatography was carried out at 4 ^{o}C. The following buffer mixtures were used in the column chromatography:

Buffer A 20 % 0.1 M sodium pyrophosphate, 0.2 mM EDTA, pH 8.5

80 % 0.05 M Tris-HCl, 0.2 mM EDTA, pH 7.8

Buffer B 30 % 0.1 M sodium pyrophosphate, 0.2 mM EDTA, pH 8.5

70 % 0.05 M Tris-HCl, 0.2 mM EDTA, pH 7.8

Post-heparin XOR was transferred into Buffer A using a PD10 column. The folate column was equilibrated with Buffer A (48 ml). XOR was then loaded onto the column and washed with Buffer B (48 ml) to remove demolybdo-XOR. Molybdo- and desulpho- XOR were then eluted with Buffer B (24 ml) containing 5 mM hypoxanthine. The column was then washed with of 0.1 M sodium pyrophosphate, 0.2 mM EDTA, pH 8.5 (36 ml).

XOR elution was monitored at 280 nm and fractions (1 ml) were collected. Fractions showing absorbance at 280 nm were assayed for absorbance at 450 nm and fractions with a PFR $\leq$ 5 were pooled.

2.3.2.3 Iso-electric point determination.

The Pharmacia Phastgel gel system and precast broad range (pH 3-9) IEF gels were used according to the manufacturer's instructions. Broad range IEF markers (Amersham-Pharmacia) and BMXO were loaded onto the gel and the following Phastgel programme was run:

SEP 1.1	2000 V	2.5 mA	3.5 W	15 °C	75 Vh	Formation of pH gradient
SEP 1.2	200 V	2.5 mA	3.5 W	15 °C	15 Vh	Sample loading
SEP 1.3	2000 V	2.5 mA	3.5 W	15 °C	410 Vh	Migration period

Proteins were visualised in the Phastgel developer unit, using the Fast Coomassie stain as described in the Phastgel manual. The following Phastgel developer programme was run:

Step	Solution	Time	Temperature
1	Fix	5 min	20 °C
2	Wash	2 min	20 °C
3	Stain	10 min	50 °C
4	Destain	10 min	50 °C

The Buffers used were as follows:

Fix	20 % w/v Trichloracetic acid
Wash/Destain	30 % v/v Methanol, 10 % v/v Acetic acid
Stain	0.02 % w/v Coomassie Blue, 0.1 % w/v $CuSO_4$, 30 % v/v Methanol, 10 % v/v Acetic acid

2.3.2.4 Gel filtration

Gel filtration was carried out on a Superdex -200 column, in 20 mM KH2PO4, pH 7.5.The column was calibrated using Blue Dextran (2000 kDa), Apoferritin (443 kDa), Alcohol dehydrogenase (150 kDa), Carbonic anhydrase (29 kDa), Lysozyme (14.3 kDa) and DNP-lysine (0.367 kDa). Post-folate BMXO was applied to the column and the elution of protein monitored at 280 nm. 1 ml fractions were collected, and those containing protein assayed for absorbance at 450 nm.

2.3.2.5 Anion exchange

Anion exchange was carried out using a 5 ml Mono-Q HiTrap column (Amersham-Pharmacia) on a BioCAD Sprint Perfusion Chromatography System (PerSeptive Biosystems). The column was run at a flow rate of 1 ml/min and was equilibrated in 50 mM Bicine, pH 8.3 containing 10 mM DTT. During a column run, pH, conductivity, pressure, A_{280} and A_{450} nm were monitored.

Post-heparin XOR was dialysed overnight against 3 L of 50 mM Bicine, pH 8.3 containing 10 mM DTT, and then loaded onto the MonoQ column in 5 ml batches until a noticeable brown colour was seen on the column. The column was then washed with 50 mM Bicine, pH 8.3 containing 10 mM DTT, until the baseline A_{280} was regained. XOR was eluted with a gradient of 0 $\rightarrow$ 0.5 M NaCl and 1 ml fractions were collected. Those fractions having a PFR $\leq$ 5.2

were pooled. The column was then washed with 50 mM Bicine, pH 8.3, 10 mM DTT, 1M NaCl and stored in the same buffer.

2.3.3 Purification of human milk XOR

2.3.3.1 Crude extraction & heparin affinity chromatography

This method is essentially that described by Sanders *et al.* (1997).

Frozen human milk was kindly donated by mothers in the Special Care Baby Units of the Royal United Hospitals, Bath; Southmead Hospital, Bristol; Bristol Royal Infirmary and Princess Margaret Hospital, Swindon. After thawing slowly, the milk was centrifuged at 3000 x g for 30 min at 4 °C. The cream was collected and resuspended in a 1:1 volume of 0.2 M K_2HPO_4, 1 mM EDTA, 10 mM DTT by stirring for 2 h at 4 °C. The resulting suspension was centrifuged at 3000 x g for 30 min. The subnatant was collected and filtered through glass wool after which, whilst stirring at 4 °C, 15 % v/v ice-cold butanol was added dropwise followed by the slow addition of 15 % w/v finely ground ammonium sulphate. The mixture was then stirred for a further hour at 4 °C after which it was centrifuged at 10,000 x g for 30 min at 4 °C. The supernatant was collected and again filtered through glass wool. Whilst stirring at 4 °C, a further 20 % w/v finely ground ammonium sulphate was added slowly. The mixture was then stirred for 45 min at 4 °C after which it was centrifuged at 10,000 g for 30 min at 4 °C. The resulting brown precipitate was collected and resuspended in a 1:1 volume of 25 mM sodium phosphate, pH 7.4, 10 mM DTT and dialysed overnight at 4 °C against 3 L of the same buffer. Any remaining precipitate was removed by centrifugation at 27,000 x g for 1 h at 4 °C, followed by filtration through a 0.22 μm filter.

The heparin column was prepared and washed as described previously (2.2.2.1), with 25 mM sodium phosphate, pH 7.4 used in place of the 20 mM MES, pH 6.5.

The crude XOR solution was loaded onto the column in 25 mM sodium phosphate, pH 7.4 containing 10 mM DTT under gravity and the XOR was observed to bind strongly, colouring the column brown. Crude XOR solution was loaded until approximately half the column was coloured deep brown. The column was then washed with approximately 50 ml 25 mM sodium phosphate, pH 7.4 containing 10 mM DTT and 0.08 M NaCl (10 column volumes). XOR was eluted with 25 mM sodium phosphate, pH 7.4 containing 10 mM DTT and 0.4 M NaCl, and all the brown coloured eluate was collected. The column was then cleaned with 10 column volumes of 25 mM sodium phosphate, pH 7.4 containing 1 M NaCl and stored in the same at 4 °C.

2.3.3.2 Anion exchange

Anion exchange was carried out using a 5 ml Mono-Q HiTrap column (Amersham-Pharmacia) on a BioCAD Sprint Perfusion Chromatography System (PerSeptive Biosystems). The column was run at a flow rate of 1 ml/min and was equilibrated in 50 mM Bicine, pH 8.3 containing 10 mM DTT. During a column run, pH, conductivity, pressure, A_{280} and A_{450} nm were monitored.

Post-heparin XOR was desalted and transferred into 50 mM Bicine, pH 8.3 containing 10 mM DTT using a HiTrap desalting column (Amersham-Pharmacia), and then loaded onto the MonoQ column in 5 ml batches until a noticeable brown colour was seen on the column. The column was then washed with 50 mM Bicine, pH 8.3 containing 10 mM DTT, until the baseline A_{280} was regained. XOR was eluted with a gradient of 0 $\rightarrow$ 0.5 M NaCl and 1 ml fractions were collected. Those fractions having a PFR $\leq$ 5.2 were pooled. The column was then washed with 50 mM Bicine, pH 8.3 containing 10 mM DTT and 1M NaCl and stored in the same buffer.

2.3.4 Crystallization of human and bovine xanthine oxidoreductase

2.3.4.1 Principles of protein crystallization

Crystallization proceeds in three phases; nucleation, growth and cessation of growth and depends on the formation of a supersaturated solution from which the molecule of interest will precipitate in a crystalline or amorphous state. The process is, perhaps, best explained through consideration of a solubility phase diagram.

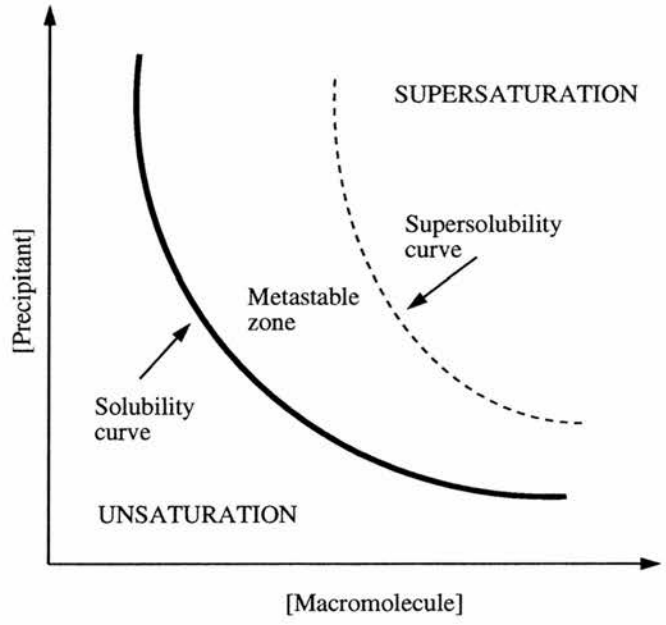

Figure 2.4: Simple phase diagram showing how solubility depends on the concentration of macromolecule and precipitant. At low concentrations of both the macromolecule remains in solution, at high concentrations it precipitates.

Crystal nuclei, small ordered cluster of a few molecules, form in the supersaturated zone. If conditions are favourable, the formation of the nuclei drives the solution into the metastable zone, where the molecule is less concentrated and crystal growth can occur with no further nucleation. At some

point, either the solution is so depleted that no further growth can occur, or the growing crystal surface is poisoned by impurities and growth stops.

The aim of a protein crystallization experiment is thus, through manipulation of the solution conditions, to drive the solution into the supersaturated zone where nucleation occurs, but not so far that amorphous precipitation occurs. It is also important to approach the supersaturation, or nucleation zone, slowly in order to allow only a few nucleation events to occur, rather than the shower of tiny crystals seen when the nucleation zone is approached too rapidly. The local depletion of protein around the nuclei produces an area of metastable solution and crystal growth can proceed further until either there is no more available protein, or the growth surface is corrupted.

It is clear from the above that in order to design a crystallization experiment, knowledge of the behaviour of the protein in solution is required. In practice, however, this information is rarely available. Although many methods for predicting the behaviour of proteins in solutions have been proposed, in order to predict likely crystallization conditions, none show general applicability, largely due to difficulties in predicting and understanding the role of salt effects.

Because of this, the design of crystallization experiments remains a largely empirical process, consisting of iterative rounds of screening and scoring through which a picture of the behaviour of the protein of interest can be built up.

The most common general screen used is the sparse matrix screen designed by Jancarik & Kim (1991) and commercialised by Hampton Research as Crystal Screen I. Jancarik & Kim collected all the crystallization conditions recorded at that time, and produced a screen of 50 conditions, in which the most common crystallization conditions were sampled. Hampton Research have since extended this in further screens (Crystal Screen II) using more recent surveys of crystallization data. Due to the wide range of precipitants, buffers and salts combined in the screens, it is likely that most proteins will produce some sort of "hit" (anything from a crystalline precipitate to large well formed crystals). Should this not be the case, the design of the screen is such that solubility information for the protein of interest can still be extracted by observing the results of each condition. Once a "hit" has been found, further screens can be designed and evaluated until the desired quality of crystals has been obtained.

Many factors influence protein crystallization including pH, precipitant type and concentration, temperature and small molecules. For a more extensive list of parameters see Giegé & Ducruix (1992).

2.3.4.2 Scoring and design of crystallization trials

In order to accurately monitor crystallization trials, a system of scoring the results of each trial is required that uncouples the effect of each parameter from that of the others. Such a system is that described by Carter (1979, 1992), which has been slightly modified for use in this project. Carter scores each trial on a scale of 1-10. Taking the mean of the scores for all trials containing a specific parameter gives an indication of the overall contribution of that parameter to the crystallization process.

The modified version of Carter's scoring scheme used in this project is as follows:

0 = clear drop
1 = amorphous precipitate
2 = unidentified [crystalline?] objects
3 = crystalline precipitate
4 = sea-urchins
5 = bundles of sticks
6 = 1D crystals - needles
7 = 2D crystals - plates
8 = small 3D crystals
9 = large 3D crystals
10 = 3D crystals diffracting to less than 2.5 Å

Figure 2.5: Examples of crystallization results. These would score as follows (reading from left to right) 1, 3, 4, 5, 6, 7, 8, 9, 10.

Once it is decided which parameters are important for crystallization, further screens are required to optimise the conditions. Designing screens that sample as much of crystallization space as possible, whilst taking into account a limited supply of protein can sometimes be complex, especially when several multivariate parameters exist.

As well as the scoring system described above, Carter has also written a simple programme, *Infac*, that uses the incomplete factorial method to produce screens that sample as much of crystallization space as possible. The incomplete factorial method seeks, rather than screening every possible combination of all parameters, to produce a screen in which every pair of variables is matched at least once. For example, consider three variables, each with two states: (a,b)(x,y)(1,2).

Factorial Screening	Incomplete factorial Screening
a,x,1 b,x,1	**a,x,1 a,y,2**
a,x,2 b,x,2	**b,x,2 b,y,1**
a,y,1 b,y,1	(a+1, b+1, a+2, b+2, a+x, b+x,
a,y,2 b,y,2	a+y, b+y, y+1, y+2, x+1, x+2)

To produce a factorial screen in which every combination of parameters is sampled requires 8 trials, an incomplete factorial screen in which every pair of variables is sampled requires only 4 trials.

2.3.4.3 Crystallization methods

Two crystallization methods were used in this project, differing in the way in which they manipulate the protein solution in order to move about phase space; hanging drop vapour diffusion and microbatch under oil.

Hanging drop vapour diffusion produces a state of supersaturation by setting up a vapour equilibrium in a sealed chamber between a small (typically 1-10 μl) drop and a large (0.5-1 ml) reservoir. The reservoir contains the crystallization solution (precipitant, buffer, additives) and the drop is made up of a mixture of this reservoir solution and protein solution in a typical ratio 1:2, although changes in the ratio of drop:reservoir can alter the rate at which equilibrium is reached. The equilibrium is produced by the precipitant concentration gradient that exists between the drop and the reservoir, as water leaves the drop (vapour diffusion) in order to equalise the precipitant concentration. If the conditions are correctly chosen, the equilibrium point produces a supersaturated protein solution in which nucleation can occur, but which is close enough to the metastable zone, that, once nuclei have formed, the local concentration of protein around the nucleus drops driving the local solution into the metastable zone where crystal growth can follow.

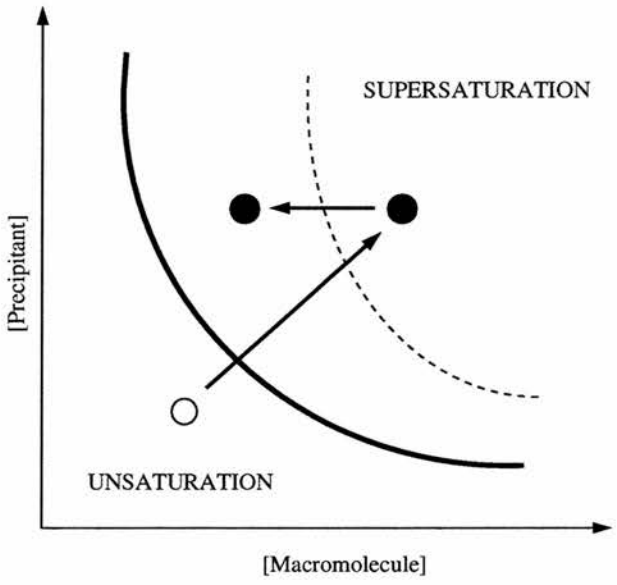

Figure 2.6 Phase diagram showing the desired movement around phase space in a hanging drop vapour diffusion experiment. Soluble protein (clear circle) is moved into the supersaturation zone as the concentration of precipitant increases, then back into the metastable zone when nucleation has occurred.

Hanging drop vapour diffusion trials were set up in 24 well Linbro plates as follows: 1 ml of appropriate precipitant solution was dispensed into each well, and the rims of the wells were greased with vacuum grease. 1µl of protein solution was mixed with 1 µl of precipitant solution in a drop on a silanised coverslip. This was upturned and placed over the Linbro well, suspending the drop above the reservoir. The well was then sealed by pushing the coverslip down carefully onto the grease, taking care that no gaps remained. Trials were stored in an incubator at 20°C and were then monitored, scored every day for a week and thereafter once or twice a week.

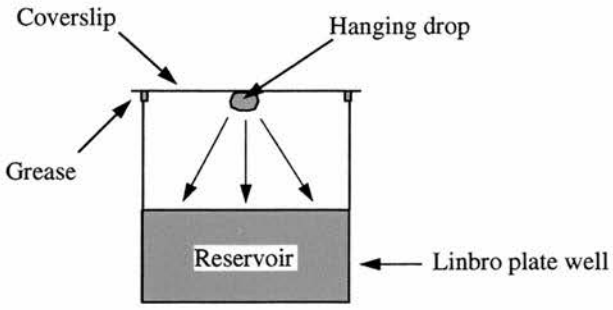

Figure 2.7 Illustration of a hanging drop vapour diffusion experiment. The droplet containing protein and precipitant solution is suspended over a reservoir of precipitant solution in a sealed chamber. The arrows within the chamber indicate the direction of vapour diffusion as the protein and precipitant concentrations in the droplet increase.

Microbatch under oil is, as its name suggests, a batch technique in which no changes in precipitant concentration occur. The protein and precipitant solutions are mixed together under paraffin oil (preventing evaporation). If the conditions are correct the protein is in an immediate state of supersaturation, and nucleation occurs. As the local protein solution is depleted around the nuclei, the solution moves into the metastable zone and crystal growth follows. The success of this method relies on the selection of conditions that are just on the border between the supersaturation and metastable zones. This allows a rapid move into the metastable zone upon nucleation, thus avoiding showers of small crystals.

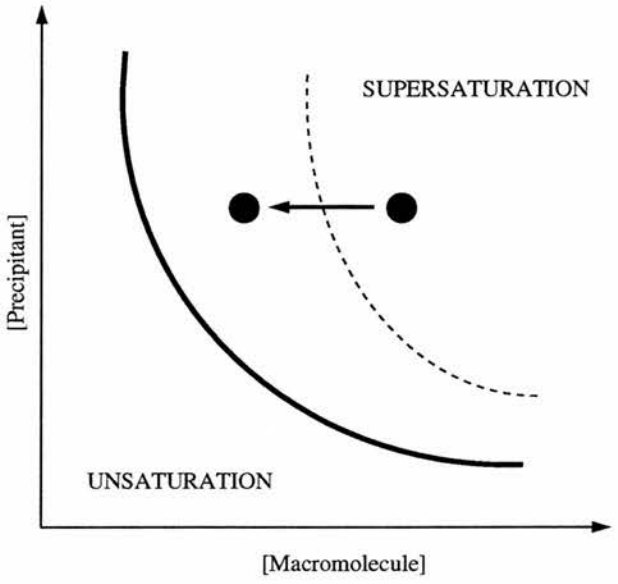

Figure 2.8 Phase diagram showing the desired movement around phase space in a microbatch experiment. The protein is immediately placed in supersaturating conditions, then when nucleation occurs, moves into the metastable zone allowing crystal growth.

Microbatch under oil trials were set up in 72 well microbatch plates (Hampton Research) as follows: paraffin oil (15 μl) was dispensed into each well. Then protein solution (1μl) and DTT solution (1μl) (concentration varied) were pipetted together under the oil in each well, and the plate was left to incubate at 20°C for 1 h. At the end of this time, appropriate precipitant solution (1μl) was added under the oil and mixed with the protein/DTT drop. The plates were then stored in an incubator set at 20°C, monitored and scored daily for one week, and once or twice a week thereafter.

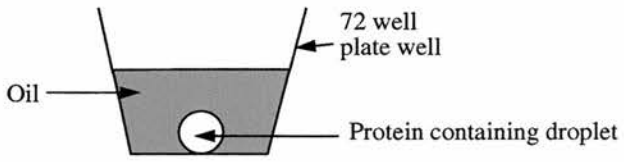

Figure 2.9 Illustration of a microbatch under oil experiment. The droplet containing the protein and precipitant solution is covered by oil, preventing evaporation.

As stated above, the presence of small molecules can have a dramatic effect on protein crystallization. Hampton Research produce 3 proprietary screens of small molecule additives which were used in the microbatch under oil trials as follows: A crystallization condition in which crystals had formed was selected, and the trial set up as described above, the sole difference being that an additive was added at the same time as the precipitant. However, in order to maintain the ratio of protein to precipitant (protein:DTT:precipitant 1:1:1) that existed in the original trials, additive trials were set up in one of two ways.

- DTT stock solution was made up at double the concentration used in the original trial, and the final drop composition was as follows: Protein 2μl, Precipitant 2μl, DTT 1μl, Additive 1μl.
- DTT was added directly to the protein solution to three times the required final concentration, and the final drop composition was as follows: Protein + DTT 1μl, Precipitant 1μl, Additive 1μl.

Both these methods maintain the total amount of DTT in the drop, whilst also retaining the protein:precipitant ratio of the original condition. There was no difference in the results obtained using these two methods.

2.3.4.4 Harvesting of crystals

Crystals were harvested and frozen for use in X-ray diffraction methods in much the same way for both vapour diffusion and microbatch under oil experiments.

For vapour diffusion trials the drops were accessed by simply removing and upturning the coverslip upon which the drop was suspended, crystals could then be "fished" from the drop using cryo-loops (Hampton Research) and either mounted in the X-ray generator immediately, or dunked in several other drops in order to soak in cryo-protectant or substrates before mounting. Drops can be resealed by replacing the coverslip over the well and sealing with grease.

Drops containing crystals grown in microbatch under oil were slightly more complex to harvest, as the oil has to be removed. This was done by pipetting off the majority of the oil, and then refilling the well to the brim with crystallization buffer (containing any cryoprotectants necessary). Any skin that had formed on the surface of the drop could then be removed with an acupuncture needle, and crystals harvested with a cryo-loop. The drops could be resealed by simply removing the excess cryo buffer and relayering oil carefully on top of the drop.

2.3.4.5 Crystallization and harvesting in the absence of oxygen

Microbatch under oil trials were also set up in the absence of oxygen using the Belle Technology anaerobic glove box at the North of England Structural Biology Centre (NESBiC) facility housed at Leeds University. This glovebox, which is specifically designed for protein crystallization, consists of 2 chambers; a large 3 glove box, with large and small entry / exit ports, for solution work and crystallisations, and a crystal mounting and freezing box, containing a built-in Leica MZ6 microscope and liquid nitrogen port, which can be isolated from the main box (see Fig 2.10).

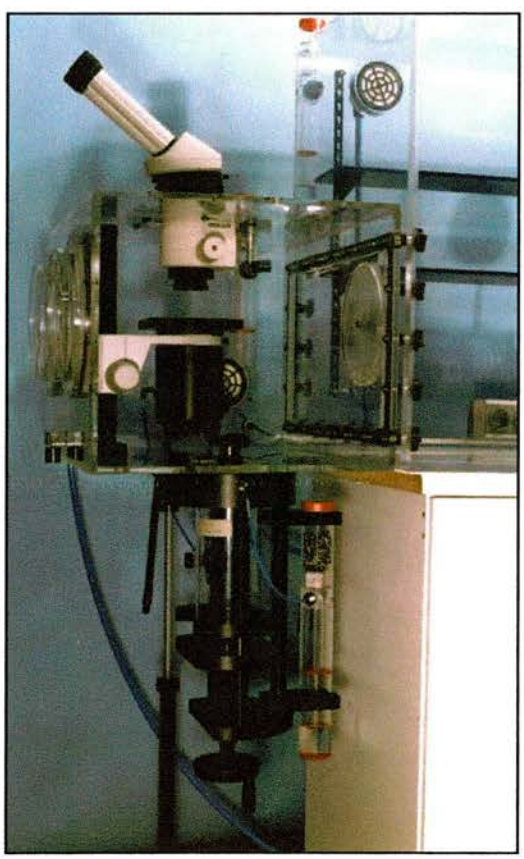

Figure 2.10: Detail of the glove box at Leeds University, showing the crystal mounting and freezing box containing the built in microscope. The port into the larger chamber is also visible, as is the liquid nitrogen port which allows protein crystal freezing.

All buffers and solutions were degassed by sparging with N_2 before being placed in the glovebox. Microbatch under oil trials were set up as described above and crystal growth was monitored. Crystals were harvested using a

cryo-loop mounted on a Magnetic Wand (Hampton Research) and frozen directly in liquid nitrogen by plunging the cryo-loop into the Dewar. Crystals harvested this way were then stored in liquid nitrogen until required. Crystal trials that were not harvested in the glovebox were sealed with parafilm before removal, and remained so until immediately prior to harvesting.

2.3.5.1 X-ray microanalysis scanning electron microscopy (X-ray SEM)

Samples of BMXOR and HMXOR, in water, were freeze dried, mounted on a thin film and carbon coated. X-ray SEM was carried out using a JEOL 8600 Electron-probe Microanalyser.

The accelerating voltage was 15 kV, wavelength was $5x10^{-8}$ Å and the count time for each measurement was 100 s. The molybdenum and iron peaks were scanned for by using solid metal standards and located as described below (Table 2.1). Mo and Fe fluorescence levels were then counted at the defined peaks for 100 s. Background readings were taken at each side of the peak to eliminate any effects from peak asymmetry. Multiple readings were taken at different positions on each sample.

Metal	Edge	Detection crystal	Peak position	Background
Molybdenum	Lα	PET crystal	173.24 mm	± 5 mm
Iron	Kα	LiF crystal	134.63 mm	± 5 mm

Table 2.2: Edge & peak positions for analysis of freeze dried BMXOR and HMXOR samples

Crystals of BMXOR (grown in 10% PEG 4000 and 50 mM potassium dihydrogen phosphate, pH 6) were also mounted on a film and coated with gold.

The accelerating voltage was 25 kV, wavelength was $5x10^{-8}$ Å and the count time for each measurement was 100 s. The molybdenum and iron peaks were scanned for by using solid metal standards and located as described below (Table 2.2). Mo and Fe fluorescence levels were then counted at the defined

peaks for 100 s. Background readings were taken at each side of the peak to eliminate any effects from peak asymmetry. Multiple readings were taken at different positions on each sample.

Metal	Edge	Detection crystal	Peak position	Background
Molybdenum	Lα	PET crystal	172.91 mm	± 5 mm
Iron	Kα	LiF crystal	134.68 mm	± 5 mm

Table 2.3: Edge & peak positions for analysis of BMXOR crystals

2.3.5.2 Micro-crystal spectrophotometer

Spectra were measured on the XSPECTRA Single Crystal Micro-spectrophotometer (http://www.4dx.se/spectrop.htm) and recorded using the Instaspec software (Oriel) at the Structural Biology Support Lab, Daresbury Laboratory, UK.

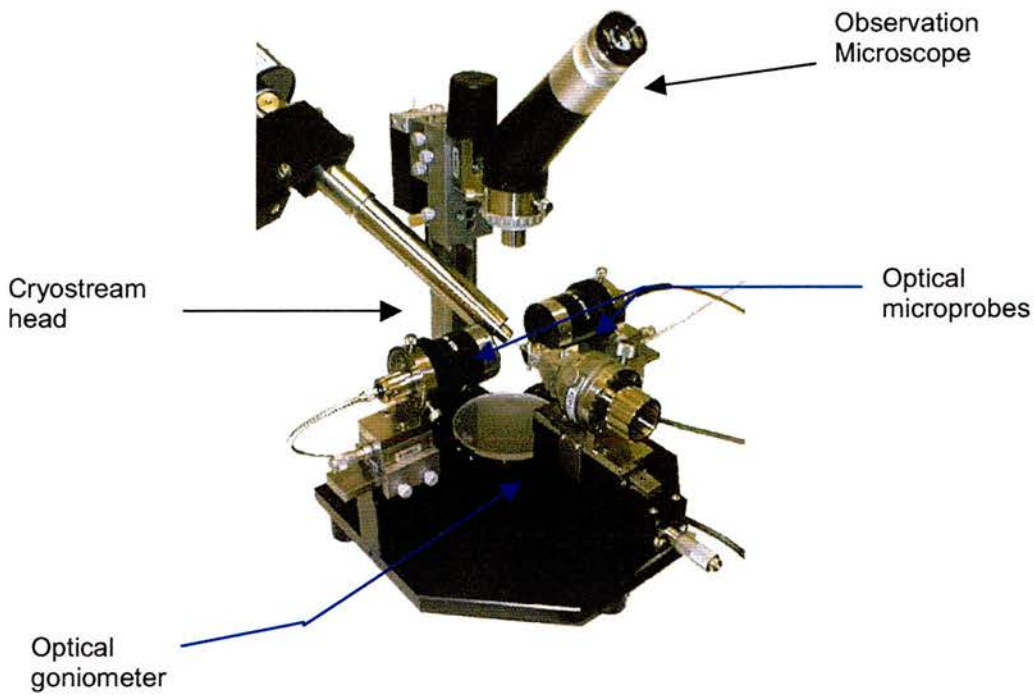

Figure 2.11: XSPECTRA Single Crystal Micro-spectrophotometer (picture taken from: http://www.4dx.se/spectrop.htm). The arrangement shown is that for collecting spectra from frozen crystals. The whole apparatus can be tipped over onto it's back (with the cryo-stream removed), so that the goniometer head points downward, and a flow cell mounted on the goniometer.

The Micro-spectrophotometer was prepared by aligning and focusing the light source using a goniometer mounted pinhole. Single crystals were harvested in cryo-loops as described in section 2.2.4.4 and frozen in liquid nitrogen. The loops were then mounted on the goniometer at 100K. Crystals were aligned in the beam using the observation microscope. Spectra were measured across

the range of the photomultiplier (~350 nm to ~550 nm) which was calibrated using the mercury fluorescence from the strip lights in the laboratory. Reference spectra were taken through a section of the loop containing only frozen cryo-solution.

In order to carry out measurements of crystal activity in the presence of substrate, the Micro-spectrophotometer was tipped onto its back, so that the goniometer head was pointing downwards and then realigned and focussed. Crystals were immobilised in a capillary as follows. A quartz capillary (0.3 mm) that was slightly tapered was selected and a few strands of cotton wool soaked in water were inserted to form a 'bung'. Care was taken not to pack them too tightly so that liquid could still flow through the capillary. The capillary was then filled with crystallization mother liquor and a small amount of G-25 or G-75 Sephadex suspended in crystallization mother liquor dropped in the top. This was allowed to settle, keeping the solution in the capillary topped up. A crystal was then harvested in a loop, dropped onto the positive meniscus at the top of the capillary and allowed to settle onto the Sephadex. More Sephadex solution was then added and allowed to settle around the crystal, effectively immobilising it. The capillary was then attached to a flow cell mounted on the goniometer avoiding air bubbles and the crystal located and centred using the observation microscope. Reference spectra were taken by translating the crystal out of the beam and measuring the spectra of the capillary and Sephadex. Care was taken not to move too far from the crystal, to avoid any artefacts due to variation in the capillary. Mother liquor was then flowed over the crystal through the flow cell (driven by a small syringe pump) and the absorbance spectra of the crystal monitored. 100 μM xanthine was

then added to the mother liquor and pumped over the crystal. The absorbance spectrum was again monitored.

2.4 Results

2.4.1 Purification of bovine milk XOR

Heparin chromatography routinely yielded preparations of XOR with PFR values 5.3 - 5.6 (Fig 2.12). 15-20 mg of XOR protein (calculated from A_{450}) were usually obtained from a litre of fresh bovine milk.

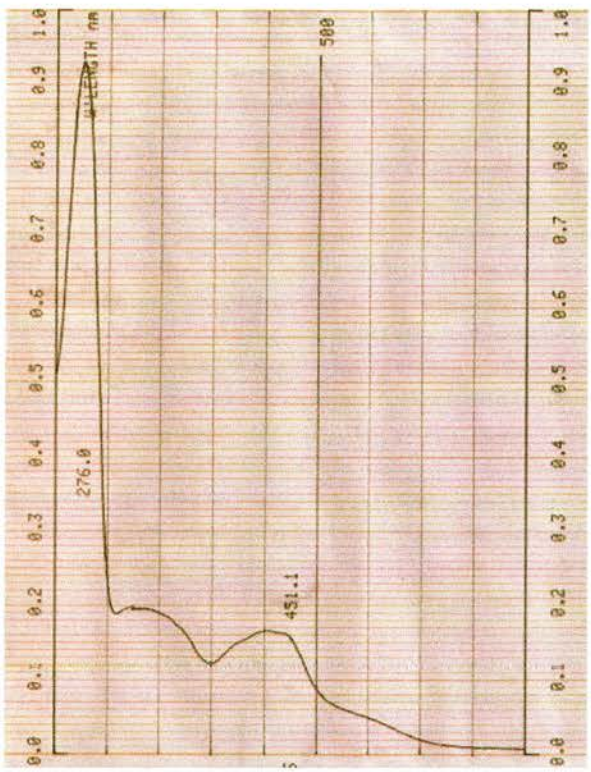

Figure 2.12:
Scan of XOR absorbance from 220 nm to 700 nm using a Cecil Series 6000 Double Beam Spectrophotometer. This preparation showed (after correction for sample turbidity) A_{280} = 0.897 and A_{450} = 0.167, giving a PFR value of 5.4.

Elution of XOR from the folate affinity column was monitored using absorbance at 450 nm, since the hypoxanthine used to elute XOR from the column is converted to urate, which has considerable absorbance at 280 nm, by XOR.

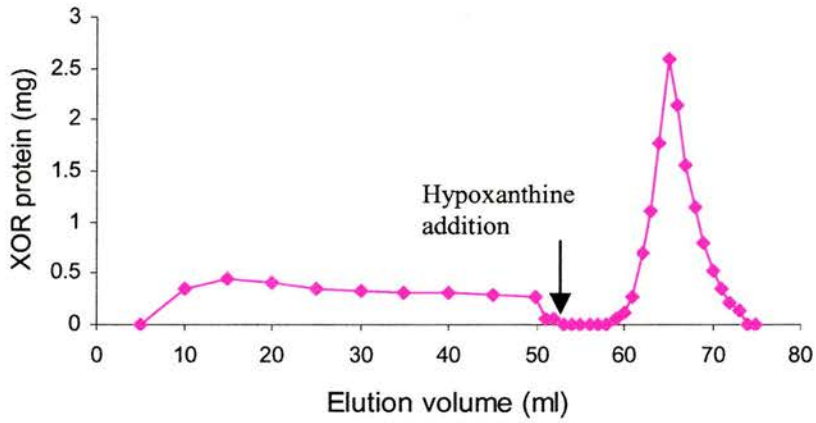

Figure 2.13:
Elution profile of XOR from the folate affinity column. XOR protein (mg) calculated from A_{450}. Arrow marks the beginning of elution (at 51 ml) with 0.5 mM hypoxanthine.

The pooled fractions from the 2nd peak gave a PFR of 5 and were immediately used in crystal trials. The unbound material had a much lower PFR of 7.3, indicating the presence of impurities. However, it still possessed xanthine oxidase activity in the fluorimetric assay suggesting that the separation of molybdo- from demolybdo- XOR was incomplete.

Iso-electric focussing (IEF) was also investigated as an alternative method of separating XOR isoforms. This method separates on the basis of differing iso-electric points. To determine whether this was a viable method, IEF gel electrophoresis of BMXOR was carried out in order to see whether individual species could be resolved.

Figure 2.14
Broad range (pH 3-9) IEF gel of BMXOR. "BMXO bound" is the bound fraction eluted from the folate column with hypoxanthine, "BMXO pre-fol" is heparin affinity purified BMXO. Marker pI values are given on the gel, markers were the broad range IEF markers from Pharmacia and are as follows: Lentil lectin-basic (8.65), Lentil lectin-middle (8.45), Lentil lectin acidic (8.15), Horse myoglobin-basic (7.34), Horse myoglobin-acidic (6.85), Human carbonic anhydrase B (6.55). The band at the lower end of both the sample lanes is an artefact caused by lowering of the sample applicator and precipitation of some of the sample onto the gel. This band was observed at whichever end of the gel the sample applicator was placed and did not migrate.

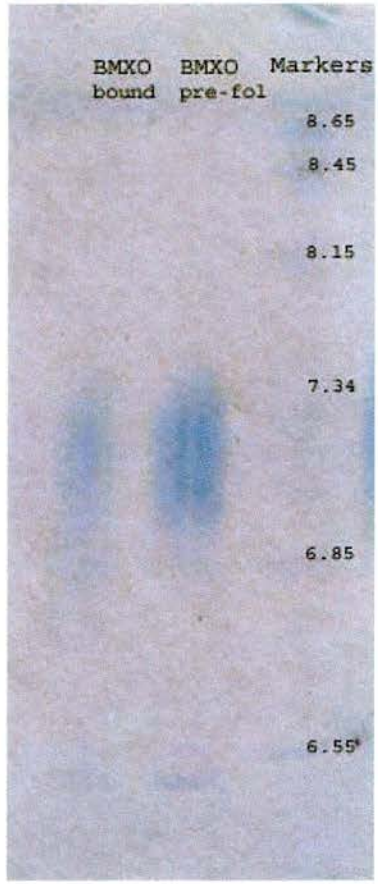

IEF gel electrophoresis did not resolve any individual species, showing only a smear of protein over the pH range 6.85 to 7.4. Attempts to improve resolution by loading different amounts of protein, and by varying the electrophoresis parameters (time, voltage) did not yield any clearer resolution of pI. Thus IEF was abandoned as a method of isoform separation.

Gel filtration of folate affinity purified BMXOR (bound fraction) was carried out in an effort to improve crystal quality by removing aggregated XOR prior to the setting down of crystallization trials.

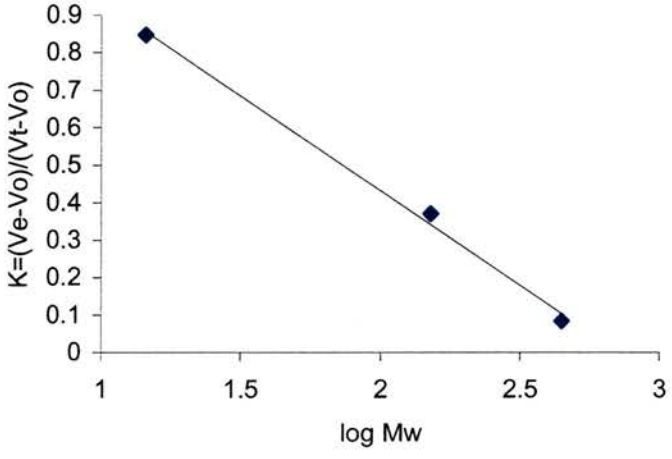

Figure 2.15:
Calibration of the Gel filtration column. Standards used were: Apoferritin (443 kDa), Alcohol dehydrogenase (150 kDa) and lysozyme (14.3 kDa). Blue Dextran and DNP-lysine were used to determine void and total volumes.
Ve = elution volume, Vo = void volume, Vt = total volume.

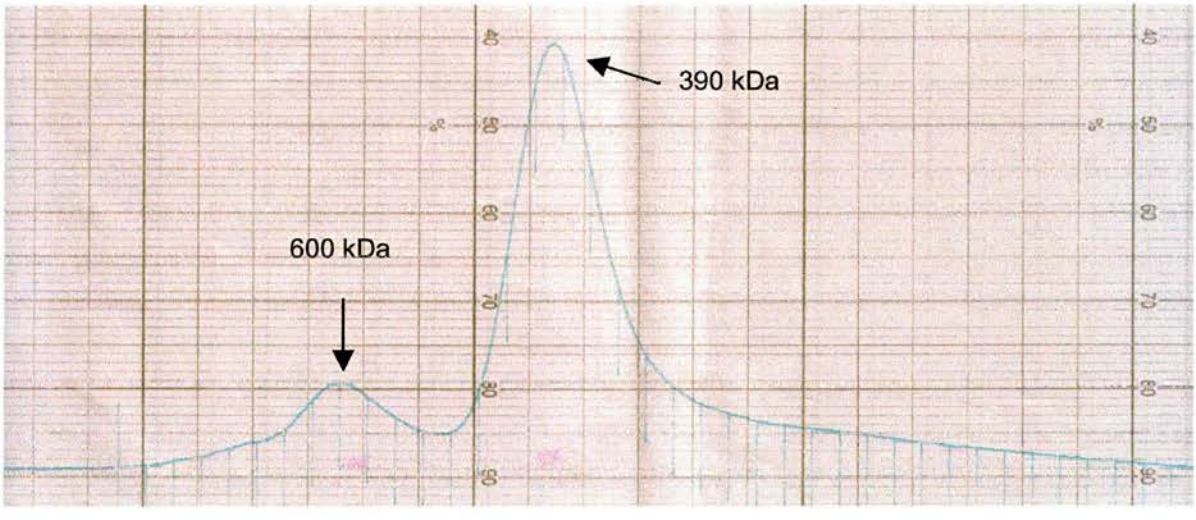

Figure 2.16:
Elution profile of BMXOR from the gel filtration column. Elution was monitored using absorbance at 280 nm. Two peaks were observed, K of peak 1 = 0.03, K of peak 2 = 0.13. 1 square = 2 ml elution volume.

Peaks at molecular weights expected for the tetramer and dimer were obtained (the 2nd peak is slightly high - 390 kDa) and dimer-containing fractions were pooled and put into crystallization trials.

At a later stage in the project, anion exchange chromatography was used as a polishing step for heparin affinity purified BMXOR. BMXOR eluted as a clean peak and was used in crystallization trials.

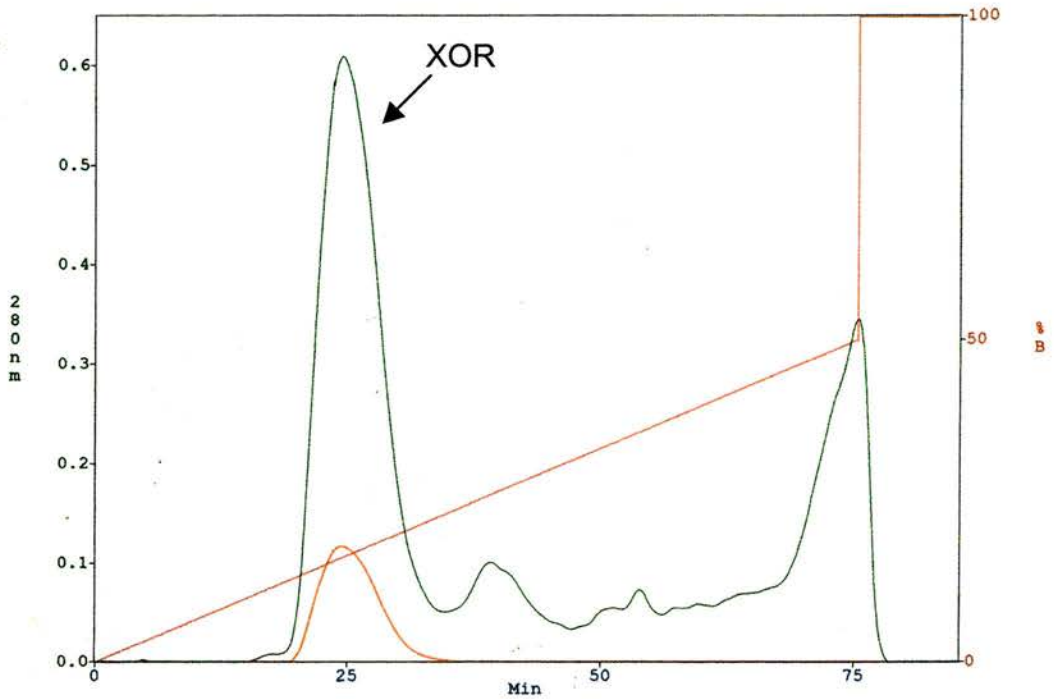

Figure 2.17: Elution of BMXOR from a MonoQ anion exchange column (Pharmacia). Absorbance at 280 nm is in green, absorbance at 450 nm (XOR specific) is in red and the gradient (Buffer B contained 1 M NaCl) is shown in pink.

2.4.2 Purification of human milk XOR

Human milk XOR was purified routinely by heparin affinity chromatography as described in Section 2.3.3.1 to a PFR of 5.2-6.0. HMXOR samples were then desalted rapidly on a HiTrap desalting column (Pharmacia) before being loaded onto an anion exchange column and eluted with a salt gradient (Fig 2.18).

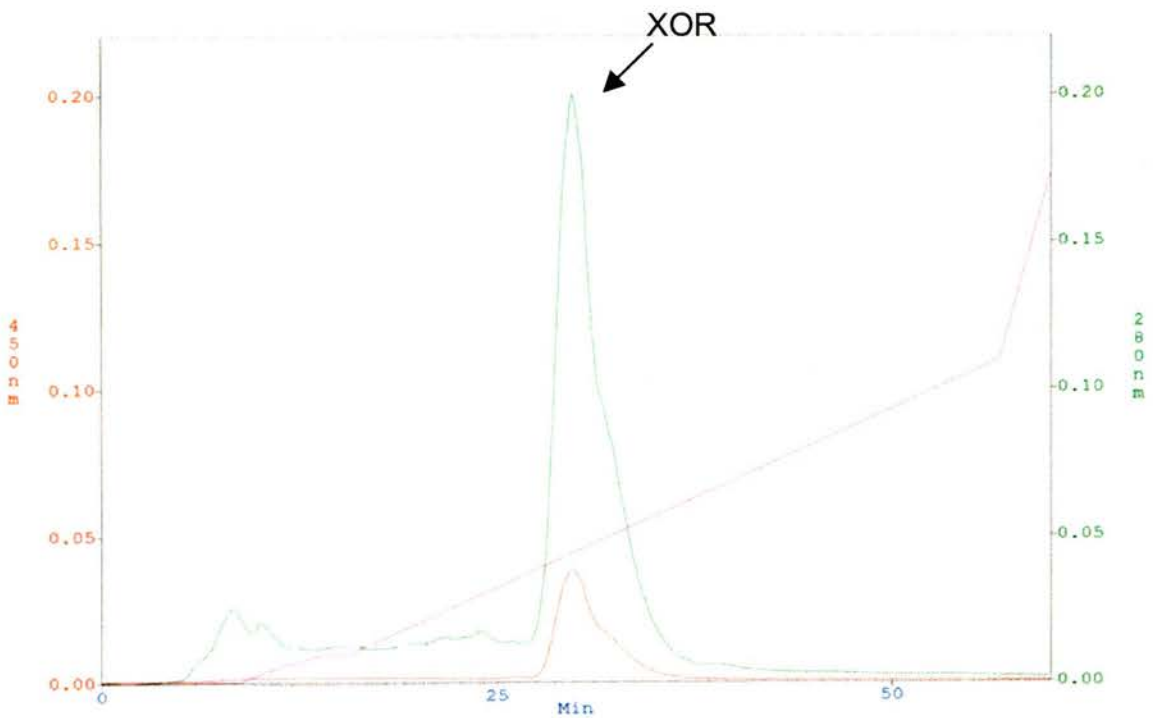

Figure 2.18 - Elution profile of HMXOR from the anion exchange column, showing (on the same scale) absorbance at 280 and 450 nm, and the salt gradient in magenta. This anion exchange preparation produced HMXOR with a PFR of 5.1-5.2.

Different preparations of HMXOR behaved very differently on the anion exchange columns; those that eluted at highest purity, as measured by PFR and SDS-PAGE, were preparations that had been done as quickly as possible and had maintained a high concentration of DTT throughout the purification. If

a high DTT concentration was not maintained, HMXOR aggregated and precipitated.

Anion exchange purified HMXOR runs as a clean single band on SDS-PAGE (Fig 2.19) at 150 kDa and preparations with a PFR 5-5.2 were used in crystallization trials.

A

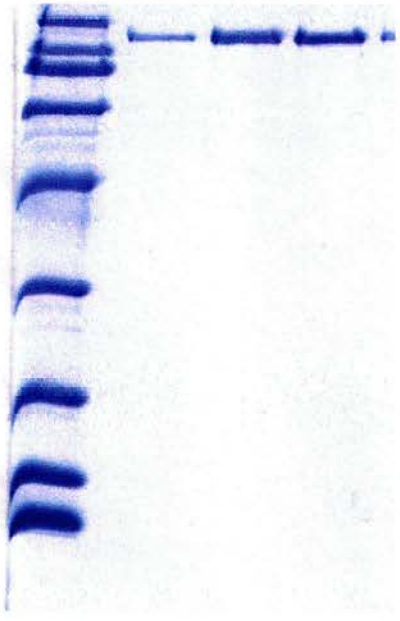

B

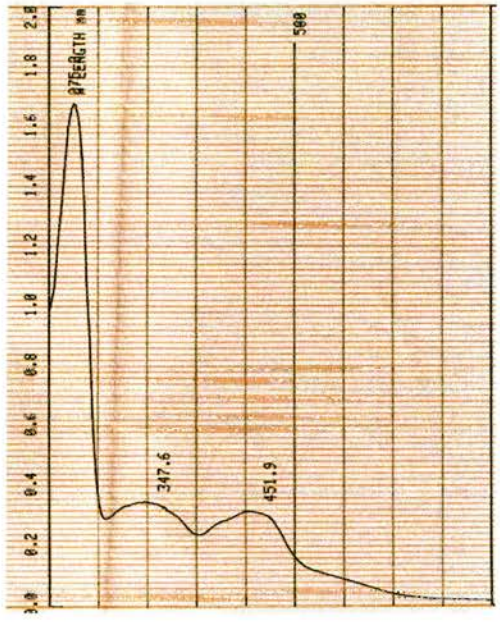

Figure 2.19: A Three fractions of post anion exchange HMXOR run on SDS-PAGE. BioRad Broad Range Markers were used and are, from top to bottom, Myosin (200 kDa), β-galactosidase (116.25 kDa), Phosphorylase b (97.4 kDa), Serum albumin (66.2 kDa), Ovalbumin (45 kDa), Carbonic anhydrase (31 kDa), Trypsin inhibitor (21.5 kDa), Lysozyme (14.4 kDa) and Aprotinin (6.5 kDa). B: Scan from 220 to 700 nm of anion exchange purified HMXOR, this preparation had a PFR of 5.1.

2.4.3 Crystallization of xanthine oxidoreductase

Early work on crystallizing XOR focussed upon the enzyme obtained from bovine milk because of the relative ease with which it could be obtained. Diffraction quality crystals of BMXOR were reported in 1993 (Eger *et al.*, 1993) and these eventually led to the solution of the bovine milk XOR structure (Enroth *et al.*, 2000). Because these crystals were grown in phosphate buffer and PEG 4K, screens designed around these conditions, using the *infac* programme in order to minimise protein use, whilst maximising the conditions searched, were used as well as the sparse matrix screens available from Hampton Research. Hanging drop vapour diffusion crystallization trials containing 10 mg/ml post-folate column BMXOR uniformly produced a thick brown precipitate. However, when the protein concentration was reduced to 1 mg/ml and azide was no longer included in the crystallization solutions as a preservative, the formation of small crystals was observed over a period of several weeks in conditions related to those described by Eger *at al.* (1993). The crystals seemed to form from the precipitate and were colourless. The maximum dimensions reached were approximately 300 x 50 x 50 μ.

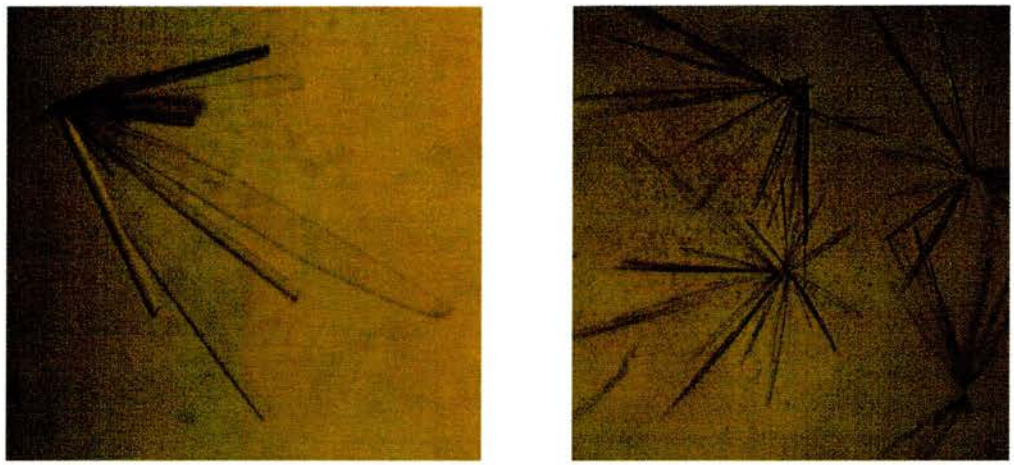

Figure 2.20: BMXOR crystals grown by hanging drop vapour diffusion in 10 % PEG 4K, 50 mM potassium dihydrogen phosphate at pH 5.8 (A) and pH 6.0 (B).

No diffraction was observed from the BMXOR crystals in house or at the EMBL Outstation at DESY, the synchrotron radiation source in Hamburg, Germany. Efforts were made to reduce microheterogeneity in the samples by removing aggregates by gel filtration and immediately setting down crystallization trials with the dimer containing fractions. However, no better crystals could be obtained.

It was then decided to turn to the human milk enzyme as, despite its low activity and molybdenum content, it was hoped that the sample would be more homogenous than BMXOR. In BMXOR, fully active XOR comprises only 30-35 % of the total XOR protein, demolybdo and desulpho XOR accounting for the remaining 65-70 %. HMXOR, on the other hand, contains 95 % demolybdo XOR.

Hanging drop vapour diffusion trials of post-monoQ HMXOR were set up using Crystal Screens 1 & 2 (Hampton Research) and screens designed,

using *infac,* around the conditions in which crystals of BMXOR had been obtained. HMXOR was used at a concentration of 2.5 mg/ml. Precipitate was observed in nearly all trials. Godber (Godber, 1998) showed that HMXOR has a strong tendency to form high molecular weight aggregates, and demonstrated, using dynamic light scattering, that the level of aggregation is reduced when HMXOR is incubated with 10 mM DTT.

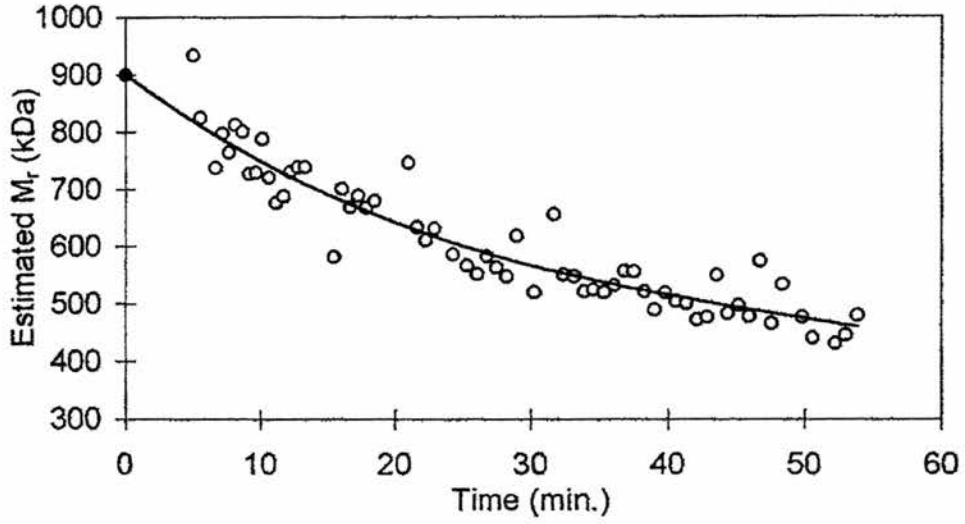

Figure 2.21: Time course showing the reduction in aggregate size of HMXOR in the presence of 10 mM DTT. 10 mM DTT was added to aggregated HMXOR and estimated molecular mass monitored using dynamic light scattering. Graph modified from Godber (Godber, 1998).

It was therefore decided to use 10 mM DTT as an additive in crystallization trials of HMXOR, as well as preincubating HMXOR with 10 mM DTT for 1 h prior to the setting down of the crystal trial. Since all previous crystals of XOR had grown over a period of weeks, a method of crystallization was sought which would maintain the reducing environment created by the presence of DTT. As DTT oxidises rapidly on exposure to air, it was feared that using the hanging drop vapour diffusion method would lead to oxidation of the DTT before crystals had formed. Microbatch crystallization under oil offered an alternative method that would slow oxidation of DTT and hence maintain the

reducing environment in the crystallization drop long enough for crystals to form. Crystal Screens 1 & 2 (Hampton Research) were used to identify initial crystallization conditions. Surprisingly, small (100 x 20 x 20 μ max.) golden brown crystals appeared overnight in several conditions, showing a trigonal prism morphology. The conditions were refined and we were able to reproducibly obtain a few single trigonal crystals in each drop (in several related conditions), with maximum dimensions of 400 x 20 x 20 μ.

Figure 2.22 HMXOR crystals grown using the microbatch under oil technique. Crystals were obtained in PEG 4K 20-30 %, pH 5-8 (100mM Tris, Acetate or Citrate), 0.15-0.25 M ammonium acetate or ammonium sulphate and 10 mM DTT.

A new batch of HMXOR was purified, but despite showing single band on SDS PAGE and having a PFR of 5, no crystals were obtained. A further batch of HMXOR was prepared, again showing a single band on SDS PAGE, and a PFR of 5 and this produced crystals in the same conditions as the first. This batch to batch variation was investigated and shown to depend on the ratio of dehydrogenase and oxidase forms of HMXOR present in the sample. If there was more than 50 % oxidase, no crystals were obtained.

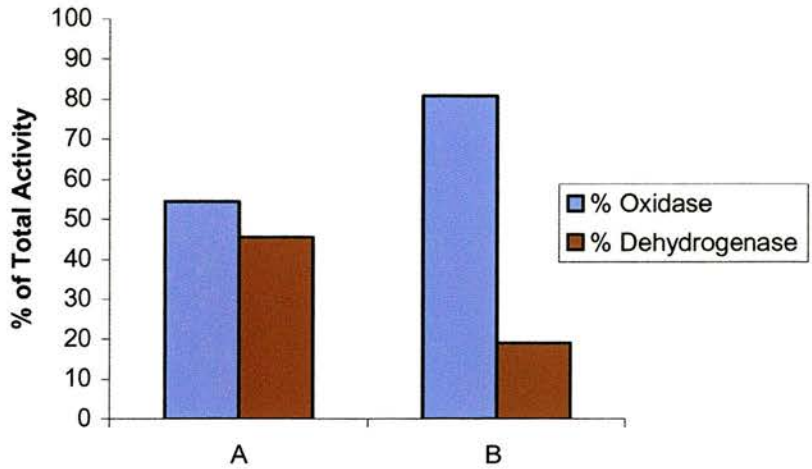

Figure 2.23 Graph showing the quantities of XDH and XO in two HXMOR preparations (A&B). A crystallized and B did not. XDH and XO activities were determined using the pterin assay.

However, although able to obtain single well shaped crystals of HMXOR, we were unable to observe any diffraction from them or to increase their size. It was thought that a possible reason for the lack of diffraction was exposure to oxygen during harvesting of the crystals. It is possible that oxidation of the crystals produced sufficient disorder to abolish diffraction. In order to test whether this was the case, microbatch under oil crystallization trials were set up in an anaerobic glove box, where there was also the facility to harvest and freeze the crystals without removing them from the nitrogen atmosphere. Crystals grown and harvested in this way were transported frozen to the EMBL Outstation at DESY, Hamburg and tested for diffraction. Some sealed microbatch plates that had been set up under nitrogen were also taken. None of the small prefrozen crystals diffracted, however, a large (800 x 50 x 50 m) but low quality crystal in one of the sealed plates was harvested at the synchrotron (i.e. exposed to oxygen) and mosaic diffraction to 7 Å was observed. This indicated that the likely reason for the lack of diffraction from

the smaller more perfect crystals was their size, rather than damage through oxidation during harvesting.

On the basis of this, it was hoped that a more intense X-ray beam would be able to produce detectable diffraction even from the smaller crystals, and time was obtained on beamline ID14-2 at the ESRF, Grenoble.

Efforts were also made to increase the size of the small crystals using the small molecule additive screens available from Hampton Research. Additives were screened against the condition in which the large, but low quality, diffracting crystal was obtained (26 % PEG 4K, 0.25 M ammonium acetate, 100 mM sodium acetate, pH 6.0 and 10 mM DTT). Crystals were obtained in the presence of many of the additives, with three additives producing large and well formed crystals (30 % w/v glucose, 1 M DTT and 5 % w/v polyvinylpyrrolidone). These and crystals obtained from previous screens were taken to ID14-2 at the ESRF where several datasets were obtained to a maximum resolution of 3.3 Å.

Figure 2.24 Crystals grown using microbatch under oil. This crystal was obtained from an additive screen containing 1 M DTT. As well as the additive, the drop contained 26 % PEG 4K, 0.25 M ammonium acetate, 100 mM sodium acetate, pH 6.0 and 10 mM DTT.

Given the success of the microbatch method in producing diffraction quality crystals of HMXOR, new attempts were made to crystallize BMXOR purified in the same way as HMXOR (heparin affinity and anion exchange). BMXOR, incubated with 10 mM DTT, was screened using Crystal Screen 1 & 2 (Hampton Research) and small golden brown clusters of plates were obtained (typical dimensions 100 x 50 x 5 μ). The conditions were optimised to give single plates grown in 22 % PEG 4K 0.2 M ammonium acetate, 100 mM sodium citrate, pH 6 and 10 mM DTT, which diffracted at the ESRF (ID14-2) to 2.7 Å.

In an attempt to extend the resolution of the human crystals beyond 3 Å, further screens were carried out, varying DTT concentration, as well as the concentrations of the other additives. A new crystal form of HMXOR was obtained (26 % PEG 4K, 100 mM Tris, pH 8, 0.25 M ammonium sulphate and 1.5-5 % w/v DTT), appearing over a period of two weeks rather than overnight, and often appearing in drops in which trigonal crystals had already formed. These crystals have a hexagonal plate morphology with average dimensions of 50 x 50 x 10 μ, and are also golden brown (Fig.2.25). On beamline ID13 at the ESRF, a dataset to 3.6 Å was obtained.

Figure 2.25 Orthorhombic HMXOR crystals obtained in 26 % PEG 4K, 100 mM Tris, pH 8, 0.25 M ammonium sulphate and 3 % w/v DTT. Maximum dimensions are 50 μ.

Attempts were also made to obtain diffraction quality crystals of HMXOR complexed with various substrates and inhibitors (NAD, xanthine, allopurinol), using both soaking and co-crystallization, with no success. Co-crystallization produced either precipitant or small non-diffracting crystals. Soaking, especially in xanthine resulted in rapid dissolution of the crystal.

2.4.4 Characterisation of XOR crystals

Because XOR exists in various forms varying in both specificity for oxidising substrate (XDH and XO) and in activity (demolybdo, desulpho), it was unclear as to precisely what was crystallizing. As the bovine milk enzyme is largely molybdo and the human milk enzyme demolybdo, it is likely that, in each case, the predominant species is that which is crystallizing. Attempts were made to determine the molybdenum content and the activity of the crystals using several methods.

2.4.4.1 X-ray microanalysis scanning electron microscopy

X-ray Microanalysis Scanning Electron Microscopy (X-ray SEM) allows the identification and quantification of elements present in a sample by measuring the characteristic X-rays emitted by the sample when an electron beam is incident upon it.

Characteristic X-rays are produced by an atom when an incoming electron has sufficient energy to eject an electron from the inner shell of the atom. The atom is then in an excited state and is able to relax to its ground state through a specific set of allowed transitions of outer shell electrons into the inner shell vacancy. The difference in energy between the outer and inner shell concerned is then emitted as a photon, the wavelength of which is specific for the atom concerned.

In order to determine whether the X-ray SEM method was a valid method for measuring molybdenum, measurements were first made upon freeze dried samples of BMXOR and HMXOR of known molybdenum content (Godber, 1998).

Metal	Peak count	Background +	Background -	Net Peak
Molybdenum	1085960	2229	3637	1083027
Iron	1106355	3595	4467	1102324

Table 2.4: Counts for the solid metal standards (at the peak wavelengths described in 2.2.5.1)

Element	Mo	Fe	Mo	Fe	Mo	Fe
Peak count	282	2561	296	2876	219	2137
Background +	239	461	236	457	198	418
Background -	218	561	224	601	203	565
Net count	54	2050	66	2347	19	1646
Mo/Fe ratio	0.026		0.028		0.011	

Table 2.5: Counts and ratio calculations for freeze dried HMXOR. Each pair of readings is from a different region of the sample.

Element	Mo	Fe	Mo	Fe	Mo	Fe	Mo	Fe
Peak count	341	1299	572	2470	315	1250	564	2461
Background +	234	517	261	537	196	517	223	520
Background -	218	609	245	731	212	670	241	708
Net count	113	736	319	1836	111	657	332	2027
Mo/Fe ratio	0.15		0.17		0.17		0.16	

Table 2.6: Counts and ratio calculations for freeze dried BMXOR. Each pair of readings is from a different region of the sample.

If the XOR sample had all molybdenum and iron sites fully occupied, a ratio of 1:4, or 0.25, would be expected. If we express the average (mean) ratios calculated above as a percentage of 100 % (0.25), this value is equivalent to the % occupancy of molybdenum in the samples. The following values are obtained:

HMXOR average Mo/Fe ratio = **0.022** → Molybdenum content = **~8.8%**

BMXOR average Mo/Fe ratio = **0.16** → Molybdenum content = **~64%**

These figures agree well with those obtained by the colourimetric method (HMXOR = 3 %, BMXOR = 63 %) and mass spectrometry (HMXOR = 6 %, BMXOR = 61 %) by Godber (Godber, 1998). The observation that the HMXOR molybdenum content is a little higher than that found by Godber can be explained if we consider his findings that one of the iron sulphur clusters is partially absent or altered. This slight decrease in iron content compared to the theoretical value, with which the maximum ratio was calculated, explains the higher than expected molybdenum content of HMXOR found using the X-ray SEM method.

Given these promising results, BMXOR crystals were mounted in the SEM as described in Section 2.2.5.1. Measurements were taken in the same way as for the freeze dried samples. However, readings obtained from the crystals were not as clear as those from the freeze dried protein. The iron reading was barely above background and the molybdenum reading abnormally high with high background readings. We then scanned across a range of wavelengths to see if any other peaks in the area could be affecting the measurements. A large sulphur peak was observed at 172 mm (very close to the Mo peak at 173 mm). This could well have affected the readings, as it is likely that, instead of reading the Lα peak from molybdenum, the abnormally high molybdenum counts came from the sulphur peak. Since there was no sulphur in the crystallization buffer the sulphur peak must come from the protein. However, were this to be the case, it would be expected that the freeze-dried sample would be similarly affected, which, given the good agreement with Mo content determined by 2 other methods seems unlikely.

In an attempt to eliminate the problems caused by the sulphur peak, we then scanned for the Mo Lβ peak (the next most intense Mo peak). This signal is, however, not significantly above background when counted over 100 s. Unfortunately, the software used to run the Electron-probe Microanalyser does not allow for count times longer than 100 s so no further data could be collected.

It was hoped that by using the iron fluorescence as in internal standard, relative amounts of molybdenum and iron present in XOR crystals could be determined. This would then have provided a relatively simple way of determining exactly which species of XOR was crystallising, demolybdo or molybdo. However, it appears that the amount of molybdenum and iron, especially given the low counts for the iron peak in the crystals, is too low to be determined by this method with the software available.

2.4.4.2 Micro-crystal spectrophotometer

HMXOR crystals were first mounted in a capillary embedded in G-25 Sephadex. After the crystal was centred, considerable care had to be taken in orienting the crystal in order to avoid edge effects from the prism shape of the crystal (Figure 2.26). However, once a favourable orientation had been found, a spectrum could be recorded that was similar to the solution spectra of XOR.

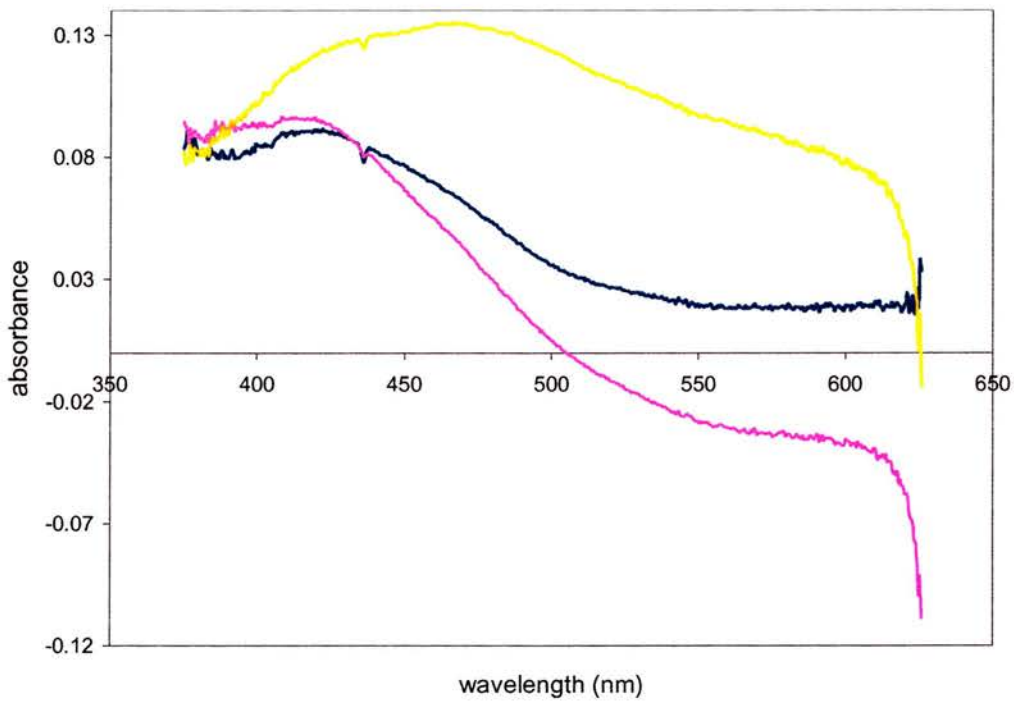

Figure 2.26: Blue trace shows the spectrum obtained from a frozen HMXOR crystal. The yellow and pink traces show spectra from the frozen crystal orientated at different angles. The large deviation from the solution spectra is likely due to edge effects from the prism shape of the crystal

We then mounted and froze a BMXOR crystal in a cryo-loop, and were able, again after careful alignment, to obtain a better and recognizably XOR spectrum (Figure 2.27).

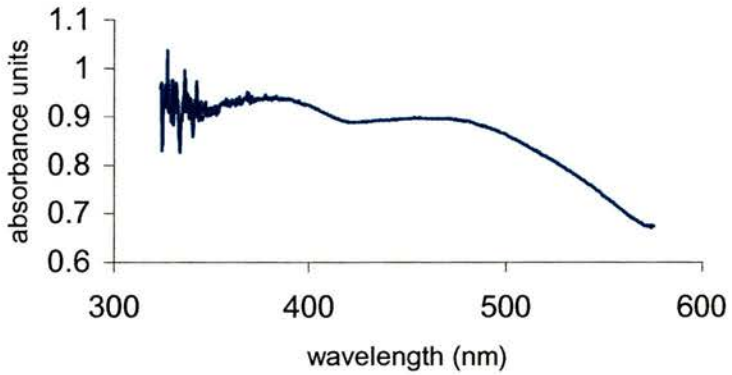

Figure 2.27: Spectrum obtained from a frozen BMXOR crystal mounted in a loop. Both the characteristic absorption peaks of XOR can be seen, although they are slightly shifted which may be due to the calibration of the photomultiplier. At around 350 nm the edge of the photomultiplier is reached.

BMXOR crystals were then mounted in a capillary embedded in G-75 Sephadex and aligned. The G-25 Sephadex is considerably more coarse than the G-25 and caused some difficulty in locating the crystal. However, once the crystal had been correctly located, a good spectrum was obtained. The syringe pump was then activated and mother liquor allowed to flow over the crystal (20 % PEG 4K, 100 mM sodium acetate pH 5.5 and 0.2 M ammonium sulphate). The crystal appeared stable and did not shift in the capillary. Once the reaction buffer (mother liquor + 100 μM xanthine) had been introduced to the system, we recorded a spectrum every two minutes, hoping to see a loss of the 450 nm peak as the flavin was reduced. Unfortunately, after 30 min, during which a very small amount of bleaching had occurred (Figure 2.28), all absorbance was lost. This was due to the crystal shifting in the capillary column and we were unable to relocate it. In the light of more recent observations, it is possible that the crystals become unstable in the presence of xanthine, and as the reaction buffer reached the crystal it began to break down. An alternative hypothesis is that the flow of the viscous mother liquor

simply dislodged the crystal and it broke into several smaller pieces that couldn't be relocated.

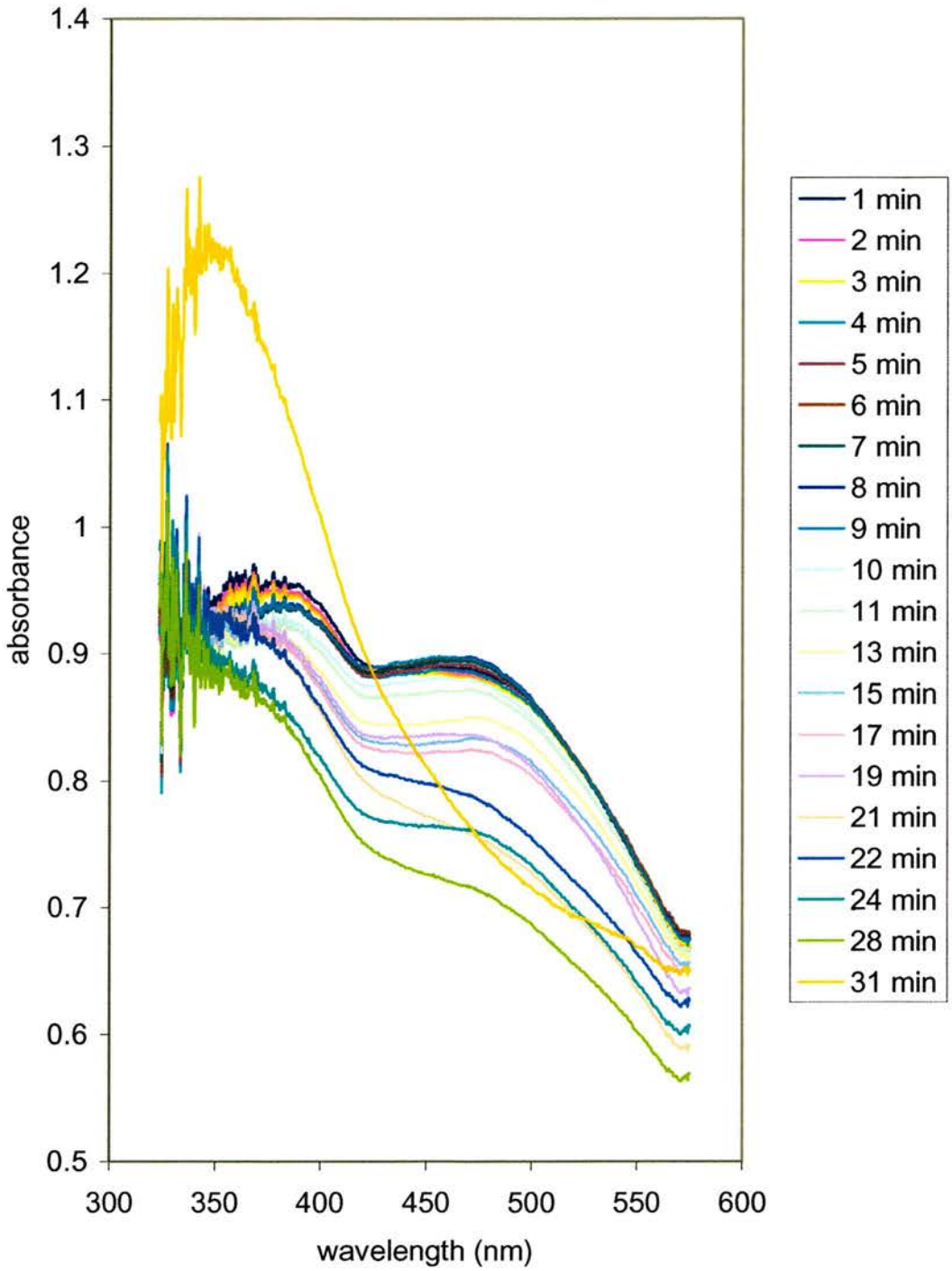

Figure 2.28: Time course absorption spectra of a BMXOR crystal mounted in G-75 Sephadex as 100 μM xanthine was pumped through the capillary. A steady loss of A_{450} is observed, indicative of flavin reduction until 17 min (pink trace) when the signal begins to lose coherency as the crystal shifts out of the beam path. By 31 min, no further data can be collected.

It was hoped that this method of mounting a XOR crystal in a capillary and monitoring absorbance changes in the presence of substrate would allow differentiation between the dehydrogenase and oxidase forms of XOR. However, although initial results were promising, it is not clear whether the loss of A450 was due to the genuine reduction of flavin, or to a gradual dissolution of the crystal.

2.5 Discussion

Several factors played a role in obtaining well-diffracting crystals, although human milk XOR seems to be more sensitive to preparation method than bovine milk.

The optimal purification procedure for HMXOR was one that was fast, simple and maintained a high level (~10 mM) of DTT at all times. The method eventually developed is a two day preparation from frozen human milk. On the first day a crude preparation of XOR is made, using ammonium sulphate cuts. This is then dialysed overnight in DTT containing buffer, before being loaded onto the heparin affinity column the following morning. After heparin affinity chromatography, the HMXOR is rapidly desalted using a HiTrap desalting column, avoiding another overnight dialysis, before being loaded onto the HiTrap MonoQ column for a final polishing step. HMXOR purified in this manner is of high purity and high dehydrogenase content, both of which have been shown in this Chapter to be vital in obtaining crystals.

Bovine milk XOR is less sensitive than HMXOR to time of purification and oxidase content. Indeed, diffracting crystals of BMXOR were obtained from a preparation that had been converted to 100 % oxidase after being purified over three days (overnight dialysis post heparin).

Despite having prepared BMXOR and HMXOR to high purity, no good quality crystal growth was observed until DTT was introduced as an additive and the

reducing conditions thus induced maintained by crystallizing under oil. In view of the observations that HMXOR will not crystallize if there is more than 50 % oxidase in the sample, it is likely that DTT aids the crystallization of HMXOR by maintaining it in its dehydrogenase form. Interestingly DTT is also absolutely required for crystallization by BMXOR, although, since the BMXOR sample was almost entirely converted to oxidase by proteolysis, DTT is not aiding crystallization by maintaining BMXOR in the dehydrogenase form. DTT was also used by Eger and co-workers in the crystallization of BMXDH and BMXO (Eger *et al.*, 2000). This suggests that DTT is also preventing non-specific aggregation and precipitation of XOR. Godber (Godber, 1998) showed that both HMXOR and, to a lesser extent, BMXOR have a tendency to aggregate that is reduced in the presence of DTT. He suggests that the aggregation of XOR may be due to the formation of inter-molecular disulphide bonds that are reduced in the presence of DTT.

HMXOR crystals were dramatically improved by the use of small molecule additives, although DTT remained the most successful of these. 30% w/v D(+)- Glucose (final concentration in the drop was 5%) gave large, well formed, trigonal crystals that diffracted to 3.3 Å at the ESRF. Unfortunately these crystals have never been reproduced, a fact which may be due to the use of an out of date additive screen in which some degradation or evaporation of additives may have occurred during storage. 5% w/v Polyvinylpyrrolidone (final concentration in the drop was 0.83%) also gave large cracked trigonal crystals. However, these did not diffract as well. 1 M DTT from the additive screen gave large trigonal crystals that were slightly

cracked, although further studies varying DTT concentration yielded cleaner, if slightly smaller, trigonal crystals and a second orthorhombic crystal form. It should be noted that all additives were used in the presence of DTT as part of the crystallization solution. No comparable improvement was observed for the BMXOR crystals.

Despite early fears that the lack of diffraction observed from apparently perfect small trigonal HMXOR crystals was due to degradation of the crystals during harvesting by exposure to oxygen, this was shown not to be the case. Indeed, as described in Section 2.4.3, the likely reason is the small size of the crystals, not oxidative damage.

It is worth noting here that the cryoprotectant used when freezing the crystals for data collection seemed to play a large role in the quality of diffraction observed for the orthorhombic crystals. This may also be the case for the trigonal crystals, although this hasn't yet been tested. This will be discussed further in Chapter Four.

Chapter 3

Sequencing of Human Mammary Gland Epithelial Cell Xanthine Dehydrogenase

3.1 Sequencing of human mammary gland XDH from HB4a cells

XOR purified from human milk was shown to have surprisingly low activity when compared to the bovine enzyme, an observation which was subsequently explained by the lack of molybdenum in the majority of HMXOR (Godber *et al.*, 1997). Further studies suggested that molybdo-XOR is expressed in a tissue-specific manner in humans, with preparations from liver (Krenitsky *et al.*, 1986; Moriwaki *et al.*, 1993) and small intestine (Sarnesto *et al.*, 1996) showing specific activity levels similar to that of BMXOR (1.8 U/mg (Krenitsky *et al.*, 1986) 960 mU/mg (Moriwaki *et al.*, 1993)), whilst XOR in human heart appeared to be of low activity (Abadeh *et al.*, 1993), like HMXOR (4.3 mU/mg) (Abadeh *et al.*, 1992). The differences in activity seen in human tissues are likely to reflect molybdenum content. This, in turn, could depend on differences in molybdopterin synthesis and post-translational incorporation into XOR or on variations in XOR primary sequence, with different abilities to coordinate molybdenum. The primary sequences of human liver* and small intestine XDH have been determined by several workers (Ichida *et al.*, 1993; Saksela and Raivio, 1996; Yamamoto *et al.*, 2001) and are identical.

In order to determine whether the low levels of molybdenum seen in human milk XOR reflect an alternative primary sequence to that observed in liver and small intestine, attempts were made to sequence human mammary gland XOR. A nearly complete sequence was obtained by Briggs (Briggs, 1997)

---

* It should be noted that the original human liver XDH sequence reported by Ichida and co-workers (1993) differed from that obtained from human small intestine at 5 bases. However, this sequence has been recently (Sep 2000) updated in the NCBI database and is now identical to the sequence reported for small intestine.

from Clonetech mammary gland cDNA that was identical to that of small intestine and liver. This sequence (tHMXO) lacked the 5' region (1-661, liver cDNA sequence numbering). It also contained some ambiguities at the 3' end (3506, 4031-4057, liver numbering), and in a central region (1618-1630, liver numbering).

Briggs (Briggs, 1997) was unable to sequence the 5' end of mammary gland XDH cDNA by using primers designed to the human liver XDH cDNA. Hence it was postulated that the 5' sequences of the two cDNAs could be different.

It was decided to use RACE (Rapid Amplification of cDNA Ends), a method that relies on the capping of all cDNA fragments at the 5' or 3' ends with a known sequence. This sequence then allows the use of a cap primer and a gene specific primer to the known internal sequence, and hence does not require knowledge of the 5' sequence for successful PCR.

Commercial RACE cDNA that has been capped is available for a variety of tissues including mammary gland. However, these cDNAs are almost exclusively from tumour tissue in which expression of XDH is reduced or absent (Pritsos, 2000). It was, therefore, decided, to generate capped cDNA from mRNA extracted from a permanent human mammary gland epithelial cell line, HB4a. These cells maintain the characteristic morphology of epithelial cells and express XDH at varying levels, depending on the point of culture (Fig. 3.1).

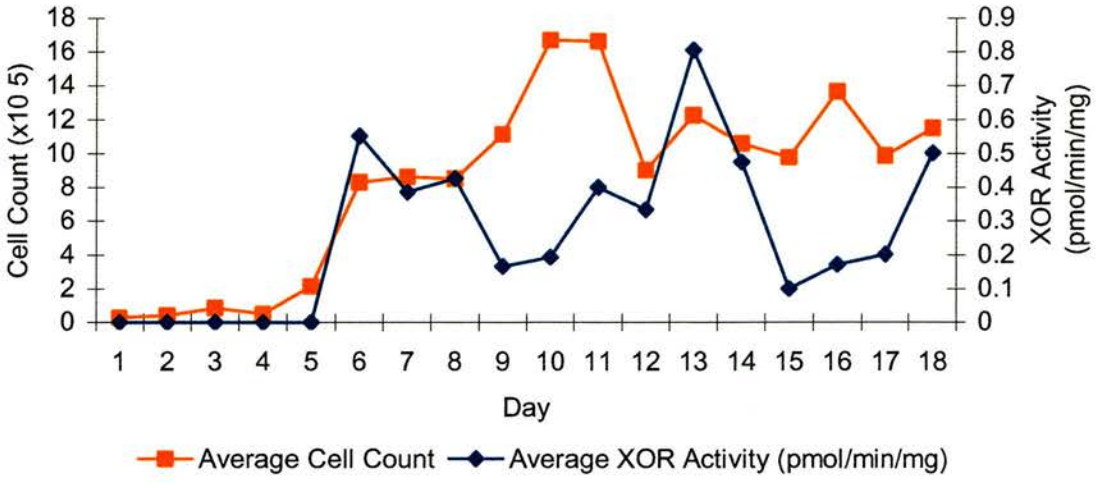

Figure 3.1: Growth curve of HB4a cells showing cell number and XDH activity. Figure kindly supplied by Catherine Hoare.

This chapter describes the determination of the 5' cDNA sequence of human mammary gland XOR and resolution of the central region ambiguities.

3.2.1 Materials

HB4a cells are a human mammary epithelial cell line, conditionally immortalised by transfection with SV40 virus and kindly donated by Dr. T. Kamalati and Prof. B. Gusterson of the Institute for Cancer Research, Royal Cancer Hospital, Sutton, UK. HB4a cells were cultured by Catherine Hoare at the University of Bath, UK. TriPure™ Isolation reagent, Expand High Fidelity PCR System and the 5'/3' RACE Kit were obtained from Roche Molecular Biochemicals, East Sussex UK. Oligonucelotide primers were obtained from MWG Biotech AG, Ebersberg, Germany. The Dynabeads mRNA Purification Kit was obtained from Dynal, Wirral, UK. Qiagen Gel extraction Kits were obtained from Qiagen, West Sussex, UK. All other reagents were obtained from Sigma, Dorset, UK.

3.2.2 Instruments

PCR reactions were carried out using a Minicycler™, MJ Research, Waltham, MA, USA.

3.3 General methods

3.3.1 Agarose gel electrophoresis

Visualisation of Polymerase Chain Reaction (PCR) products was carried out using horizontal agarose gel electrophoresis. A 1% (w/v) TAE-agarose gel containing ethidium bromide (50 μg) was poured. Samples were mixed with loading dye (6x dye contained: 0.25 % w/v bromophenol blue, 0.25 % w/v xylene cyanol and 40 % w/v sucrose) and gels were run in TAE buffer [50 x buffer contained: Tris base (242 g), glacial acetic acid (57.1 ml) and 0.5 M EDTA (100 ml) per litre]. PCR products were visualised under UV light and were extracted from the gel using a Qiagen Gel Extraction kit according to the manufacturers' instructions.

3.3.2 PCR

Target cDNAs were amplified using the PCR method (Saiki *et al.*, 1985). Template cDNA was incubated with primers to the target sequence, a thermostable high fidelity DNA polymerase, dNTPs, and a Mg^{2+}-containing buffer in a thermocycler. The temperature of the reaction was then cycled to allow sequential denaturation of DNA, primer annealing and template extension (Fig. 3.2). With each cycle, the number of target cDNA fragments doubles and, at the end of the reaction, the target cDNA is the predominant species in solution. PCR reactions (50 μl or 100 μl) were carried out in 500 μl thin walled eppendorf tubes under mineral oil to prevent sample evaporation.

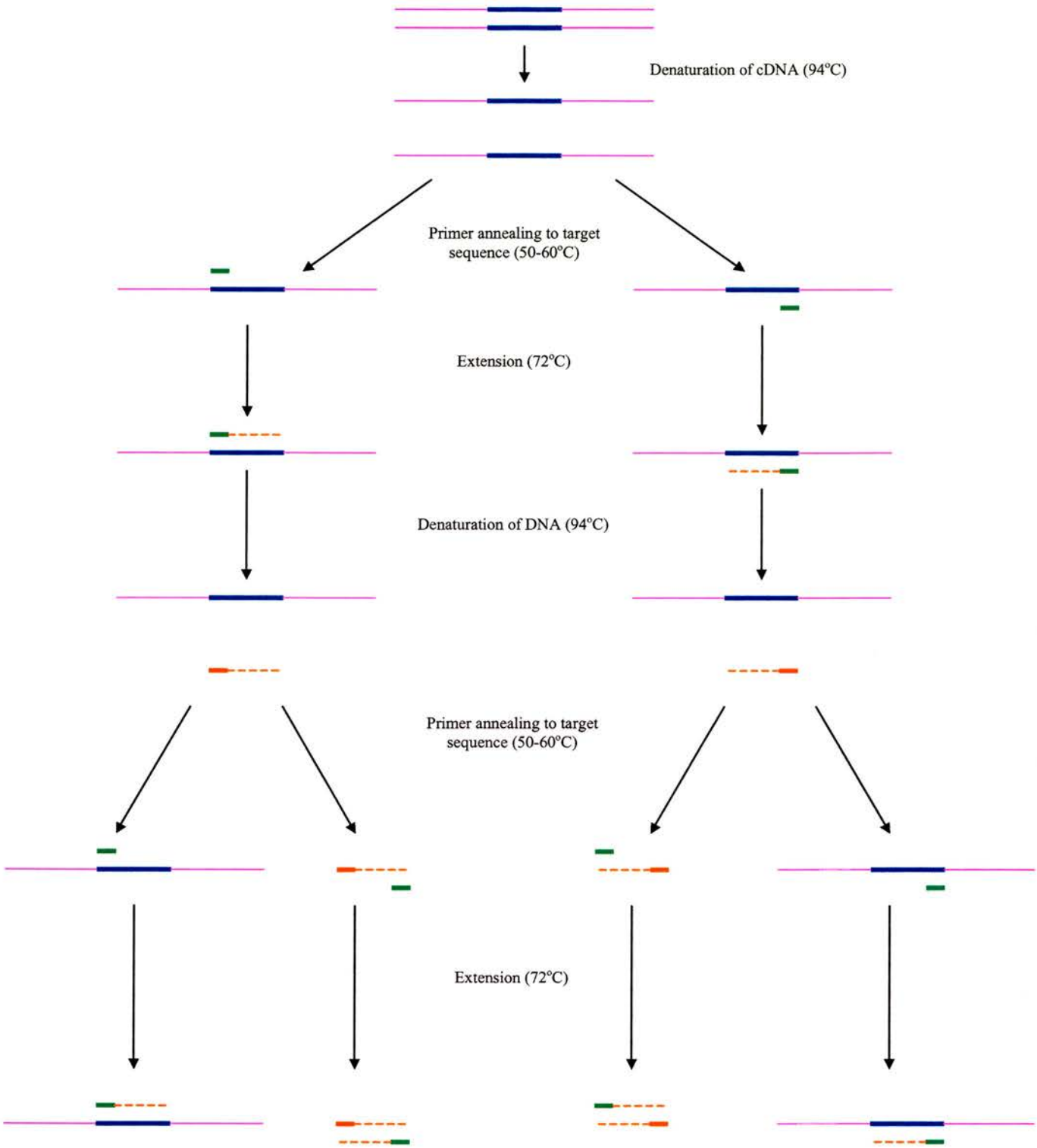

Figure 3.2: Schematic diagram showing two cycles of a PCR reaction. cDNA containing the target sequence is denatured at high temperature. The temperature is then reduced to allow the primers to bind to their target sequence. Template extension then takes place at a higher temperature, before redenaturation. The whole process is dependent on the use of thermostable DNA polymerases which are able to withstand the degree and variation in temperature over the period of the reaction.

3.3.3 Sequencing

PCR products were sequenced by Alex Houston using an ABI PRISM™ 377 DNA Sequencer (Perkin-Elmer) at the St. Andrews University DNA Sequencing Unit. Samples containing 250-300 μg of PCR product and 3-5 pmol of primer in water (total volume 12 μl) were submitted for sequencing. PCR products were quantified using horizontal agarose gel electrophoresis with markers of known quantity.

3.3.4 Computing programmes used

The **Blast** server at the NCBI (http://www.ncbi.nlm.nih.gov/BLAST/) was used to generate alignments between sequence pairs and to search for sequence matches to primers and sequences obtained from PCR products.

The **GCG** (http://www.gcg.com/products/wis-package.html) suite (Wisconsin Package™, SeqLab®, SeqWeb®, Wisconsin Package Version 8.0.1-Unix Genetics Computer Group (GCG), Madison, Wisc.) was used for a variety of tasks, including the generation of multiple sequence alignments, primer design and generation of full length sequences from overlapping PCR fragments.

Chromas© (Technelysium Pty Ltd.) was used to visualise and edit DNA sequences obtained from PCR products.

3.4 Methods

3.4.1 Isolation of total RNA from HB4a cells

HB4a cells were harvested at confluence when the activity of XDH is at its highest (Fig 3.1). Total RNA was extracted from the cells using TriPure™ Isolation Reagent, essentially according to the manufacturers' instructions. In brief 20 x 10^6 HB4a cells were washed and pelleted in PBS. TriPure™ reagent (2ml) was added to the pelleted cells in a 15 ml glass corex tube and the cells were lysed by repeated pipetting. The lysate was incubated at room temperature for 5 min before the addition of chloroform (0.4 ml) after which the tube was capped and shaken vigorously for 15 s. After a further incubation at room temperature for 15 min, the sample was centrifuged at 9,000 x g for 25 min at 4 °C. Three phases were formed and the upper clear aqueous phase containing the RNA was transferred to a clean tube. Isopropanol (1 ml) was added and the tube was mixed thoroughly by being inverted several times. The sample was then incubated at room temperature for 10 min to allow the RNA to precipitate before being centrifuged at 9,000 x g for 20 min at 4 °C. The supernatant was discarded and the RNA washed by vortexing in 75 % ethanol (2 ml). After centrifugation at 7,500 x g for 5 min at 4 °C, the supernatant was discarded and the RNA left to air-dry for 10 min. The RNA was resuspended in sterile RNase-and-DNase free water (100 µl) by passing the solution through a pipette tip several times to loosen the pellet and then incubating at 55-60 °C for 15 min.

3.4.2 Isolation of mRNA from total HB4a RNA

mRNA was isolated from total HB4a RNA using the Dynabeads mRNA Purification Kit. This technique uses Oligo-$(dT)_{25}$ bound to magnetic beads in order to purify poly A^+ RNA from total RNA. A magnetic particle concentrator (MPC) is used to concentrate all the beads in one part of the tube allowing removal of the supernatant. The Dynabeads mRNA purification kit was used in accordance with the manufacturers' instructions. In brief, Dynabeads-Oligo$(dT)_{25}$ (250 µl) were washed in Binding buffer (20 mM Tris-HCl, pH 7.5 containing 1 M LiCl and 2mM EDTA) (100 µl) and then resuspended in Binding buffer (100 µl). Total HB4a cell RNA (100 µl) was then added and mixed at room temperature for 5 min. The supernatant was removed and the beads washed twice with Washing buffer (10 mM Tris-HCl, pH 7.5 containing 0.15 M LiCl and 1 mM EDTA) (200 µl). mRNA was eluted from the magnetic beads in 10 mM Tris-HCl, pH 7.5 (20 µl) by incubating at 65 °C for 2 min, then placing the tube immediately into the MPC and removing the supernatant rapidly. mRNA not used immediately was stored at -70 °C.

3.4.3 Isolation of mRNA from cytoplasmic total RNA

HB4a cells were harvested at confluence as before (3.4.1) and lysed gently in the presence of a non-ionic detergent to release cellular RNA without lysing the nucleus. The cells were washed in PBS and then resuspended in lysis buffer (10 mM Tris, pH 7.8 containing 10 mM NaCl, 10 mM $MgCl_2$ and 1% Triton X-100) (4 ml) and mixed gently. The lysed mixture was then spun for 3

min at 13,000 x g to remove cell debris and the pellet discarded. TriPure™ reagent (2ml) was added to the supernatant and RNA isolated as described in Section 3.4.1. mRNA was then isolated from total cytoplasmic RNA using the Dynabeads mRNA Purification Kit, described above (3.4.2).

3.4.4 Rapid amplification of 5' cDNA ends (5' RACE)

5' RACE allows the amplification of unknown sequences at the 5' end of mRNA in the following manner. First strand cDNA is synthesised from the mRNA using a gene specific primer (SP1), the resulting 3' end is then capped with a poly A tail using a terminale transferase. Tailed target cDNA is then amplified by PCR using a second genespecific primer (SP2) and an oligo dT anchor primer (Fig 3.3). A second round of PCR is then carried out using a third gene specific primer (SP3) and a PCR anchor primer (Fig 3.3) to produce a largely homogeneous product. The sequence of reactions is summarised in Fig. 3.4.

The 5'/3' RACE kit from Boehringer-Mannheim was selected. This kit uses AMV reverse transcriptase for the first strand synthesis because of its heat stability. This allows the first strand synthesis reaction to be carried out at 55 ^{o}C (instead of the more normal 42 ^{o}C) encouraging reverse transcription to proceed through regions of difficult RNA 2^{o} structure. It also contains control neo-RNA (an *in vitro* transcribed RNA from the neomycin resistance gene) and primers which can be used as controls at the various stages of the reaction.

Oligo d(T)-anchor primer: V=A,C,G
5'-GACCACGCGTATCGATGTCGACTTTTTTTTTTTTTTTV-3'

PCR anchor primer:
5'-GACCACGCGTATCGATGTCGAC-3'

Figure 3.3: Sequences of the Oligo d(T)-anchor primer and the PCR anchor primer supplied with the 5'/3' RACE kit.

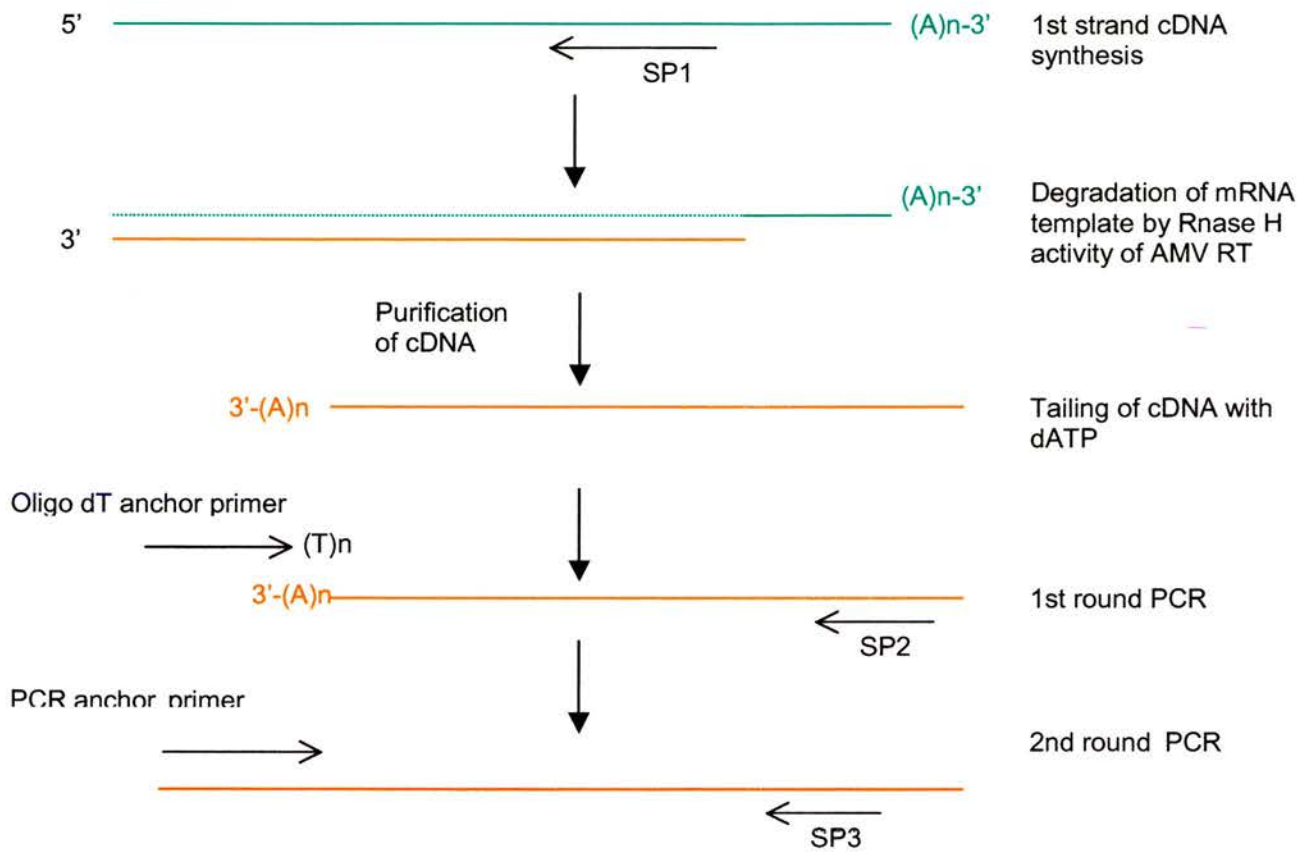

Figure 3.4: Schematic summary of the 5' RACE protocol, mRNA is in green, cDNA in red

5' RACE and control reactions were carried out according to the manufacturers' instructions. The steps are briefly described below.

3.4.4.1 First strand cDNA synthesis

HB4a mRNA (5μl) was combined with cDNA Synthesis buffer (250 mM Tris-HCl, pH 8.5 containing 40 mM $MgCl_2$, 150 mM KCl and 5 mM DTT) (4 μl), deoxynucleotide mixture (2 μl), SP1 primer (10-20 pmol) (1 μl), AMV reverse transcriptase (20 U, 1μl) and made up to a final volume of 20 μl with sterile water. The tube was mixed and incubated at 55 °C for 60 min, then at 65 °C for 10 min. The resulting cDNA was purified using the High Pure PCR Product Purification Kit according to the instructions contained in the 5'/3' RACE pack insert and eluted in 10 mM Tris-HCl, pH 8.03 (50 μl).

Control reactions were performed according to the 5'/3' RACE pack insert.

A modification of this protocol was used to improve 5' CDNA synthesis. In this modified version, the mRNA and SP1 primer were heated to 94 °C for 5 min before being chilled rapidly by plunging into iced water where the other reaction components were added. After this, the rest of the reaction proceeded as above with incubation at 55 °C for 60 min.

3.4.4.2 Tailing reaction of cDNA

Purified cDNA (19 μl) was combined with of Reaction buffer (100 mM Tris-HCl, pH 8.3 containing 15 mM $MgCl_2$ and 500 mM KCl) (2.5 μl) and 2 mM dATP (2.5 μl) and incubated at 94 °C for 3 min. It was then chilled rapidly on ice and terminale transferase (10 U, 1 μl) added. After mixing the reaction mixture was then incubated at 37 °C for 30 min before 10 min incubation at 70 °C to inactivate the terminale transferase. The sample was then chilled on ice.

3.4.4.3 PCR

In the first PCR reaction, dA-tailed cDNA (5 µl) was combined with oligo dT-anchor primer (1 µl), SP2 (10-20 pmol) (1 µl), deoxynucleotide mixture (1 µl) and Expand HF buffer (5 µl), containing 15 mM $MgCl_2$ in a final aqueous volume of 49.5 µl. Expand High Fidelity PCR system DNA polymerase mix (1.75 U, 0.5 µl) was added after 2 min incubation at 94 °C. The PCR protocol is given in Table 3.1.

In the 2nd PCR reaction, 1 µl of 1st PCR product mix was combined with 1 µl of PCR anchor primer, 1 µl of SP3 (10-20 pmol), 1 µl of deoxynucleotide mix and 5 µl of Expand HF buffer, 10x with 15 mM $MgCl_2$ in a final volume of 49.5 µl with water. 0.5 µl of Expand DNA polymerase mix was added after two minutes incubation at 94 °C. The PCR reaction cycle was as described in table 3.x.

Control reactions were performed according to the 5'/3' RACE pack insert.

Products of the second PCR reaction and the control reactions were visualised using TAE-agarose gel electrophoresis on a 1 % gel.

1	2 minutes	94 °C	
	Pause		*add Expand DNA polymerase mix*
2	15 seconds	94 °C	
3	30 seconds	60 °C	
4	40 seconds	72 °C	
5	*Cycle 2-4 10 times*		
6	15 seconds	94 °C	
7	30 seconds	60 °C	
8	40 seconds	72 °C	+ 20 seconds/cycle
9	*Cycle 6-8 25 times*		
10	7 minutes	72 °C	

Table 3.1 PCR protocol for 1st and 2nd PCR reactions.

3.5 Results of the sequencing of human mammary gland XDH

Three gene specific primers were designed for the 5' RACE protocol (Fig. 3.5) using the mammary gland sequence already derived by Briggs (Briggs, 1997). The primers were designed to bind well into the known sequence, in order to ensure that if the 5' end of the gene was indeed different, there would be sufficient known mammary XDH sequence to accurately identify the PCR products as XDH.

SP1-a 5'-CTGGGTCTTCATGGTGTTCTGTGTAG-3' (3' end binds human liver XDH at 2380)
SP2-a 5'-GTAGCGAGGAATGTCGTCACAGTACA-3' (3' end binds human liver XDH at 1858)
SP3-a 5'-GGGTCCAGTTTACCACAGTTGTCTTC-3' (3' end binds human liver XDH at 1680)

Figure 3.5: Sequences of the gene specific primers used in the 5' RACE. All primers had a Tm of 64.8 °C and were designed using the liver sequence and the mammary gland sequence already determined (Briggs, 1997). 1 µl of primer contained: SP1-a - 16.6 pmol, SP2-a - 18.7 pmol, SP3-a - 18 pmol.

A product of size 1.6 kb was expected from the primers, and a product of approximately 1 kb (xdh1) was obtained (Figure 3.6).

Figure 3.6
1 % TAE-agarose gel of the product of the 2nd RACE PCR. Markers used are a 1 kb DNA ladder (Gibco BRL). These markers include a mass reference band at 1613b which contains 100 ng DNA, indicating that the PCR band contains ~ 500 ng DNA.

This was sequenced as described, using SP3-a as the reverse primer and a 526 bp sequence obtained. Using the BLAST search programme it was observed that the first 333 bases of xdh1 matched human liver XDH cDNA, however, the entire 526 bp matched the XDH genomic sequence (figure 3.7). This indicated that the HB4a cell mRNA contained incompletely spliced mRNA.

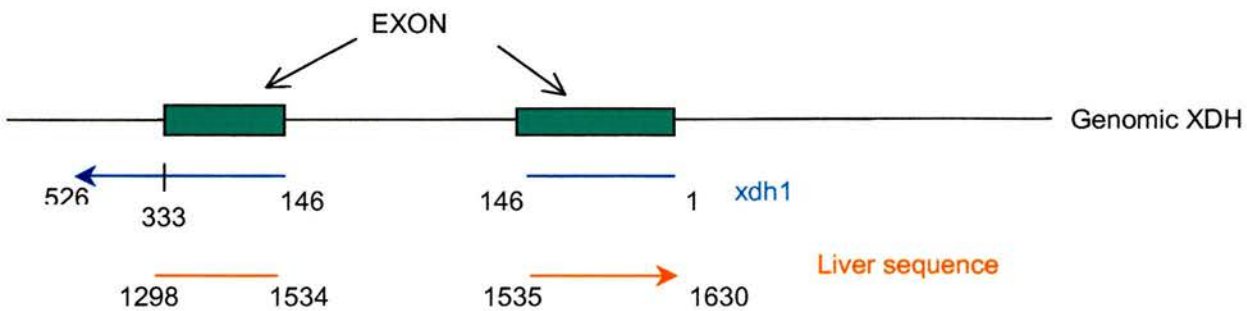

Figure 3.7: Schematic diagram showing the relationship between the human liver XDH sequence, the genomic sequence and xdh1. It can be seen that xdh1 crosses one exon break (1534-1535, liver) but deviates from the correctly spliced cDNA from 333 (xdh1) onwards.

A new set of RACE primers were designed (Fig. 3.8) to the mammary gland sequence derived by Briggs (1997) beyond the point where xdh1 deviated from the human liver cDNA and continued with intronic sequence and a new 5' RACE was carried out. The 5' RACE protocol was also modified slightly, introducing an incubation at 94 °C of the mRNA and SP1 before first strand cDNA synthesis in order to relax any secondary structure in the 5' region of the gene. It was hoped that this would further improve the ability of the AMV RT to proceed to the 5' end of the mRNA.

SP1-b TGTAGCCAGGGAAGAAGGTG
SP2-b CTTGCTTCCCAGCAAACCAG
SP3-b ATGCCAATCTCCGTGTTCCC
SP4 ACACGCTCCCCTTCAAATCG

Figure 3.8: New primers designed beyond the exon break for the 2nd 5' RACE reaction. 1 µl of primer contained: SP1-b - 13.5 pmol, SP2-b - 12.5 pmol, SP3-b - 14.2 pmol.

From the new 5' RACE primers, a product size of ~ 700 bp was expected, a slightly lighter product (xdh2) of ~ 500 bp was obtained (Fig. 3.9) and 460 bp sequenced using an internal primer designed to the already obtained mammary gland sequence, SP4 (Fig. 3.8), before the poly A+ 5' tail was reached.

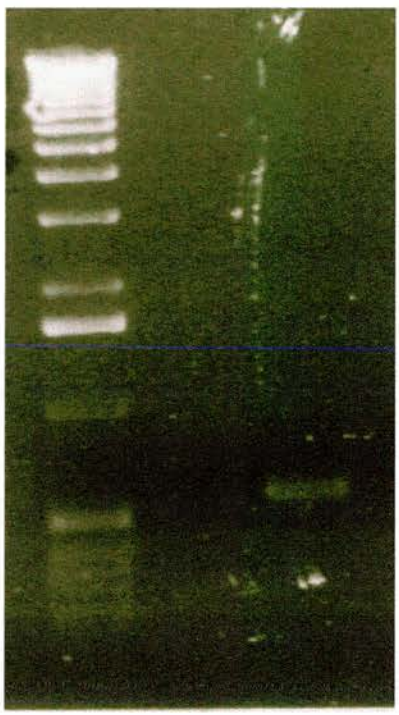

Figure 3.9:
1% TAE-agarose gel showing PCR product xdh2, obtained from the 2nd 5' RACE. Markers are the 1kb DNA markers described above.

This product aligned to the human liver cDNA sequence (268-728) and did not contain any intronic sequences. However, it appeared that the cDNA was truncated at the 5' end, as the sequence obtained from xdh2 ran into the poly A+ cap introduced in the 5' tailing reaction. It appeared to be possible that an intact copy of the 5' end of XDH was present in the mRNA but was truncated at the 3' end so that the binding region of the primers thus far designed was missing. Accordingly, a further set of 5' RACE primers was designed (Fig. 3.10) using the new sequence obtained from xdh2 and the 5' RACE reaction

was again repeated. The extra heating step at the start of first strand cDNA synthesis was again used.

SP1-c ATCCACCATCCCTGGCAAAG
SP2-c AGCGGCACAGATTTCCTTGG
SP3-c CACTGCAACATGGTGCAAGG

Figure 3.10: 5' RACE primers designed using the xdh2 sequence obtained in the second RACE. 1 µl of primer contained: SP1-c - 12.75 pmol, SP2-c -12.2 pmol, SP3-c - 14.3 pmol.

The expected product size using the new primers was 280 bp. A fragment of ~ 300 bp (Fig. 3.11) was obtained (xdh3) and sequenced using SP3-c as a sequencing primer. A 259 bp sequence was obtained that aligned exactly to the beginning of the coding region of human liver XDH cDNA (23-282).

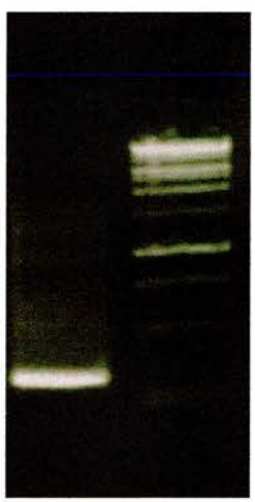

Figure 3.11:
1% TAE-agarose gel showing PCR product xdh3, obtained from the 3rd 5' RACE. Markers are the 1kb DNA markers described above.

The sequences were combined using the GCG package and ambiguous bases resolved by resequencing those regions. This produced a clear sequence for the 5' region of human mammary gland XDH, and resolved the ambiguities in the sequence obtained by Briggs (Briggs, 1997) (Fig. 3.12). Alignment of the newly derived 5' mammary gland XDH sequence with that of XDH from small intestine and liver shows that they are identical.

```
xdh1        >                                   GAAGGACTGTCAGGTAGAACTTGAAGAAGAAG 32
xdh1 reseq  >          GGTTCTCTTGGCCCAGCTTCTGAAGGACTGTCAGGTAGAACTTGAAGAANAAG 53
Briggs seq  < ..TCTTCCAGGTTCTCTTGGCCCAGCTTCtrAArgactkTcaGGTAGAACTTGAAGAAGAAG 1062
Consensus   >   TCTTCCAGGTTCTCTTGGCCCAGCTTCTGAAGGACTGTCAGGTAGAACTTGAAGAAGAAG 1576

xdh1        > CTGAGGGTGAGGGTGCACCGGAAGTCCACCATGCCACCAGGGGCATCGGGAGGCAGATGC 92
xdh1 reseq  > CTGAGGGTGAGGGTGCACCGGAAGTCCACCATGCCACCAGGGGCATCGGGAGGCAGATGC 113
Briggs seq  < CTGAGGGTGAGGGTGCACCGGAAGTCCACCATGCCACCAGGGGCATCGGGAGGCAGATGC 1122
consensus   > CTGAGGGTGAGGGTGCACCGGAAGTCCACCATGCCACCAGGGGCATCGGGAGGCAGATGC 1516

xdh1        > AGCTCCTCTGCCAGTCCTGCACACACGTCCTGCAGCAGCTCCTCCTTCCAGAGCTTGGAA 152
xdh1 reseq  > AGCTCCTCTGCCAGTCCTGCACACACGTCCTGCAGCAGCTCCTCCTTCCAGAGCTTGGAA 173
Briggs seq  < AGCTCCTCTGCCAGTCCTGCACACACGTCCTGCAGCAGCTCCTCCTTCCAGAGCTTGGAA 1182
consensus   > AGCTCCTCTGCCAGTCCTGCACACACGTCCTGCAGCAGCTCCTCCTTCCAGAGCTTGGAA 1456

xdh1        > AGCTGCCTCTGAGTGGTCTTGAGGGCTGAGATGGTTCTGTTGGCCATTCCACCATAGCAA 212
xdh1 reseq  > AGCTGCCTCTGAGTGGTCTTGAGGGCTGAGATGGTTCTGTTGGCCATTCCACCATAGCAA 233
Briggs seq  < AGCTGCCTCTGAGTGGTCTTGAGGGCTGAGATGGTTCTGTTGGCCATTCCACCATAGCAA 1242
consensus   > AGCTGCCTCTGAGTGGTCTTGAGGGCTGAGATGGTTCTGTTGGCCATTCCACCATAGCAA 1396

xdh1        > AGGGCCAGCTCCTGTACCTCTGTGGTTCCTGGCTTGAATAAAACTCTCATGCCACTGGTT 272
xdh1 reseq  > AGGGCCAGCTCCTGTACCTCTGTGGTTCCTGGCTTGAATAAAACTCTCATGCCACTGGTT 293
Briggs seq  < AGGGCCAGCTCCTGTACCTCTGTGGTTCCTGGCTTGAATAAAACTCTCATGCCACTGGTT 1302
consensus   > AGGGCCAGCTCCTGTACCTCTGTGGTTCCTGGCTTGAATAAAACTCTCATGCCACTGGTT 1336

xdh1        > ACCTTGGCAATGTCATCTTCTCTCCGGGAGGCCTGCTTGAATGCTGAGAAATACTCCNCC 332
xdh1 reseq  > ACCTTGGCAATGTCATCTTCTCTCCGGGAGGCCTGCTTGAATGCTGAGAAATACTNCCCN 353
Briggs seq  < ACCTTGGCAATGTCATCTTCTCTCCGGGAGGCCTGCTTGAATGCTGAGAAATACTCCCCC 1362
consensus   > ACCTTGGCAATGTCATCTTCTCTCCGGGAGGCCTGCTTGAATGCTGAGAAATACTCCCCC 1276

xdh1        > T                                                           333
xdh1 reseq  > T                                                           354
Briggs seq  < TCCCTGCTGTAGGGGATCTCTATGGAGAGCAGTATCTCCTCCGGGCTCAGCAGGGTCTTT 1422
consensus   > TCCCTGCTGTAGGGGATCTCTATGGAGAGCAGTATCTCCTCCGGGCTCAGCAGGGTCTTT 1216

Briggs seq  < CTGTAGCCAGGGAAGAAGGTGTGGTCCATCTGGACAGTTCTCCTGGTGCCTCTGGACACA 1482
consensus   > CTGTAGCCAGGGAAGAAGGTGTGGTCCATCTGGACAGTTCTCCTGGTGCCTCTGGACACA 1156

Briggs seq  < AGTGTCAGCTTGGCCCCACTGGCCATGAACACGGGGTTGAGGTCGGAGATGGGGCTGGCA 1542
consensus   > AGTGTCAGCTTGGCCCCACTGGCCATGAACACGGGGTTGAGGTCGGAGATGGGGCTGGCA 1096

Briggs seq  < GTGATGATGTTCCCTCCAACGGACGCCACAGACTTGACTTGCTTCCCAGCAAACCAGCGC 1602
consensus   > GTGATGATGTTCCCTCCAACGGACGCCACAGACTTGACTTGCTTCCCAGCAAACCAGCGC 1036

Briggs seq  < AGCTGCTCCAGGACCCCTCTGAACACCTCTGTCTTTTGGGCAGGAAGCTTAGCAACAGCA 1662
consensus   > AGCTGCTCCAGGACCCCTCTGAACACCTCTGTCTTTTGGGCAGGAAGCTTAGCAACAGCA 976

Briggs seq  < TCCACCAGGGTTTTTTCCACAATGCTCAGGGGGCAAGCAGCTCCAAAGGAGATACCGTCG 1722
consensus   > TCCACCAGGGTTTTTTCCACAATGCTCAGGGGGCAAGCAGCTCCAAAGGAGATACCGTCG 916
Briggs seq  < GGTCCATGTTCTACCGAATTCAGCTCAGGGATCCAGGCTGGGCAGACAATCATAGGAAAC 1782
consensus   > GGTCCATGTTCTACCGAATTCAGCTCAGGGATCCAGGCTGGGCAGACAATCATAGGAAAC 856

Briggs seq  < AGCATATTCTTGAACTTCATCTCAATGCCAATCTCCGTGTTCCCCACGACCAGCTTGGCG 1842
consensus   > AGCATATTCTTGAACTTCATCTCAATGCCAATCTCCGTGTTCCCCACGACCAGCTTGGCG 796

Briggs seq  < TCAGGGTGCTGAGCCTTGAGGTCCAGCAGCTCCTTGAGGGTTGAGGCCTGTATCCACGTC 1902
consensus   > TCAGGGTGCTGAGCCTTGAGGTCCAGCAGCTCCTTGAGGGTTGAGGCCTGTATCCACGTC 736

xdh2        >                                   CGAGGAGTGTCTTTCAGCCTCAGCAACTCT 43
Briggs seq  < ACACGCTCCCCTTCAAATCGCAGCTGCTTCCGAGGAGTGTCTTTCAGCCTCAGCAACTCT 1962
consensus   > ACACGCTCCCCTTCAAATCGCAGCTGCTTCCGAGGAGTGTCTTTCAGCCTCAGCAACTCT 676

xdh2        > GGGGGAAAAATGGGCTCCTGGGTTGGATCCAGGGGCGTGAACTCCTCTGGTTTGAATAAA 103
Briggs seq  < GGGGGAAAAATGGGCTCCTGGGTTGGATCCAGGGGCGT                        2000
consensus   > GGGGGAAAAATGGGCTCCTGGGTTGGATCCAGGGGCGTGAACTCCTCTGGTTTGAATAAA 616

xdh2        > GATGGCGAGAGGCTGACTGAGTGGTCTTTCTTCTGGTTCATGCAGCAATTTGGATTATTC 163
consensus   > GATGGCGAGAGGCTGACTGAGTGGTCTTTCTTCTGGTTCATGCAGCAATTTGGATTATTC 556

xdh2        > CCATCTCCTCCACAGCATCCACCATCCCTGGCAAAGGTCCGGAAGCCCTGGAGGATGGGT 223
consensus   > CCATCTCCTCCACAGCATCCACCATCCCTGGCAAAGGTCCGGAAGCCCTGGAGGATGGGT 496

xdh2        > CTGTAGCCTGTGCAGCGGCACAGATTTCCTTGGAAGGCATTCTCAATCTCCTCCATGGTG 283
consensus   > CTGTAGCCTGTGCAGCGGCACAGATTTCCTTGGAAGGCATTCTCAATCTCCTCCATGGTG 436
```

Figure 3.12 This figure continues on the following page.

```
xdh2       > GGCTCGGGCTGATTCCGGAGCAGTGTGTACATACTCATGACGATGCCAGGGGTGCAGAAC 343
consensus  > GGCTCGGGCTGATTCCGGAGCAGTGTGTACATACTCATGACGATGCCAGGGGTGCAGAAC 376

xdh2       > CCGCACTGGGAGCCGTGGCTTTTGGCAATTCTCTCCTGCACAGGATGCAGCCTCGTCTTG 403
consensus  > CCGCACTGGGAGCCGTGGCTTTTGGCAATTCTCTCCTGCACAGGATGCAGCCTCGTCTTG 316

xdh3       >                                                       GGCC 4
xdh2       > GTGCTTCCTATTCCTTCCACAGTTGTCACTGCAACATGGTGCAAGGAGCAGATGGGGGCC 463
consensus  > GTGCTTCCTATTCCTTCCACAGTTGTCACTGCAACATGGTGCAAGGAGCAGATGGGGGCC 256

xdh3       > AGGCNGGCATTGGCAGAAAAGTGGACGATCTTGTTCTGCAGACGATCATACTTGGAGAGC 64
xdh2       > AGGCAGGCATT                                                  474
consensus  > AGGCAGGCATTGGCAGAAAAGTGGACGATCTTGTTCTGCAGACGATCATACTTGGAGAGC 196

xdh3       > ATCACTGTGCAAGCCCCGCAGCCCCCCTCTCCACAGCCGAGCTTGGTTCCACTCAGCCCC 124
consensus  > ATCACTGTGCAAGCCCCGCAGCCCCCCTCTCCACAGCCGAGCTTGGTTCCACTCAGCCCC 136

xdh3       > AACTTTCTTCTCAGGTAGGCCAAAAGGGTTGTCTCTGGATCTGCATTTTTCTCCACCACC 184
consensus  > AACTTTCTTCTCAGGTAGGCCAAAAGGGTTGTCTCTGGATCTGCATTTTTCTCCACCACC 76

xdh3       > TTTCTGCCATTCACAAAGAAAACCAATTTGTCTGCTGTCATTGTCACAGGTTGGGGTCCC 244
consensus  > TTTCTGCCATTCACAAAGAAAACCAATTTGTCTGCTGTCATTGTCACAGGTTGGGGTCCC 16

xdh3       > CGAACTCCAGGTACC 259
consensus  > CGAACTCCAGGTACC 1
```

Figure 3.12: Combination of xdh1, xdh2 & xdh3 to produce a full sequence for the 5' end of human mammary XDH. Sequence runs from midway through the mammary gland sequence to the 5' end. The consensus sequence is in red.

3.6 Discussion

The work described in this chapter was carried out in order to determine the basis of differences in XOR activity observed in different human tissues. Two possibilities exist, one that a single XOR transcript is expressed in all cells, and post-translational modifications account for the observed differences in activity. The alternative is that "high" and "low" activity XOR sequences exist, that are expressed in different levels in the various tissues. As stated in the introduction to this chapter, a near complete cDNA sequence of human mammary gland XOR cDNA was obtained by Briggs which was identical to the sequence of human small intestine and liver XOR. This sequence has now been completed (apart from 9 unresolved bases at the 3' end) and shown to be identical to that of small intestine and liver XDH, suggesting that regulation of XOR activity does indeed occur at a post-translational level.

The complete identity of the sequenced mammary gland cDNA to that of the small intestine and liver still does not rule out the possibility of an alternative low-level "low" activity transcript of XOR in human cells. During the course of this work, the genomic sequence of human XOR was deposited in the NCBI as part of 2 larger BAC sequences (AL121654, AL121657) (Hazan *et al.*, 1999). These sequences show the presence of very large introns in the 5' region of the XOR gene which could conceivably contain an alternative exon. This possibility was investigated by analysing possible translations of the 5' introns (1 & 2) of the genomic sequence using the various utilities of the GCG program suite and the BLAST search server at NCBI. No potential sequences

possessing any homology to XOR, or indeed to anything else, seemed to be present, suggesting strongly that there is a single XOR transcript coded for in the genome.

It is also possible that the XOR expressed by the HB4a cell line is not that truly present *in vivo* in the mammary gland and there remains an alternative "low" activity XOR sequence which we have not yet succeeded in isolating. In this context it is worth mentioning very recent work by Choudhury and colleagues (Personal Communication) on purified human liver XOR, which indicates that the activity of human liver XOR in its pure state is considerably lower than that reported in cell extracts or purified enzyme by other workers (Krenitsky *et al.*, 1986; Parks and Granger, 1986; Sarnesto *et al.*, 1996). These very recent results suggest the possibility that human tissues traditionally regarded as being "high" activity may in fact contain much less XOR activity than previously thought. Indeed, the only other purifications of human liver XOR reported (Krenitsky *et al.*, 1986; Moriwaki *et al.*, 1993) used active site affinity ligands to obtain pure XOR. Such a procedure, unlike the immunoaffinity methods used by Choudhury and colleagues, would, of course, result in the purification only of active XOR and the loss of known inactive XOR species such as demolybdo-XOR. This artificial enrichment of fully active molybdo-XOR in the preparation of Krenitsky *et. al.* could well account for their reported high XOR activity in liver. As yet, no determination of molybdenum content of the immunoaffinity-purified XOR has been carried out.

Chapter 4

Solution of the Crystal Structure of Human Milk Xanthine Oxidoreductase

4.1 Introduction

Crystals of BMXOR were first reported in 1955 (Avis, Bergel, and Bray, 1955), produced during a recrystallization step in the last stage of purification of the enzyme. However, it was not until 1993 that Eger and coworkers (Eger *et al.*, 1993) reported diffraction from BMXOR crystals to 3.5 Å. Despite this, no solution was reported, largely due to the lack of a good model for molecular replacement. In 1998 diffraction from two rat liver XOR crystal forms was reported to 2.6 Å (Carvalho *et al.*, 1998) and similar problems in finding a solution were encountered (Carvalho, personal communication), despite the publication of a related structure, MOP, in 1995 (Romão *et al.*, 1995).

The crystal structure of BMXOR was eventually obtained very recently at a resolution of 2.1 Å (Enroth *et al.*, 2000) using similar techniques to those used to solve the structure of another related enzyme, CODH (Dobbek *et al.*, 1999), combining a weak molecular replacement solution found using the MOP structure (Romão *et al.*, 1995), correlation coefficient = 0.231 (next highest peak = 0.189) and *R*-factor = 57.4 % (next highest peak = 59.0%), with phases from a MAD dataset collected at three wavelengths near the Iron edge.

This chapter describes the collection of X-ray diffraction data from crystals of BMXOR and HMXOR and the solution and preliminary refinement of the crystal structure of the human milk enzyme.

4.2 Programmes

4.2.1 CCP4 programme suite

The CCP4 programme suite is a set of programmes for protein crystallography containing many utilities for manipulation of file formats and data (CCP4, 1994). Several of its programmes have been used during the course of this project, these will be indicated in following manner: PROGRAMME NAME (CCP4).

4.2.2 AMoRe

AMoRe (**A**utomated **Mo**lecular **Re**placement), part of the CCP4 suite, contains a set of programmes for Molecular Replacement written by Navaza (Navaza, 1994). **SORTING** packs and sorts the observed amplitudes into a P1 cell. In the **TABLING** section of the programme the model is placed in a small box, its coordinates rotated so that its principal axes of inertia are parallel to the box axes and then translated so that its centre of gravity is at the origin of the cell. This ensures that the model is placed optimally within the smallest box for the later stages of calculation. TABLING also calculates pseudo electron density from the model coordinates and Fourier transforms this to produce Structure factors calculated in a fine grid for use in calculating the model Patterson function. **ROTING** then takes the two sets of data (observed and model) and generates structure factors for each possible orientation of the model by interpolating them between the Structure factors generated in

TABLING. A list of top peaks from the rotation function are then output, along with several correlation coefficients and an R factor which give an indication of the likelihood of the peak being a correct solution. The two most popular "scoring" values are the CC_F and the RF_F. The CC_F is the correlation coefficient between the observed amplitudes for the crystal and the calculated amplitudes for the model; RF_F is the R_{factor} between the observed amplitudes of the crystal and the calculated amplitudes for the model (12).

$$R = \frac{\sum \left| |F_{obs}| - |F_{calc}| \right|}{\sum |F_{obs}|} \qquad (12)$$

At this stage, when a set of possible rotation solutions has been found, AMoRe does not require a choice to be made between them. Rather the entire set of possible rotation solutions are fed into **TRAING** to carry out a Translation function peak search. Sets of translation solutions are generated for each rotation function peak, and then for each rotation function peak the top scoring (usually sorted on CC_F) translation solution is read out. Again, the same "scoring" parameters are calculated. If it is known from calculation of the solvent fraction of the crystal, or from derivation of NCS, that there is more than one molecule in the unit cell, then the best solution can be fixed, and TRAING rerun to determine the translation of the 2nd molecule (and again for the third etc.). The final sub-programme in AMoRe, **FITING**, carries out a rigid body refinement of the selected solution(s). If the solutions are indeed correct, it is expected that the correlation coefficients should increase and the R_{factor} drop; if this does not occur, it is unlikely that the solution(s) are correct.

Finally, FITING calculates the rotation and translation that need to be applied to the original model (before it was moved to the origin) in order to superimpose it on the target molecule.

4.2.3 REFMAC

Part of the CCP4 suite, REFMAC is a refinement programme that contains utilities for least squares and maximum likelihood refinement (Murshudov *et al.*, 1999; Murshudov, Vagin, and Dodson, 1996; Murshudov, Vagin, and Dodson, 1997). It has been used in this project for ML refinement of both the orthorhombic and trigonal data sets.

4.2.4 PROCHECK

PROCHECK is a CCP4 programme for the validation of protein structure. It checks the geometry of the structure against ideal values and provides a variety of graphs and plots indicating, residue by residue, the "correctness" of the structure compared to ideal geometry.

4.2.5 Xplor and CNS

Xplor and CNS are also suites of programmes for crystallographers (Brunger *et al.*, 1998), that utilise slightly different algorithms, in places, to the CCP4 programmes. Certain operations in MR, such as 1-dimensional rotation

searches were easier to carry out using Xplor and CNS than CCP4. Use of CNS programmes will be indicated as (CNS).

4.2.6 DENZO/SCALEPACK

DENZO and SCALEPACK (Otwinowski and Minor, 1997) are two programmes for the indexing, processing and scaling of diffraction images. Their use will be discussed in Section 4.3.2.2.

4.2.7 Moleman

Moleman is a programme containing routines for the manipulation of pdb coordinate files (Kleywegt, 1995; Kleywegt, 1996; Kleywegt, 1997; Kleywegt and Jones, 1996; Kleywegt and Jones, 1997) and was used for a variety of tasks. These included rotation and translation of the search model, renaming of chains and the creation of trimmed models containing only main chain atoms or only a poly-Ala chain.

4.2.8 O

O is a graphics package for the visualisation of protein models and electron density (Jones *et al.*, 1991). It was used both to check the packing of possible solutions (by generating symmetry related molecules) and for model building when a solution had been found.

4.2.9 GRASP

GRASP (Nicholls, Sharp, and Honig, 1991) is a programme for the visualisation of protein structures, especially protein surfaces.

4.2.10 MOLSCRIPT

MOLSCRIPT (Kraulis, 1991) is a programme for the visualisation of protein structure.

4.3 Data collection and processing

4.3.1 Principles of diffraction from a crystal

A protein crystal comprises a regularly repeating arrangement of protein molecules in 3 dimensions. The fundamental volume, or repeating unit, of a crystal is the unit cell, a parallelepiped specified by the basis vectors a, b and c. It should be noted that the basis vectors are not unit vectors, they carry dimensions of length and may be considered to be along the directions of infinite axes x, y & z.

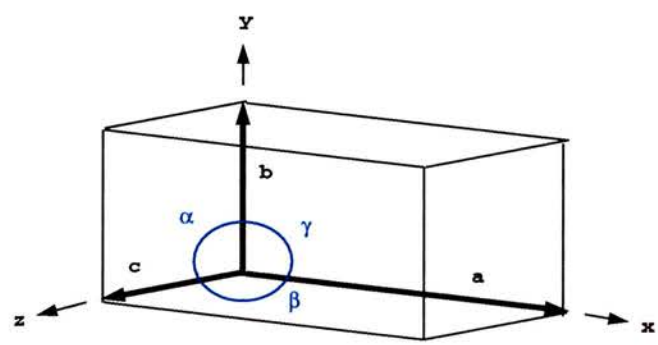

Figure 4.1 Schematic representation of the unit cell, showing the basis vectors a, b & c and the resulting intervector angles α, β & γ.

By consideration of symmetry, the possible unit cells of all crystals can be divided into seven different 3 dimensional crystal systems; triclinic, monoclinic, orthorhombic, tetragonal, trigonal, hexagonal and cubic. These seven can be further classified into 14 crystal lattices, the Bravais lattices. The crystal lattice is a simplified geometric representation of the translational repetition within the crystal in which each unit cell is represented by a single point. The 14 crystal lattices can be subdivided into 32 crystal classes which reflect the arrangement of the symmetry elements of the crystal, giving rise to 230

possible crystallographic space groups. However, due to the inherent "hand" of proteins, protein crystals can only grow in 65 enantiomeric space groups.

In most protein crystals, the unit cell is large and contains several identical molecules, or sets of molecules in an arrangement that produces crystallographic symmetry elements. In the unit cell, the smallest set of molecules that possesses no crystallographic symmetry elements (i.e. crystallographic symmetry operations will not map part of the set onto another identical part) but can be translated onto other identical sets using crystallographic symmetry is known as the asymmetric unit. Hence a single unit cell can contain several asymmetric units, the number of which is determined by the crystallographic symmetry present. In the simplest case found in a protein crystal, the asymmetric unit would contain a single monomer.

It is possible for parts of the asymmetric unit to be related to other parts through a symmetry operation that does not extend throughout the crystal. This type of symmetry is known as "local symmetry" or "non-crystallographic symmetry" (NCS).

Since any atom in the unit cell will be found in the same position throughout the crystal, the position of that atom can also be visualised as a set of planes in the crystal*.

---

* It should be noted that, because of thermal motion and static disorder, each atom is in a slightly different position within the many unit cells of a crystal, and that this position may change slightly over the course of the diffraction experiment. This causes a reduction in the contribution of that atom to the overall scattering factor that depends on the extent of the disorder. The effect is modelled by multiplying the scattering factor by an exponential function of scattering angle:

$$F \rightarrow F \times \exp[-B \sin^2\theta/\lambda^2]$$

Where B is a measure of thermal disorder, F is the scattering factor, λ the wavelength of incident radiation and θ the scattering angle.

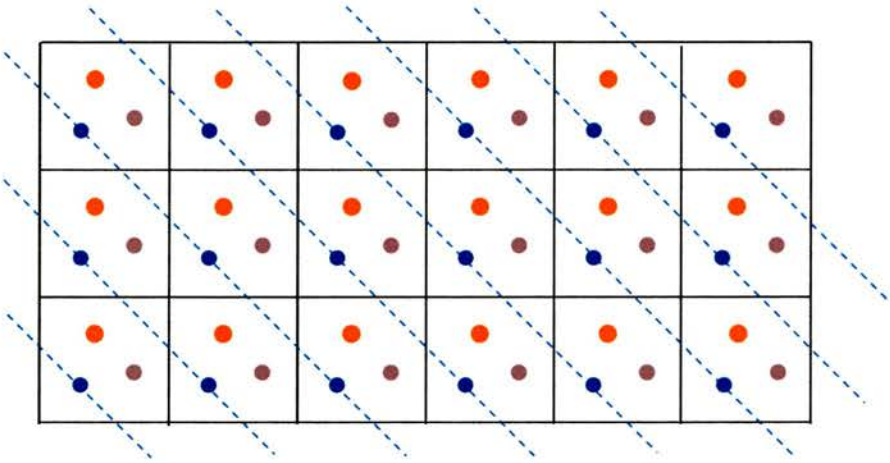

Figure 4.2 A 2-dimensional representation of a crystal illustrating how the position of a single atom (blue dot) in the unit cell forms a set of planes throughout the crystal.

Although the dimensions of the unit cell can be described in Angstroms, and the position of atoms within the unit cell in fractional coordinates, an alternative system for describing the location of an atom in the unit cell exists, which rather than describing the position of a single atom within the unit cell, describes a set of planes throughout the crystal. The planes are described using a set of indices, *hkl*, known as Miller indices. These are derived by considering a set of planes to be defined by the point at which they cross the unit cell axes, these intersection points are defined as multiples of the unit cell lengths. To eliminate infinity in these coordinates, the reciprocal is taken, to produce Miller indices. Hence, a plane intersecting the unit cell axes at (a,b/2,∞) is described in Miller indices (*hkl*) as (120).

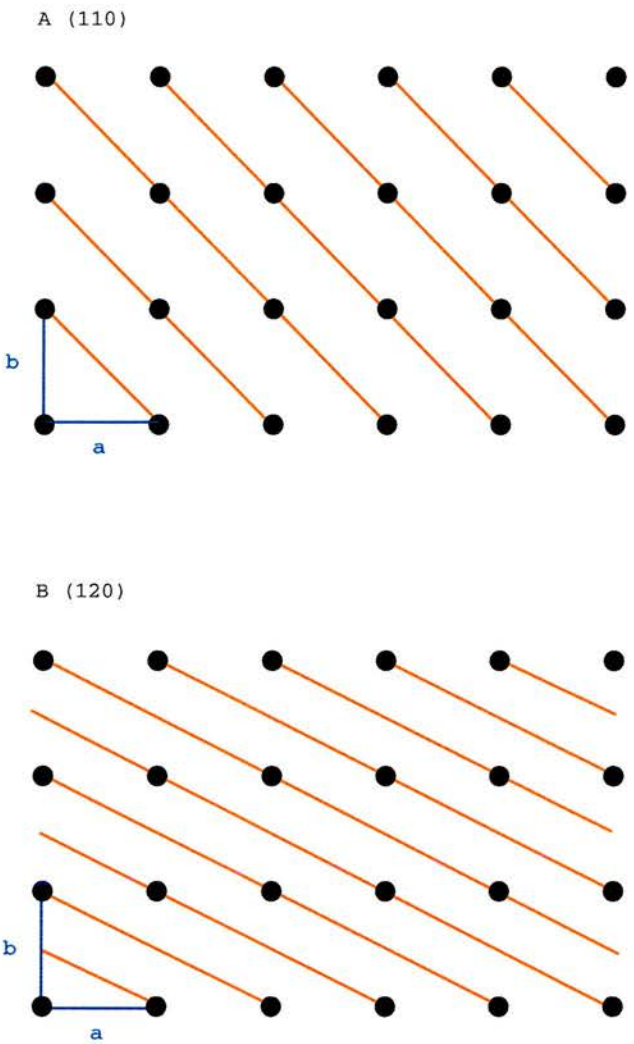

Figure 4.3

Illustrates two sets of planes that can be drawn through the same lattice (the points represent the corners of the unit cell) and their corresponding Miller indices. If the lattice array is considered as a top view of a three dimensional rectangular lattice in which the unit cell has a length *c* along the axis perpendicular to the page (z), then both sets of planes intersect the z axis at infinity.

A shows planes intersecting the unit cell axes at (a,b,∞), and B shows planes at (a,b/2,∞), resulting in the Miller indices (110) and (120) respectively.

Since the Miller indices are the reciprocal of the real space positions of the planes, they are describing positions in reciprocal space.

A characteristic property of any set of waves, including X-rays, is that they interfere with one another. This interference is additive, giving a greater amplitude where their displacements are in phase and a smaller amplitude where their displacements are out of phase. Because the intensity of electromagnetic radiation is proportional to the square of the amplitudes of its component waves, the regions of constructive and destructive interference

appear as regions of enhanced and diminished intensities. Diffraction occurs when a set of waves that are in phase (all interfering in a constructive fashion) encounter an object in their path which scatters the waves and causes some to become out of phase with others. If a detector is then placed beyond the object the varying intensities that result from the diffraction can be recorded as a varying pattern of dark and light.

In 1913, Laue suggested that X-rays might be diffracted when passed through a crystal, since the wavelength of X-rays is comparable to the separation of atoms within a molecule, this prediction was proved in an experiment performed by two of Laue's students (Friedrich, Knipping and Laue, 1913). Diffraction is the scattering of a incoming X-ray when it collides with an atom, or to be more precise, with the electron shell of an atom.

The intensity distribution obtained from diffraction of a wave by a single object, such as an atom, is continuous in space, but variable in amplitude. Repeating the object in a regular array amplifies the intensity of observed diffraction and also introduces sampling of the diffraction pattern. The underlying intensity distribution remains the same, the sampling is the result of diffraction from sets of planes formed by the regular array, rather than from a single object (Bragg, 1913). As the size of the array increases, the sampling becomes increasingly restrictive until, as described by Bragg's Law (see below), the diffraction pattern is measurable only in specific directions distributed in a regular spatial pattern.

As discussed above, we can consider diffraction of X-rays in a crystal to be diffraction from a set of planes, rather than from a single atom.

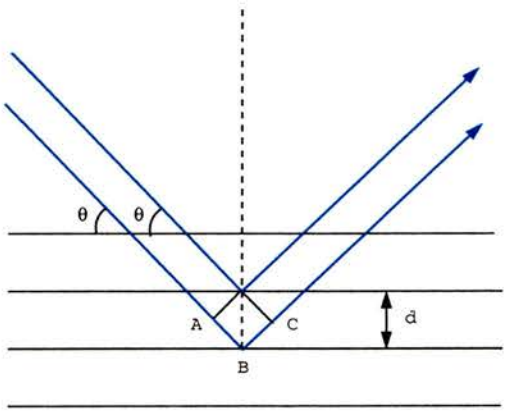

Figure 4.4 Schematic diagram of two X-ray beams of wavelength λ incident on two planes within a crystal. The path length travelled by the diffracted beams differs by AB + BC, and depends on the angle of incidence of the beams, θ.

Bragg showed that when the difference in pathlength travelled by two rays (AB +BC) is equal to the wavelength of the incident radiation, λ, the two diffracted waves are in phase and will interfere constructively to produce a diffraction maxima, or spot on the detector. Since the path length difference is dependent on the angle of incidence of the X-rays (1), it follows that a set of planes should be in a diffracting condition when Braggs Law (2) is satisfied.

$$AB + BC = 2d\sin\theta \quad (1)$$

$$\lambda = 2d\sin\theta \quad (2)$$

The treatment of diffraction in crystals as reflection of X-rays from a set of planes has led to the use of the term *reflection* to describe the intensity peaks arising from constructive interference.

4.3.2.1 Data collection

All X-ray diffraction data were collected at two synchrotron radiation sources (BW7a - DESY, Hamburg & ID14-2 & ID13 - ESRF, Grenoble). Due to the high intensity of synchrotron radiation, crystals were flash frozen in liquid nitrogen before mounting in the diffractometer. In order to prevent the formation of ice-crystals, some of the crystals were treated with cryoprotectant before freezing. The nature and quantity of cryprotectant will be described in Section 4.3.3. A flow of nitrogen gas at 100 K maintained the frozen state of the crystals.

During data collection, crystals were rotated in a stepwise fashion around an axis perpendicular to the X-ray beam in oscillation steps of 1°, each corresponding to a single frame. Collection times per frame were typically 30 - 90 seconds.

Data collection was controlled using the MarResearch interface (http://www.marresearch.com/) at Hamburg and the ProDC software (http://www.esrf.fr/computing/bliss/gui/prodc/) at Grenoble.

4.3.2.2 Data processing

Diffraction data were processed and scaled using the Denzo/Scalepack software package (Otwinowski and Minor, 1997). Denzo enables autoindexing of the first diffraction image from a subset of bright spots, determining unit cell and likely space group, followed by a refinement of crystal and detector parameters. The programme then uses the refined parameters and unit cell information to predict reflection positions in ensuing frames and integrate the

reflection intensities across the data set. The data are then reduced to a set of unique reflections for the specified space group. Data processing is monitored by a χ^2 value which represents the average ratio, squared, of the error in fitting, divided by the expected error.

Scalepack then scales the data set, correcting for changes in parameters such as beam intensity and crystal decay during data collection. Scalepack also carries out a post-refinement of cell and detector parameters by an iterative reintegration of intensities and refinement of mosaicity and spot size in order to improve data statistics. As well as merging the data into a single set of indices and associated errors, Scalepack allows determination of any screw axes using systematic absences. Several sets of statistics are produced by Scalepack, including a measure of the ratio of intensity to noise (I/σ) and a measure of the agreement in position and intensity of symmetry related reflections, R_{merge}. Scalepack is also monitored by the use of a χ^2 value, which represents the weighted ratio of the difference between the observed and average value of I, <I>, squared, divided by the square of the error model, effectively providing a measure of how accurately the error model being used to scale the data reflects the true errors in the data.

TRUNCATE (CCP4) (French and Wilson, 1978) was used to provide an output of structure factors and corresponding standard deviations from Scalepack's list of intensities and associated errors and to provide an estimate of the average B_{factor} of the data from a Wilson distribution.

4.3.3 Results

As described in Chapter 2, diffraction was first obtained on BW7A (DESY, Hamburg, Germany) from a large cracked HMXOR crystal, grown under anaerobic conditions. The crystal was trigonal in morphology and was flash frozen by dunking in liquid nitrogen, after being soaked for ~20 sec in mother liquor + 20% glycerol as cryoprotectant.

The choice of cryoprotectant and concentration was based on the list of cryoprotectants that would produce a glassy freezing for each of the 50 conditions of the Hampton Sparse Matrix Screen, described by Garman and Mitchell (Garman and Mitchell, 1996). Since HMXOR crystals grew in conditions closely related to Hampton Sparse Matrix Screen conditions 6 and 17, the suggested cryoprotectant for condition 6, 20 % glycerol, was used. Crystals were harvested as described in Chapter 2, and then transferred to mother liquor + 20 % glycerol.

Very low resolution and very mosaic diffraction (due to the cracked nature of the crystal) was observed (Fig. 4.5). Although the data were not suitable for any sort of analysis, not even unit cell determination, they supplied the impetus to further optimise these HMXOR crystallization conditions.

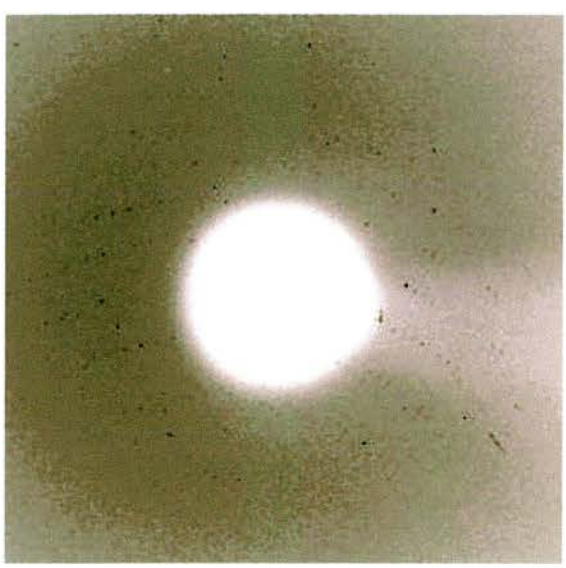

Figure 4.5
Diffraction observed from a cracked HMXOR crystal at BW7A (DESY, Hamburg, Germany). The resolution at the edge of the picture is ~ 7Å. The diffraction image was visualised using the DENZO package.

After further optimisation of crystallization conditions, crystals were obtained that diffracted to a maximum of 3.3 Å at ID14-2 (ESRF, Grenoble, France). As before, since the conditions remained close to those of the Hampton Screen, 20 % glycerol was used as cryoprotectant. Three HMXOR datasets were collected, two from large crystals grown in 26 % PEG 4K, 100 mM Na-acetate, pH 6 containing 0.25 M Ammonium acetate, 10 mM DTT and 30 % w/v D(+)-glucose that diffracted to 3.5 Å, and one very incomplete dataset from a smaller crystal grown in 26 % PEG 4K, 100 mM Na-acetate, pH 6 containing 0.25 M Ammonium acetate, 10 mM DTT and 5 % w/v polyvinylpyrrolidone K15 which diffracted to 3.3 Å.

The higher resolution dataset proved to be mosaic and incomplete. However, the first dataset (max. res. 3.5 Å) was processed and scaled using DENZO/SCALEPACK.

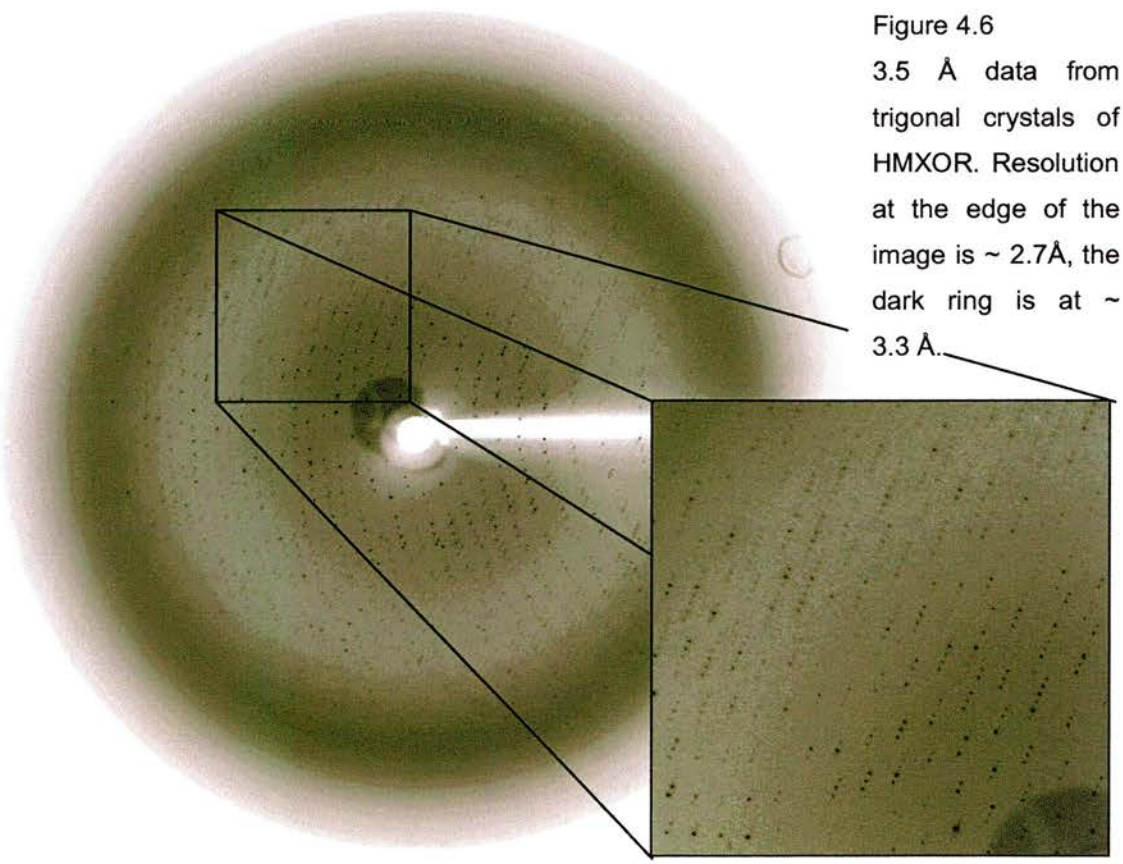

Figure 4.6
3.5 Å data from trigonal crystals of HMXOR. Resolution at the edge of the image is ~ 2.7Å, the dark ring is at ~ 3.3 Å.

First attempts at auto indexing with DENZO seemed to indicate that the data were hexagonal, and indeed scaled acceptably to 6 Å as P622. However, on scaling to higher resolution, it became clear that the data were in fact of crystal class 32. Study of the systematic absences indicated the presence of a screw axis, defining the possible space groups as $P3_121$ or $P3_221$. These differ in the degree of screw, in $P3_121$, there is a screw of 1/3 along the c axis, and in $P3_221$, there is a screw of 2/3. The two possible space groups are not distinguishable at this stage of analysis; however, a correct solution is only possible in one of them. This will be discussed later.

Wavelength	0.9326 Å
Space Group	$P3_121$ or $P3_221$
Cell	a = b = 192.7 A, c = 278.6 Å, $\alpha = \beta = 90^\circ$, $\gamma = 120^\circ$
Resolution range	30 - 3.5 Å
# Observations	614949 (of which 75088 are unique)
% Completeness	98.2 (98.2)
I/σ	3.6 (1.5)
R_{merge}	0.12 (0.47)
Highest shell	3.62-3.5 Å
Average B_{factor}	30 $Å^2$ (from Wilson Plot)

Table 4.1 Summary of data statistics for the 3.5 Å trigonal HMXOR dataset, output from Scalepack and Truncate. Figures in parentheses indicate values in the highest resolution bin.

An estimate of the number of HMXOR monomers present in the asymmetric unit was made by calculating the % solvent content, as originally described by Matthews (Matthews, 1968). In brief, the volume of the unit cell ($Å^3$) is calculated, and is divided by the number of asymmetric units x the estimated molecular mass of the contents of the asymmetric unit to give a measure of volume per unit mass ($Å^3Da^{-1}$). Thus, if a monomer of XOR was present in the asymmetric unit, the volume of the unit cell would be divided by 6 (the number

of asymmetric units in a trigonal space group) multiplied by 150,000. The solvent fraction is then calculated by the following equation:

1-(1.23/[volume per unit mass]) = solvent fraction

Typical values for the solvent fraction range from ~ 0.4 - 0.7; if a tetramer (2 XOR dimers) is assumed in the asymmetric unit, then a reasonable solvent fraction value of 0.51 is obtained.

As described in Chapter 2, reproducing the large HMXOR trigonal crystals that were used to obtain the above dataset proved impossible. However, smaller clean trigonal crystals of HMXOR were routinely obtained. In view of this, time was obtained on the microfocus beamline, ID13, at the ESRF, a beamline designed specifically for very small crystals. Just prior to the beamtime, a second crystal form of HMXOR was obtained, with an apparent hexagonal morphology. Again, these crystals were very small (max. dimensions 50 μ).

Small trigonal crystals were mounted first, again using 20 % glycerol as a cryoprotectant (Fig. 4.7).

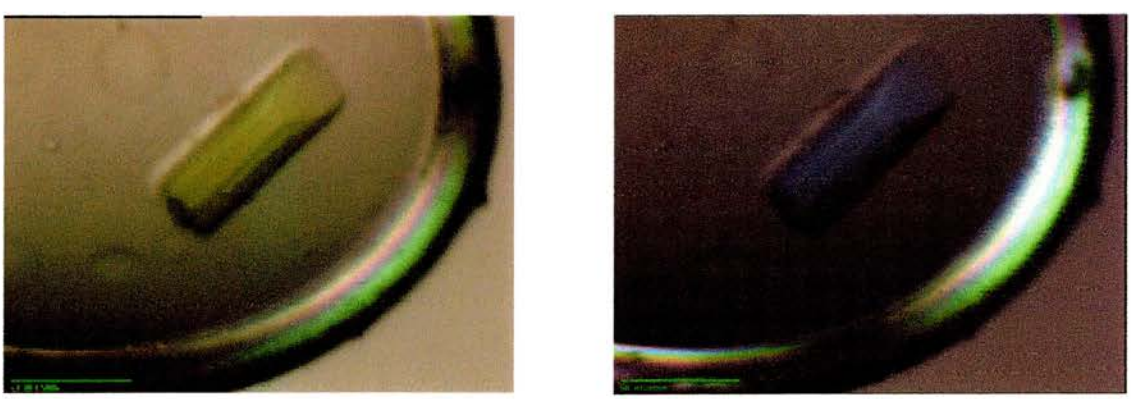

Figure 4.7 Small trigonal crystals mounted in ID13, the green bar at the bottom is 50 μ. These crystals were grown in 29 % PEG 4K, 100 mM Tris, pH 8, 0.25 M ammonium sulphate and 3 % w/v DTT. 20 % glycerol was used a cryoprotectant. The image on the left shows the crystal under normal lighting, that on the right shows the crystal viewed under polarised light, demonstrating the single nature of the crystal.

The quality of diffraction observed varied greatly from crystal to crystal (Fig. 4.8), and a maximum resolution of 5.5 Å was obtained.

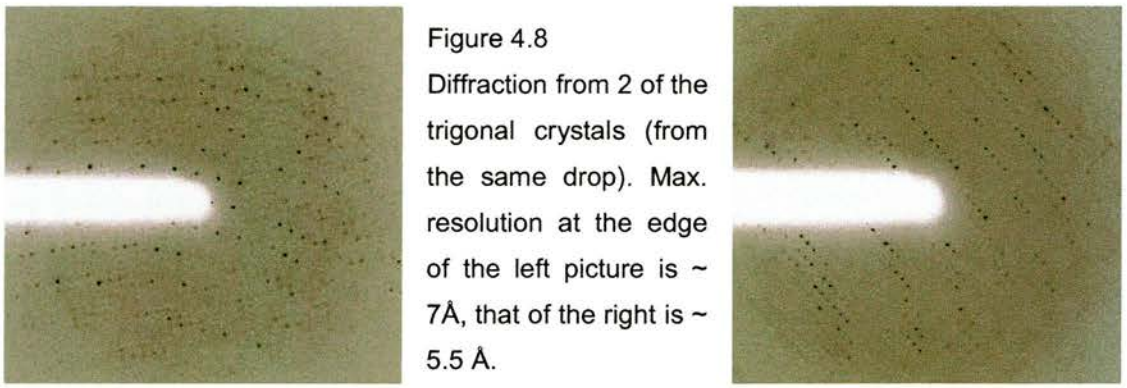

Figure 4.8
Diffraction from 2 of the trigonal crystals (from the same drop). Max. resolution at the edge of the left picture is ~ 7Å, that of the right is ~ 5.5 Å.

The diffraction of the new crystal form of HMXOR (hexagonal morphology) was then tested using crystals grown in 26 % PEG 4K, 100 mM Tris, pH 8 containing 0.25 M ammonium sulphate and 1.5-5 % w/v DTT. Again, given the success of 20 % glycerol as a cryoprotectant for the closely related trigonal conditions, this was used again. Surprisingly, these crystals diffracted to beyond 3 Å, however, the diffraction was only clear at low resolution, and became very smeary towards the edge of the plate. This suggested that, although the crystals were freezing glassily in the presence of 20 % glycerol, the amount of cryoprotectant was incorrect. Various concentrations of glycerol (5-30 %) were tried with no improvement in diffraction. An attempt at crystal annealing was made (anecdotal evidence suggests that a rapid thawing and refreezing of a crystal can improve diffraction in certain cases. It is likely this occurs by allowing slightly misaligned regions of the crystal lattice to shift into a more ordered position) but this abolished all diffraction.

PEG 4K is also a possible cryoprotectant, so crystals were soaked into higher concentrations of PEG 4K, whilst maintaining similar salt concentration and pH. This brought about some improvement in resolution and quality of

diffraction, and it was clear that the closer the concentration of PEG 4K was to that of the mother liquor of the crystal, the better the diffraction. This led to an eventual attempt at freezing a crystal straight from the drop with no cryoprotectant at all, which produced the best quality diffraction yet observed, to a maximum resolution of 3.6 Å.

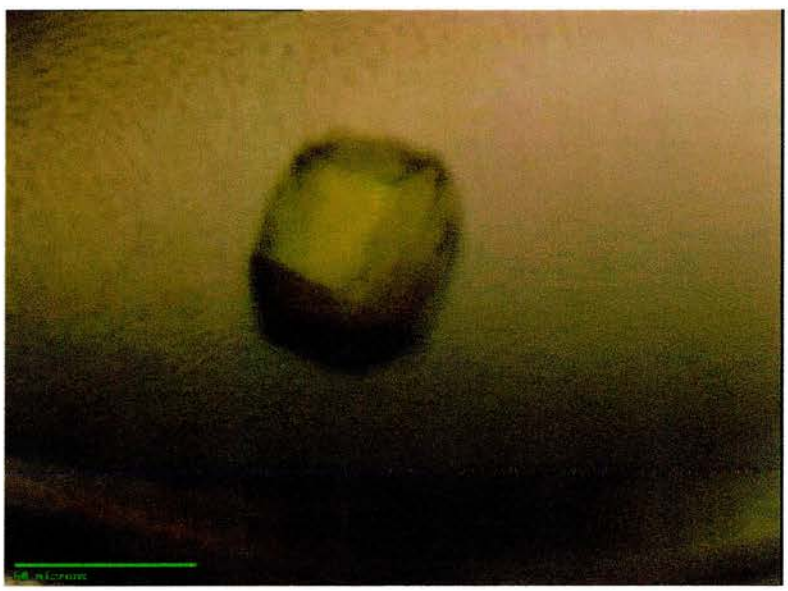

Figure 4.9
Orthorhombic crystals of HMXOR grown in 26 % PEG 4K, 100 mM Tris, pH 8, 0.25 M ammonium sulphate and 1.5-5 % w/v DTT. The crystal is shown mounted in the beam at ID13, the green bar is 50μ. This crystal was frozen directly from the drop.

The data were collected in two parts, due to a beam dump in the middle of collection, (ϕ = 1-12°, ϕ = 10-90°, $\Delta\phi$ = 1°), processed separately using DENZO and then scaled together in SCALEPACK. Surprisingly, given the hexagonal morphology of the crystals, the data indexed as orthorhombic. After scaling, examination of systematic absences indicated the presence of two screw axes, defining the spacegroup as $P2_12_12$.

Wavelength	0.9640 Å
Space Group	$P2_12_12$
Cell	a = 143.4 b = 156.1 Å, c = 131.8 A, $\alpha = \beta = \gamma = 90^o$
Resolution range	48 - 3.6 Å
# Observations	277780 (of which 35036 are unique)
% Completeness	98.5 (97.0)
I/σ	4.5 (1.7)
R_{merge}	0.18 (0.51)
Highest shell	3.88-3.6 Å
Average B_{factor}	40.5 $Å^2$ (from Wilson Plot)

Table 4.2 Summary of data statistics for the 3.6 Å orthorhombic HMXOR dataset, output from Scalepack and Truncate.

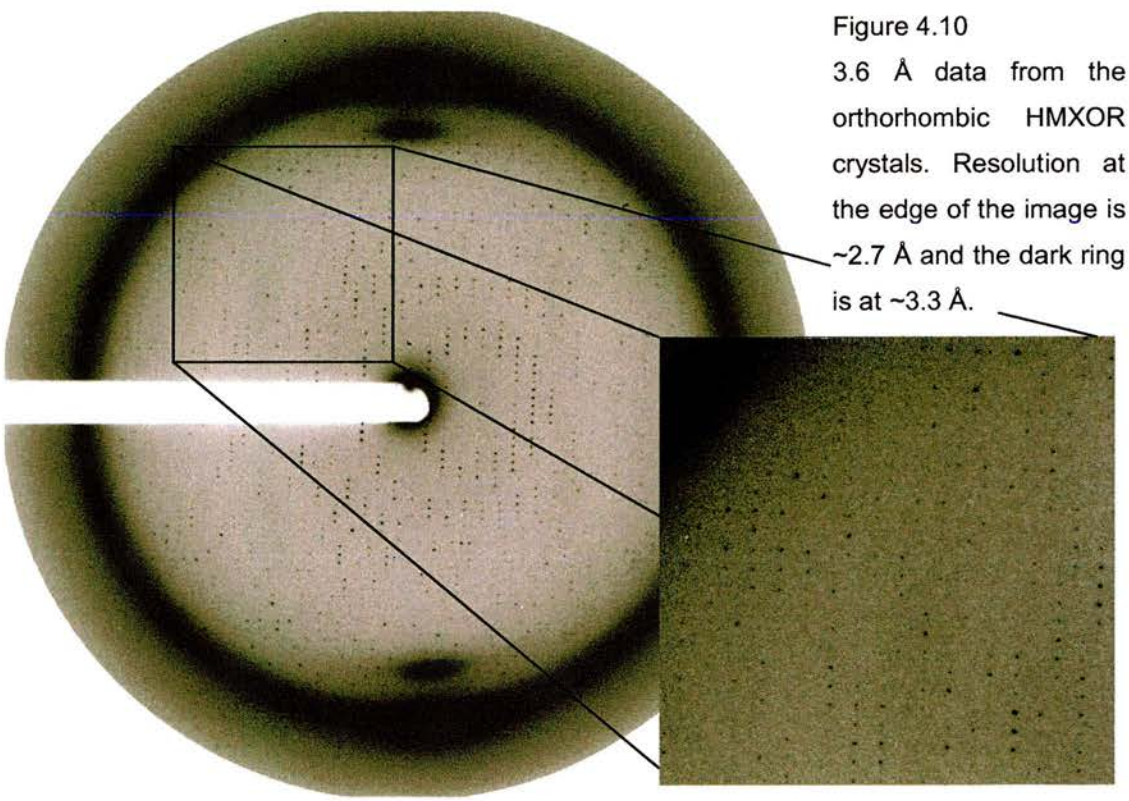

Figure 4.10
3.6 Å data from the orthorhombic HMXOR crystals. Resolution at the edge of the image is ~2.7 Å and the dark ring is at ~3.3 Å.

It should be noted (and this again may be due to the freezing) that the data obtained from this crystal were considerably better in one direction, extending to 3.3 Å. However, at 90° rotation, diffraction was barely beyond 3.6 Å. This is reflected in the high R_{merge} in the highest resolution shell of the data (Tab. 4.2).

Calculation of the solvent fraction, as described above, indicated that the asymmetric unit of the crystal contained a dimer of HMXOR (Solvent fraction = 0.5).

One BMXOR dataset was also collected on ID14-2 at the ESRF. A BMXOR crystal grown in 22 % PEG 4K, 100 mM Na-citrate, pH 6 containing 0.2 M ammonium acetate and 10 mM DTT was harvested as described in Chapter 2 and flash frozen in liquid nitrogen. Again in this case 20 % glycerol was used as a cryoprotectant. The crystals froze well and a partial dataset (ϕ = 0-50°) was collected (data collection was stopped by a beam dump). The data were processed and scaled as described, and indexed in the spacegroup $P2_1$. Due to the low completeness of the dataset, it was not used in any further structure determination.

Wavelength	0.9326 Å
Space Group	$P2_1$
Cell	a = 124.4 b = 143.7 Å, c = 168.5 A, α = 90°, β = 94.6° γ = 90°
Resolution range	30-3 Å
# Observations	217439 (of which 118487 are unique)
% Completeness	32.5 (24.3)
I/σ	7.9 (1.3)
R_{merge}	0.07 (0.31)
Highest shell	3.11-3.0 Å
Average B_{factor}	52 $Å^2$ (from Wilson Plot)

Table 4.3 Summary of data statistics for the 3.0 Å monoclinic BMXOR dataset, output from Scalepack and Truncate.

Further attempts to collect a complete BMXOR dataset were unsuccessful. All crystals mounted proved to be either very mosaic, or to contain several

lattices. The thin plate morphology of BMXOR is the likely root of the problem, as it was often the case that a thicker plate that appeared to be a single crystal was in fact composed of several very slightly offset thin crystals.

4.4 Molecular Replacement

4.4.1 The phase problem

A wave is described in terms of a sine or cosine function with the following parameters; F, the maximum amplitude of wave; h, the frequency (the reciprocal of the wavelength) and ϕ, the phase of the wave. Thus the amplitude of a wave at any point in space $f(x)$ can be described in terms of these three parameters (1).

$$f(x) = F \cos 2\pi (hx + \phi) \qquad (1)$$

There are many versions of the wave equation, the most useful form for crystallography is a complex exponential form with no explicit time dependence (2).

$$f(x) = F \exp(i\theta) \qquad (2)^*$$

This allows us to conveniently represent waves as vectors in the complex plane and to add waves by graphical or algebraic vector addition (Fig. 4.11).

---

* Where $\theta = 2\pi(hx)$, from (1), and implicitly contains the phase, ϕ, which is dependent only h and x.

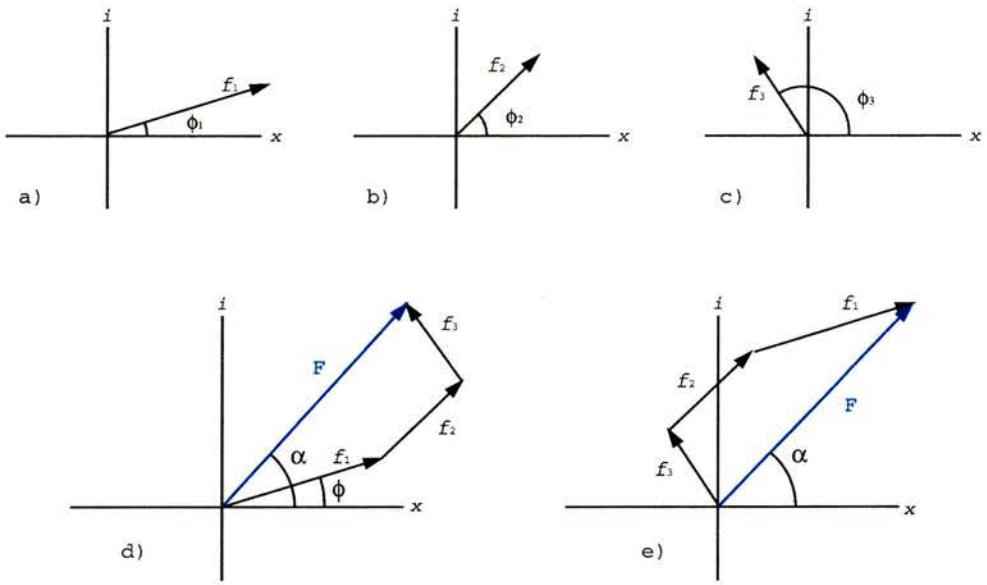

Figure 4.11 a), b) & c) show vectors f_1, f_2 and f_3 representing three waves of different amplitude and phase. d) shows the resultant vector F after addition, e) illustrates that after addition in reverse order the resultant vector F is the same.

The resultant wave can be described by means of a Fourier series as the sum of all the component waves, or in this case, the resultant vector can be described as the sum of the series of vectors (3).

$$F = f_1 + f_2 + f_3 \qquad (3)$$

By extension, in the case of n vectors, the resultant would be described by the equation (4).

$$F = f_1 + f_2 + f_3 + \ldots\ldots + f_{(n-1)} + f_n \qquad (4)$$

As described in section 4.2.1, in a crystal X-rays may be considered to be diffracted from planes of atoms. The diffraction pattern obtained is the resultant of the net additive effect of the interference of all the X-rays

scattered by the crystal, thus *every* plane (or every atom) contributes to *every* reflection observed in the diffraction pattern. Each reflection *hkl* can be described as the sum of all contributing scattered waves. This sum is known as a structure factor and each reflection, *hkl*, has a corresponding structure factor, F_{hkl}. The scattering contribution of each atom to the structure factor depends on two parameters, the scattering factor, *f*, of the atom (a measure of how strongly an atom can scatter an incoming X-ray, this is dependent on atomic number) and the disorder of the atom (discussed in 4.2.1). As described above, the structure factor can be expressed in terms of a Fourier series in which each term gives the contribution of one atom at position (x,y,z) to the observed reflection *hkl* (5).

$$F_{hkl} = \sum_{j=1}^{n} f_j \exp\left[-B_j \frac{\sin^2\theta}{\lambda^2}\right] \exp[2\pi i(hx_j + ky_j + lz_j)] \qquad (5)$$

Where f_j is the scattering factor of the jth atom, the following term corrects for disorder of the jth atom (see 4.2.1) and the final term contains information about the phase of the jth wave and the position of the jth atom.

Thus F_{hkl} possesses amplitude, frequency and phase; the frequency is that of the X-ray source and the amplitude is proportional to the square root of I_{hkl}, the intensity of the recorded reflections.

F_{hkl} can also be considered as the sum of scattering not from individual atoms, but from a volume element of electron density, ρ, in the unit cell. The electron density at a point in the unit cell (x,y,z) is thus given as $\rho(x,y,z)$. The electron density of a cubic volume element of dimensions δ^3 centred at (x,y,z) is the

average of $\rho(x+\delta,y+\delta,z+\delta)$ in that region. As $\delta^3 \rightarrow 0$, we approach precise values for electron density at every point (x,y,z). Thus F_{hkl} can be considered not as the sum, but as the integral of $\rho(x,y,z)$ over the unit cell volume (6).

$$F_{hkl} = \int_V \rho(x,y,z)\exp[2\pi i(hx+ky+lz)]\delta v \qquad (6)$$

$\rho(x,y,z)$ is the Fourier transform of F_{hkl}, allowing us to write an expression describing the electron density at any point in the unit cell (x,y,z) as (7).

$$\rho(x,y,z) = \frac{1}{V}\sum_h\sum_k\sum_l F_{hkl}\exp[-2\pi i(hx+ky+lz)] \qquad (7)$$

Thus, calculation of the electron density across the unit cell requires knowledge of the structure factors F_{hkl}. These are complex and vectorial and cannot be directly measured. However, F_{hkl} can be calculated if the frequency, amplitude and phase of a reflection are known. Frequency is defined in a diffraction experiment by the wavelength of the incident radiation and amplitude can be calculated from the observed intensities I_{hkl}. However, no phase information is available from single measurements of intensities, as although the phase is implicit in the reflection, it cannot be directly measured.

This is the crux of the phase problem, that the phase cannot be extracted from observed data. However, since phase information is inherent in the observed reflections, it is possible to develop a model of the actual atomic structure for which the calculated phases closely approximate those of reality.

4.4.1.1 Solution of the phase problem

Several methods exist to resolve the phase problem in crystallography. In this project molecular replacement (MR) was used. MR depends on using the phases calculated from a known structure as an estimation of the actual phases in the data. The improvement of these starting phases to give a final model that reflects the observed data as closely as possible will be discussed later.

Molecular replacement (MR) relies on a starting structure that closely resembles the structure that is to be determined. There are various ways of predicting structural similarity; the search model may be the same protein from another source, or a related protein with sequence homology to the unknown protein. Once a search model has been decided upon, MR is used to place the model in the same orientation and position in the unit cell as the molecule under study. Phases calculated from the model can then be combined with the observed amplitudes to create an electron density map.

Defining the correct orientation and position of the model in the unit cell requires six dimensional parameters; three angles which describe the rotation needed to place the model in the same orientation as the molecule and three translational coordinates that describe where in the unit cell (with respect to the origin) the model is to be placed in order to superimpose on the molecule.

MR is complicated by the presence of symmetry in the crystal. In most spacegroups, except P1 which contains no rotational symmetry, the crystal

will contain several molecules in different orientations (related by crystallographic symmetry) within the unit cell. In most cases the spacegroup is unambiguously determined by the systematic absences of the observed diffraction pattern. However, certain spacegroups, including $P3_121$ and $P3_221$, cannot be distinguished on the basis of systematic absences alone. Thus, when considering the position of the symmetry related molecules in the unit cell, there is an ambiguity in the translation required to position the model within the unit cell. This can only be resolved by trial and error, a consistent solution is only possible in one of the two spacegroups.

An added complication is the presence of non-crystallographic symmetry (NCS) within the asymmetric unit of the crystal. Many protein crystals, as is the case with the data described here, contain two or more copies of a molecule in each asymmetric unit. The presence of NCS is both a blessing and a curse; it can provide additional information that can be used when deciding on a solution - the solution found must satisfy the observed NCS, however, the presence of two or more molecules can produce high levels of noise that make a solution difficult to detect.

The basis of MR is the Patterson function (which will be described in more detail in the following Section). In brief, the Patterson function, P, describes the set of vectors relating every atom in the unit cell. MR seeks to maximise the correlation between the Patterson map calculated from the observed data, P_{obs}, and that calculated from the model, P_{mod}. This can be done by finding the set of 3 angles, Ω, and 3 coordinates, τ, that maximises the value of the product, $S(\Omega,\tau)$, of P_{obs} and P_{mod} (8).

$$S(\Omega,\tau) = \sum_i P_{obs}(\mathbf{u}_i) \cdot P_{mod}(\mathbf{u}_i, \Omega, \tau) \qquad (8)$$

P_{obs} and P_{mod} both vary with the vector $\mathbf{u}_i$ which defines position in the Patterson map. P_{mod} also depends on the orientational and positional parameters, Ω and τ. If the peaks of P_{mod} and P_{obs} occur in the same position, then $S(\Omega,\tau)$ will sum to a large value. However, for a single molecule in the asymmetric unit, this requires a search in 6 dimensions, and for 2 molecules a search in 12 dimensions. Whilst possible, such a method would require a large amount of computing power and time.

Most MR methods split this six dimensional search into two parts; a rotation search to define the orientation of the model, followed by a translation search to locate its position in the unit cell. This is the method that proved successful in this project using the programme AMoRe (Navaza, 1994). Recently different programmes have been developed, such as EPMR (Kissinger, Gehlhaar, and Fogel, 1999) and Queen of Spades (Glykos and Kokkinidis, 2000), that use a maximum likelihood approach to MR and generate many copies of the model in random orientations in the unit cell, then select those that have the highest correlation to observed data and vary these candidate solutions iteratively to converge on the correct solution.

4.4.1.2 The Patterson function

The Patterson function is a Fourier transform of the set of squared but not phased reflection amplitudes. Since amplitude is proportional to the square root of intensity, this is equivalent to the Fourier transform of observed intensities. The general form of the Patterson function, describing the height of the Patterson function, P, at a point (u,v,w) is shown in equation (9).

$$P(u,v,w)=\frac{1}{V}\sum_{h}\sum_{k}\sum_{l}\left|F_{hkl}^{2}\right|\exp[-2\pi i(hu+kv+lw)] \qquad (9)$$

Unlike the functions described in the previous section, the Patterson function does not define a map of the electron density within a unit cell, rather a density map of the vectors between atoms in the unit cell. If we consider a simple molecule of three atoms within the unit cell (Fig. 4.12) and draw vectors between each pair of atoms, then place all these vectors at the origin of the cell, peaks are obtained at the 'heads' of each of the vectors.

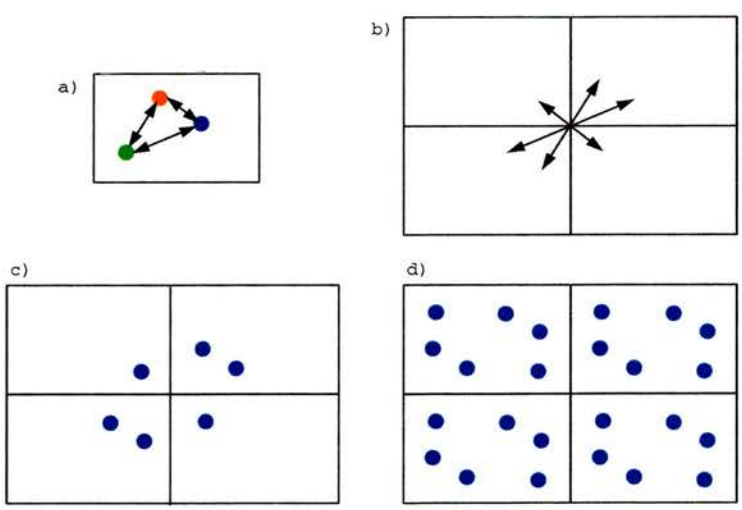

Figure 4.12. a) Shows three atoms in a unit cell and the interatomic vectors. b) shows the vectors placed at the origin of the lattice. Note that there are 6 vectors as vectors are directional, therefore, the vector from atom-1 to atom-2 is not equivalent to the vector from atom-2 to atom-1. c) Shows the Patterson function peaks from a single molecule, d) shows the Patterson function peaks for a repeating array of molecules.

It is clear (Fig. 4.13) that for a single molecule in the unit cell, as long as the orientation remains unchanged, it can be translated to any point in the unit cell and still produce the same Patterson map, as the interatomic vectors of the molecule remain the same.

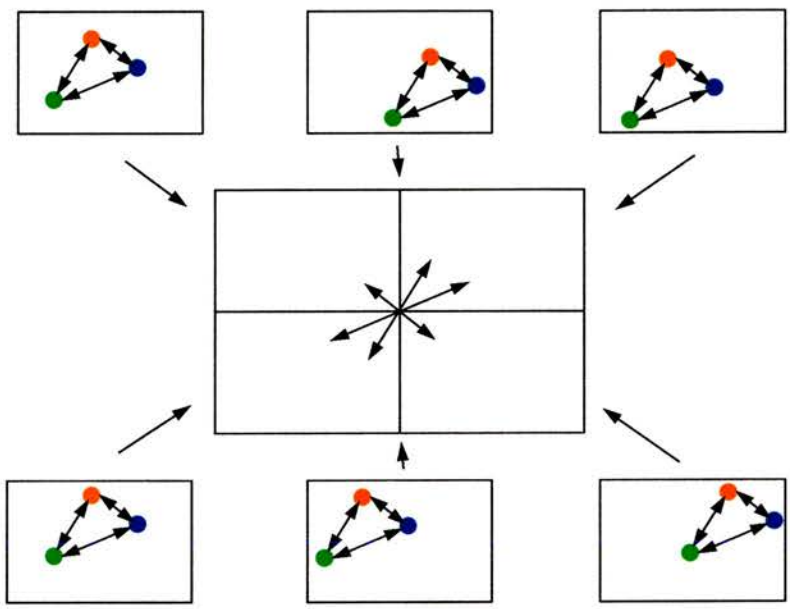

Figure 4.13. Illustration of the independence of the Patterson map from the position of the molecule within the unit cell.

If there are two or more molecules in the unit cell, then there will also be vectors between all the atoms within the two molecules, producing a much more complex and noisy Patterson map (Fig. 4.14).

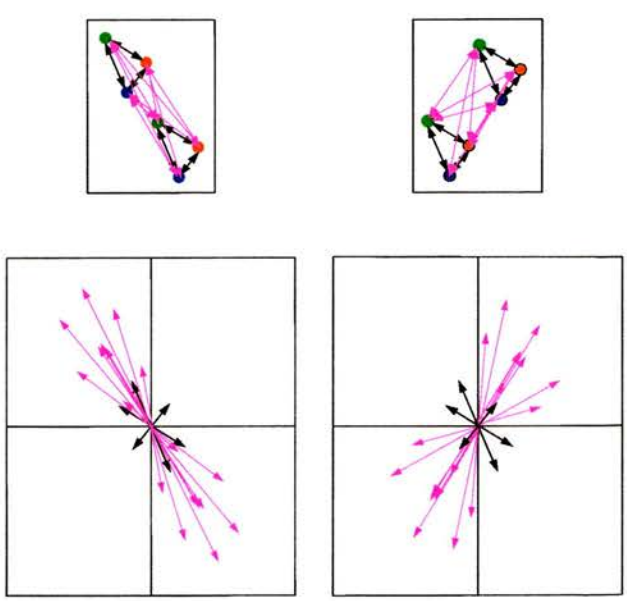

Figure 4.14
Illustration of the inter-atomic vectors generated between two molecules within the unit cell. Vectors within a single molecule are indicated in black, those between the molecules in pink. It should be noted that the intra-molecular vectors are independent of relative position within the cell, whereas the relative position of the two molecules affects the inter-molecular vectors.

4.4.1.3 The cross rotation and translation functions

As described in previously, most MR methods divide the six dimensional search for the correct orientation and position of the model into two three dimensional searches, determining first the rotation and then the translation of the model required to superimpose it on the target molecule.

This separation of the search into two halves takes advantage of a property of the Patterson function. As the Patterson function is a map of inter-atomic vectors, in the calculated Patterson maps there will be both *intra*-molecular vectors within one molecule and *inter*-molecular vectors relating the atoms of one molecule to those of the other molecules within the unit cell (related by crystallographic and non-crystallographic symmetry). The intra-molecular set of vectors depends only on the orientation of the molecule (Fig. 4.13), as the relative arrangement of the vectors to each other doesn't change as the molecule is rotated, it is merely the direction of the vectors that is altered. In contrast, the inter-molecular set of vectors depends on both the orientation and the position of the two molecules (Fig. 4.14).Hence, it should be possible, by defining the set of intra-molecular vectors in the observed Patterson map, to use these to determine the rotation required to place the model in the correct orientation. Without knowing the structure of the target molecule there is no mathematical way to distinguish between intra- and inter-molecular vectors. However, differentiation in a purely empirical fashion is possible as the inter-molecular vectors tend to be longer than the intra-molecular vectors. Therefore, the six dimensional search can be divided into two halves, by using only the vectors within a spherical envelope around the origin when

determining the orientation of the model, and only the vectors outside the sphere to determine the translation.

In practice, this means determining two product functions; one for the rotation, $R(\Omega)$ (10), and one for the translation, $T(\Omega,)$ (11) each with three variable parameters.

$$R(\Omega) = \sum_{i \in \text{intra}} P_{\text{obs}}(\mathbf{u}_i) \cdot P_{\text{mod}}(\mathbf{u}_i, \Omega) \tag{10}$$

$$T(\Omega, \tau) = \sum_{i \in \text{inter}} P_{\text{obs}}(\mathbf{u}_i) \cdot P_{\text{mod}}(\mathbf{u}_i, \Omega, \tau) \qquad \text{where } \Omega \text{ is constant} \tag{11}$$

4.4.1.4 The Self Rotation Function

Just as the Rotation function can be used to compare an observed Patterson map with a model Patterson map (Cross Rotation), it can also be used to rotate an observed Patterson map against itself (Self Rotation). A Self Rotation function will contain peaks at angles corresponding to a rotation of one Patterson that brings it back into alignment with the unrotated Patterson. If we reconsider the simple Patterson calculated from one molecule in Figure 4.12, it becomes clear that choosing a lattice point in the Patterson map as the origin and rotating the map around that point will produce an exact overlay at certain angles of rotation.

Thus, a Self rotation function would be expected to yield peaks at angles corresponding to crystallographic axes, however, if there are two or molecules in the unit cell related by rotational symmetry, the Self Rotation function will also yield peaks corresponding to the NCS of the crystal. These will be weaker than the peaks resulting from CS, but their position and height can yield information about the position and type of NCS found in the unit cell. However, Self Rotation functions can be notoriously difficult to interpret, and are often only really explained with the benefit of hindsight, when the actual crystal structure is solved.

4.4.2 Molecular Replacement results

At the beginning of this project, there was only one MR model available, MOP from *D.gigas* (Romão *et al.*, 1995). As described in the introduction, MOP is a homodimer of 907 residues and contains a molybdenum domain (binding the Mo-MPT) and an iron sulphur domain (containing the 2 [2Fe2S] iron sulphur clusters). Despite the lack of an FAD domain, it was hoped that given the relatively high sequence similarity of MOP to HXOR (44 % identity in the iron sulphur domain and 32 % identity in the molybdenum domain) that a MR solution could be found with MOP as a search model. Before the first dataset was obtained, however, a second XOR related structure was published; the CODH from *O. carboxidovorans* (Dobbek *et al.*, 1999). As well as molybdenum (23 % identity to HXOR) and iron sulphur domains (35 % identity to HXOR), CODH also contained a FAD domain (18 % identity to HXOR). Interestingly, despite the high degree of structural similarity between the molybdenum and iron sulphur domains of CODH and MOP, the dimer formation is quite different (Fig 4.15).

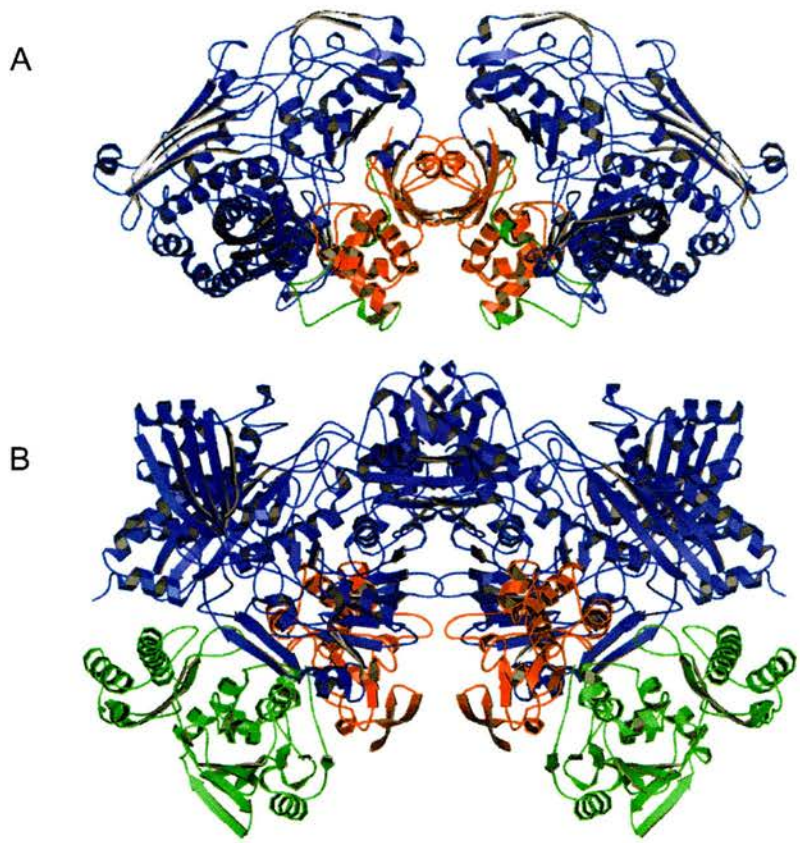

Figure 4.15. Different dimer formation in MOP and CODH. A shows the MOP dimer, B shows the CODH dimer. Colouring is the same for both molecules; blue the molybdenum domains, red the iron sulphur domains and green the FAD domains. Picture generated with Molscript.

When the first trigonal dataset was obtained, attempts were made to find a MR solution with AMoRe, using CODH as a model. Both the dimer and monomer were used, as well as Cα and poly-ala models. Attempts were also made using just the molybdenum and iron sulphur domains of CODH, in case the FAD domain was located in a different place in XOR, and using all three single domains of CODH. Composite models comprising the molybdenum and iron sulphur domains of CODH overlaid onto the MOP structure were also tried. Despite occasionally finding promising solutions, that appeared to improve during the FITING step of AMoRe, they failed to pack well.

The strong pseudo hexagonal nature of the trigonal data indicated the existence of an NCS 2-fold axis, and calculation of the self rotation function (POLARRFN, CCP4) indicated that this 2-fold axis was at 30° to the a-axis of the crystal and was 95% of the origin peak (Fig. 4.16).

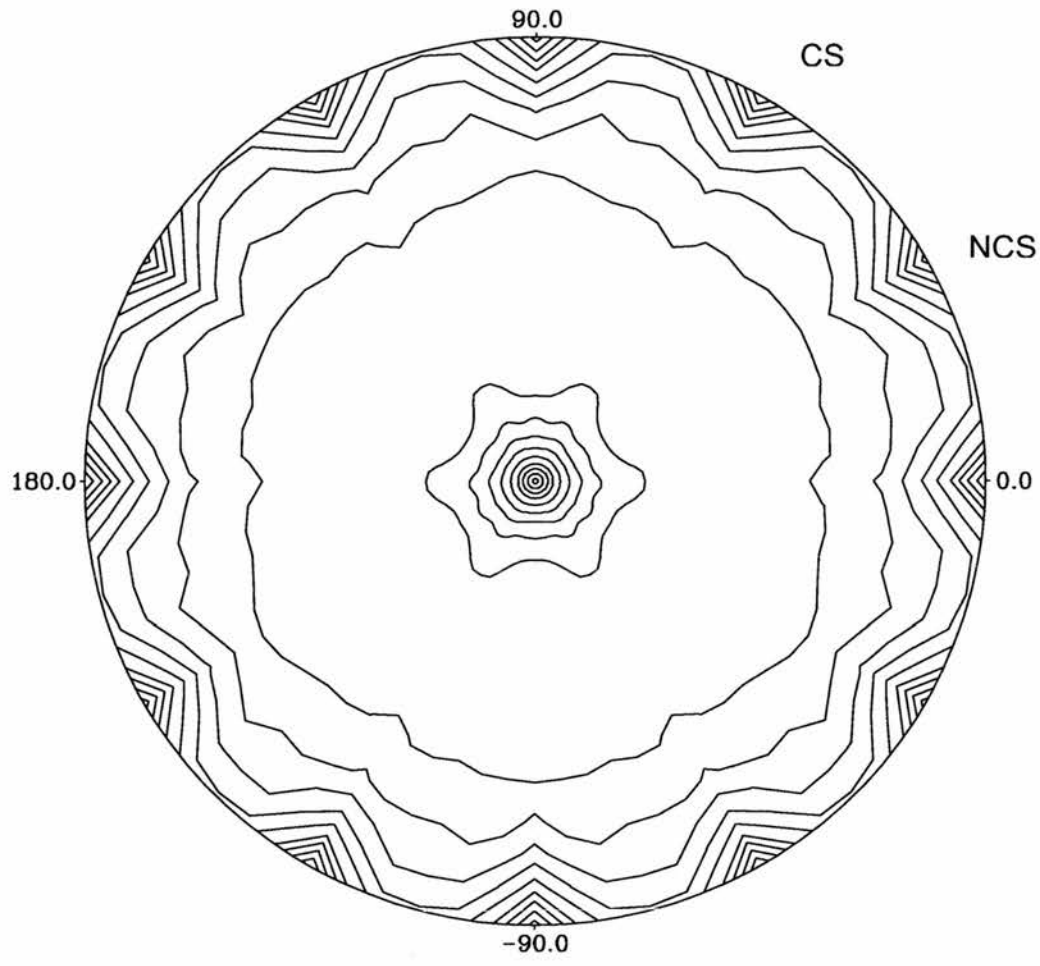

Figure 4.16 Self Rotation function of the trigonal dataset obtained from HMXOR crystals. Calculated with a 25 Å sphere, 10-4 Å data. Section shown is $\kappa = 180°$. Peaks corresponding to the CS 2-folds can be seen at 60° intervals, the NCS 2-fold peaks appear at 30° intervals.

A native Patterson map was calculated to detect any significant translation vectors that might suggest a pseudocentering of molecules in the unit cell. The native Patterson, calculated with data to 8Å, revealed a peak at (0, 0, ½) that was 50 % of the origin peak.

Since calculation of the solvent fraction had indicated that there were two dimers of XOR within the asymmetric unit, it was thought likely that the NCS 2-fold lay down the dimer axis and the two dimers were stacked on top of each other and related by (0, 0, ½). This led to two alternative strategies for improving the detection of correct MR solutions. Both made the assumption that the HMXOR dimer formation resembled that of CODH, not MOP.

The first strategy was to carry out a rotation search with AMoRe and then to select pairs of peaks that were related by a 30° rotation. RFCORR (CCP4) was used to find pairs of peaks, and those related by the rotation 90° 30° 180° were used in a translation search. However, although pairs of peaks were found, no solutions were obtained that packed well.

The second strategy was to take advantage of the fact that if the NCS 2-fold did lie down the dimer axis and the dimer arrangement was the same as that in CODH, then 2 of the rotation angles were already defined and it only remained to ascertain the degree of rotation around the NCS 2-fold (Fig. 4.17).

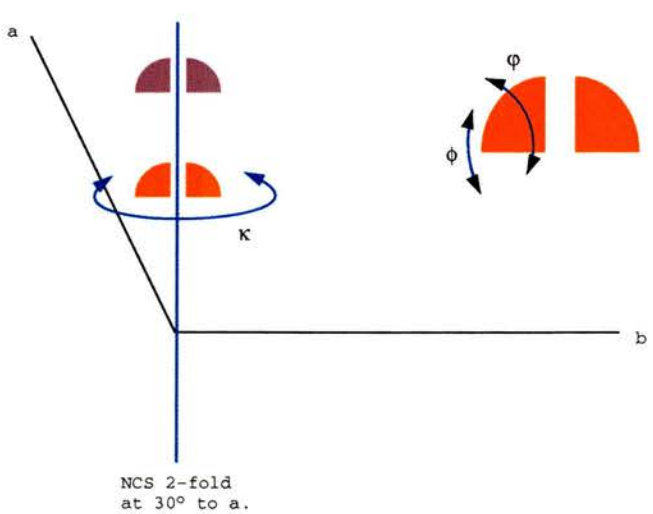

Figure 4.17
Illustrates that if the position of the NCS 2-fold with respect to the crystallographic axes is known and the dimer axis assumed to lie along the NCS 2-fold, then both ϕ and φ are defined and only κ remains to be determined.

From the self rotation function, we know that both dimers should be in the same orientation, therefore, after the rotation (κ only) and translation of the first dimer are determined, the second dimer can be generated by the translation (0, 0, ½).

The MR programmes within the XPLOR programme suite allow the calculation of a cross rotation function with two of the rotation angles locked at zero. Therefore the CODH dimer model was moved so that the dimer axis lay at 30° to a and then a 1 dimensional cross rotation search was carried out using XPLOR. The search was carried out twice with the dimer flipped through 180°. As before, no correctly packing solutions were found.

MR can prove difficult when either the model doesn't sufficiently resemble the target structure, or there is considerably more scattering matter in the asymmetric unit than in the model creating noise in the rotation function that makes it difficult to discern peaks corresponding to correct solutions. Searching with a CODH dimer should reduce this noise as, if there are two dimers within the unit cell, we are searching with 50 % of the scattering matter within the cell. However, if the dimer axis is considerably different, then a CODH dimer doesn't constitute an accurate search model. If we search with a monomer, we do not have the potential problem of the dimer formation being different, but we are only searching with 25 % of the scattering matter of the cell, and hence may not detect a solution above noise.

Again, it was thought possible that the strong NCS might be utilised to overcome these problems. It has already been noted that the trigonal data were strongly pseudo-hexagonal and, as mentioned previously, they scale acceptably as P622 at 6 Å resolution. Scaling as P622 treats the NCS 2-fold

as a crystallographic axis, reducing the size of the asymmetric unit by half. This means that, given a tetramer in the trigonal asymmetric unit, there will be a dimer in the hexagonal asymmetric unit. This then allows us to search with a monomer of CODH, thus avoiding any difficulties with dimer arrangement, whilst reducing the noise levels by reducing extra scattering matter within the asymmetric unit.

However, MR searches in P622, $P6_222$ and $p6_422$ with MOP and CODH, monomers and dimers, trimmed models and composite models all failed to yield any solutions that would pack correctly.

At this point, the new crystal form of HMXOR was obtained and a dataset collected that processed and scaled as $P2_12_12$ and had a considerably smaller unit cell. Calculation of the solvent fraction, as described, indicated the presence of only a dimer in the asymmetric unit. AMoRe was immediately used in an attempt to find a MR solution using the CODH monomer Cαs as a model and resolution limits of 20 - 4 Å. Solutions for two monomers were found (Tab. 4.4) whose CC_F and RF_F improved during the rigid body refinement step of AMoRe. The packing was checked using O, and the second solution found to generate a symmetry related molecule that formed a dimer with the first solution. PDBSET (CCP4) was used to translate the second monomer into its symmetry related position to produce the dimer (Fig. 4.18).

	Peak#	Rotation angles			Translation positions			CC_F	RF_F
SOLUTIONRC	1	44.05	76.50	65.00	0.0000	0.0000	0.0000	14.2	55.3
SOLUTIONRC	2	112.00	77.23	201.79	0.0000	0.0000	0.0000	13.6	55.4
SOLUTIONRC	3	9.69	44.50	223.58	0.0000	0.0000	0.0000	14.0	55.2
SOLUTIONRC	4	154.37	78.11	341.49	0.0000	0.0000	0.0000	14.0	55.3
SOLUTIONRC	5	119.84	22.36	19.89	0.0000	0.0000	0.0000	13.3	55.5
SOLUTIONRC	6	27.10	36.42	302.21	0.0000	0.0000	0.0000	13.4	55.5
SOLUTIONRC	7	13.26	41.28	218.84	0.0000	0.0000	0.0000	13.5	55.4
SOLUTIONRC	8	173.43	49.15	195.88	0.0000	0.0000	0.0000	13.6	55.3
SOLUTIONRC	9	125.25	77.88	64.03	0.0000	0.0000	0.0000	14.3	55.2
SOLUTIONRC	10	138.79	41.79	8.89	0.0000	0.0000	0.0000	13.7	55.4
SOLUTIONRC	11	83.39	53.98	145.72	0.0000	0.0000	0.0000	13.4	55.4
SOLUTIONRC	12	98.90	52.09	244.73	0.0000	0.0000	0.0000	13.6	55.2
SOLUTIONRC	13	112.19	27.04	104.88	0.0000	0.0000	0.0000	14.1	55.2
SOLUTIONRC	14	174.86	54.55	151.93	0.0000	0.0000	0.0000	13.1	55.5
SOLUTIONRC	15	10.42	37.06	6.16	0.0000	0.0000	0.0000	13.9	55.2
SOLUTIONRC	16	109.51	90.00	228.08	0.0000	0.0000	0.0000	13.3	55.4
SOLUTIONRC	17	71.65	90.00	48.23	0.0000	0.0000	0.0000	13.4	55.4
SOLUTIONRC	18	1.65	66.88	326.76	0.0000	0.0000	0.0000	13.0	55.6
SOLUTIONRC	19	27.29	52.97	150.63	0.0000	0.0000	0.0000	13.7	55.4
SOLUTIONRC	20	113.99	76.48	59.39	0.0000	0.0000	0.0000	13.8	55.3
SOLUTIONTF1	1	44.05	76.50	65.00	0.1777	0.2994	0.4333	18.7	55.1
SOLUTIONTF1	2	112.00	77.23	201.79	0.4270	0.4000	0.1236	16.8	55.5
SOLUTIONTF1	3	9.69	44.50	223.58	0.4763	0.0136	0.4118	17.2	55.7
SOLUTIONTF1	4	154.37	78.11	341.49	0.0561	0.0609	0.1519	17.1	55.5
SOLUTIONTF1	5	119.84	22.36	19.89	0.4865	0.9997	0.0566	17.2	55.7
SOLUTIONTF1	6	27.10	36.42	302.21	0.0556	0.0280	0.0574	17.3	55.6
SOLUTIONTF1	7	13.26	41.28	218.84	0.4723	0.4428	0.0491	16.8	55.9
SOLUTIONTF1	8	173.43	49.15	195.88	0.4799	0.4700	0.2036	17.7	55.4
SOLUTIONTF1	9	125.25	77.88	64.03	0.2613	0.1101	0.0237	18.8	55.3
SOLUTIONTF1	10	138.79	41.79	8.89	0.1148	0.0301	0.0364	17.0	55.8
SOLUTIONTF1	11	83.39	53.98	145.72	0.0053	0.0304	0.2097	16.8	55.8
SOLUTIONTF1	12	98.90	52.09	244.73	0.0827	0.0154	0.4818	17.7	55.6
SOLUTIONTF1	13	112.19	27.04	104.88	0.0454	0.4858	0.4355	17.5	55.5
SOLUTIONTF1	14	174.86	54.55	151.93	0.0015	0.3628	0.2918	16.2	55.9
SOLUTIONTF1	15	10.42	37.06	6.16	0.3652	0.0605	0.0688	18.1	55.1
SOLUTIONTF1	16	109.51	90.00	228.08	0.4325	0.0517	0.3599	17.1	55.6
SOLUTIONTF1	17	71.65	90.00	48.23	0.0672	0.0529	0.1403	16.8	55.7
SOLUTIONTF1	18	1.65	66.88	326.76	0.0043	0.3582	0.4926	16.5	55.6
SOLUTIONTF1	19	27.29	52.97	150.63	0.4308	0.0309	0.3279	17.1	55.7
SOLUTIONTF1	20	113.99	76.48	59.39	0.4476	0.3293	0.1627	17.6	55.5
SOLUTIONTF2	2	112.00	77.23	201.79	0.5636	0.3816	0.4536	18.0	54.7
SOLUTIONTF2	3	9.69	44.50	223.58	0.4833	0.0121	0.5924	18.6	54.7
SOLUTIONTF2	4	154.37	78.11	341.49	0.0877	0.4613	0.4944	18.9	54.3
SOLUTIONTF2	5	119.84	22.36	19.89	0.0826	0.8611	0.4247	18.1	54.6
SOLUTIONTF2	6	27.10	36.42	302.21	0.4882	0.3895	0.6012	18.4	54.7
SOLUTIONTF2	7	13.26	41.28	218.84	0.0150	0.8031	0.5427	18.5	54.4
SOLUTIONTF2	8	173.43	49.15	195.88	0.0276	0.3890	0.7519	18.4	54.5
SOLUTIONTF2	9	125.25	77.88	64.03	0.7618	0.1092	0.0239	21.7	54.2
SOLUTIONTF2	10	138.79	41.79	8.89	0.6185	0.9463	0.7071	18.5	54.4
SOLUTIONTF2	11	83.39	53.98	145.72	0.5227	0.8180	0.5972	18.6	54.5
SOLUTIONTF2	12	98.90	52.09	244.73	0.6844	0.7000	0.2431	18.4	54.8
SOLUTIONTF2	13	112.19	27.04	104.88	0.0370	0.5570	0.4314	18.6	54.6
SOLUTIONTF2	14	174.86	54.55	151.93	0.2586	0.7875	0.7869	18.1	54.7
SOLUTIONTF2	15	10.42	37.06	6.16	0.7336	0.5896	0.4795	18.7	54.6
SOLUTIONTF2	16	109.51	90.00	228.08	0.3151	0.2745	0.5659	18.3	54.6
SOLUTIONTF2	17	71.65	90.00	48.23	0.1827	0.7787	0.4307	18.4	54.7
SOLUTIONTF2	18	1.65	66.88	326.76	0.7698	0.3085	0.4686	18.2	54.6
SOLUTIONTF2	19	27.29	52.97	150.63	0.5340	0.1778	0.4349	18.7	54.4
SOLUTIONTF2	20	113.99	76.48	59.39	0.5502	0.1105	0.1930	18.5	54.5

Table 4.4. Showing the solutions obtained from an AMoRe MR search of the orthorhombic data, using a CODH monomer Cα search model. No solutions stand out in the rotation function as clearly correct, although peaks 1 & 9 which were found to be solutions in the translation searches do have the highest CC_F. Both peaks 1 & 9 stood out as solutions in the 1st translation search, as peak 1 had the lower RF_F that solution was fixed during the 2nd translation search, from which peak 9 was clearly the correct solution.

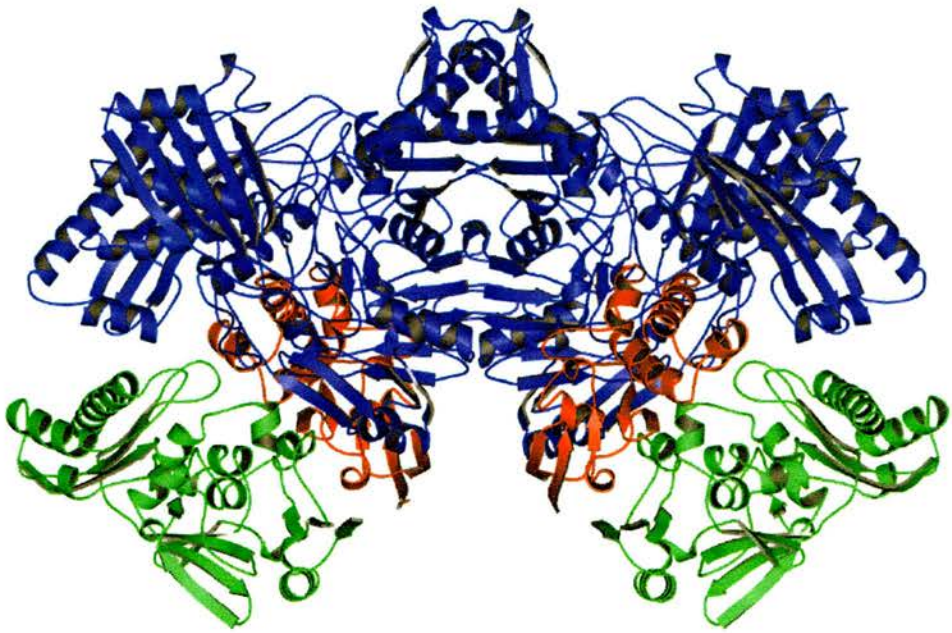

Figure 4.18 The 2 solutions found using the CODH monomer as a MR search model in AMoRe form a dimer. The dimer interface can be seen to closely resemble that of CODH (Fig. 4.15). The molybdenum domain is blue, the FAD domain green and the iron sulphur domain red. Picture generated with Molscript.

The CCP4 suite (SFALL, SIGMAA & FFT) was used to generate an electron density map using phases from the correctly positioned model dimer. The correctness of the solution was verified by contouring the map (generated from a poly-ala model) at 3σ and checking for the presence of the two iron sites. Both iron sites were clearly visible at the position expected from the CODH model.

However, this solution did not behave well during refinement. The electron density for one of the FAD domains appeared very disordered, and rigid body refinement (CNS) seemed unable to find a stable position for it.

Attempts were made to find an improved solution, indeed to confirm the solution described above, using a variety of search models; the molybdenum and iron sulphur domains of CODH, composite search models of MOP and CODH (with and without the FAD domain). A MOP search model was

superimposed on the first monomer found in the CODH monomer solution, and fixed as the solution for the first monomer and then rotation and translation searches attempted to locate the second monomer. None of the these approaches met with success, often the first monomer would be found with passable CC_F and RF_F, but either no second monomer solution was obtained, or the second monomer solution would not pack well. All of this led to a loss of confidence in the original solution as correct.

At this stage the coordinates of the bovine milk xanthine oxidase (Enroth *et al.*, 2000) became available to us (with the kind permission of E. Pai). Given the very high sequence identity between the two enzymes (90%) it was expected that this would provide a much better search model than either MOP or CODH. AMoRe was used to find a MR solution using the BMXO monomer (all atoms except the cofactors) as a model with resolution limits of 20-4 Å. Clear solutions were obtained for each monomer (Tab. 4.5) and both the CC_F and the RF_F improved during FITING.

Solution 1	40.55	76.62	243.83	0.1864	0.2910	0.4400	45.3 47.8
Solution 2	120.01	75.71	243.99	0.7728	0.1155	0.0359	64.0 38.9
After FITING							CC_F RF_F
Solution 1	40.25	76.71	243.58	0.1864	0.2908	0.4393	69.0 37.7
Solution 2	119.88	76.16	243.85	0.7728	0.1154	0.0354	69.0 37.7

The packing of the two solutions was checked in O and found to be very good. Interestingly, the dimer formation was very similar to that seen in the solution found using CODH as a model (Fig. 4.19). However, the FAD domain can be seen to packed more intimately against the iron sulphur and molybdenum domains. Electron density maps were generated for this solution

using only a poly-ala model for phasing (CNS) and again a map contoured at 3σ clearly showed the presence of the iron sulphur clusters. The same map contoured at 1σ also showed good density for the FAD isoalloxazine ring, indicating that the FAD domain model position was closer to that of HMXOR than in the CODH solution.

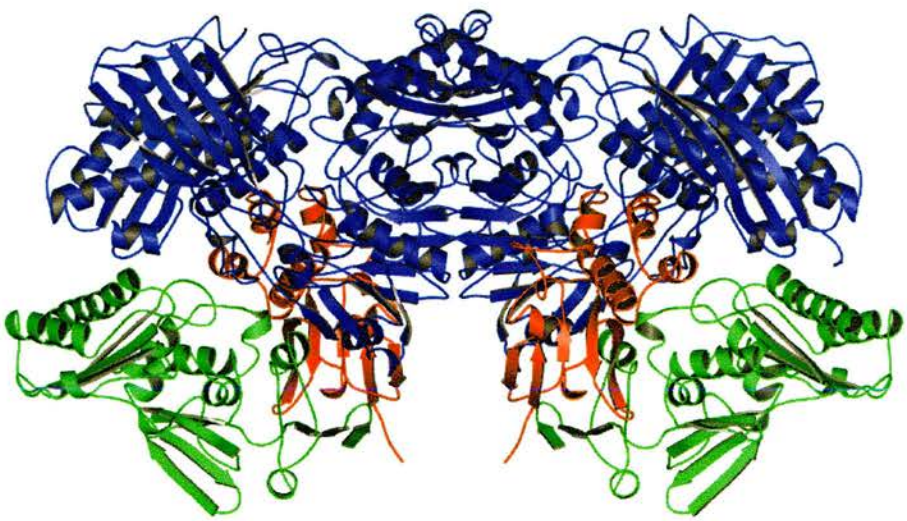

Figure 4.19 The dimer formed by the 2 solutions found using the BMXO monomer as a MR search model in AMoRe. The dimer arrangement is very similar to that found using CODH as the search model, however, the FAD domain packs more closely against the molybdenum and iron sulphur domains. The molybdenum domain is blue, the FAD domain green and the iron sulphur domain red. Picture generated with Molscript.

The BMXDH coordinates also became available at this stage and the same solution was found, with slightly better $R_{factors}$ and clearer maps.

	Peak#	Rotation angles			Translation positions			CC_F	RF_F
SOLUTIONRC	1	40.55	76.62	243.83	0.0000	0.0000	0.0000	25.6	53.7
SOLUTIONRC	2	120.01	75.71	243.99	0.0000	0.0000	0.0000	24.7	54.1
SOLUTIONRC	3	83.11	48.01	141.28	0.0000	0.0000	0.0000	20.5	55.2
SOLUTIONRC	4	116.79	75.55	43.23	0.0000	0.0000	0.0000	20.7	55.3
SOLUTIONRC	5	159.63	41.50	205.01	0.0000	0.0000	0.0000	19.4	55.6
SOLUTIONRC	6	152.50	59.44	46.42	0.0000	0.0000	0.0000	20.0	55.4
SOLUTIONRC	7	92.14	86.50	99.49	0.0000	0.0000	0.0000	20.1	55.3
SOLUTIONRC	8	166.33	81.08	341.67	0.0000	0.0000	0.0000	19.5	55.5
SOLUTIONRC	9	91.42	90.00	280.89	0.0000	0.0000	0.0000	20.0	55.3
SOLUTIONRC	10	56.90	74.92	246.97	0.0000	0.0000	0.0000	20.3	55.2
SOLUTIONRC	11	139.37	41.42	67.40	0.0000	0.0000	0.0000	19.9	55.5
SOLUTIONRC	12	2.50	51.50	139.93	0.0000	0.0000	0.0000	19.3	55.6
SOLUTIONRC	13	124.11	18.59	58.26	0.0000	0.0000	0.0000	19.6	55.5
SOLUTIONRC	14	10.26	65.39	247.26	0.0000	0.0000	0.0000	19.5	55.6
SOLUTIONRC	15	118.20	84.08	288.94	0.0000	0.0000	0.0000	19.6	55.5
SOLUTIONRC	16	74.84	33.57	278.91	0.0000	0.0000	0.0000	19.7	55.5
SOLUTIONRC	17	158.11	78.21	80.38	0.0000	0.0000	0.0000	20.2	55.4
SOLUTIONRC	18	138.46	83.50	182.02	0.0000	0.0000	0.0000	19.3	55.6
SOLUTIONRC	19	3.79	90.00	95.04	0.0000	0.0000	0.0000	19.4	55.6
SOLUTIONRC	20	177.42	90.00	275.72	0.0000	0.0000	0.0000	19.5	55.5
SOLUTIONTF1	1	40.55	76.62	243.83	0.1864	0.2910	0.4400	45.3	47.8
SOLUTIONTF1	2	120.01	75.71	243.99	0.2729	0.1154	0.0359	41.9	49.3
SOLUTIONTF1	3	83.11	48.01	141.28	0.9979	0.4062	0.0765	25.3	55.1
SOLUTIONTF1	4	116.79	75.55	43.23	0.0361	0.0195	0.1227	25.6	55.0
SOLUTIONTF1	5	159.63	41.50	205.01	0.4597	0.3600	0.1201	24.2	55.4
SOLUTIONTF1	6	152.50	59.44	46.42	0.1373	0.4432	0.0960	25.1	54.9
SOLUTIONTF1	7	92.14	86.50	99.49	0.4126	0.0617	0.1605	24.4	55.4
SOLUTIONTF1	8	166.33	81.08	341.67	0.0570	0.0390	0.2399	24.4	55.4
SOLUTIONTF1	9	91.42	90.00	280.89	0.1234	0.2963	0.0319	24.6	54.9
SOLUTIONTF1	10	56.90	74.92	246.97	0.0279	0.4483	0.0422	25.1	55.2
SOLUTIONTF1	11	139.37	41.42	67.40	0.4050	0.4536	0.1275	24.2	55.5
SOLUTIONTF1	12	2.50	51.50	139.93	0.0556	0.4650	0.2765	24.0	55.5
SOLUTIONTF1	13	124.11	18.59	58.26	0.1425	0.3799	0.0954	24.1	55.5
SOLUTIONTF1	14	10.26	65.39	247.26	0.4805	0.4842	0.3128	24.6	55.4
SOLUTIONTF1	15	118.20	84.08	288.94	0.1155	0.3241	0.4307	24.3	55.2
SOLUTIONTF1	16	74.84	33.57	278.91	0.1039	0.4240	0.0825	24.3	55.3
SOLUTIONTF1	17	158.11	78.21	80.38	0.0721	0.4369	0.1948	24.9	55.1
SOLUTIONTF1	18	138.46	83.50	182.02	0.4486	0.4373	0.3281	24.2	55.5
SOLUTIONTF1	19	3.79	90.00	95.04	0.0415	0.1074	0.0459	23.9	55.4
SOLUTIONTF1	20	177.42	90.00	275.72	0.4659	0.3510	0.4442	24.2	55.3
SOLUTIONTF2	2	120.01	75.71	243.99	0.7728	0.1155	0.0359	64.0	38.9
SOLUTIONTF2	3	83.11	48.01	141.28	0.5109	0.8866	0.5586	33.6	51.9
SOLUTIONTF2	4	116.79	75.55	43.23	0.7395	0.1088	0.7852	33.6	51.8
SOLUTIONTF2	5	159.63	41.50	205.01	0.3818	0.1377	0.7221	33.4	52.0
SOLUTIONTF2	6	152.50	59.44	46.42	0.0916	0.6343	0.8692	33.8	51.6
SOLUTIONTF2	7	92.14	86.50	99.49	0.7225	0.5928	0.3477	33.8	51.5
SOLUTIONTF2	8	166.33	81.08	341.67	0.0944	0.2010	0.0124	33.4	51.9
SOLUTIONTF2	9	91.42	90.00	280.89	0.7840	0.0821	0.6533	33.4	51.6
SOLUTIONTF2	10	56.90	74.92	246.97	0.3955	0.3393	0.4742	33.4	51.7
SOLUTIONTF2	11	139.37	41.42	67.40	0.3270	0.1002	0.2804	33.3	51.7
SOLUTIONTF2	12	2.50	51.50	139.93	0.3513	0.6079	0.8928	33.3	51.7
SOLUTIONTF2	13	124.11	18.59	58.26	0.8695	0.2525	0.4342	33.5	51.6
SOLUTIONTF2	14	10.26	65.39	247.26	0.4757	0.9925	0.4204	33.1	52.1
SOLUTIONTF2	15	118.20	84.08	288.94	0.9893	0.7579	0.4160	33.4	52.0
SOLUTIONTF2	16	74.84	33.57	278.91	0.5447	0.9019	0.3810	33.1	51.8
SOLUTIONTF2	17	158.11	78.21	80.38	0.4458	0.1224	0.4509	33.6	51.7
SOLUTIONTF2	18	138.46	83.50	182.02	0.0207	0.6884	0.4662	33.1	52.0
SOLUTIONTF2	19	3.79	90.00	95.04	0.7743	0.5704	0.5540	33.1	51.9
SOLUTIONTF2	20	177.42	90.00	275.72	0.8722	0.3892	0.6261	33.0	52.1

Table 4.5. Showing the solutions obtained from an AMoRe MR search of the orthorhombic data, using the BMXO monomer Cα search model. Two solutions are already evident in the rotation function (peaks 1 & 2) and these are clearly confirmed in the two translation searches.

Given the success of the BMXOR models in solving the orthorhombic data, it was decided to return to the slightly higher resolution (3.5 Å) trigonal data. AMoRe MR searches were carried out, using either the BMXDH monomer, or the dimer found in the orthorhombic space group. Searches with the dimer found only 1 solution, and no second dimer could be found, however, searching with the BMXDH monomer found four clear solutions (Tab. 4.6) which refined well in the rigid body refinement carried out by FITING and pack well together. Note the two sets of solutions with very similar Eulerian angles but related by approximately (0, 0, ½) as indicated in the native Patterson.

Solution 1	57.50	11.61	332.17	0.7154	0.5222	0.4794	26.4	53.3
Solution 2	57.50	11.61	332.17	0.7180	0.5251	0.9792	33.5	64.6
Solution 3	114.00	11.45	336.00	0.1950	0.3355	0.3929	39.5	52.5
Solution 4	114.00	11.45	336.00	0.1908	0.3289	0.8937	43.2	57.4

After FITING							CC_F	RF_F
Solution 1	58.97	11.69	330.55	0.7113	0.5176	0.4803	67.5	37.4
Solution 2	53.26	12.10	336.95	0.7232	0.5313	0.9771	67.5	37.4
Solution 3	112.25	11.35	340.02	0.2001	0.3425	0.3917	67.5	37.4
Solution 4	110.59	12.58	337.32	0.1819	0.3192	0.8952	67.5	37.4

	Peak#	Rotation angles			Translation positions			CC_F	RF_F
SOLUTIONRC	1	57.50	11.61	332.17	0.0000	0.0000	0.0000	15.3	56.0
SOLUTIONRC	2	114.00	11.45	336.00	0.0000	0.0000	0.0000	14.0	56.3
SOLUTIONRC	3	58.54	48.78	203.50	0.0000	0.0000	0.0000	11.6	57.0
SOLUTIONRC	4	27.78	63.67	141.67	0.0000	0.0000	0.0000	11.6	57.0
SOLUTIONRC	5	54.97	41.31	41.74	0.0000	0.0000	0.0000	12.5	56.8
SOLUTIONRC	6	59.33	87.51	221.06	0.0000	0.0000	0.0000	12.0	56.9
SOLUTIONRC	7	114.00	41.98	43.58	0.0000	0.0000	0.0000	12.3	56.8
SOLUTIONRC	8	83.34	81.27	243.15	0.0000	0.0000	0.0000	12.1	56.9
SOLUTIONRC	9	16.71	16.76	304.00	0.0000	0.0000	0.0000	12.3	56.7
SOLUTIONRC	10	116.00	61.22	41.17	0.0000	0.0000	0.0000	12.5	56.8
SOLUTIONRC	11	6.95	87.74	231.25	0.0000	0.0000	0.0000	11.9	57.0
SOLUTIONRC	12	82.41	66.21	239.66	0.0000	0.0000	0.0000	11.9	56.9
SOLUTIONRC	13	113.14	90.00	50.60	0.0000	0.0000	0.0000	11.8	57.0
SOLUTIONRC	14	118.78	48.75	202.32	0.0000	0.0000	0.0000	11.5	57.1
SOLUTIONRC	15	54.96	64.78	40.56	0.0000	0.0000	0.0000	12.5	56.8
SOLUTIONRC	16	94.55	43.62	211.92	0.0000	0.0000	0.0000	11.7	57.0
SOLUTIONRC	17	7.09	80.73	291.03	0.0000	0.0000	0.0000	12.3	56.8
SOLUTIONRC	18	111.20	65.30	43.50	0.0000	0.0000	0.0000	12.2	56.9
SOLUTIONRC	19	114.00	13.66	98.84	0.0000	0.0000	0.0000	12.4	56.8
SOLUTIONRC	20	59.00	90.00	41.00	0.0000	0.0000	0.0000	11.9	56.9
SOLUTIONTF1	1	57.50	11.61	332.17	0.7154	0.5222	0.4794	26.4	53.3
SOLUTIONTF1	2	114.00	11.45	336.00	0.1842	0.3233	0.3954	21.8	54.8
SOLUTIONTF1	3	58.54	48.78	203.50	0.0076	0.0371	0.0382	16.6	56.8
SOLUTIONTF1	4	27.78	63.67	141.67	0.9692	0.0642	0.0831	16.3	56.9
SOLUTIONTF1	5	54.97	41.31	41.74	0.1306	0.0124	0.0574	17.2	56.5
SOLUTIONTF1	6	59.33	87.51	221.06	0.0378	0.0285	0.0150	17.2	56.6
SOLUTIONTF1	7	114.00	41.98	43.58	0.6249	0.0161	0.2789	17.5	56.2
SOLUTIONTF1	8	83.34	81.27	243.15	0.9924	0.0343	0.0246	16.9	56.6
SOLUTIONTF1	9	16.71	16.76	304.00	0.9440	0.8744	0.1256	17.1	56.5
SOLUTIONTF1	10	116.00	61.22	41.17	0.8775	0.8995	0.0021	16.9	56.4
SOLUTIONTF1	11	6.95	87.74	231.25	0.0526	0.0092	0.3433	16.7	56.7
SOLUTIONTF1	12	82.41	66.21	239.66	0.9928	0.0313	0.0157	16.8	56.6
SOLUTIONTF1	13	113.14	90.00	50.60	0.0119	0.0530	0.4408	16.7	56.7
SOLUTIONTF1	14	118.78	48.75	202.32	0.9813	0.0147	0.2642	16.4	56.8
SOLUTIONTF1	15	54.96	64.78	40.56	0.0557	0.0194	0.1091	17.3	56.4
SOLUTIONTF1	16	94.55	43.62	211.92	0.0098	0.9944	0.4856	16.2	56.9
SOLUTIONTF1	17	7.09	80.73	291.03	0.9907	0.0764	0.4871	16.6	56.7
SOLUTIONTF1	18	111.20	65.30	43.50	0.0361	0.9789	0.2504	16.9	56.7
SOLUTIONTF1	19	114.00	13.66	98.84	0.0794	0.0531	0.2293	16.5	56.6
SOLUTIONTF1	20	59.00	90.00	41.00	0.0206	0.9756	0.0454	16.9	56.8
SOLUTIONTF2	1	57.50	11.61	332.17	0.7180	0.5251	0.9792	33.5	64.6
SOLUTIONTF2	2	114.00	11.45	336.00	0.1969	0.3385	0.3926	31.6	51.4
SOLUTIONTF2	3	58.54	48.78	203.50	0.9428	0.5433	0.8853	19.7	55.0
SOLUTIONTF2	4	27.78	63.67	141.67	0.3099	0.0125	0.3794	19.9	55.0
SOLUTIONTF2	5	54.97	41.31	41.74	0.7981	0.0457	0.5832	20.0	55.0
SOLUTIONTF2	6	59.33	87.51	221.06	0.5436	0.4900	0.8164	19.7	55.0
SOLUTIONTF2	7	114.00	41.98	43.58	0.7313	0.8973	0.0173	20.4	54.9
SOLUTIONTF2	8	83.34	81.27	243.15	0.3252	0.7142	0.9870	20.1	54.9
SOLUTIONTF2	9	16.71	16.76	304.00	0.2540	0.6412	0.7587	20.0	55.0
SOLUTIONTF2	10	116.00	61.22	41.17	0.5429	0.5593	0.0000	20.3	55.0
SOLUTIONTF2	11	6.95	87.74	231.25	0.5439	0.1047	0.6854	20.0	54.8
SOLUTIONTF2	12	82.41	66.21	239.66	0.7152	0.3699	0.4905	19.9	54.9
SOLUTIONTF2	13	113.14	90.00	50.60	0.5364	0.1750	0.7355	19.9	54.9
SOLUTIONTF2	14	118.78	48.75	202.32	0.6168	0.0821	0.5523	19.7	55.1
SOLUTIONTF2	15	54.96	64.78	40.56	0.5265	0.3294	0.0797	20.0	55.1
SOLUTIONTF2	16	94.55	43.62	211.92	0.4325	0.8469	0.2741	19.6	55.1
SOLUTIONTF2	17	7.09	80.73	291.03	0.5574	0.9674	0.0686	20.3	54.8
SOLUTIONTF2	18	111.20	65.30	43.50	0.5020	0.4408	0.9965	19.9	55.2
SOLUTIONTF2	19	114.00	13.66	98.84	0.0546	0.3001	0.6420	20.0	55.1
SOLUTIONTF2	20	59.00	90.00	41.00	0.4641	0.1482	0.2873	19.8	55.2

Cont'd

Table 4.6 For the full table legend see the following page.

SOLUTIONTF3	1	57.50	11.61	332.17	0.7162	0.5231	0.4793	33.2	57.1
SOLUTIONTF3	2	114.00	11.45	336.00	0.1950	0.3355	0.3929	39.5	52.5
SOLUTIONTF3	3	58.54	48.78	203.50	0.6815	0.0837	0.7290	30.6	55.5
SOLUTIONTF3	4	27.78	63.67	141.67	0.4765	0.5042	0.4603	30.5	55.6
SOLUTIONTF3	5	54.97	41.31	41.74	0.5937	0.5579	0.0885	30.7	55.6
SOLUTIONTF3	6	59.33	87.51	221.06	0.5015	0.0042	0.2868	30.6	55.6
SOLUTIONTF3	7	114.00	41.98	43.58	0.3520	0.7884	0.6975	30.9	55.5
SOLUTIONTF3	8	83.34	81.27	243.15	0.6011	0.7642	0.5128	30.4	55.6
SOLUTIONTF3	9	16.71	16.76	304.00	0.1204	0.3698	0.6834	30.8	55.6
SOLUTIONTF3	10	116.00	61.22	41.17	0.6402	0.4926	0.8337	31.0	55.5
SOLUTIONTF3	11	6.95	87.74	231.25	0.0092	0.4000	0.6705	30.7	55.5
SOLUTIONTF3	12	82.41	66.21	239.66	0.7158	0.3702	0.4897	30.5	55.8
SOLUTIONTF3	13	113.14	90.00	50.60	0.4010	0.0105	0.3303	30.6	55.7
SOLUTIONTF3	14	118.78	48.75	202.32	0.6385	0.4878	0.8791	30.5	55.6
SOLUTIONTF3	15	54.96	64.78	40.56	0.7641	0.3504	0.1512	30.7	55.8
SOLUTIONTF3	16	94.55	43.62	211.92	0.2357	0.6485	0.1032	30.4	55.8
SOLUTIONTF3	17	7.09	80.73	291.03	0.0925	0.6913	0.9039	30.7	55.5
SOLUTIONTF3	18	111.20	65.30	43.50	0.5038	0.4415	0.4970	30.7	55.8
SOLUTIONTF3	19	114.00	13.66	98.84	0.6052	0.3643	0.4354	30.8	55.5
SOLUTIONTF3	20	59.00	90.00	41.00	0.0036	0.5052	0.7133	30.4	55.7
SOLUTIONTF4	1	57.50	11.61	332.17	0.7160	0.5229	0.4792	38.6	52.9
SOLUTIONTF4	2	114.00	11.45	336.00	0.1908	0.3289	0.8937	43.2	57.4
SOLUTIONTF4	3	58.54	48.78	203.50	0.8811	0.3362	0.1427	35.3	52.5
SOLUTIONTF4	4	27.78	63.67	141.67	0.5378	0.1261	0.5660	35.4	52.3
SOLUTIONTF4	5	54.97	41.31	41.74	0.1655	0.5420	0.0909	35.6	52.4
SOLUTIONTF4	6	59.33	87.51	221.06	0.4027	0.2740	0.9049	35.5	52.4
SOLUTIONTF4	7	114.00	41.98	43.58	0.4606	0.9823	0.9070	35.7	52.3
SOLUTIONTF4	8	83.34	81.27	243.15	0.2878	0.6413	0.9543	35.6	52.2
SOLUTIONTF4	9	16.71	16.76	304.00	0.1440	0.8248	0.5649	36.4	52.1
SOLUTIONTF4	10	116.00	61.22	41.17	0.6426	0.4922	0.8348	35.8	52.2
SOLUTIONTF4	11	6.95	87.74	231.25	0.9801	0.7327	0.5633	35.5	52.4
SOLUTIONTF4	12	82.41	66.21	239.66	0.4310	0.0491	0.8650	35.7	52.4
SOLUTIONTF4	13	113.14	90.00	50.60	0.3982	0.0098	0.3293	35.4	52.3
SOLUTIONTF4	14	118.78	48.75	202.32	0.4642	0.1943	0.8074	35.4	52.4
SOLUTIONTF4	15	54.96	64.78	40.56	0.7656	0.3515	0.1499	35.7	52.4
SOLUTIONTF4	16	94.55	43.62	211.92	0.8190	0.4288	0.5283	35.4	52.3
SOLUTIONTF4	17	7.09	80.73	291.03	0.3942	0.5169	0.0266	35.8	52.1
SOLUTIONTF4	18	111.20	65.30	43.50	0.7411	0.1192	0.6847	35.6	52.4
SOLUTIONTF4	19	114.00	13.66	98.84	0.0552	0.3041	0.6413	35.7	52.3
SOLUTIONTF4	20	59.00	90.00	41.00	0.6907	0.5184	0.6486	35.4	52.3

Figure 4.6. Showing the solutions obtained from an AMoRe MR search of the trigonal data using the BMXO monomer as a model (all atoms except cofactors were included). Two solutions (peaks 1 & 2) stand out already in the rotation function. These are then confirmed in the translation seraches. Since the four solutions consists of two pairs of monomers in exactly the same orientation, it was necessary to use all rotation solutions in the translation searches, rather than fixing a solution and then removing that rotation from the input to the translation search. Examination of the packing and the position of symmetry related molecules indicates clearly that pairs of solutions in the same orientation are not equivalent.

Interestingly, although 4 solutions were found using the BMXDH monomer, there were not two dimers lying down the NCS 2-fold. Rather, two of the monomer solutions lie along the crystallographic 2-fold and form dimers with their symmetry generated partners, and a third dimer is formed by the 3rd and 4th solutions, its dimer axis lies at 30° to *a* along the NCS-2-fold. Finding the solution was further complicated by the fact that solutions 1 and 2, and

solutions 3 and 4 are in nearly the identical orientation. The four solutions were moved as close as possible to each other using symmetry operations (CNS) and a further check of the correctness of the solution carried out by generating structure factors for the shifted model and calculating a self rotation function (CCP4). It can be seen (Fig 4.20) that the self rotation function closely resembles that of the native data (Fig 4.16).

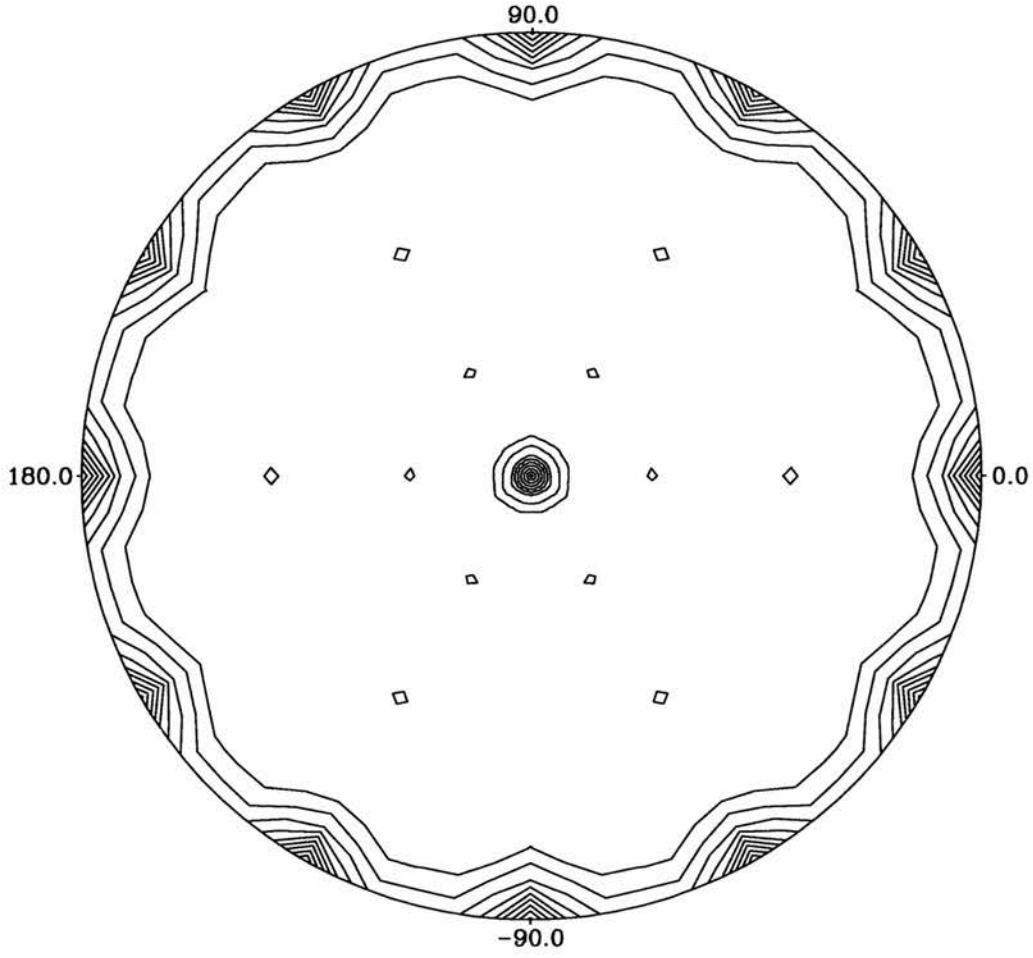

Figure 4.20 Self Rotation function of the calculated structure factors from the 4 molecule solution of the trigonal HMXOR dataset. Calculated with a 25 Å sphere, 10-4 Å data. Section shown is $\kappa = 180^{\circ}$. Peaks corresponding to the CS 2-folds can be seen at 60° intervals, the NCS 2-fold peaks appear at 30° intervals.

4.5 Refinement

4.5.1 Principles of refinement

Once a solution to the phase problem has been found, and the MR search model correctly placed in the unit cell, the model phases need to be refined until they approach closely the true phases of the target molecule. Crudely, this is an iterative process in which a starting map is calculated, and then the model adjusted to fit more closely with the density. From this new model new phases are generated, the calculated structure factors refined against the observed structure factors and a new map made. After which, the model is again adjusted to fit the observed density.

This iterative method again takes advantage of the properties of Fourier transforms. The electron density $\rho(x,y,z)$ produced from model phases can be calculated and viewed in real space, and the model manipulated (real space refinement). Using reverse Fourier transform, structure factor amplitudes are calculated for the modified model and compared to the observed amplitudes. This allows both a measure of the quality of the new model (how well it reflects the actual structure) and a further opportunity for refinement (reciprocal space refinement).

Reciprocal space refinement proceeds by minimising a residual that includes an X-ray term based on $(|F_o|-|F_c|)$, and a number of pseudo energy terms that enforce stereochemical restraints. These stereochemical restraints are used

to improve the effective number of observations, as macromolecular diffraction data are not usually in the atomic range. By applying restraints, the ratio of degrees of freedom (or parameters to be refined) to the number of observations is reduced, allowing a more accurate refinement with limited observations. Such restraints include restraining bond lengths and angles, as well as the application of non-crystallographic symmetry.

Two methods are in common use for reciprocal space refinement; the minimisation of a least squares function (12) that describes the difference between observed and calculated structure factor amplitudes.

$$\Phi = \sum_{hkl} w_{hkl} \left(|F_o| - k|F_c| \right)^2_{hkl} \qquad (12)$$

Where $(|F_o| - |F_c|)_{hkl}$ describes the difference between the observed ($|F_o|$) and calculated ($|F_c|$) amplitudes for reflection *hkl*, w_{hkl} is a weighting term that reflects the quality of the observed data for that reflection and *k* represents the overall scale factor between $|F_o|$ and $|F_c|$.

An alternative to least squares minimisation is Maximum Likelihood (ML) refinement. This relies on the fact that the best model is the one that is most consistent with experimental observations, and calculates the likelihood of the data given that the model is correct. Using Bayesian statistics it can be shown that the probability that the model is correct, p(B), and the probability that the data is correct, p(A), are related (13).

$$p(\mathrm{B};\mathrm{A}) = \frac{p(\mathrm{B})p(\mathrm{A};\mathrm{B})}{p(\mathrm{A})} \qquad (13)$$

Putting this in terms of data and models and treating p(A) as a constant (since the probability of the data is fixed), we obtain the following expression (14).

$$p(\text{model};\text{data}) = p(\text{model})p(\text{data};\text{model}) \qquad (15)$$

Hence, the probability (or likelihood) of the model given the observed data, p(model;data), is equivalent to the product of the probability of the model being correct, p(model), and the probability of obtaining the observed data, given the current model, p(data;model). p(model) contains a priori information about the model (restraints) such as ideal geometry and NCS.

ML refinement seeks to maximise the likelihood function describing the likelihood of the data given the model is correct, in practice, a minimisation function is used, minimising the -log of the likelihood.

This minimisation, either of a -log likelihood or of a least squares function, can take various forms; rigid body refinement, in which various parts of the structure are defined as units and can be refined with respect to their relative position, but not their internal arrangement; refinement of all atomic positions with restraints applied using known molecular geometry such as bond lengths and angles and refinement of atomic B factors as a measure of the disorder of individual atoms.

Refinement is monitored by two criteria; the R_{factor} (R) and the *free* R_{factor} (R_{free}). Both $R_{factors}$ are calculated in a similar fashion, but from different sets of data, and measure the convergence of the observed and calculated structure factors (13).

$$R = \frac{\sum \| F_o | - | F_c \|}{\sum | F_o |} \qquad (13)$$

R_{free} is calculated using a small set of randomly chosen intensities (test set) that are set aside at the beginning of refinement and not used other than to act as a cross validation of the agreement of the model with the observed data. In other words, calculation of R_{free} allows assessment of how well the model predicts a set of observed intensities that have not been included in the model refinement. R, on the other hand, measures how well the model predicts the entire observed data set. For a set of random amplitudes compared to a set of observed amplitudes R is ~ 0.6, for a perfect model of the observed data R would be 0. Use of R_{free} also gives an indication of when the data is over refined and the model is introducing a degree of accuracy that is not present in the data. At this point, although R may continue to drop, R_{free} will either stall, or begin to rise.

4.5.2 Refinement results

Refinement of the orthorhombic data was begun using CNS. First maps were generated using a poly-ala trace with no cofactors and showed a clear protein/solvent boundary and 2^{o} structure. Density was also visible for the iron sulphur clusters and the FAD, although no density was found for the molybdenum or MPT cofactor.

Refinement of the orthorhombic data using a poly-ala model in CNS (cycles of rigid body refinement followed by minimisation and manual model building in O) did not go well. After an initial drop in R and R_{free}, there was no further improvement (R=0.35, R_{free}=0.46). Due to the size of the asymmetric unit of the trigonal data (4 monomers, each 1332 residues), it was impossible to use CNS as currently compiled.

Since the bovine and human milk XOR sequences are 90 % identical, it was decided to attempt to refine the human data against a full BMXDH model in which the 10% of non-identical residues were mutated to alanine (or glycine), rather than attempting to build in side chains into a 3.6 Å map. Hence, the BMXDH structure was mutated using O to create the new model. Refinement of the trigonal data with this new model was attempted first, as it was hoped that the presence of 4 monomers and the use of tight NCS restraints would improve the refinement. Because of the size of the asymmetric unit of the trigonal data, as mentioned above, REFMAC5 was used as the refinement programme.

Rigid body and TLS refinement in REFMAC5 to 3.6 Å did not produce an improvement in R factor or in model quality (monitored by PROCHECK, CCP4).

The refinement strategy giving the best results in REFMAC5 refinement of the trigonal solution was very simple. The starting model was bovine milk XDH, containing all protein atoms (mutated to the human sequence) but lacking the cofactors. A ML refinement of all atoms was carried out using conjugate gradient minimization and applying tight NCS restraints. Overall B factors were refined, applying the average B factor obtained from the Wilson plot. Tight NCS restraints were used for each domain, although not for entire monomers. Geometric restraints were also applied, some trial and error was involved to find the restraint level that gave the best geometry and R factor combination.

$2F_o$-F_c and F_o-F_c maps generated from this refined model showed clear density for the iron-sulphur clusters. They were accordingly introduced into the model and refinement continued using the same set of restraints as before.

After 15 cycles of maximum likelihood refinement in REFMAC (CCP4), the structure appears to be refining well; R=0.305 and R_{free}=0.321.

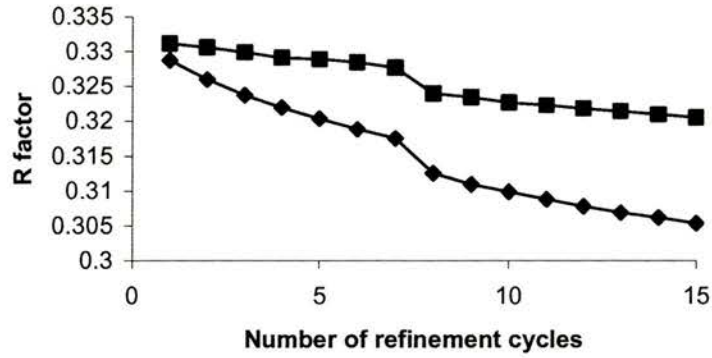

Figure 4.21 Graph showing the decrease in R and R_{free} during refinement. The iron sulphur clusters were added before cycle 8. ♦ indicates the R factor, ■ indicates R_{free}.

At the current stage of refinement of the trigonal data, $2F_o$-F_c maps show clear protein solvent boundaries and readily interpretable density for most of the peptide chain (Fig. 4.22). Strong density is visible for the two iron sulphur clusters (Fig. 4.23) and, although not yet included in the refinement, weaker density is also visible for the FAD (Fig. 4.24). No density is visible for the molybdenum or molybdopterin (Fig. 4.25).

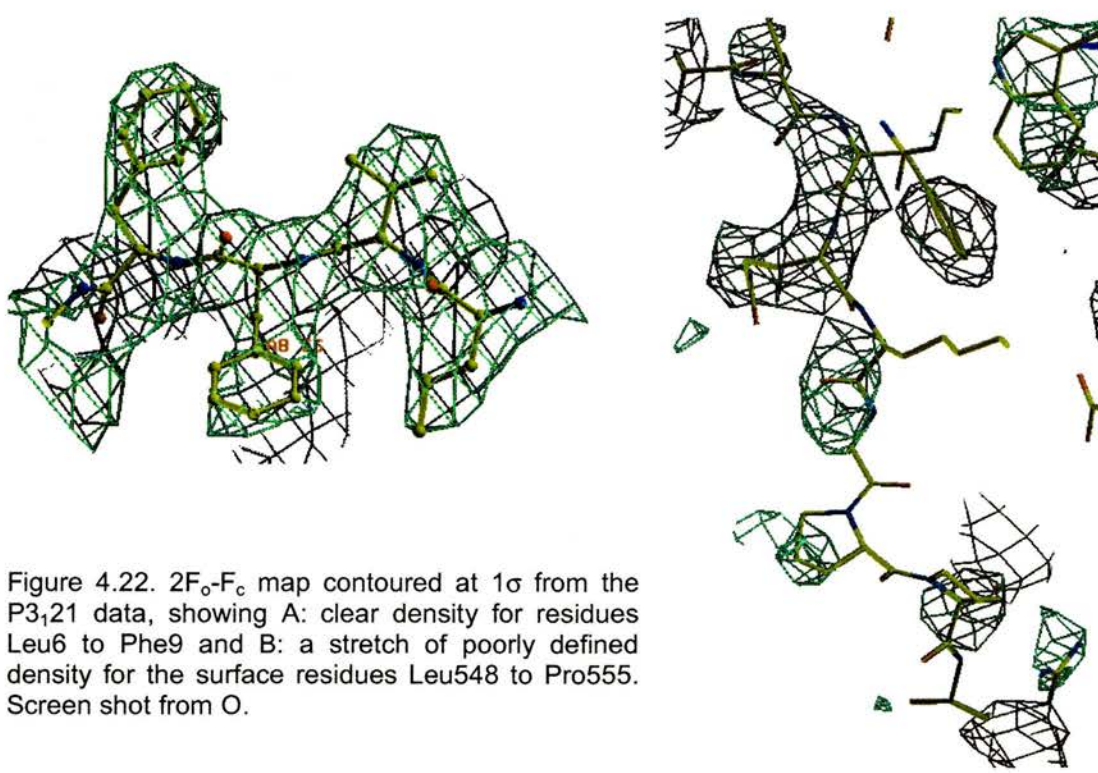

Figure 4.22. $2F_o$-F_c map contoured at 1σ from the $P3_121$ data, showing A: clear density for residues Leu6 to Phe9 and B: a stretch of poorly defined density for the surface residues Leu548 to Pro555. Screen shot from O.

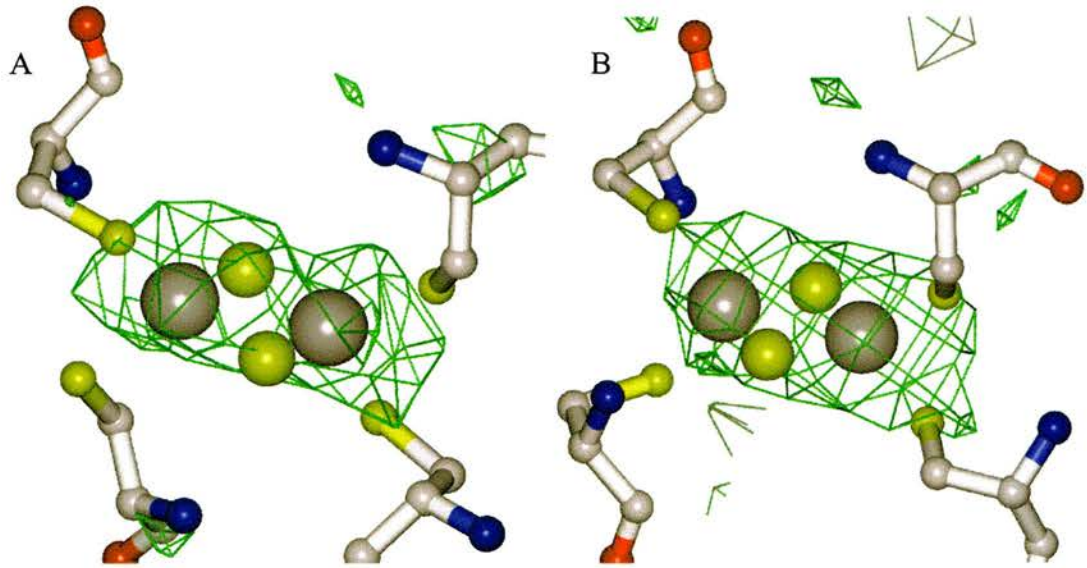

Figure 4.23. F_o-F_c map contoured at 4 σ from the $P3_121$ data, showing density for FeS1 (A) and FeS2 (B) and the four coordinating cysteines (A113, A116, A148 & A150 for FeS1 and A43, A48, A51 and A73 for FeS2). Picture generated with Molscript.

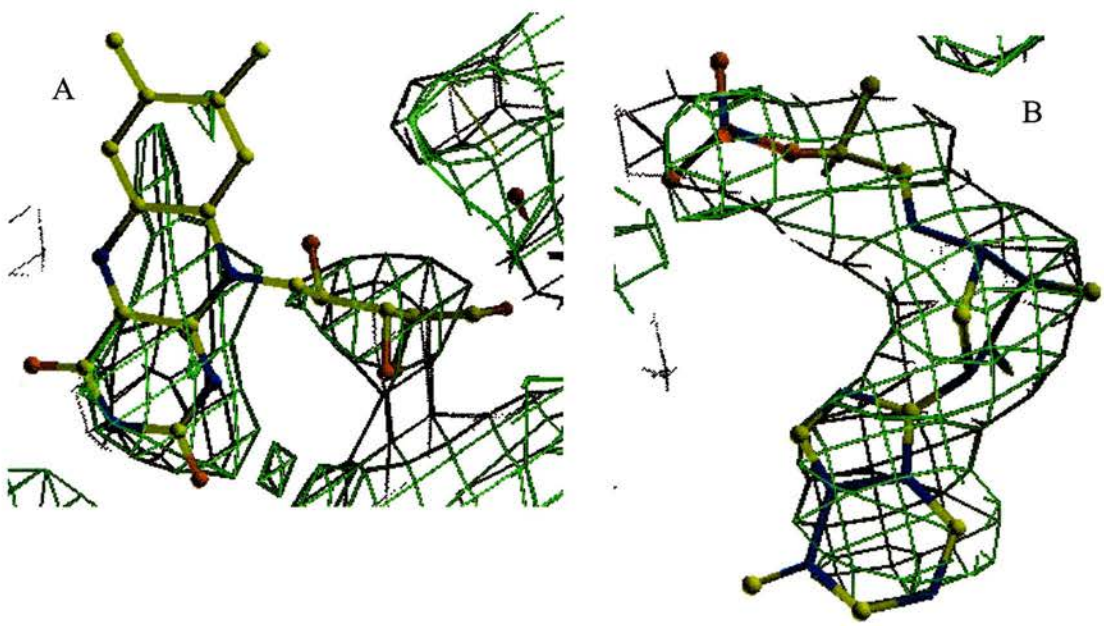

Figure 4.24. $2F_o$-F_c map contoured at 1σ from the $P3_121$ data, showing the isoalloxazine ring (A) and the adenosine moiety (B) of the FAD. Weak density, in particular for the isoalloxazine ring, is seen for the FAD although it is not yet included in the refinement model. Screen shot from O.

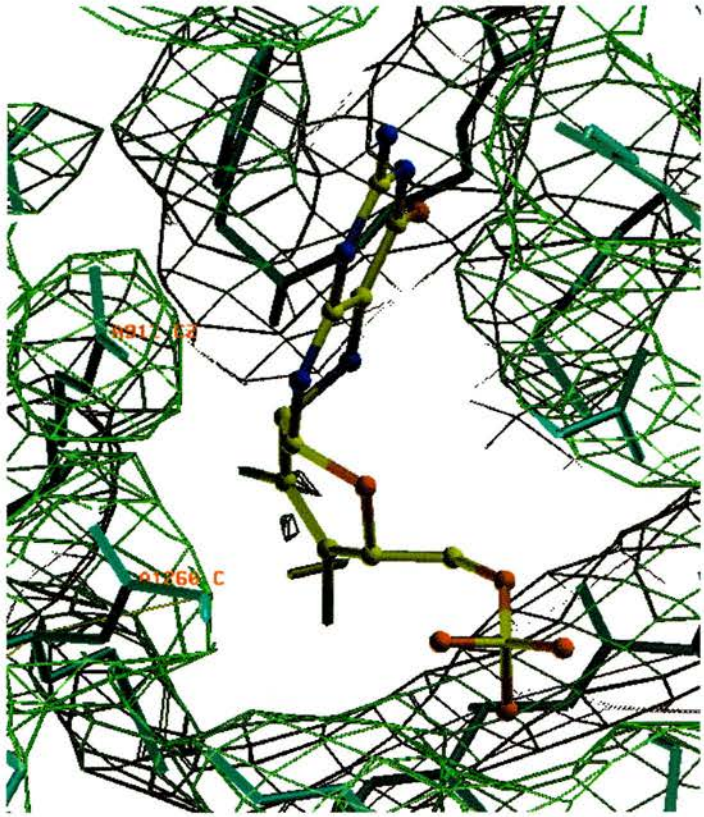

Figure 4.25. $2F_oF_c$ map contoured at 1 σ from the $P3_121$ data, showing the lack of any visible density for the molybdopterin or molybdenum. Screen shot from O.

4.6 Discussion

This chapter presents the collection of XOR diffraction data sets in two space groups ($P3_121$ and $P2_12_12$) to a maximum resolution of 3.5 Å; the solution of these two data sets using the bovine milk xanthine oxidase structure as a molecular replacement search model and the preliminary refinement of both data sets using maximum likelihood methods.

Collection of diffraction data from the orthorhombic crystal form was very dependent on freezing conditions. The best diffraction was observed from a crystal containing no cryoprotectant that was frozen rapidly by plunging into liquid nitrogen. Even this crystal, however, showed smeary diffraction beyond 3.6 Å suggesting that further manipulation of freezing conditions could yield improved data. To date, the only datasets collected from the trigonal crystals were from larger (800 μ) crystals frozen using 20 % glycerol as a cryoprotectant. No trigonal crystals have been mounted in the absence of cryoprotectant and it may be the case that the smaller trigonal crystals will show improved diffraction when frozen in this manner. Beam intensity was also a factor in obtaining good diffraction. Both datasets solved were collected at the ESRF, Grenoble on two very high intensity beam lines. ID-13, the microfocus beamline at ESRF, was particularly useful in obtaining data from the very small (50 μ) orthorhombic crystals.

Molecular replacement solutions were sought using three search models, aldehyde oxidoreductase from *D. gigas* (Romão *et al.*, 1995), carbon monoxide dehydrogenase from *O. carboxidovorans* (Dobbek *et al.*, 1999) and

xanthine dehydrogenase/oxidase from *B. taurus* (Enroth *et al.*, 2000). No MR solution of the trigonal data was found using MOP as a search model, despite the relatively good fit of the MOP structure to BMXDH (r.m.s.d = 2.5 Å, calculated using the VAST structural alignment server at http://www.ncbi.nlm.nih.gov/Structure/VAST/vast.shtml). This is likely due to the low percentage of scattering matter within the trigonal asymmetric unit actually represented by the MOP model. This could have been improved by searching with the dimer, but as is described previously, the dimer interface in MOP is radically different to CODH or XOR and so also did not lead to a solution. A MR solution was found in the $P2_12_12$ data using the CODH monomer, but did not behave well during further analysis and was discarded, although subsequent comparison with the true solution indicates that the solution found was correct. As with MOP, no solution of the trigonal data was found using CODH. The difficulty in refining the CODH solution found for the orthorhombic data and the lack of any solution for the trigonal data may reflect the low sequence homology of CODH and human XOR (35 % in the iron sulphur domain, 23 % in the molybdenum domain and only 18 % in the FAD domain). Structural comparison of XOR with CODH also indicates considerable differences in loop regions.

MR replacement solutions were finally found using the coordinates of BMXO (kindly supplied by E. Pai) in both the trigonal and orthorhombic datasets. As expected a single dimer was found in the orthorhombic asymmetric unit. The solutions found in the trigonal data were slightly more surprising in that, rather than the expected two dimers, one dimer and 2 monomers (forming dimers with crystallographically related molecules) were found. Both sets of data

were resolved with the BMXDH coordinates (Enroth *et al.*, 2000), finding the same solutions that proved slightly easier to refine.

Refinement of the trigonal solution is underway using maximum likelihood methods in REFMAC (CCP4). Iron sulphur centres have been introduced into the refinement and the structure currently has an R_{factor} of 0.305 and an R_{free} of 0.321. Calculation of a Ramachandran plot (PROCHECK, CCP4) indicates that only 0.7 % of residues are in disallowed conformations.

Visual inspection of both the orthorhombic and trigonal solutions in O reveals that the dimer formation is identical in both space groups (CS and NCS trigonal dimers and orthorhombic dimer). Both structures also show strong density for the iron sulphur clusters in F_o-F_c maps contoured at 3 σ as well as clear density for the FAD. No density is observed in either crystal form for the molybdenum or molybdopterin.

Chapter 5

Discussion

5.1 Summary of results

The purification procedure of HMXOR described by Sanders and colleagues, (Sanders *et al.*, 1997) and modified by Godber, (Godber, 1998) was further optimised during this work by the substitution of a desalting column for an overnight dialysis step. This reduces the purification to a two-day protocol and yields enzyme of high purity and dehydrogenase content suitable for crystallization.

Crystals of HMXOR suitable for X-ray diffraction studies were obtained using the microbatch under oil technique in the presence of DTT. DTT was absolutely required for crystallization. It is likely that it is acting both to reduce non-specific aggregation of HMXOR (possibly by reducing intermolecular disulphide bonds) as described by Godber (Godber, 1998) as well as maintaining the dehydrogenase form. Two crystal forms of HMXOR can be reproducibly obtained; a trigonal form that appears rapidly and a slower growing orthorhombic form that appears over 1-2 weeks.

Complete X-ray diffraction datasets were collected from both HMXOR crystal forms to a maximum resolution of 3.5 Å (trigonal) and the structure solved using the molecular replacement method with the bovine milk XDH and XO structures as search models. Refinement of both structures is currently underway using REFMAC (CCP4).

The cDNA sequence of human mammary gland epithelial cell XDH has been determined (with the exception of 9 ambiguous bases in the 3' region). It is identical to those sequences already determined for human liver and small intestine (Ichida *et al.*, 1993; Saksela and Raivio, 1996; Yamamoto *et al.*, 2001).

5.2 Sequencing of human mammary gland XDH.

In this study, the molecular basis for the low molybdenum content of human milk XOR was addressed. Several identical cDNA sequences of human XDH have been reported (Ichida *et al.*, 1993; Saksela and Raivio, 1996; Yamamoto *et al.*, 2001) from liver and small intestine. However, these sequences are all from tissues traditionally regarded as "high" XOR activity (Abadeh *et al.*, 1992; Harrison, 1997). In order to determine whether the low molybdenum observed in human milk XOR is due to the expression of an alternative transcript of XDH with inherently lower affinity for molybdenum in the mammary gland, the sequence of human mammary gland XDH was nearly completely determined by Briggs (Briggs, 1997). In this study the sequence was completed, apart from a stretch of 26 bases at the 3' end in which 8 bases remain ambiguous and one ambiguous base at position 3506 (liver numbering). The derived sequence from human mammary gland epithelial cells is identical to those human cDNA sequences already determined.

As mentioned in Chapter 3, the complete identity of the determined sequence does not rule out the possibility of an alternative transcript of XDH being expressed at low levels within the mammary gland. However, several other observations suggest that this is unlikely.

The genomic sequence of human XDH was reported by Xu and colleagues (Xu *et al.*, 1996), although the sequence was not released. It has since been reported as part of two larger BAC sequences (Hazan *et al.*, 1999). Study of

the intronic regions revealed no alternative exons, therefore if an alternative transcript of human XDH does exist it must be on another section of the genome. All gene localization studies carried out to date report a single copy of the XDH gene located at chromosome 2p22 (Ichida *et al.*, 1993; Xu *et al.*, 1994). The two BAC sequences reported are also from this region (chromosome 2p2-1p22) (Hazan *et al.*, 1999). This strongly suggests that there is indeed a single human XDH transcript.

In addition, several workers have shown that under certain conditions human XOR is upregulated in a manner that appears to involve activation of a pool of inactive XOR rather than de-novo synthesis of XOR. Brown and coworkers (Brown *et al.*, 1995) showed wide variation (50 fold) of XOR specific activity in breast milk after parturition that was not mirrored in the amount of XOR protein present. Page and colleagues (Page *et al.*, 1998) have shown that XOR specific activity in a human mammary gland epithelial cell line is also upregulated by various cytokines. They reported an 8-fold increase in XOR activity, accompanied by only a 2-3 fold increase in XDH mRNA and protein.

Godber (Godber, 1998) suggested that increases in specific activity can be at least partially accounted for by conversion of the desulpho form of XOR to the active sulpho form. As desulpho-XOR comprises at least 40 % of molybdopterin containing human milk XOR (Harrison, 1997) it is plausible that conversion of desulpho- to sulpho-XOR accounts for the cytokine driven 2-3 fold upregulation of XOR observed by Page and coworkers (Page *et al.*, 1998).

More recently, upregulation of XOR in response to the lactogenic hormones, prolactin and cortisol, has been reported in mouse mammary gland (McManaman *et al.*, 2000). These workers reported a 5.5-fold increase in XOR activity, accompanied by a 4-fold increase in XOR protein. They were able to attribute most of the increase in activity observed to an increase in XOR synthesis and also showed a reduction in the rate of XOR degradation. They demonstrated that most of the newly synthesised XOR is active towards xanthine, indicating that molybdopterin is correctly incorporated.

The sulphuration of desulpho-XOR and a possible reduction in XOR degradation, however, are unable to account for the massive upregulation of XOR activity seen *post partum* by Brown and coworkers (Brown *et al.*, 1995). This 50 fold activation of XOR, unaccompanied by an increase in XOR protein levels indicates that an alternative pathway of XOR activation exists. The most likely candidate for this activation is the incorporation of molybdopterin into the demolybdo-enzyme known to comprise 95 % of human milk XOR (Harrison, 1997).

The human genes involved in the biosynthesis of molybdopterin have been identified on the basis of sequence comparisons to bacterial and fungal counterparts. Molybdopterin synthesis begins with the conversion of a guanosine derivative to a compound known as precursor Z by the products of two contiguous genes, *MOCS1A* and *MOCS1B* (Reiss *et al.*, 1998). Precursor Z is then converted to molybdopterin through generation of the dithiolene group required for molybdenum chelation by molybdopterin synthase, a

heterodimeric product of the bicistronic gene *MOCO1* (Sloan *et al.*, 1999; Stallmeyer *et al.*, 1999a). Molybdopterin synthase is regenerated by a sulphurylase encoded by *MOCO2* (Unkles *et al.*, 1999; Kinghorn, personal communication). The final step in the synthesis of Mo-molybdopterin, incorporation of molybdenum, is catalysed by the gene product of *MOCO3*. The gene product of *MOCO3* shows high similarity to gephyrin, a rat protein involved in glycine receptor clustering suggesting a possible dual role for gephyrin (Feng *et al.*, 1998; Stallmeyer *et al.*, 1999b).

It is not yet clear whether gephyrin is able to incorporate Mo-MPT directly into XOR, SO and AO or whether a further enzyme is responsible. To date, no case of Mo-MPT incorporation into purified demolybdo-XOR has been reported. However, it is likely that a similar mechanism to that observed in prokaryotes (Santini *et al.*, 1992; Temple and Rajagopalan, 2000) exists in humans for the insertion of molybdopterin into demolybdo-XOR. Such a mechanism would allow for the massive upregulation of XOR activity observed by Brown and coworkers (Brown *et al.*, 1995).

Therefore, the transcription-independent activation of human milk XOR by cytokines and *post partum* appears to be due to both the re-sulphuration of desulpho XOR and the incorporation of molybdopterin into a pool of demolybdo-XOR. It is likely that tissue-specific variation in XOR activity is also determined by regulation of the molybdopterin synthesis and incorporation pathway. Preliminary northern blot studies seem to show some degree of tissue specific expression of the molybdopterin synthesis genes (Kinghorn

and Unkles, personal communication), although it is not yet clear whether these reflect the tissue distribution of active molybdopterin enzymes.

Therefore, given the presence of a single gene for human XDH, with no alternative exons, as well as several mechanisms allowing for the activation and regulation of the activity of human XOR, it can be concluded that a single XDH transcript is expressed in human tissues. In general the specific activity of human XOR is considerably lower than that of other species and this low specific activity is due to a low molybdenum content, compounded by the presence of desulpho XOR in that fraction of XOR which contains molybdenum.

5.3 The structure of human milk XOR

The human and bovine XDH sequences are 90 % identical. Of the 10 % of differing residues, only 12 % (17 residues) are completely unconserved. 40 % of changes are semiconservative and 48 % are highly conservative.

Comparison of the human milk XOR structure (as so far refined) with that of the bovine XDH structure shows that the two structures are very similar. There are no gross structural changes or rearrangements (Fig 5.1).

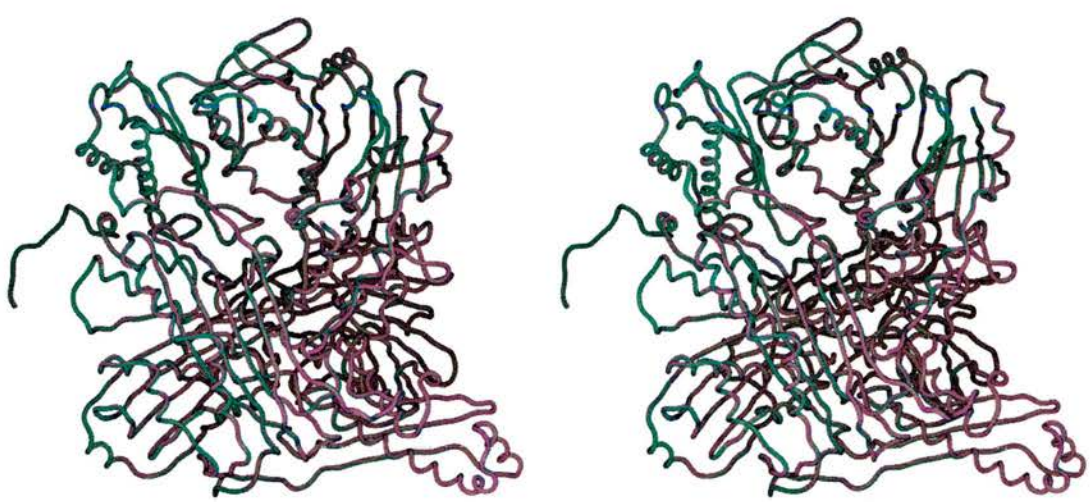

Figure 5.1 Stereo image showing the overlay of the bovine (blue) and human (lilac) XOR monomer structures.

Localisation of the differing residues on to the bovine milk XDH structure show that they are not localised to any specific areas of the structure, and that no differing residues are involved in cofactor binding.

It is clear that the structure determined in both crystal forms is that of the demolybdo enzyme, although both the iron-sulphur clusters and the FAD moiety are present. Less clear is whether the structure is that of the dehydrogenase or oxidase form of XOR.

Probably the most striking difference between the bovine milk XO and XDH structures is the shifted loop (423-433) which in the oxidase form has moved to occlude the NAD^+ binding site. Study of the electron density for this loop in the human milk XOR structure shows that it is largely disordered. The $2F_o$-F_c map does seem to show more density in the region of the dehydrogenase loop than the oxidase loop, however this could simply be due to model bias as the dehydrogenase structure was the starting point for refinement. F_o-F_c maps are less convincing in this area with little density for either version of the loop. It appears likely, at least at this resolution, that this loop is disorded. It is possible that the crystals contain a mixture of oxidase and dehydrogenase and that both confirmations exist within the structure. At the current stage of refinement this cannot be determined. However, biochemical observations that HMXOR runs as a single band on SDS-PAGE, absolutely requires DTT for crystallization and will only crystallize when there is less than 50 % oxidase present suggest that it is likely that the structure determined is indeed that of the dehydrogenase form.

5.4 Structure of the human milk XOR molybdenum binding site

In this part of the study, a possible structural basis for the low molybdenum content of human milk XOR was investigated.

Comparison of the molybdopterin binding cleft of bovine and human milk XOR shows that the protein structure of the molybdopterin binding cleft in HMXOR appears (at the current stage of refinement) to be identical to that of the bovine molybdopterin-containing enzyme (Fig. 5.2). Figure 4.25 also shows clearly that while there is no visible density for the molybdopterin or molybdenum, clear and well defined density is visible for the local protein environment.

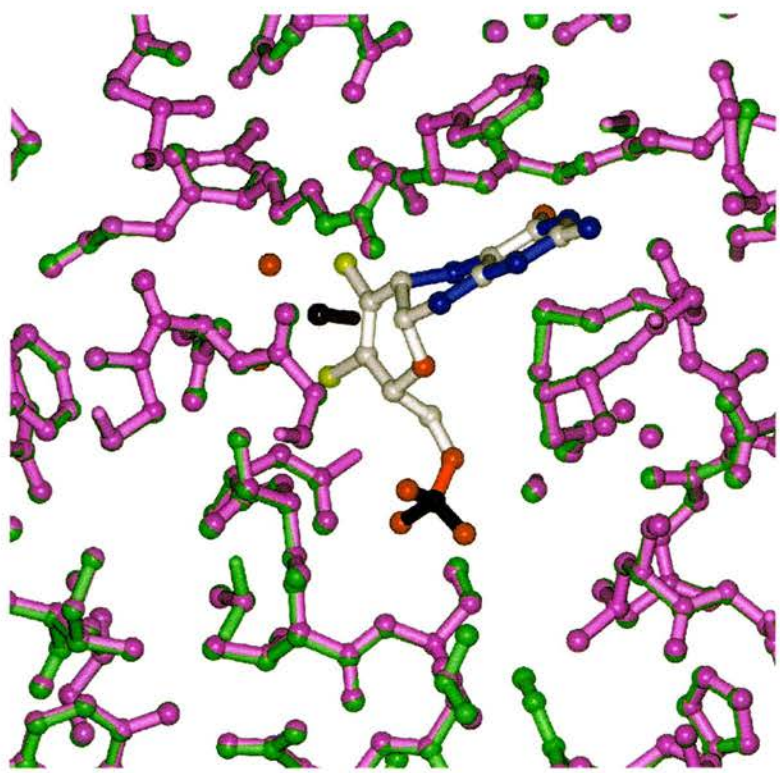

Figure 5.2 Ball and stick representation of the molybdenum binding cleft of human milk XOR (magenta) and bovine milk XDH (green). The molybdopterin is that of the bovine XDH structure and is coloured by atom type. Image generated using Molscript.

The stability of the molybdenum binding site in the absence of molybdopterin suggests that the low molybdenum content of the human milk enzyme cannot be accounted for by structural changes in this area of the protein.

This situation is similar to that seen in the demolybdo form of CODH, reported by Hänzelmann and co-workers (Hänzelmann and Meyer, 1998). They observed that demolybdo CODH was obtained from cells cultured in the presence of tungsten and low intracellular molybdenum and determined the structure of both the molybdo and demolybdo forms of CODH (Hänzelmann *et al.*, 2000). As observed in the case of demolybdo human milk xanthine oxidase, the molybdenum and molybdopterin moieties were absent from the protein, although the binding cleft remained intact.

XOR deficiency in humans causes xanthinuria. This classifies into two types, xanthinuria type 1 where no detectable XOR activity or protein can be observed (Yamamoto *et al.*, 2001) and type 2 in which XOR protein is present, but no activity is observed. In xanthinuria type 2 aldehyde oxidase activity is also missing (Ichida *et al.*, 1997). This suggests that xanthinuria type 1 is likely to be caused by mutations in the XDH gene or its promoter regions, whereas xanthinuria type 2 has been suggested to be caused by a defect in the sulphuration of the desulpho enzyme (Yamamoto *et al.*, 2001). Patients suffering from either of these conditions may develop urinary tract calculi, acute renal failure or myositis due to tissue deposition of xanthine (Ichida *et al.*, 1997).

Defects in molybdenum uptake or in the molybdopterin biosynthesis pathway cause a more serious disease that usually results in premature death in early childhood. In these cases, no enzyme activities (xanthine oxidase, aldehyde oxidase and sulfite oxidase) requiring molybdopterin are observed in the cell, even though mRNA levels for the enzymes are detectable (Falciani *et al.*, 1994).

These observations suggest that the low molybdopterin incorporation into human XOR is not caused by an alteration in the structure of the enzyme, nor does the lack of molybdopterin cause a change in XOR structure. It is therefore probable that molybdopterin incorporation is regulated through control of the molybdopterin synthesis pathway rather than by the sequence or structure of XOR.

Very recently, Bray and co-workers have reported that FeS1 appears altered or deficient in approximately 30 % human milk demolybdo-XOR (Bray *et al.*, 1999). Examination of the human milk demolybdo-XOR structure reveals that FeS1 and its coordinating cysteines are identical to that of FeS1 in the molybdopterin containing BMXOR structures. This may reflect a bias towards the BMXDH model used in refinement. However, examination of the molybdo and demolybdo forms of CODH, the only XOR family member for which molybdo and demolybdo structures have been determined from the same species (*Hydrogena pseudoflava*), shows no difference in FeS1 or the surrounding peptide chain in either structure. Bray and co-workers comment on the lower stability of demolybdo-XOR, and it is probable that FeS deficient-demolybdo-XOR is even less stable. In view of this it is possible that the

demolybdo-XOR lacking FeS1 is too unstable to crystallize and the crystals obtained during this work are of the slightly more stable demolybdo-XOR with FeS1 intact.

5.5 Final conclusions

This study reports the crystallization and solution of the crystal structure of human milk demolybdo-XOR to a resolution of 3.5 Å. Also reported is the cDNA sequence of human mammary gland XDH.

Both the sequence and the crystal structure of human milk XOR suggest strongly that neither sequence or structure is responsible for the low level of molybdopterin incorporation into human milk XOR. As discussed above, it is likely that human milk XOR molybdopterin content is determined by regulation of the molybdopterin synthesis and incorporation machinery. As also discussed, the activation of a pool of inactive XOR seen under certain conditions is likely due to the resulphuration of desulpho enzyme and incorporation of molybdopterin into demolybdo-XOR.

Although the crystal structure is clearly demolybdo, whether it is oxidase or dehydrogenase remains unclear. The most striking structural determinant of this, loop 423 to 433, is disorded in the HMXOR structure.

Refinement of the HMXOR structure is underway using maximum likelihood methods. Given the low resolution and low quality of the data in the higher resolution bins, it is unlikely that any further conclusions can be drawn with respect to the structure. However, it is hoped that higher resolution data can be obtained from both crystal forms through modification of the freezing conditions.

Appendices

Appendix 1

Alignment of the human milk XDH sequence (Briggs, 1997 and this work) to the human small intestine sequence (Saksela and Raivio, 1996). The human milk XDH sequence is on top, the small intestine XDH sequence on the bottom. Highlighted in red are the 9 ambiguous bases. Highlighted in blue is a cytosine I believe to be missequenced, as it does not appear in any of the other human sequences, and introduces a frame shift that removes the stop codon. Study of Briggs' data (Briggs, 1997) reveals that this section of the sequence is very unclear. Highlighted in green is the thymine that starts the TAA stop codon.

```
  1 GGTACCTGGAGTTCGGGGACCCCAACCTGTGACAATGACAGCAGACAAAT 50
    ||||||||||||||||||||||||||||||||||||||||||||||||||
  1 GGTACCTGGAGTTCGGGGACCCCAACCTGTGACAATGACAGCAGACAAAT 50

 51 TGGTTTTCTTTGTGAATGGCAGAAAGGTGGTGGAGAAAAATGCAGATCCA 100
    ||||||||||||||||||||||||||||||||||||||||||||||||||
 51 TGGTTTTCTTTGTGAATGGCAGAAAGGTGGTGGAGAAAAATGCAGATCCA 100

101 GAGACAACCCTTTTGGCCTACCTGAGAAGAAAGTTGGGGCTGAGTGGAAC 150
    ||||||||||||||||||||||||||||||||||||||||||||||||||
101 GAGACAACCCTTTTGGCCTACCTGAGAAGAAAGTTGGGGCTGAGTGGAAC 150

151 CAAGCTCGGCTGTGGAGAGGGGGGCTGCGGGGCTTGCACAGTGATGCTCT 200
    ||||||||||||||||||||||||||||||||||||||||||||||||||
151 CAAGCTCGGCTGTGGAGAGGGGGGCTGCGGGGCTTGCACAGTGATGCTCT 200

201 CCAAGTATGATCGTCTGCAGAACAAGATCGTCCACTTTTCTGCCAATGCC 250
    ||||||||||||||||||||||||||||||||||||||||||||||||||
201 CCAAGTATGATCGTCTGCAGAACAAGATCGTCCACTTTTCTGCCAATGCC 250

251 tGCCTGGCCCCCATCTGCTCCTTGCAcCATGTTGCAGTGACAACTGTGGA 300
    ||||||||||||||||||||||||||||||||||||||||||||||||||
251 TGCCTGGCCCCCATCTGCTCCTTGCACCATGTTGCAGTGACAACTGTGGA 300

301 AGGAATAGGAAGCACCAAGACGAGGCTGCATCCTGTGCAGGAGAGAATTG 350
    ||||||||||||||||||||||||||||||||||||||||||||||||||
301 AGGAATAGGAAGCACCAAGACGAGGCTGCATCCTGTGCAGGAGAGAATTG 350

351 CCAAAAgCCACGGCTCCCAGTGCGGGTTcTGCACCCCTGGCATCGTCATG 400
    ||||||||||||||||||||||||||||||||||||||||||||||||||
351 CCAAAAGCCACGGCTCCCAGTGCGGGTTCTGCACCCCTGGCATCGTCATG 400
```

```
 401 AGTATGTACACACTGCTCCGGAATCAGCCCGAGCCCACCATGGAGGAGAT 450
     ||||||||||||||||||||||||||||||||||||||||||||||||||||
 401 AGTATGTACACACTGCTCCGGAATCAGCCCGAGCCCACCATGGAGGAGAT 450

 451 TGAGAATGCCTTCCAAGGAAATCTGTGCCGCTGCACAGGCTACAGACCCA 500
     ||||||||||||||||||||||||||||||||||||||||||||||||||||
 451 TGAGAATGCCTTCCAAGGAAATCTGTGCCGCTGCACAGGCTACAGACCCA 500

 501 TCCTCCAGGGCTTCCGGACCTTTGCCAgGGATGGTGGATGCTGTGGAGGA 550
     ||||||||||||||||||||||||||||||||||||||||||||||||||||
 501 TCCTCCAGGGCTTCCGGACCTTTGCCAGGGATGGTGGATGCTGTGGAGGA 550

 551 GATGGGAATAATCCAAATTGCTGCATGAACCAGAAGAAAGACCACTCaGT 600
     ||||||||||||||||||||||||||||||||||||||||||||||||||||
 551 GATGGGAATAATCCAAATTGCTGCATGAACCAGAAGAAAGACCACTCAGT 600

 601 CAGCCTCTCGCCATCTTTATTCAAACCAgAGGAGTTCACGCCCCTGGATC 650
     ||||||||||||||||||||||||||||||||||||||||||||||||||||
 601 CAGCCTCTCGCCATCTTTATTCAAACCAGAGGAGTTCACGCCCCTGGATC 650

 651 CAACCCAGGAGCCCATTTTTCCCCCAGAGTTGCTgAGGCTGAAAGACACT 700
     ||||||||||||||||||||||||||||||||||||||||||||||||||||
 651 CAACCCAGGAGCCCATTTTTCCCCCAGAGTTGCTGAGGCTGAAAGACACT 700

 701 CCTCGGAAGCAGCTGCGATTTGAAGGGGAGCGTGTGACGTGGATACAGGC 750
     ||||||||||||||||||||||||||||||||||||||||||||||||||||
 701 CCTCGGAAGCAGCTGCGATTTGAAGGGGAGCGTGTGACGTGGATACAGGC 750

 751 CTCAACCCTCAAGGAGCTGCTGGACCTCAAGGCTCAGCACCCTGACGCCA 800
     ||||||||||||||||||||||||||||||||||||||||||||||||||||
 751 CTCAACCCTCAAGGAGCTGCTGGACCTCAAGGCTCAGCACCCTGACGCCA 800

 801 AGCTGGTCGTGGGGAACACGGAGATTGGCATTGAGATGAAGTTCAAGAAT 850
     ||||||||||||||||||||||||||||||||||||||||||||||||||||
 801 AGCTGGTCGTGGGGAACACGGAGATTGGCATTGAGATGAAGTTCAAGAAT 850

 851 ATGCTGTTTCCTATGATTGTCTGCCCAGCCTGGATCCCTGAGCTGAATTC 900
     ||||||||||||||||||||||||||||||||||||||||||||||||||||
 851 ATGCTGTTTCCTATGATTGTCTGCCCAGCCTGGATCCCTGAGCTGAATTC 900

 901 GGTAGAACATGGACCCGACGGTATCTCCTTTGGAGCTGCTTGCCCCCTGA 950
     ||||||||||||||||||||||||||||||||||||||||||||||||||||
 901 GGTAGAACATGGACCCGACGGTATCTCCTTTGGAGCTGCTTGCCCCCTGA 950

 951 GCATTGTGGAAAAAACCCTGGTGGATGCTGTTGCTAAGCTTCCTGCCCAA 1000
     ||||||||||||||||||||||||||||||||||||||||||||||||||||
 951 GCATTGTGGAAAAAACCCTGGTGGATGCTGTTGCTAAGCTTCCTGCCCAA 1000

1001 AAGACAGAGGTGTTCAGAGGGGTCCTGGAGCAGCTGCGCTGGTTTGCTGG 1050
     ||||||||||||||||||||||||||||||||||||||||||||||||||||
1001 AAGACAGAGGTGTTCAGAGGGGTCCTGGAGCAGCTGCGCTGGTTTGCTGG 1050

1051 GAAGCAAGTCAAGTCTGTGGCGTCCGTTGGAGGGAACATCATCACTGCCA 1100
     ||||||||||||||||||||||||||||||||||||||||||||||||||||
1051 GAAGCAAGTCAAGTCTGTGGCGTCCGTTGGAGGGAACATCATCACTGCCA 1100
```

```
1101 GCCCCATCTCCGACCTCAACCCCGTGTTCATGGCCAGTGGGGCCAAGCTG 1150
     ||||||||||||||||||||||||||||||||||||||||||||||||||
1101 GCCCCATCTCCGACCTCAACCCCGTGTTCATGGCCAGTGGGGCCAAGCTG 1150

1151 ACACTTGTGTCCAGAGGCACCAGGAGAACTGTCCAGATGGACCACACCTT 1200
     ||||||||||||||||||||||||||||||||||||||||||||||||||
1151 ACACTTGTGTCCAGAGGCACCAGGAGAACTGTCCAGATGGACCACACCTT 1200

1201 CTTCCCTGGCTACAGAAAGACCCTGCTGAGCCCGGAGGAGATACTGCTCT 1250
     ||||||||||||||||||||||||||||||||||||||||||||||||||
1201 CTTCCCTGGCTACAGAAAGACCCTGCTGAGCCCGGAGGAGATACTGCTCT 1250

1251 CCATAGAGATCCCCTACAGCAGGGAgGgGgAGTATTTCTCAGCATTCAAG 1300
     ||||||||||||||||||||||||||||||||||||||||||||||||||
1251 CCATAGAGATCCCCTACAGCAGGGAGGGGGAGTATTTCTCAGCATTCAAG 1300

1301 CAGGCCTCCCGGAGAGAAGATGACATTGCCAAGGTAACCAGTGGCATGAG 1350
     ||||||||||||||||||||||||||||||||||||||||||||||||||
1301 CAGGCCTCCCGGAGAGAAGATGACATTGCCAAGGTAACCAGTGGCATGAG 1350

1351 AGTTTTATTCAAGCCAGGAACCACAGAGGTACAGGAGCTGGCCCTTTGCT 1400
     ||||||||||||||||||||||||||||||||||||||||||||||||||
1351 AGTTTTATTCAAGCCAGGAACCACAGAGGTACAGGAGCTGGCCCTTTGCT 1400

1401 ATGGTGGAATGGCCAACAGAACCATCTCAGCCCTCAAGACCACTCAGAGG 1450
     ||||||||||||||||||||||||||||||||||||||||||||||||||
1401 ATGGTGGAATGGCCAACAGAACCATCTCAGCCCTCAAGACCACTCAGAGG 1450

1451 CAGCTTTCCAAGCTCTGGAAGGAGGAGCTGCTGCAGGACGTGTGTGCAGG 1500
     ||||||||||||||||||||||||||||||||||||||||||||||||||
1451 CAGCTTTCCAAGCTCTGGAAGGAGGAGCTGCTGCAGGACGTGTGTGCAGG 1500

1501 ACTGGCAGAGGAGCTGCATCTGCCTCCCGATGCCCCTGGTGGCATGGTGG 1550
     ||||||||||||||||||||||||||||||||||||||||||||||||||
1501 ACTGGCAGAGGAGCTGCATCTGCCTCCCGATGCCCCTGGTGGCATGGTGG 1550

1551 ACTTCCGGTGCACCCTCACCCTCAGCTTcTTCTTCAAGTTCTACCTGAcA 1600
     ||||||||||||||||||||||||||||||||||||||||||||||||||
1551 ACTTCCGGTGCACCCTCACCCTCAGCTTCTTCTTCAAGTTCTACCTGACA 1600

1601 GTCcTTcAGAAGCTGGGCCAAGAGAACCTGGAAGACAAGTGTGGTAAACT 1650
     ||||||||||||||||||||||||||||||||||||||||||||||||||
1601 GTCCTTCAGAAGCTGGGCCAAGAGAACCTGGAAGACAAGTGTGGTAAACT 1650

1651 GGACCCCACTTTCGCCAGTGCAACTTTACTGTTTCAGAAAGACCCCCCAG 1700
     ||||||||||||||||||||||||||||||||||||||||||||||||||
1651 GGACCCCACTTTCGCCAGTGCAACTTTACTGTTTCAGAAAGACCCCCCAG 1700

1701 CCGATGTCCAGCTCTTCCAAGAGGTGCCCAAGGGTCAGTCTGAGGAGGAC 1750
     ||||||||||||||||||||||||||||||||||||||||||||||||||
1701 CCGATGTCCAGCTCTTCCAAGAGGTGCCCAAGGGTCAGTCTGAGGAGGAC 1750

1751 ATGGTGGGCCGGCCCCTGCCCCACCTGGCAGCGGACATGCAGGCCTCTGG 1800
     ||||||||||||||||||||||||||||||||||||||||||||||||||
1751 ATGGTGGGCCGGCCCCTGCCCCACCTGGCAGCGGACATGCAGGCCTCTGG 1800
```

```
1801 TGAGGCCGTGTACTGTGACGACATTCCTCGCTACGAGAATGAGCTGTCTC 1850
     ||||||||||||||||||||||||||||||||||||||||||||||||||
1801 TGAGGCCGTGTACTGTGACGACATTCCTCGCTACGAGAATGAGCTGTCTC 1850

1851 TCCGGCTGGTCACCAGCACCCGGGCCCACGCCAAGATCAAGTCCATAGAT 1900
     ||||||||||||||||||||||||||||||||||||||||||||||||||
1851 TCCGGCTGGTCACCAGCACCCGGGCCCACGCCAAGATCAAGTCCATAGAT 1900

1901 ACATCAGAAGCTAAGAAGGTTCCAGGGTTTGTTTGTTTCATTTCCGCTGA 1950
     ||||||||||||||||||||||||||||||||||||||||||||||||||
1901 ACATCAGAAGCTAAGAAGGTTCCAGGGTTTGTTTGTTTCATTTCCGCTGA 1950

1951 TGATGTTCCTGGGAGTAACATAACTGGAATTTGTAATGATGAGACAGTCT 2000
     ||||||||||||||||||||||||||||||||||||||||||||||||||
1951 TGATGTTCCTGGGAGTAACATAACTGGAATTTGTAATGATGAGACAGTCT 2000

2001 TTGCGAAGGATAAGGTTACTTGTGTTGGGCATATCATTGGTGCTGTGGTT 2050
     ||||||||||||||||||||||||||||||||||||||||||||||||||
2001 TTGCGAAGGATAAGGTTACTTGTGTTGGGCATATCATTGGTGCTGTGGTT 2050

2051 GCTGACACCCCGGAACACACACAGAGAGCTGCCCAAGGGGTGAAAATCAC 2100
     ||||||||||||||||||||||||||||||||||||||||||||||||||
2051 GCTGACACCCCGGAACACACACAGAGAGCTGCCCAAGGGGTGAAAATCAC 2100

2101 CTATGAAGAACTACCAGCCATTATCACAATTGAGGATGCTATAAAGAACA 2150
     ||||||||||||||||||||||||||||||||||||||||||||||||||
2101 CTATGAAGAACTACCAGCCATTATCACAATTGAGGATGCTATAAAGAACA 2150

2151 ACTCCTTTTATGGACCTGAGCTGAAGATCGAGAAAGGGGACCTAAAGAAG 2200
     ||||||||||||||||||||||||||||||||||||||||||||||||||
2151 ACTCCTTTTATGGACCTGAGCTGAAGATCGAGAAAGGGGACCTAAAGAAG 2200

2201 GGGTTTTCCGAAGCAGATAATGTTGTGTCAGGGGAGATATACATCGGTGG 2250
     ||||||||||||||||||||||||||||||||||||||||||||||||||
2201 GGGTTTTCCGAAGCAGATAATGTTGTGTCAGGGGAGATATACATCGGTGG 2250

2251 CCAAGAGCACTTCTACCTGGAGACTCACTGCACCATTGCTGTTCCAAAAG 2300
     ||||||||||||||||||||||||||||||||||||||||||||||||||
2251 CCAAGAGCACTTCTACCTGGAGACTCACTGCACCATTGCTGTTCCAAAAG 2300

2301 GCGAGGCAGGGGAGATGGAGCTCTTTGTGTCTACACAGAACACCATGAAG 2350
     ||||||||||||||||||||||||||||||||||||||||||||||||||
2301 GCGAGGCAGGGGAGATGGAGCTCTTTGTGTCTACACAGAACACCATGAAG 2350

2351 ACCCAGAGCTTTGTTGCAAAAATGTTGGGGGTTCCAGCAAACCGGATTGT 2400
     ||||||||||||||||||||||||||||||||||||||||||||||||||
2351 ACCCAGAGCTTTGTTGCAAAAATGTTGGGGGTTCCAGCAAACCGGATTGT 2400

2401 GGTTCGAGTGAAGAGAATGGGAGGAGGCTTTGGAGGCAAGGAGACCCGGA 2450
     ||||||||||||||||||||||||||||||||||||||||||||||||||
2401 GGTTCGAGTGAAGAGAATGGGAGGAGGCTTTGGAGGCAAGGAGACCCGGA 2450

2451 GCACTGTGGTGTCCACGGCAGTGGCCCTGGCTGCATATAAGACCGGCCGC 2500
     ||||||||||||||||||||||||||||||||||||||||||||||||||
2451 GCACTGTGGTGTCCACGGCAGTGGCCCTGGCTGCATATAAGACCGGCCGC 2500
```

```
2501 CCTGTGCGATGCATGCTGGACCGTGATGAGGACATGCTGATAACTGGTGG 2550
     ||||||||||||||||||||||||||||||||||||||||||||||||||
2501 CCTGTGCGATGCATGCTGGACCGTGATGAGGACATGCTGATAACTGGTGG 2550

2551 CAGACATCCCTTCCTGGCCAGATACAAGGTTGGCTTCATGAAGACTGGGA 2600
     ||||||||||||||||||||||||||||||||||||||||||||||||||
2551 CAGACATCCCTTCCTGGCCAGATACAAGGTTGGCTTCATGAAGACTGGGA 2600

2601 CAGTTGTGGCTCTTGAGGTGGACCACTTCAGCAATGTGGGGAACACCCAG 2650
     ||||||||||||||||||||||||||||||||||||||||||||||||||
2601 CAGTTGTGGCTCTTGAGGTGGACCACTTCAGCAATGTGGGGAACACCCAG 2650

2651 GATCTCTCTCAGAGTATTATGGAACGAGCTTTATTCCACATGGACAACTG 2700
     ||||||||||||||||||||||||||||||||||||||||||||||||||
2651 GATCTCTCTCAGAGTATTATGGAACGAGCTTTATTCCACATGGACAACTG 2700

2701 CTATAAAATCCCCAACATCCGGGGCACTGGGCGGCTGTGCAAAACCAACC 2750
     ||||||||||||||||||||||||||||||||||||||||||||||||||
2701 CTATAAAATCCCCAACATCCGGGGCACTGGGCGGCTGTGCAAAACCAACC 2750

2751 TTCCCTCCAACACGGCCTTCCGGGGCTTTGGGGGGCCCCAGGGGATGCTC 2800
     ||||||||||||||||||||||||||||||||||||||||||||||||||
2751 TTCCCTCCAACACGGCCTTCCGGGGCTTTGGGGGGCCCCAGGGGATGCTC 2800

2801 ATTGCCGAGTGCTGGATGAGTGAAGTTGCAGTGACCTGTGGGATGCCTGC 2850
     ||||||||||||||||||||||||||||||||||||||||||||||||||
2801 ATTGCCGAGTGCTGGATGAGTGAAGTTGCAGTGACCTGTGGGATGCCTGC 2850

2851 AGAGGAGGTGCGGAGAAAAAACCTGTACAAAGAAGGGGACCTGACACACT 2900
     ||||||||||||||||||||||||||||||||||||||||||||||||||
2851 AGAGGAGGTGCGGAGAAAAAACCTGTACAAAGAAGGGGACCTGACACACT 2900

2901 TCAACCAGAAGCTTGAGGGTTTCACCTTGCCCAGATGCTGGGAAGAATGC 2950
     ||||||||||||||||||||||||||||||||||||||||||||||||||
2901 TCAACCAGAAGCTTGAGGGTTTCACCTTGCCCAGATGCTGGGAAGAATGC 2950

2951 CTAGCAAGCTCTCAGTATCATGCTCGGAAGAGTGAGGTTGACAAGTTCAA 3000
     ||||||||||||||||||||||||||||||||||||||||||||||||||
2951 CTAGCAAGCTCTCAGTATCATGCTCGGAAGAGTGAGGTTGACAAGTTCAA 3000

3001 CAAGGAGAATTGTTGGAAAAAGAGAGGATTGTGCATAATTCCCACCAAGT 3050
     ||||||||||||||||||||||||||||||||||||||||||||||||||
3001 CAAGGAGAATTGTTGGAAAAAGAGAGGATTGTGCATAATTCCCACCAAGT 3050

3051 TTGGAATAAGCTTCACAGTTCCTTTTCTGAATCAGGCAGGAGCCCTACTT 3100
     ||||||||||||||||||||||||||||||||||||||||||||||||||
3051 TTGGAATAAGCTTCACAGTTCCTTTTCTGAATCAGGCAGGAGCCCTACTT 3100

3101 CATGTTTACACAGATGGCTCTGTGCTGCTGACCCACGGGGGGACTGAGAT 3150
     ||||| ||||||||||||||||||||||||||||||||||||||||||||
3101 CATGTGTACACAGATGGCTCTGTGCTGCTGACCCACGGGGGGACTGAGAT 3150

3151 GGGCCAAGGCCTTCATACCAAAATGGTCCAGGTGGCCAGTAGAGCTCTGA 3200
     ||||||||||||||||||||||||||||||||||||||||||||||||||
3151 GGGCCAAGGCCTTCATACCAAAATGGTCCAGGTGGCCAGTAGAGCTCTGA 3200
```

```
3201 AAATCCCCACCTCTAAGATTTATATCAGCGAGACAAGCACTAACACTGTG 3250
     ||||||||||||||||||||||||||||||||||||||||||||||||||
3201 AAATCCCCACCTCTAAGATTTATATCAGCGAGACAAGCACTAACACTGTG 3250

3251 CCCAACACCTCTCCCACGGCTGCCTCTGTCAGCGCTGACCTCAATGGACA 3300
     ||||||||||||||||||||||||||||||||||||||||||||||||||
3251 CCCAACACCTCTCCCACGGCTGCCTCTGTCAGCGCTGACCTCAATGGACA 3300

3301 GGCCGTCTATGCGGCTTGTCAGACCATCTTGAAAAGGCTGGAACCCTACA 3350
     ||||||||||||||||||||||||||||||||||||||||||||||||||
3301 GGCCGTCTATGCGGCTTGTCAGACCATCTTGAAAAGGCTGGAACCCTACA 3350

3351 AGAAGAAGAATCCCAGTGGCTCCTGGGAAGACTGGGTCACAGCTGCCTAC 3400
     ||||||||||||||||||||||||||||||||||||||||||||||||||
3351 AGAAGAAGAATCCCAGTGGCTCCTGGGAAGACTGGGTCACAGCTGCCTAC 3400

3401 ATGGACACAGTGAGCTTGTCTGCCACTGGGTTTTATAGAACACCCAATCT 3450
     ||||||||||||||||||||||||||||||||||||||||||||||||||
3401 ATGGACACAGTGAGCTTGTCTGCCACTGGGTTTTATAGAACACCCAATCT 3450

3451 GGGCTACAGCTTTGAGACTAACTCAGGGAAmCCCTTCCACTACTTCAGCT 3500
     ||||||||||||||||||||||||||||||:||||||||||||||||||
3451 GGGCTACAGCTTTGAGACTAACTCAGGGAACCCCTTCCACTACTTCAGCT 3500

3501 ATGGGGTGGCTTGCTCTGAAGTAGAAATCGACTGCCTAACAGGAGATCAT 3550
     ||||||||||||||||||||||||||||||||||||||||||||||||||
3501 ATGGGGTGGCTTGCTCTGAAGTAGAAATCGACTGCCTAACAGGAGATCAT 3550

3551 AAGAACCTCCGCACAGATATTGTCATGGATGTTGGCTCCAGTCTAAACCC 3600
     ||||||||||||||||||||||||||||||||||||||||||||||||||
3551 AAGAACCTCCGCACAGATATTGTCATGGATGTTGGCTCCAGTCTAAACCC 3600

3601 TGCCATTGATATTGGACAGGTGGAAGGGGCATTTGTCCAGGGCCTTGGCC 3650
     ||||||||||||||||||||||||||||||||||||||||||||||||||
3601 TGCCATTGATATTGGACAGGTGGAAGGGGCATTTGTCCAGGGCCTTGGCC 3650

3651 TCTTCACCCTAGAGGAGCTACACTATTCCCCCGAGGGGAGCCTGCACACC 3700
     ||||||||||||||||||||||||||||||||||||||||||||||||||
3651 TCTTCACCCTAGAGGAGCTACACTATTCCCCCGAGGGGAGCCTGCACACC 3700

3701 CGTGGCCCTAGCACCTACAAGATCCCGGCATTTGGCAGCATCCCCATTGA 3750
     ||||||||||||||||||||||||||||||||||||||||||||||||||
3701 CGTGGCCCTAGCACCTACAAGATCCCGGCATTTGGCAGCATCCCCATTGA 3750

3751 GTTCAGGGTGTCCCTGCTCCGCGACTGCCCCAACAAGAAGGCCATCTATG 3800
     ||||||||||||||||||||||||||||||||||||||||||||||||||
3751 GTTCAGGGTGTCCCTGCTCCGCGACTGCCCCAACAAGAAGGCCATCTATG 3800

3801 CATCGAAGGCTGTTGGAGAGCCGCCCCTCTTCCTGGCTGCTTCTATCTTC 3850
     ||||||||||||||||||||||||||||||||||||||||||||||||||
3801 CATCGAAGGCTGTTGGAGAGCCGCCCCTCTTCCTGGCTGCTTCTATCTTC 3850

3851 TTTGCCATCAAAGATGCCATCCGTGCAGCTCGAGCTCAGCACACAGGTAA 3900
     ||||||||||||||||||||||||||||||||||||||||||||||||||
3851 TTTGCCATCAAAGATGCCATCCGTGCAGCTCGAGCTCAGCACACAGGTAA 3900
```


3901 TAACGTGAAGGAACTCTTCCGGCTAGACAGCCCTGCCACCCCGGAGAAGA 3950
3901 TAACGTGAAGGAACTCTTCCGGCTAGACAGCCCTGCCACCCCGGAGAAGA 3950
3951 TCCGCAATGCCTGCGTGGACAAGTTCACCACCCTGTGTGTCACTGGTGTC 4000
3951 TCCGCAATGCCTGCGTGGACAAGTTCACCACCCTGTGTGTCACTGGTGTC 4000
4001 CCAGAAAAyTrCAAACCCTsGCTCTbCkwbCGTyT 4035
4001 CCAGAAAACTGCAAACCCTGG.TCTGTGAGGGTCT 4034

Appendix 2

Alignment of the human XDH sequence (Ichida *et al.*, 1993; Saksela & Raivio, 1996; Yamamoto *et al.*, 2001) with the bovine XDH sequence (Berglund *et al.*, 1996). The human sequence is on the top, the bovine on the bottom. Conservative changes are marked in blue, semiconservative changes in green and unconservative changes in red.

```
  1 MTADKLVFFVNGRKVVEKNADPETTLLAYLRRKLGLSGTKLGCGEGGCGA 50
    ||||.|||||||:||||||||||||||||||||.||||||||||||||
  1 mtadelvffvngkkvveknadpettllaylrrklglrgtklgcgeggcga 50

 51 CTVMLSKYDRLQNKIVHFSANACLAPICSLHHVAVTTVEGIGSTKTRLHP 100
    ||||||||||||:||:||||||||||||.||||||||||||||||||||
 51 ctvmlskydrlqdkiihfsanaclapictlhhvavttvegigstktrlhp 100

101 VQERIAKSHGSQCGFCTPGIVMSMYTLLRNQPEPTMEEIENAFQGNLCRC 150
    ||||||||||||||||||||||||||||||||||:||||:|||||||||
101 vqeriakshgsqcgfctpgivmsmytllrnqpeptveeiedafqgnlcrc 150

151 TGYRPILQGFRTFARDGGCCGGDGNNPNCCMNQKKDHSVSLSPSLFKPEE 200
    ||||||||||||||::||||||:||||||||||||||.|.||||||.|||
151 tgyrpilqgfrtfaknggccggngnnpnccmnqkkdhtvtlspslfnpee 200

201 FTPLDPTQEPIFPPELLRLKDTPRKQLRFEGERVTWIQASTLKELLDLKA 250
    | ||||||||||||||||||.|.|||||||||||||||||||||||||||
201 fmpldptqepifppellrlkdvppkqlrfegervtwiqastlkelldlka 250

251 QHPDAKLVVGNTEIGIEMKFKNMLFPMIVCPAWIPELNSVEHGPDGISFG 300
    |||:||||||||||||||||| |||||:|||||||||.|||||:|||||
251 qhpeaklvvgnteigiemkfknqlfpmiicpawipelnavehgpegisfg 300

301 AACPLSIVEKTLVDAVAKLPAQKTEVFRGVLEQLRWFAGKQVKSVASVGG 350
    |||:|| |||||::||||||.||||||||||||||||||||||||:||
301 aacalssvektlleavaklptqktevfrgvleqlrwfagkqvksvaslgg 350

351 NIITASPISDLNPVFMASGAKLTLVSRGTRRTVQMDHTFFPGYRKTLLSP 400
    ||||||||||||||||||.|||:|||||||||.|||||||:||||||:|
351 niitaspisdlnpvfmasgtkltivsrgtrrtvpmdhtffpsyrktllgp 400

401 EEILLSIEIPYSREGEYFSAFKQASRREDDIAKVTSGMRVLFKPGTTEVQ 450
    |||||||||||||:|:||||||||||||||||:||||||.||. :|.
401 eeillsieipysredeffsafkqasrreddiakvtcgmrvlfqpgsmqvk 450

451 ELALCYGGMANRTISALKTTQRQLSKLWKEELLQDVCAGLAEELHLPPDA 500
    ||||||||||:||||||||||:||||:|.|.|||||||||||||| |.||
451 elalcyggmadrtisalkttqkqlskfwnekllqdvcaglaeelslspda 500
```

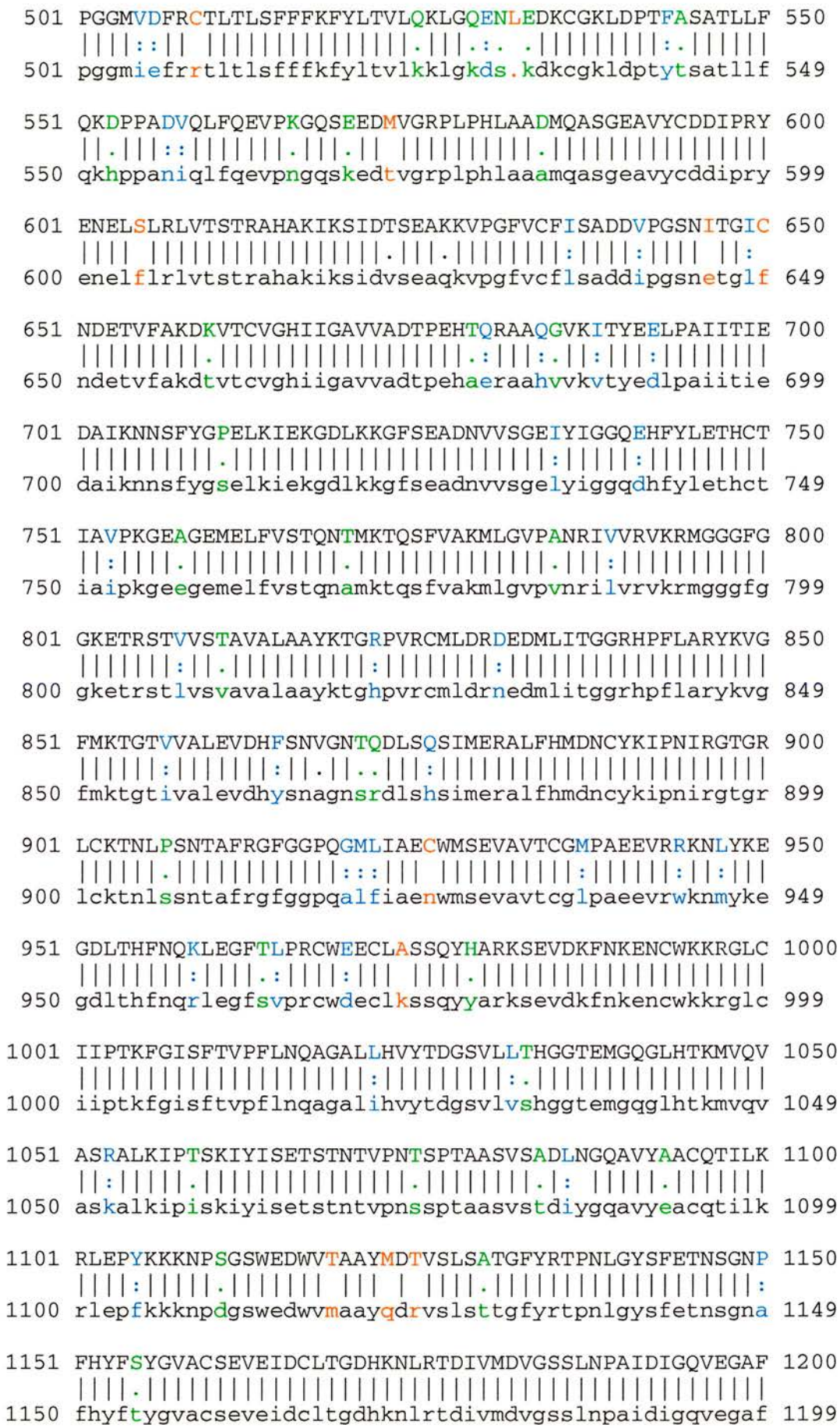
501 PGGMVDFRCTLTLSFFFKFYLTVLQKLGQENLEDKCGKLDPTFASATLLF 550
501 pggmiefrrtltlsfffkfyltvlkklgkds.kdkcgkldptytsatllf 549
551 QKDPPADVQLFQEVPKGQSEEDMVGRPLPHLAADMQASGEAVYCDDIPRY 600
550 qkhppaniqlfqevpngqskedtvgrplphlaaamqasgeavycddipry 599
601 ENELSLRLVTSTRAHAKIKSIDTSEAKKVPGFVCFISADDVPGSNITGIC 650
600 enelflrlvtstrahakiksidvseaqkvpgfvcflsaddipgsnetglf 649
651 NDETVFAKDKVTCVGHIIGAVVADTPEHTQRAAQGVKITYEELPAIITIE 700
650 ndetvfakdtvtcvghiigavvadtpehaeraahvvkvtyedlpaiitie 699
701 DAIKNNSFYGPELKIEKGDLKKGFSEADNVVSGEIYIGGQEHFYLETHCT 750
700 daiknnsfygselkiekgdlkkgfseadnvvsgelyiggqdhfylethct 749
751 IAVPKGEAGEMELFVSTQNTMKTQSFVAKMLGVPANRIVVRVKRMGGGFG 800
750 iaipkgeegemelfvstqnamktqsfvakmlgvpvnrilvrvkrmgggfg 799
801 GKETRSTVVSTAVALAAYKTGRPVRCMLDRDEDMLITGGRHPFLARYKVG 850
800 gketrstlvsvavalaayktghpvrcmldrnedmlitggrhpflarykvg 849
851 FMKTGTVVALEVDHFSNVGNTQDLSQSIMERALFHMDNCYKIPNIRGTGR 900
850 fmktgtivalevdhysnagnsrdlshsimeralfhmdncykipnirgtgr 899
901 LCKTNLPSNTAFRGFGGPQGMLIAECWMSEVAVTCGMPAEEVRRKNLYKE 950
900 lcktnlssntafrgfggpqalfiaenwmsevavtcglpaeevrwknmyke 949
951 GDLTHFNQKLEGFTLPRCWEECLASSQYHARKSEVDKFNKENCWKKRGLC 1000
950 gdlthfnqrlegfsvprcwdeclkssqyyarksevdkfnkencwkkrglc 999
1001 IIPTKFGISFTVPFLNQAGALLHVYTDGSVLLTHGGTEMGQGLHTKMVQV 1050
1000 iiptkfgisftvpflnqagalihvytdgsvlvshggtemgqglhtkmvqv 1049
1051 ASRALKIPTSKIYISETSTNTVPNTSPTAASVSADLNGQAVYAACQTILK 1100
1050 askalkipiskiyisetstntvpnssptaasvstdiygqavyeacqtilk 1099
1101 RLEPYKKKNPSGSWEDWVTAAYMDTVSLSATGFYRTPNLGYSFETNSGNP 1150
1100 rlepfkkknpdgswedwvmaayqdrvslsttgfyrtpnlgysfetnsgna 1149
1151 FHYFSYGVACSEVEIDCLTGDHKNLRTDIVMDVGSSLNPAIDIGQVEGAF 1200
1150 fhyftygvacseveidcltgdhknlrtdivmdvgsslnpaidigqvegaf 1199

```
1201 VQGLGLFTLEELHYSPEGSLHTRGPSTYKIPAFGSIPIEFRVSLLRDCPN 1250
     ||||||||||||||||||||||||||||||||||||.||||||||||||
1200 vqglglftleelhyspegslhtrgpstykipafgsiptefrvsllrdcpn 1249

1251 KKAIYASKAVGEPPLFLAASIFFAIKDAIRAARAQHTGNNVKELFRLDSP 1300
     ||||||||||||||||||:||:||||||||||||||||.||.|||||||||
1250 kkaiyaskavgepplflgasvffaikdairaaraqhtnnntkelfrldsp 1299

1301 ATPEKIRNACVDKFTTLCVTGVPENCKPWSVRV 1333
     ||||||||||||||||||||.|:||||||:||
1300 atpekirnacvdkfttlcvtgapgnckpwslrv 1332
```

References

ABADEH, S., CASE, P. C., and HARRISON, R. (1993). Purification of xanthine oxidase from human heart. *Biochemical Society Transactions* **21**(2), 99S.

ABADEH, S., KILLACKY, J., BENBOUBETRA, M., and HARRISON, R. (1992). Purification and partial characterization of xanthine oxidase from human milk. *Biochimica et Biophysica Acta* **1117**, 25-32.

ADACHI, T., FUKUSHIMA, T., USAMI, Y., and HIRANO, K. (1993). Binding of human xanthine oxidase to sulphated glycosaminoglycans on the endothelial-cell surface. *Biochemical Journal* **289**(Pt 2), 523-527.

AMAYA, Y., YAMAZAKI, K., SATO, M., NODA, K., and NISHINO, T. (1990). Proteolytic conversion of xanthine dehydrogenase from the NAD-dependent type to the O2-dependent type. Amino acid sequence of rat liver xanthine dehydrogenase and identification of the cleavage sites of the enzyme protein during irreversible conversion by trypsin. *Journal of Biological Chemistry* **265**(24), 14170-14175.

AVIS, P. G., BERGEL, F., and BRAY, R. C. (1955). Cellular constituents. The chemistry of xanthine oxidase. Part I. The preparation of a crystalline xanthine oxidase from cow's milk. *Journal of the Chemical Society* **227**, 1100-1106.

AVIS, P. G., BERGEL, F., and BRAY, R. C. (1956a). Cellular Constituents. The Chemistry of Xanthine Oxidase. Part III. Estimations of the co-factors and the catalytic activities of enzyme fractions from cow's milk. *Journal of the Chemical Society*(Part I), 1219-1226.

AVIS, P. G., BERGEL, F., BRAY, R. C., JAMES, D. W. F., and SHOOTER, K. V. (1956b). Cellular Constituents. The Chemistry of Xanthine Oxidase. Part II. The Homogeneity of Crystalline Metalloflavoprotein Fractions. *Journal of the Chemical Society*(Part I), 1212-1219.

BALL, E. G. (1939). Xanthine Oxidase: Purification and Properties. *Journal of Biological Chemistry* **128**, 51-67.

BARATA, B. A., LEGALL, J., and MOURA, J. J. (1993). Aldehyde oxidoreductase activity in Desulfovibrio gigas: in vitro reconstitution of an electron-transfer chain from aldehydes to the production of molecular hydrogen. *Biochemistry* **32**(43), 11559-11568.

BECKMAN, J. S., PARKS, D. A., PEARSON, J. D., MARSHALL, P. A., and FREEMAN, B. A. (1989). A sensitive fluorometric assay for measuring xanthine dehydrogenase and oxidase in tissues. *Free Radical Biology and Medicine* **6**(6), 607-615.

BENBOUBETRA, M., GLEESON, A., HARRIS, C. P., KHAN, J., ARRAR, L., BRENNAND, D., REID, J., RECKLESS, J. D., and HARRISON, R. (1997). Circulating anti-(xanthine oxidoreductase) antibodies in healthy human adults. *European Journal of Clinical Investigation* **27**(7), 611-9.

BENSON, T. E., WALSH, C. T., and HOGLE, J. M. (1996). The structure of the substrate-free form of MurB, an essential enzyme for the synthesis of bacterial cell walls. *Structure* **4**(1), 47-54.

BERGLUND, L., RASMUSSEN, J. T., ANDERSEN, M. D., RASMUSSEN, M. S., and PETERSEN, T. E. (1996). Purification of the bovine xanthine oxidoreductase from milk fat globule membranes and cloning of complementary deoxyribonucleic acid. *Journal of Dairy Science* **79**(2), 198-204.

BLASE, M., BRUNTNER, C., TSHISUAKA, B., FETZNER, S., and LINGENS, F. (1996). Cloning, expression, and sequence analysis of the three genes encoding quinoline 2-oxidoreductase, a molybdenum-containing hydroxylase from Pseudomonas putida 86. *Journal of Biological Chemistry* **271**(38), 23068-23079.

BOOTH, V. H. (1938). The Specificity of Xanthine Oxidase. *Biochemical Journal* **32,** 494-502.

BORDAS, J., BRAY, R. C., GARNER, C. D., GUTTERIDGE, S., and HASNAIN, S. S. (1980). X-ray absorption spectroscopy of xanthine oxidase. The molybdenum centres of the functional and the desulpho forms. *Biochemical Journal* **191**(2), 499-508.

BOURNE, P. E., GRIBSKOV, M., JOHNSON, G., MORELAND, J., and WEISSIG, H. (1998). A prototype molecular interactive collaborative environment (MICE). *In* "Pacific Symposium on Biocomputing." (R. Altman, K. Dunker, L. Hunter, and T. Klein, Eds.) pp. 118-129 World Scientific Publishing Company.

BOYINGTON, J. C., GLADYSHEV, V. N., KHANGULOV, S. V., STADTMAN, T. C., and SUN, P. D. (1997). Crystal structure of formate dehydrogenase H: catalysis involving Mo, molybdopterin, selenocysteine, and an Fe4S4 cluster. *Science* **275**(5304), 1305-1308.

BRAGG, W. (1913). The diffraction of short electromagnetic waves by a crystal. *Proceedings of the Cambridge Philosophical Society* **17,** 43-57.

BRAY, R. C. (1975). Molybdenum iron-sulfur flavin hydroxylases and related enzymes. 3rd ed. *In* "The Enzymes" (P. D. Boyer, Ed.), Vol. 12, pp. 299-419. Academic Press, New York.

BRAY, R. C., GODBER, B., HARRISON, R., and EISENTHAL, R. (1999). Properties of xanthine oxidase from human milk: the enzyme is grossly deficient in molybdenum and substantially deficient in iron-sulphur centres. *In* "Flavins and Flavoproteins 1999: Proc. 13th Int. Symp., Konstanz, Germany." (S. Ghisla, P. M. H. Kroneck, P. Macheroux, and H. Sund, Eds.) Agency for Scientific Publication, Berlin.

BRIGGS, T. (1997). Sequencing of the human mammary gland xanthine dehydrogenase. *Final Year Project Report.* The University of Bath.

BRINKMANN, H., EILERS, T., NIEDER, J., and MENDEL, R. R. (1999). Cloning and sequencing of sulfite oxidase cDNA from *Arabidopsis thaliana. Unpublished.*

BROWN, A. M., BENBOUBETRA, M., ELLISON, M., POWELL, D., RECKLESS, J. D., and HARRISON, R. (1995). Molecular activation-deactivation of xanthine oxidase in human milk. *Biochimica et Biophysica Acta* **1245**(2), 248-254.

BRUNGER, A. T., ADAMS, P. D., CLORE, G. M., DELANO, W. L., P, G., GROSSE-KUNSTLEVE, R. W., JIANG, J.-S., KUSZEWSKI, J., NILGES, N., PANNU, N. S., READ, R. J., RICE, L. M., SIMONSON, T., and WARREN, G. L. (1998). Crystallography and NMR system (CNS): A new software system for macromolecular structure determination. *Acta Crystallographica* **D54,** 905-921.

BURIAN, R. (1905). Über die oxydative und die vermeintliche synthetische Bildung von Harnsäure in Rinderleberauszug. *Zeitschrift für Physiologisches Chemie* **43,** 497-531.

CARTER, C. W. (1979). Protein crystallization using incomplete factorial experiments. *Journal of Biological Chemistry* **254**(23), 12219-12223.

CARTER, C. W. (1992). Design of crystallization experiments and protocols. *In* "Crystallization of nucleic acids and proteins - A practical approach" (A. Ducruix, and R. Giegé, Eds.), pp. 47-71. IRL Press at Oxford University Press, Oxford, New York and Tokyo.

CARVALHO, A., DIAS, J. M., TEIXEIRA, S., BOURENKOV, G., BARTUNIK, H., HUBER, R., MAIA, L., MIRA, L., and ROMAO, M. J. (1998). X-ray diffraction data collection of Xanthine Oxidase crystals purified from rat liver. *HASYlab Annual Report* **Part II**.

CCP4. (1994). The CCP4 suite: Programmes for Protein Crystallography. *Acta Crystallographica* **D50,** 760-763.

CHAN, M. K., MUKUND, S., KLETZIN, A., ADAMS, M. W., and REES, D. C. (1995). Structure of a hyperthermophilic tungstopterin enzyme, aldehyde ferredoxin oxidoreductase. *Science* **267**(5203), 1463-1469.

CORRAN, H. S., DEWAN, J. G., GORDON, A. H., and E, G. D. (1939). Xanthine Oxidase and Milk Flavoprotein. *Biochemical Journal* **33,** 1694-1706.

CRICK, F. H. C., and KENDREW, J. C. (1957). X-ray analysis and protein structure. *Advances in Protein Chemistry* **12,** 133-214.

CRUZ RAMOS, H., BOURSIER, L., MOSZER, I., KUNST, F., DANCHIN, A., and GLASER, P. (1995). Anaerobic transcription activation in Bacillus subtilis: identification of distinct FNR-dependent and -independent regulatory mechanisms. *Embo Journal* **14**(23), 5984-5994.

DE RENZO, E. C., KALEITA, E., HEYTLER, P., OLESON, J. J., HUTCHINGS, B. L., and WILLIAMS, J. H. (1953). The nature of the xanthine oxidase factor. *Journal of the American Chemical Society* **75,** 753.

DIAS, J. M., THAN, M. E., HUMM, A., HUBER, R., BOURENKOV, G. P., BARTUNIK, H. D., BURSAKOV, S., CALVETE, J., CALDEIRA, J., CARNEIRO, C., MOURA, J. J., MOURA, I., and ROMAO, M. J. (1999). Crystal structure of the first dissimilatory nitrate reductase at 1.9 A solved by MAD methods. *Structure Folding and Design* **7**(1), 65-79.

DIXON, M. (1926). Studies on Xanthine Oxidase.
VII. The specificity of the system. *Biochemical Journal* **20,** 703-718.

DIXON, M. (1938). On the question of the identity of the Schardinger enzyme with xanthine oxidase and aldehyde mutase. *Enzymologia* **5,** 198-225.

DIXON, M., and THURLOW, S. (1924a). Studies on Xanthine Oxidase.
I. Preparation and properties of the active material. *Biochemical Journal* **18,** 971-975.

DIXON, M., and THURLOW, S. (1924b). Studies on Xanthine Oxidase.
II. The dynamics of the oxidase system. *Biochemical Journal* **18,** 976-988.

DIXON, M., and THURLOW, S. (1924c). Studies on Xanthine Oxidase.
III. The reduction of Nitrates. *Biochemical Journal* **18,** 989-992.

DOBBEK, H., GREMER, L., MEYER, O., and HUBER, R. (1999). Crystal structure and mechanism of CO dehydrogenase, a molybdo iron-sulfur flavoprotein containing S-selanylcysteine. *Proceedings of the National Academy of Sciences USA* **96**(8884-8889).

DOEL, J. J., GODBER, B. L. J., GOULT, T. A., EISENTHAL, R., and HARRISON, R. (2000). Reduction of organic nitrites to nitric oxide catalyzed by xanthine oxidase: possible role in metabolism of nitrovasodilators. *Biochemical and Biophysical Research Communications* **270**(880-885).

DUARTE, R. O., ARCHER, M., DIAS, J. M., BURSAKOV, S., HUBER, R., MOURA, I., ROMÃO, M. J., and MOURA, J. J. G. (2000). Biochemical/spectroscopic characterization and preliminary X-ray analysis of a new aldehyde oxidoreductase isolated from *Desulfovibrio desulfuricans* ATCC 27774. *Biochemical and Biophysical Research Communications* **268,** 745-749.

EGER, B. T., EIKMANNS, U., PAI, E. F., SATO, M., OKAMOTO, K., and NISHINO, T. (1993). Crystallization and preliminary X-ray diffraction of xanthine oxidase isolated from bovine milk. *In* "Flavins and Flavoproteins 1993", pp. 727-729. Walter de Gruyter & Co., Berlin New York.

EGER, B. T., OKAMOTO, K., ENROTH, C., SATO, M., NISHINO, T., and PAI, E. F. (2000). Purification, crystallization and preliminary X-ray diffraction studies of xanthine dehydrogenase and xanthine oxidase isolated from bovine milk. *Acta Crystallographica* **D56**(Pt 12), 1656-8.
ENROTH, C., EGER, B. T., OKAMOTO, K., NISHINO, T., and PAI, E. F. (2000). Crystal structures of bovine milk xanthine dehydrogenase and xanthine oxidase: structure-based mechanism of conversion. *Proceedings of the National Academy of Sciences U S A* **97**(20), 10723-10728.

FALCIANI, F., TERAO, M., GOLDWURM, S., RONCHI, A., GATTI, A., MINOIA, C., LI CALZI, M., SALMONA, M., CAZZANIGA, G., and GARATTINI, E. (1994). Molybdenum(VI) salts convert the xanthine oxidoreductase apoprotein into the active enzyme in mouse L929 fibroblastic cells. *Biochemical Journal* **298**(Pt 1), 69-77.

FENG, G., TINTRUP, H., KIRSCH, J., NICHOL, M. C., KUHSE, J., BETZ, H., and SANES, J. R. (1998). Dual requirement for gephyrin in glycine receptor clustering and molybdoenzyme activity [see comments]. *Science* **282**(5392), 1321-4.

FRAAIJE, M. W., VAN BERKEL, W. J., BENEN, J. A., VISSER, J., and MATTEVI, A. (1998). A novel oxidoreductase family sharing a conserved FAD-binding domain [published erratum appears in Trends Biochem Sci 1998 Jul;23(7):271]. *Trends in Biochemical Sciences* **23**(6), 206-207.

FRENCH, S., and WILSON, K. S. (1978). On the treatment of negative intensity observations. *Acta Crystallographica* **A34**, 517-525.

FRIEDRICH, W., KNIPPING, P., and LAUE, M. (1913). Interferenzerscheinungen bei Röntgenstrahlen. *Annalen der Physik* **41**, 971-988.

GARDLIK, S., BARBER, M. J., and RAJAGOPALAN, K. V. (1987). A molybdopterin-free form of xanthine oxidase. *Archives of Biochemistry and Biophysics* **259**(2), 363-371.

GARMAN, E. F., and MITCHELL, E. (1996). Glycerol concentrations required for cryoprotection of 50 typical protein crystallization solutions. *Journal of Applied Crystallography* **29**, 584-587.

GARRETT, R. M., BELLISSIMO, D. B., and RAJAGOPALAN, K. V. (1995). Molecular cloning of human liver sulfite oxidase. *Biochimica et Biophysica Acta* **1262**(2-3), 147-149.

GIEGÉ, R., and DUCRUIX, A. (1992). An introduction to the crystallogenesis of biological macromolecules. *In* "Crystallization of nucleic acids and proteins - A practical approach" (A. Ducruix, and R. Giegé, Eds.), pp. 1-18. IRL Press at Oxford University Press, Oxford, New York and Tokyo.

GLYKOS, N. M., and KOKKINIDIS, M. (2000). A stochastic approach to molecular replacement. *Acta Crystallographica* **D56**, 169-174.

GODBER, B., SANDERS, S., HARRISON, R., EISENTHAL, R., and BRAY, R. C. (1997). 95% of xanthine oxidase in human milk is present as the demolybdo form, lacking molybdopterin. *Biochemical Society Transactions* **25**(3), 519S.

GODBER, B. L., DOEL, J. J., DURGAN, J., EISENTHAL, R., and HARRISON, R. (2000a). A new route to peroxynitrite: a role for xanthine oxidoreductase. *FEBS Letters* **475**(2), 93-6.

GODBER, B. L. J. (1998). Physicochemical and Kinetic Properties of Human Milk Xanthine Oxidoreductases. *PhD Thesis*. The University of Bath, Bath.

GODBER, B. L. J., DOEL, J. J., SAPKOTA, G. P., BLAKE, D., STEVENS, C., EISENTHAL, R., and HARRISON, R. (2000b). Reduction of nitrite to nitric oxide catalysed by xanthine oxidoreductase. *Journal of Biological Chemistry* **275**(11), 7757-7763.

GRANGER, D. N., RUTILI, G., and MCCORD, J. M. (1981). Superoxide radicals in feline intestinal ischemia. *Gastroenterology* **81**(1), 22-29.

GREEN, D. E., and BEINERT, H. (1953). Xanthine oxidase, a molybdoflavo protein. *Biochimica et Biophysica Acta* **11**, 599-600.

HÄNZELMANN, P., DOBBEK, H., GREMER, L., HUBER, R., and MEYER, O. (2000). The Effect of Intracellular Molybdenum in Hydrogenophaga pseudoflava on the Crystallographic Structure of the Seleno-Molybdo-Iron-Sulfur Flavoenzyme Carbon Monoxide Dehydrogenase. *Journal of Molecular Biology* **301**(5), 1221-1235.

HÄNZELMANN, P., and MEYER, O. (1998). Effect of molybdate and tungstate on the biosynthesis of CO dehydrogenase and the molybdopterin cytosine-dinucleotide-type of molybdenum cofactor in *Hydrogenophaga pseudoflava*. *European Journal of Biochemistry* **255**, 755-765.

HARRISON, R. (1997). Human xanthine oxidoreductase: in search of a function. *Biochemical Society Transactions* **25**(3), 786-791.

HARRISON, R., BENBOUBETRA, M., BRYSON, S., THOMAS, R. D., and C, E. P. (1990). Antibodies to xanthine oxidase: elevated levels in patients with acute myocardial infarction. *Cardioscience* **1**, 183-189.

HART, L. I., MCGARTOLL, M. A., CHAPMAN, H. R., and BRAY, R. C. (1970). The composition of milk xanthine oxidase. *Biochemical Journal* **116**(5), 851-864.

HAWKES, T. R., and BRAY, R. C. (1984). Studies by electron-paramagnetic-resonance spectroscopy of the environment of the metal in the molybdenum cofactor of molybdenum- containing enzymes. *Biochemical Journal* **222**(3), 587-600.

HAZAN, J., FONKNECHTEN, N., MAVEL, D., PATERNOTTE, C., SAMSON, D., ARTIGUENAVE, F., DAVOINE, C. S., CRUAUD, C., DURR, A., WINCKER, P., BROTTIER, P., CATTOLICO, L., BARBE, V., BURGUNDER, J. M., PRUD'HOMME, J. F., BRICE, A., FONTAINE, B., HEILIG, B., and WEISSENBACH, J. (1999). Spastin, a new AAA protein, is altered in the most frequent form of autosomal dominant spastic paraplegia. *Nature Genetics* **23**(3), 296-303.

HILLE, R. (1996). The Mononuclear Molybdenum Enzymes. *Chemical Reviews* **96**, 2757-2816.

HILLE, R., HAGEN, W. R., and DUNHAM, W. R. (1985). Spectroscopic studies on the iron-sulfur centers of milk xanthine oxidase. *Journal of Biological Chemistry* **260**(19), 10569-10575.

HORBACZEWSKI, J. (1891). Beiträge sur Kenntniss der Bildung der Harnsäure und der Xanthinbasen, sowie der Entstehung der Leucocytosen im Säugethierorganismus. *Monatshefte für Chemie* **12,** 221-275.

HUBER, R., HOF, P., DUARTE, R. O., MOURA, J. J. G., MOURA, I., LIU, M.-Y., LEGALL, J., HILLE, R., ARCHER, M., and ROMÃO, M. J. (1996). A structure-based catalytic mechanism for the xanthine oxidase family of molybdenum enzymes. *Proceedings of the National Academy of Sciences USA* **93,** 8846-8851.

HUNT, J., and MASSEY, V. (1994). Studies of the reductive half-reaction of milk xanthine dehydrogenase. *Journal of Biological Chemistry* **269**(29), 18904-18914.

ICHIDA, K., AMAYA, Y., KAMATANI, N., NISHINO, T., HOSOYA, T., and SAKAI, O. (1997). Identification of two mutations in human xanthine dehydrogenase gene responsible for classical type I xanthinuria. *Journal of Clinical Investigation* **99**(10), 2391-2397.

ICHIDA, K., AMAYA, Y., NODA, K., MINOSHIMA, S., HOSOYA, T., SAKAI, O., SHIMIZU, N., and NISHINO, T. (1993). Cloning of the cDNA encoding human xanthine dehydrogenase (oxidase): structural analysis of the protein and chromosomal location of the gene. *Gene* **133**(2), 279-284.

IKEGAMI, T., and NISHINO, T. (1986). The presence of desulfo xanthine dehydrogenase in purified and crude enzyme preparations from rat liver. *Archives of Biochemistry Biophysics* **247**(2), 254-260.

IWASAKI, T., OKAMOTO, K., NISHINO, T., MIZUSHIMA, J., HORI, H., and NISHINO, T. (2000). Sequence motif-specific assignment of two [2Fe-2S] clusters in rat xanthine oxidoreductase studied by site directed mutagenesis. *Journal of Biochemistry (Tokyo)* **127,** 771-778.

JANCARIK, J., and KIM, S.-H. (1991). Sparse matrix sampling: a screening method for crystallization of proteins. *Journal of Applied Crystallography* **24,** 409-411.

JARASCH, E.-D., BRUDER, G., and HEID, H. (1986). Significance of xanthine oxidase in capillary endothelial cells. *Acta Physiologica Scandinavia* **548S,** 39-46.

JOHNSON, J. L., and RAJAGOPALAN, K. V. (1982). Structural and metabolic relationship between the molybdenum cofactor and urothione. *Proceedings of the National Academy of Sciences U S A* **79**(22), 6856-6860.

JONES, T. A., ZOU, J. Y., COWAN, S., and KJELDGAARD, M. (1991). Improved methods for building protein models in electron density maps and the location of errors in these models. *Acta Crystallographica* **A47,** 110-119.

KAWARABAYASI, Y., SAWADA, M., HORIKAWA, H., HAIKAWA, Y., HINO, Y., YAMAMOTO, S., SEKINE, M., BABA, S., KOSUGI, H., HOSOYAMA, A., NAGAI, Y., SAKAI, M., OGURA, K., OTSUKA, R., NAKAZAWA, H., TAKAMIYA, M., OHFUKU, Y., FUNAHASHI, T., TANAKA, T., KUDOH, Y., YAMAZAKI, J., KUSHIDA, N., OGUCHI, A., AOKI, K., and KIKUCHI, H. (1998). Complete sequence and gene organization of the genome of a hyper- thermophilic archaebacterium, Pyrococcus horikoshii OT3. *DNA Research* **5**(2), 55-76.

KEITH, T. P., RILEY, M. A., KREITMAN, M., LEWONTIN, R. C., CURTIS, D., and CHAMBERS, G. (1987). Sequence of the structural gene for xanthine dehydrogenase (rosy locus) in Drosophila melanogaster. *Genetics* **116**(1), 67-73.

KISKER, C., SCHINDELIN, H., BAAS, D., RÉTEY, J., MECKENSTOCK, R. U., and KRONECK, P. M. H. (1999). A Structural comparison of molybdenum cofactor-containing enzymes. *FEMS Microbiology Reviews* **22,** 503-521.

KISKER, C., SCHINDELIN, H., PACHECO, A., WEHBI, W. A., GARRETT, R. M., RAJAGOPALAN, K. V., ENEMARK, J. H., and REES, D. C. (1997). Molecular basis of sulfite oxidase deficiency from the structure of sulfite oxidase. *Cell* **91**(7), 973-983.

KISSINGER, C. R., GEHLHAAR, D. K., and FOGEL, D. B. (1999). Rapid automated molecular replacement by evolutionary search. *Acta Crystallographica* **D55,** 484-491.

KLEYWEGT, G. J. (1995). Dictionaries for Heteros. *CCP4/ESF-EACBM Newsletter on Protein Crystallography* **31,** 45-50.

KLEYWEGT, G. J. (1996). Making the most of your search model. *CCP4/ESF-EACBM Newsletter on Protein Crystallography* **32,** 32-36.

KLEYWEGT, G. J. (1997). Validation of protein models from CA coordinates alone. *Journal of Molecular Biology* **273,** 371-376.

KLEYWEGT, G. J., and JONES, T. A. (1996). Phi/Psi-chology: Ramachandran revisited. *Structure* **4,** 1395-1400.

KLEYWEGT, G. J., and JONES, T. A. (1997). Model Building and refinement practice. *Methods in Enzymology* **277,** 208-230.

KOMAI, H., MASSEY, V., and PALMER, G. (1969). The preparation and properties of deflavo xanthine oxidase. *Journal of Biological Chemistry* **244**(7), 1692-1700.

KRAULIS, P. J. (1991). Molscript: a programme to produce both detailed and schematic plots of protein structures. *Journal of Applied Crystallography* **24,** 946-950.

KRENITSKY, T. A. (1978). Aldehyde oxidase and xanthine oxidase--functional and evolutionary relationships. *Biochemical Pharmacology* **27**(24), 2763-2764.

KRENITSKY, T. A., SPECTOR, T., and HALL, W. W. (1986). Xanthine oxidase from human liver: purification and characterization. *Archives of Biochemistry and Biophysics* **247**(1), 108-119.

LAEMMLI, U. K. (1970). Cleavage of structural proteins during the assembly of the head of bacteriophage T4. *Nature* **227**(259), 680-685.

LEHMANN, M., TSHISUAKA, B., FETZNER, S., and LINGENS, F. (1995). Molecular cloning of the isoquinoline 1-oxidoreductase genes from Pseudomonas diminuta 7, structural analysis of iorA and iorB, and sequence comparisons with other molybdenum-containing hydroxylases. *Journal of Biological Chemistry* **270**(24), 14420-14429.

LOWRY, O. H., BESSEY, O. A., and CRAWFORD, E. J. (1949). Pterine oxidase. *Journal of Biological Chemistry* **180,** 399-410.

LU, G., LINDQVIST, Y., SCHNEIDER, G., DWIVEDI, U., and CAMPBELL, W. (1995). Structural studies on corn nitrate reductase: refined structure of the cytochrome b reductase fragment at 2.5 A, its ADP complex and an active-site mutant and modeling of the cytochrome b domain. *Journal of Molecular Biology* **248**(5), 931-948.

MASSEY, V., BRUMBY, P. E., and KOMAI, H. (1969). Studies on milk xanthine oxidase. Some spectral and kinetic properties. *Journal of Biological Chemistry* **244**(7), 1682-1691.

MASSEY, V., and EDMONDSON, D. (1970). On the mechanism of inactivation of xanthine oxidase by cyanide. *Journal of Biological Chemistry* **245,** 6595-6598.

MASSEY, V., SCHOPFER, L. M., NISHINO, T., and NISHINO, T. (1989). Differences in protein structure of xanthine dehydrogenase and xanthine oxidase revealed by reconstitution with flavin active site probes. *Journal of Biological Chemistry* **264,** 10567- 10573.

MATTHEWS, B. W. (1968). Solvent content of protein crystals. *Journal of Molecular Biology* **33**(2), 491-497.

MCCORD, J. M., and ROY, R. S. (1982). The pathophysiology of superoxide: roles in inflammation and ischemia. *Canadian Journal of Physiology and Pharmacology* **60**(11), 1346-1352.

MCMANAMAN, J. L., HANSON, L., NEVILLE, M. C., and WRIGHT, R. M. (2000). Lactogenic hormones regulate xanthine oxidoreductase and b-casien levels in mammary epithelial cells by distinct mechanisms. *Archives of Biochemistry and Biophysics* **373**(2), 318-327.

MEYER, O., FRUNZKE, K., and MÖRSDORF, G. (1993). *In* "Microbial growth on C_1 compounds" (J. C. Murrel, and D. P. Kelly, Eds.), pp. 433-459. Intercept, Andover, UK.

MILLAR, T. M., STEVENS, C. R., BENJAMIN, N., EISENTHAL, R., HARRISON, R., and BLAKE, D. R. (1998). Xanthine oxidoreductase catalyses the reduction of nitrates and nitrite to nitric oxide under hypoxic conditions. *FEBS Letters* **427**(2), 225-228.

MORGAN, E. J., STEWART, C. P., and HOPKINS, F. G. (1922). On the Anaerobic and Aerobic Oxidation of Xanthin and Hypoxanthin by Tissues and by Milk. *Proceedings of the Royal Society of London Series B* **94,** 109-131.

MORIWAKI, Y., YAMAMOTO, T., SUDA, M., NASAKO, Y., TAKAHASHI, S., AGBEDANA, O. E., HADA, T., and HIGASHINO, K. (1993). Purification and immunohistochemical tissue localization of human xanthine oxidase. *Biochimica et Biophysica Acta* **1164**(3), 327-30.

MURSHUDOV, G., LEBEDEV, A., VAGIN, A., WILSON, K. S., and DODSON, E. (1999). Efficient anisotropic refinement of Macromolecular structures using FFT. *Acta Crystallographica* **D55,** 247-255.

MURSHUDOV, G., VAGIN, A., and DODSON, E. (1996). Application of Maximum Likelihood Refinement. *In* "Proceedings of the Daresbury Study Weekend 1996".

MURSHUDOV, G., VAGIN, A., and DODSON, E. (1997). Refinement of Macromolecular Structures by the Maximum-Likelihood Method. *Acta Crystallographica* **D53,** 240-255.

NAKAMURA, M., and YAMAZAKI, I. (1982). Preparation of bovine milk xanthine oxidase as a dehydrogenase form. *Journal of Biochemistry (Tokyo)* **92**(4), 1279-1286.

NAVAZA, J. (1994). AMoRe: an automated package for molecular replacement. *Acta Crystallographica* **A50,** 157-163.

NEAME, P. J., and BARBER, M. J. (1989). Conserved domains in molybdenum hydroxylases. The amino acid sequence of chicken hepatic sulfite oxidase. *Journal of Biological Chemistry* **264**(35), 20894-20901.

NICHOLLS, A., SHARP, K. A., and HONIG, B. (1991). Protein folding and association: insights from the interfacial and thermodynamic properties of hydrocarbons. *Proteins* **11**(4), 281-296.

NISHINO, T. (1989). The nicotinamide adenine dinucleotide-binding site of chicken liver xanthine dehydrogenase. Evidence for alteration of the redox potential of the flavin by NAD binding or modification of the NAD-binding site and isolation of a modified peptide. *Journal of Biological Chemistry* **264**(10), 5468-73.

NISHINO, T., and TSUSHIMA, K. (1981). Purification of highly active milk xanthine oxidase by affinity chromatography on Sepharose 4B/folate gel. *FEBS Letters* **131**(2), 369-372.

OKAMOTO, P. M., FU, Y. H., and MARZLUF, G. A. (1991). Nit-3, the structural gene of nitrate reductase in Neurospora crassa: nucleotide sequence and regulation of mRNA synthesis and turnover. *Molecular and General Genetics* **227**(2), 213-223.

OTWINOWSKI, Z., and MINOR, W. (1997). Processing of X-ray diffraction data collected in oscillation mode. *Methods in Enzymology* **276,** 307-325.

PAGE, S., POWELL, D., BENBOUBETRA, M., STEVENS, C. R., BLAKE, D. R., SELASE, F., WOLSTENHOLME, A. J., and HARRISON, R. (1998). Xanthine oxidoreductase in human mammary epithelial cells: activation in response to inflammatory cytokines. *Biochimica et Biophysica Acta* **1381**(2), 191-202.

PALMER, G., and MASSEY, V. (1969). Electron paramagnetic resonance and circular dichroism studies on milk xanthine oxidase. *Journal of Biological Chemistry* **244**(10), 2614-2620.

PARKS, D. A., and GRANGER, D. N. (1986). Xanthine Oxidase: biochemistry, distribution and physiology. *Acta Physiologica Scandinavia* **548S,** 87-99.

PATEMAN, J. A., COVE, D. J., REVER, B. M., and ROBERTS, D. B. (1964). A common co-factor for nitrate reductase and xanthine dehydrogenase which also regulates the synthesis of nitrate reductase. *Nature* **201,** 58-60.

PORRAS, A. G., and PALMER, G. (1982). The room temperature potentiometry of xanthine oxidase. pH-dependent redox behavior of the flavin, molybdenum, and iron-sulfur centers. *Journal of Biological Chemistry* **257**(19), 11617-11626.

PRITSOS, C. A. (2000). Cellular distribution, metabolism and regulation of the xanthine oxidoreductase enzyme system. *Chemico-biological Interactions* **129**(1-2), 195-208.

RASMUSSEN, J. T., RASMUSSEN, M. S., and PETERSEN, T. E. (2000). Cysteines involved in the interconversion between dehydrogenase and oxidase forms of bovine xanthine oxidoreductase. *Journal of Dairy Science* **83,** 499-506.

REBELO, J., MACIEIRA, S., DIAS, J. M., HUBER, R., ASCENSO, C. S., RUSNAK, F., MOURA, J. J. G., MOURA, I., and ROMÃO, M. J. (2000). Gene sequence and crystal structure of the aldehyde oxidoreductase from *Desulfovibrio desulfuricans* ATCC 27774. *Journal of Molecular Biology* **297,** 135-146.

REISS, J., COHEN, N., DORCHE, C., MANDEL, H., MENDEL, R. R., STALLMEYER, B., ZABOT, M. T., and DIERKS, T. (1998). Mutations in a polycistronic nuclear gene associated with molybdenum cofactor deficiency. *Nature Genetics* **20**(1), 51-3.

RICHERT, D. A., and WESTERFIELD, W. W. (1953). Isolation and identification of the xanthine oxidase factor as molybdenum. *Journal of Biological Chemistry* **203,** 915-923.

RICHERT, D. A., and WESTERFIELD, W. W. (1954). The relationship of iron to xanthine oxidase. *Journal of Biological Chemistry* **209,** 179-183.

ROMÃO, M. J., ARCHER, M., MOURA, I., MOURA, J. J. G., LEGALL, J., ENGH, R., SCHNEIDER, M., HOF, P., and HUBER, R. (1995). Crystal structure of the xanthine oxidase related aldehyde oxidoreductase from *D. gigas*. *Science* **270,** 1170-1176.

SAIKI, R. K., SCHARF, S., FALOONA, F., MULLIS, K. B., HORN, G. T., ERLICH, H. A., and ARNHEIM, N. (1985). Enzymatic amplification of beta-globin genomic sequences and restriction site analysis for diagnosis of sickle cell anemia. *Science* **230**(4732), 1350-1354.

SAKSELA, M., and RAIVIO, K. O. (1996). Cloning and expression in vitro of human xanthine dehydrogenase/oxidase. *Biochemical Journal* **315**(Pt 1), 235-239.

SANDERS, S. A., EISENTHAL, R., and HARRISON, R. (1997). NADH oxidase activity of human xanthine oxidoreductase. *European Journal of Biochemistry* **245,** 541-548.

SANTINI, C. L., IOBBI-NIVOL, C., ROMANE, C., BOXER, D. H., and GIORDANO, G. (1992). Molybdoenzyme biosynthesis in Escherichia coli: in vitro activation of purified nitrate reductase from a chlB mutant. *Journal of Bacteriology* **174**(24), 7934-40.

SARNESTO, A., LINDER, N., and RAIVIO, K. O. (1996). Organ distribution and molecular forms of human xanthine dehydrogenase/xanthine oxidase protein. *Laboratory Investigation* **74**(1), 48-56.

SATO, A., NISHINO, T., NODA, K., and AMAYA, Y. (1995). The structure of chicken liver xanthine dehydrogenase. cDNA cloning and the domain structure. *Journal of Biological Chemistry* **270**(6), 2818-2826.

SCHARDINGER, F. (1902). Ueber das Verhalten der Kuhmilch gegen Methylenblau und seine Verwendung zur Unterscheidung von ungekochter und gekochter Milch. *Zeitschrift fuer Untersuchung der Nahrungs- und Genussmittel* **5**(22), 1113-1121.

SCHINDELIN, H., KISKER, C., HILTON, J., RAJAGOPALAN, K. V., and REES, D. C. (1996). Crystal structure of DMSO reductase: redox-linked changes in molybdopterin coordination. *Science* **272**(5268), 1615-1621.

SCHNEIDER, F., LOWE, J., HUBER, R., SCHINDELIN, H., KISKER, C., and KNABLEIN, J. (1996). Crystal structure of dimethyl sulfoxide reductase from Rhodobacter capsulatus at 1.88 A resolution. *Journal of Molecular Biology* **263**(1), 53-69.

SCHUBEL, U., KRAUT, M., MORSDORF, G., and MEYER, O. (1995). Molecular characterization of the gene cluster coxMSL encoding the molybdenum-containing carbon monoxide dehydrogenase of Oligotropha carboxidovorans. *Journal of Bacteriology* **177**(8), 2197-2203.

SENSEN, C. W., KLENK, H. P., SINGH, R. K., ALLARD, G., CHAN, C. C., LIU, Q. Y., PENNY, S. L., YOUNG, F., SCHENK, M. E., GAASTERLAND, T., DOOLITTLE, W. F., RAGAN, M. A., and CHARLEBOIS, R. L. (1996). Organizational characteristics and information content of an archaeal genome: 156 kb of sequence from Sulfolobus solfataricus P2. *Molecular Microbiology* **22**(1), 175-191.

SHAW, A. L., HANSON, G. R., and MCEWAN, A. G. (1996). Cloning and sequence analysis of the dimethylsulfoxide reductase structural gene from Rhodobacter capsulatus. *Biochimica et Biophysica Acta* **1276**(3), 176-180.

SLOAN, J., KINGHORN, J. R., and UNKLES, S. E. (1999). The two subunits of human molybdopterin synthase: evidence for a bicistronic messenger RNA with overlapping reading frames. *Nucleic Acids Research* **27**(3), 854-8.

SPITZER, W. (1899). Die Ueberführung von Nucleïnbasen in Harnsäure durch die sauerstoffübertragende Wirkung von Gewebsauszügen. *Archiv für Physiologie* **76**, 192-203.

STALLMEYER, B., DRUGEON, G., REISS, J., HAENNI, A. L., and MENDEL, R. R. (1999a). Human molybdopterin synthase gene: identification of a bicistronic transcript with overlapping reading frames. *American Journal of Human Genetics* **64**(3), 698-705.

STALLMEYER, B., SCHWARZ, G., SCHULZE, J., NERLICH, A., REISS, J., KIRSCH, J., and MENDEL, R. R. (1999b). The neurotransmitter receptor-anchoring protein gephyrin reconstitutes molybdenum cofactor biosynthesis in bacteria, plants, and mammalian cells. *Proceedings of the National Academy of Sciences USA* **96**(4), 1333-8.

STEVENS, C. R., MILLAR, T. M., CLINCH, J. G., KANCZLER, J. M., BODAMYALI, T., and BLAKE, D. R. (2000). Antibacterial properties of xanthine oxidase in human milk. *Lancet* **356**(9232), 829-830.

TAKAMI, H., NAKASONE, K., TAKAKI, Y., MAENO, G., SASAKI, R., MASUI, N., FUJI, F., HIRAMA, C., NAKAMURA, Y., OGASAWARA, N., KUHARA, S., and HORIKOSHI, K. (2000). Complete genome sequence of the alkaliphilic bacterium bacillus halodurans and genomic sequence comparison with bacillus subtilis. *Nucleic Acids Research* **28**(21), 4317-4331.

TATE, J. G., MORELAND, J., and BOURNE, P. E. (1999).MSG (Molecular Scene Generator): a Web-based application for the visualization of macromolecular structures. *Journal of Applied Crystallography* **32**, 1027-1028.

TEMPLE, C. A., and RAJAGOPALAN, K. V. (2000). Mechanism of assembly of the Bis(Molybdopterin guanine dinucleotide)molybdenum cofactor in Rhodobacter

sphaeroides dimethyl sulfoxide reductase. *Journal of Biological Chemistry* **275**(51), 40202-10.

THOENES, U., FLORES, O. L., NEVES, A., DEVREESE, B., VAN BEEUMEN, J. J., HUBER, R., ROMAO, M. J., LEGALL, J., MOURA, J. J., and RODRIGUES-POUSADA, C. (1994). Molecular cloning and sequence analysis of the gene of the molybdenum- containing aldehyde oxido-reductase of Desulfovibrio gigas. The deduced amino acid sequence shows similarity to xanthine dehydrogenase. *European Journal of Biochemistry* **220**(3), 901-910.

TOPHAM, R., GOGER, M., PEARCE, K., and SCHULTZ, P. (1989). The mobilization of ferritin iron by liver cytosol. A comparison of xanthine and NADH as reducing substrates. *Biochemical Journal* **261**(1), 137-143.

TOPHAM, R. W., WALKER, M. C., and CALISCH, M. P. (1982a). Liver xanthine dehydrogenase and iron mobilization. *Biochemical and Biophysical Research Communications* **109**(4), 1240-1246.

TOPHAM, R. W., WALKER, M. C., CALISCH, M. P., and WILLIAMS, R. W. (1982b). Evidence for the participation of intestinal xanthine oxidase in the mucosal processing of iron. *Biochemistry* **21**(19), 4529-4535.

TOTTER, J. R., BURNETT JR., W. T., MONROE, R. A., WHITNEY, I. B., and COMAR, C. L. (1953). Evidence that Molybdenum is a non-dialyzable component of Xanthine Oxidase. *Science* **118**, 555.

TSUCHIDA, S., and TAGAWA, M. (2000). Molecular Cloning of a cDNA coding for feline liver xanthine dehydrogenase. *Unpublished.*

TURNER, N. A., DOYLE, W. A., VENTOM, A. M., and BRAY, R. C. (1995). Properties of rabbit liver aldehyde oxidase and the relationship of the enzyme to xanthine oxidase and dehydrogenase. *European Journal of Biochemistry* **232**(2), 646-57.

UNKLES, S. E., HECK, I. S., APPLEYARD, M. V., and KINGHORN, J. R. (1999). Eukaryotic molybdopterin synthase. Biochemical and molecular studies of Aspergillus nidulans cnxG and cnxH mutants. *Journal of Biological Chemistry* **274**(27), 19286-93.

VAN DER OOST, J., SCHUT, G., KENGEN, S. W., HAGEN, W. R., THOMM, M., and DE VOS, W. M. (1998). The ferredoxin-dependent conversion of glyceraldehyde-3-phosphate in the hyperthermophilic archaeon Pyrococcus furiosus represents a novel site of glycolytic regulation. *Journal of Biological Chemistry* **273**(43), 28149-28154.

VENTOM, A. M., DEISTUNG, J., and BRAY, R. C. (1988). The isolation of demolybdo xanthine oxidase from bovine milk. *Biochemical Journal* **255**(3), 949-956.

WALLACE, A. C., LASKOWSKI, R. A., and THORNTON, J. M. (1995). LIGPLOT: A program to generate schematic diagrams of protein-ligand interactions. *Protein Engineering* **8,** 127-134

WARBURG, O., and CHRISTIAN, W. (1938). Isolierung der prosthetischen Gruppe der d-Aminosäureoxydase. *Biochemische Zeitschrift* **298,** 150-168.

WESTERFIELD, W. W., and RICHERT, D. A. (1950). Dietary factors related to liver xanthine oxidase. *Journal of Biological Chemistry* **184,** 163-173.

WRIGHT, R. M., VAITAITIS, G. M., WILSON, C. M., REPINE, T. B., TERADA, L. S., and REPINE, J. E. (1993). cDNA cloning, characterization, and tissue-specific expression of human xanthine dehydrogenase/xanthine oxidase. *Proceedings of the National Academy of Sciences USA* **90**(22), 10690-10694.

XIA, M., DEMPSKI, R., and HILLE, R. (1999). The reductive half-reaction of xanthine oxidase. Reaction with aldehyde substrates and identification of the catalytically labile oxygen. *Journal of Biological Chemistry* **274**(6), 3323-30.

XU, P., HUECKSTEADT, T. P., and HOIDAL, J. R. (1996). Molecular cloning and characterization of the human xanthine dehydrogenase gene (XDH). *Genomics* **34**(2), 173-180.

XU, P., ZHU, X. L., HUECKSTEADT, T. P., BROTHMAN, A. R., and HOIDAL, J. R. (1994). Assignment of human xanthine dehydrogenase gene to chromosome 2p22. *Genomics* **23**(1), 289-291.

YAMAMOTO, T., MORIWAKI, Y., SHIBUTANI, Y., MATSUI, K., UEO, T., TAKAHASHI, S., TSUTSUMI, Z., and HADA, T. (2001). Human xanthine dehydrogenase cDNA sequence and protein in an atypical case of type I xanthinuria in comparison with normal subjects. *Clinica Chimica Acta* **304**(1-2), 153-158.